# DOCTOR OF PHILOSOPHY

## Palmitoylation of the Cardiac Sodium-Calcium Exchanger

Reilly, Louise

*Award date:*
2014

# Palmitoylation Of The Cardiac Sodium-Calcium Exchanger

Louise Reilly

A thesis submitted for the Degree of Doctor of Philosophy

University of Dundee
December 2014

**Table Of Contents**

Table Of Contents ii
List Of Figures vii
List Of Tables xi
Abbreviations xii
Acknowledgements xvii
Declaration xix
Supervisors Declaration xix
Abstract xx

**1 Introduction** 1
1.1 Cardiac Ion Transport 2
1.1.1 SLC8 – $Na^+$-$Ca^{2+}$ Exchanger Family 3
1.1.2 Structural Features Of NCX 4
1.1.3 Function Of NCX1 11
1.1.4 Modes Of Function 12
i Forward Mode 12
ii Reverse Mode 12
1.1.5 Structure-Function Of NCX1 14
i Function Of The α-repeats 14
ii Function Of The XIP Region 16
iii Function Of The $Ca^{2+}$ Regulatory Domain 18
1.1.6 Regulation Of NCX1 22
i $Na^+$-dependent Inactivation 22
ii $Ca^{2+}$ Regulation 24
iii ATP Regulation 29
iv $PIP_2$ Regulation 30
v Phosphorylation Of NCX1 32
vi Contribution Of NCX1 To Cardiovascular Disease 33
1.2 Palmitoylation 37
1.2.1 Overview Of Palmitoylation Mechanism 37
1.2.2 Control Of Palmitoylation 39
i Protein Acyl Transferases 39
ii Thioesterases 42

iii Hydrolases 46
1.2.3 Palmitoylation And Control Of Protein Biology 47
i Membrane Targeting 47
ii Membrane Cycling 49
iii Regulation Of Ion Transport 51
iv Massive Endocytosis (MEND) 54
1.3 Project Aims 57
**2 Materials And Methods** 58
2.1 Chemicals And Reagents 59
2.2 Ethics Statement 59
2.3 Adult Rat Ventricular Myocyte Isolation 59
2.3.1 Myocyte Isolation 59
2.3.2 Assessment Of Healthy Viable Cells 61
2.4 Cell Culture 62
2.4.1 Culture Conditions 62
2.4.2 Subculture Of Cells 62
2.4.3 Freezing And Revival Of Cell Stocks 62
2.5 Cell Based Assays 65
2.5.1 Transient Transfection Of Cell Lines 65
2.5.2 Generation Of Stable Cell Lines 65
2.5.3 Treatment Of Cells With Global Palmitoylation Inhibitior, 2-Bromohexadecanoic Acid 68
2.5.4 Labelling Of Cell Surface Proteins With Biotin 68
2.5.5 Confocal Microscopy Analysis Of Transiently Transfected Cell Lines 68
2.6 Protein Analysis 69
2.6.1 Bradford Assay 69
2.6.2 Purification Of Palmitoylated Proteins By Resin Assisted Capture 69
2.6.3 Purification Of Biotin Labelled Cell Surface Proteins Via Streptavidin Affinity Capture 71
2.6.4 Co-Immunoprecipitation 71
2.6.5 Cell Fractionation 72
2.6.6 Sucrose Gradient Fractionation Of Caveolin-enriched Membranes 72
2.7 Gel Electrophoresis 73
2.7.1 Gel Preparation 73
2.7.2 Sample Preparation 74

2.7.3 Sodium Dodecyl Sulphate – Polyacrylamide Gel Electrophoresis (SDS PAGE) 75
2.7.4 Western Blotting 75
2.7.5 Detection Of Total Protein Using SimplyBlue™ SafeStain Gel Stain 77
2.8 mRNA Preparation And Quantitative PCR 77
2.8.1 Rat Heart Isolation 77
2.8.2 RNA Preparation 77
2.8.3 cDNA Preparation 78
2.8.4 Quantitative PCR 78
2.9 Cloning Using TOPO® TA Cloning System 79
2.9.1 Amplification Of DNA For Cloning 79
2.9.2 Visualisation Of PCR Products By Agarose Gel Electrophoresis 80
2.9.3 TOPO Reaction For Ligation Of DNA Into TOPO Vector 81
2.9.4 Preparation Of Agar Plates 81
2.9.5 Transformation Of Top10 Competent Cells 82
2.9.6 Extraction Of DNA From Positive Clones 82
2.9.7 Restriction Enzyme Digest Of DNA 83
2.9.8 Ligation Of DNA Into FRT/TO Expression Vector 83
i Transformation Of DH5α Competent Cells 84
2.10 Mutagenesis 85
2.10.1 Single-Site Mutagenesis 85
i Transformation Of XL-1 Blue Supercompetent Cells 86
2.10.2 Multiple-Site Mutagenesis 87
i Transformation Of XL-10 Gold Ultracompetent Cells 88
2.10.3 Generation Of NCX-YFP Fusion Construct 88
2.11 Mass Spectrometry 92
2.11.1 Filter Aided Sample Preparation 92
2.12 Electrophysiology 94
2.12.1 Cell-attached Configuration 95
2.12.2 Whole-cell Configuration 96
2.12.3 IV Ramps 97
2.13 Left Ventricular Heart Failure 98
2.14 Cardiac Hypertrophy In Vivo Model 98
**3 Determining NCX1.1 Palmitoylation In Cardiac Muscle** 99
3.1 NCX1.1 Displays Intramolecular Aggregation Following Prolonged Heating

100
3.2 NCX1 Is Sensitive To Temperature And Reducing Agent 101
3.3 NCX1 Is Palmitoylated In Adult Rat Ventricular Myocytes 102
3.4 NCX1 Is Sub-Stoichiometrically Palmtioylated In ARVM 104
3.5 Palmitoylation Of NCX1 Is Not Splice Variant Specific 105
3.6 SDS Is Essential For Elution Of Palmitoylated Proteins Captured By Acyl Rac 107
3.7 PANTHER Analysis Reveals Functions Of Proteins In Cardiac Palmitoyl Proteome 108
3.8 DAVID Analysis Indicates Functional Pathways That Are Palmitoylated In Cardiac Tissue 110
3.9 Verification Of Specific Targets Identified By Mass Spectrometry 112
3.10 Mass Spectrometry Reveals Cys557 Is Not A Potential Palmitoylation Site 114
3.11 Discussion 118
**4 Mapping Palmitoylation Site(s) In NCX1.1** 127
4.1 Comparison Of NCX1 Palmitoylation In BHK, HeLa And HEK293 Cell Lines 128
4.2 Expression And Palmitoylation Of NCX1 Site Mutations In HeLa And HEK293 Cell Lines 129
4.3 Expression And Palmitoylation Of NCX1 Intracellular Loop Site Mutants In HeLa And HEK293 Cell Lines 131
4.4 Expression And Palmitoylation Of NCX-YFP Fusion Mutants In HEK293 Cell Line 133
4.5 Localisation Of WT NCX, Cysless And C739 Intracellular Loop Domains Fused to YFP 134
4.6 Discussion 140
**5 Identification Of Protein Acyl Transfereases That Palmitoylate NCX1.1** 146
5.1 Expression Profile Of PATs In Adult Rat Heart 147
5.2 Co-Immunoprecipitation Of Candidate DHHCs with NCX1.1 148
5.3 Effect Of Candidate DHHCs On Full Length NCX1 Palmitoylation 149
5.4 Effect Of DHHS Mutants On Full Length NCX1 Palmitoylation 151
5.5 Discussion 156
**6 Effect Of Palmitoylation On NCX1 Function** 162
6.1 Effect Of Pharmacological And Mutational Inhibition Of Palmitoylation On

WT NCX1 163
6.2 Effect Of Pharmacological And Mutational Inhibition Of Palmitoylation On NCX1 Cell Surface Localisation 165
6.3 Targeting Of NCX1 To Ventricular Myocyte Caveolae By Palmitoylation 167
6.4 NCX1 Exchange Current In HEK293 Cell Line 169
6.5 Discussion 173
**7 NCX1 Palmitoylation In Disease** 179
7.1 NCX1 Palmitoylation In Left Ventricular Heart Failure 180
7.2 NCX1 Palmitoylation During Development Of Left Ventricular Hypertrophy 185
7.3 Changes In Caveolin-3 And SERCA2a During Development Of Left Ventricular Hypertrophy 187
7.4 Discussion 194
**8 Concluding Remarks And Future Work** 199
**9 References** 210
**10 Appendix** 231

**List Of Figures**

**1 Introduction**

1.1 The Transport Of $Ca^{2+}$ In Ventricular Myocytes 2
1.2 Schematic Structure Of $Na^{+}$-$Ca^{2+}$ Exchanger 5
1.3 Helix Packing Of TMS 2, 3, 7 And 8 In The Cardiac $Na^{+}$-$Ca^{2+}$ Exchanger 7
1.4 New Helix Packing Model Of Cardiac $Na^{+}$-$Ca^{2+}$ Exchanger 8
1.5 Computer-Generated Model Of NCX Helix Packing 9
1.6 Topology Of NCX_Mj 10
1.7 Schematic Of Alternative NCX1 Topologies 11
1.8 Mutations Of The XIP Region Of NCX Have Different Effects On Outward Exchange Current 18
1.9 Schematic Representation Of $Ca^{2+}$ Regulatory Domains 20
1.10 Structure Of CBD1 And CBD2 25
1.11 Excision Of Exon 11 Deletes Amino Acids 722-813 37
1.12 Addition Of Fatty Acids To Cysteine Residues Via S-Palmitoylation And N-Palmitoylation 38
1.13 DHHC-containing protein topology 40
1.14 Schematic Representation Of Thioesterases 44
1.15 Human ABHD Family 47
1.16 Palmitoylation And Depalmitoylation Are Required For Ras Trafficking 51
1.17 Hypothetical MEND Pathway 56

**2 Materials And Methods**

2.1 Isolated Adult Rat Ventricular Myocytes (ARVM) 61
2.2 Schematic Of Methodology For Generation Of Inducible Stable Cell Lines 66
2.3 Bright Field Images Comparing Effects of Hygromycin And Zeocin On Flp-In 293 Inducible Cell Lines 67
2.4 Representative Image Of PCR Product Visualisation 81
2.5 Positive Clones Identified By Restriction Enzyme Digestion 85
2.6 SimplyBlue™ Stained SDS-PAGE Polyacrylamide Gel Of FASP Analysis 94
2.7 IV Ramp Protocol For Electrophysiology 97

**3 Determining NCX1.1 Palmitoylation In Cardiac Muscle**

3.1 NCX1 Displays Intramolecular Aggregation Following Prolonged Heating

100
3.2 NCX1 Is Sensitive To Temperature And Reducing Agent 101
3.3 NCX1 Is Palmitoylated In ARVM 103
3.4 NCX1 Is Sub-Stoichiometrically Palmitoylated In ARVM 105
3.5 Palmitoylation Is Not Specific To The Cardiac Splice Variant Of NCX1 106
3.6 SDS Is Essential For Elution Of Proteins From Thiopropyl Sepharose 107
3.7 PANTHER Analysis Reveals Respective Functions Of Palmitoylated Proteins Identified By Mass Spectrometry 109
3.8 DAVID Analysis Reveals An Array Of Biological Functional Clusters As Palmitoylated Within Cardiac Muscle 111
3.9 Verification Of Proteins Identified By Mass Spectrometry 113
3.10 Coverage Map Of NCX1 114
3.11 Cys557 Is Not Palmitoylated In NCX1 116
3.12 Clustal Alignment Of NCX1 Splice Variants 121
**4 Mapping Palmitoylation Site(s) In NCX1.1**
4.1 NCX1 Is Palmitoylated To A Greater Extent In HeLa And HEK293 Cell Lines 128
4.2 Site-directed Mutagenesis Reveals Cys739 As The Principal Palmitoylation Site In NCX1 130
4.3 Cys739 Is Necessary And Sufficient For Palmitoylation Of NCX1 132
4.4 NCX-YFP Fusion Proteins Are Palmitoylated In HEK293 Cell Line 133
4.5 WT And C739$^{Only}$ YFP Fusion Proteins Are Anchored To Membranes In HEK293 Cell Line 135
4.6 Confocal Microscopy Of YFP-Fusion Proteins Do Not Localise To The ER 137
4.7 Confocal Microscopy Of YFP-Fusion Proteins Reveal Localisation To The Golgi 139
4.8 Schematic Of NCX1 Predicted Topology 141
4.9 Sequence Surrounding C739 Is Negatively Charged 142
4.10 JPred3 Secondary Structure Prediction Of NCX1 Intracellular Loop 143
4.11 Structural Comparison Of Outward-Facing And Inward-Facing Conformations 144
**5 Identification Of Protein Acyl Transferases That Palmitoylate NCX1.1**
5.1 DHHC Expression Profile In Cardiac Muscle 147
5.2 Co-Immunoprecipiation Of Candidate DHHCs With WT NCX-YFP 148

5.3 Candidate DHHCs Have No Effect On Palmitoylation Of WT NCX1 150
5.4 Candidate DHHCs Do Not Increase C739A NCX1 Palmitoylation 151
5.5 Flotillin-2 And Ras Palmitoylation In Response To DHHC Overexpression 152
5.6 DHHS9 Significantly Decreases WT NCX1 Palmitoylation 153
5.7 Effect Of DHHS Overexpression On Flotillin-2 And Ras Palmitoylation 155
5.8 Clustal Alignment Of Human NCX1, H-Ras and N-Ras 158
**6 Effect Of Palmitoylation On NCX1 Function**
6.1 2-BP Decreases WT NCX1 Palmitoylation 164
6.2 NCX1 Cell Surface Localisation Is Not Decreased By Inhibiting Palmitoylation 166
6.3 Palmitoylation Is Not Involved In Targeting NCX1 To Caveolae 168
6.4 WT NCX1 And C739A NCX1 IV Relationship In FT293 Cell Line 170
6.5 C739A NCX1 Current Is Decreased Compared To WT NCX1 At Positive Voltages 172
6.6 T-Tubule Network And Protein Organisation 175
6.7 Hypothetical Dual Electrostatic Switch Mechanism In NCX Regulation 177
**7 NCX1 Palmitoylation In Disease**
7.1 NCX1 Expression and Palmitoylation Are Unchanged In Heart Failure 181
7.2 SERCA2a Expression Is Unchanged In Heart Failure 182
7.3 SERCA2a:NCX1 Ratio In Heart Failure 183
7.4 Caveolin-3 Expression And Palmitoylation Is Unchanged In Heart Failure 184
7.5 NCX1 Palmitoylation Is Unchanged In Heart Failure When Normalised To Caveolin-3 Palmitoylation 185
7.6 NCX1 Palmitoylation Does Not Change During Development Of Left Ventricular Hypertrophy 186
7.7 Caveolin-3 Expression And Palmitoylation Does Not Change During Development Of Hypertrophy 188
7.8 NCX1 Palmitoylation Is Significantly Increased At 4 Weeks Post Banding Relative To Caveolin-3 Palmitoylation 189
7.9 SERCA2a Is Downregulated At 2 Weeks Post Banding In Hypertrophy 191
7.10 SERCA:NCX1 Ratio Significantly Decreased By 3 Days During Development Of Left Ventricular Hypertrophy 193
**8 Concluding Remarks And Future Work**

8.1 Clustal Alignment Of Exchanger Superfamily Members 201
8.2 TMD6 Moves Considerably During NCX1 Transport 204
8.3 In Silico Mutagenesis Of Proline At Position 737 (771) to Alanine Results In Loss Of Palmitoylation Prediction 207

**List Of Tables**

**2 Materials And Methods**

2.1 Cardiac Myocyte Cell Isolation Buffers 60

2.2 Details Of Cell Lines 64

2.3 Buffer Compositions For Acyl Rac 70

2.4 Gradient Gel Recipe 73

2.5 Alternative Gel Recipe 73

2.6 Stacking Gel Recipe 74

2.7 Buffers For Protein Gel Electrophoresis And Western Blotting 74

2.8 Antibodies Used In Western Blotting Analysis 76

2.9 Ligation Reaction Set-Up 84

2.10 PCR and Sequencing Primer Details 90

2.11 Buffers Used In FASP 93

2.12 Composition Of Electrophysiology Buffers 95

**5 Identification Of Protein Acyl Transferases That Palmitoylate NCX1.1**

5.1 Summary Of DHHCs Purified By Co-Immunoprecipitation 149

**Abbreviations**

| | |
|---|---|
| 17-ODYA | 17-octadecynoic acid |
| 2-BP | 2-bromohexadecanoic acid |
| ABE | Acyl Biotin Exchange |
| ABHD | α/β-hydrolase domain |
| Acyl Rac | resin assisted capture |
| Akr | Ankyrin repeat-containing protein |
| AMPA | α-Amino-3-hydroxy-5-methyl-4-isoxazolepropionic acid |
| APS | ammonium persulfate |
| APT | Acyl protein thioesterase |
| AQP | aquaporin |
| ARVM | Adult Rat Ventricular Myocytes |
| ATP | Adenosine Tri Phosphate |
| AU | arbitrary units |
| B | bound |
| β-me | β-mercaptoethanol |
| BHK | Baby Hamster Kidney |
| BK | Large-conductance potassium channel |
| BRET | Bioluminescence resonance energy transfer |
| BSA | bovine serum albumin |
| C12E10 | octaethylene glycol monododecyl ether |
| CBD1 | Calcium binding domain 1 |
| CBD2 | Calcium binding domain 2 |
| cDNA | complementary DNA |
| CFP | Cyan Fluorescent Protein |
| CHO | Chinese Hamster Ovary |
| CLD | catenin-like domain |
| Co-IP | co-immunoprecipitation |
| CoA | Co enzyme A |
| CRD | Cysteine Rich Domain |
| CSP | Cysteine-string protein |
| Dabco | 1,4-diazabicyclo[2.2.2]octane |
| DAPI | 4',6-diamidino-2-phenylindole |
| DAVID | database for annotation, visualization and integrated discovery |

| | |
|---|---|
| DHHC | Aspartate-Histidine-Histidine-Cysteine |
| DHHS | Aspartate-Histidine-Histidine-Serine |
| DMEM | Dulbecco’s modified Eagle's medium |
| DMF | Dimethylformamide |
| DMSO | Dimethyl Sulphoxide |
| DNA | Deoxyribonucleic acid |
| dNTP | deoxy nucleoside triphosphates |
| DSA | DNase Stop Solution |
| DTT | Dithiotheritol |
| EDTA | Ethylenediaminetetraacetic acid |
| EGTA | ethylene glycol tetraacetic acid |
| ENaC | epithelial sodium channel |
| eNOS | endothelial nitric oxide synthase |
| ENU | N-ethyl-N-nitrosourea |
| ER | Endoplasmic Reticulum |
| ERF | Effectors Of Ras Function |
| EV | empty vector |
| FASP | Filter Aided Sample Preparation |
| FCS | Fetal Calf Serum |
| FRET | Fluorescence Resonance Energy Transfer |
| $GABA_A$ | γ-Aminobutyric acid |
| GAP | Growth Associated Protein |
| GAPDH | Glyceraldehyde 3-phosphate dehydrogenase |
| GFP | Green Fluorescent Protein |
| GT | gene-trapped |
| GTP | Guanosine-5'-triphosphate |
| HA | hemagglutinin |
| ha | hydroxylamine |
| HCl | hydrochloride |
| HDFP | hexadecyl fluorophosphonate |
| HEF | hemagglutinin-esterase-fusion |
| HEK293 | Human Embryonic Kidney 293 |
| HEPES | 4-(2-hydroxyethyl)-1-piperazineethanesulfonic acid |
| HPDP | N-[6-(Biotinamido)hexyl]-3'-(2'-pyridyldithio)propionamide |
| HPLC | High-performance liquid chromatography |

| | |
|---|---|
| HRP | Horseradish peroxidase |
| IAA | iodoacetamide |
| INCL | infantile neuronal ceroid lipofuscinosis |
| iTRAQ | Isobaric tags for relative and absolute quantitation |
| IV | current-voltage |
| KB-R7943 | 2-[2-[4-(4-nitrobenzyloxy)phenyl]ethyl]isothiourea methane |
| KCM | Potassium Calcium Magnesium |
| LB | Lysogeny broth |
| LGMD1C | autosomal dominant limb-girdle muscular dystrophy 1C |
| LV | left ventricular |
| MCS | multiple cloning site |
| MEND | Massive endocytosis |
| MES | 2-(N-morpholino)ethanesulfonic acid |
| MIB | Myocyte Isolation Buffer |
| MMTS | methyl methanethiosulfonate |
| mRNA | messenger RNA |
| MS | mass spectrometry |
| MUC | Mucin |
| mV | millivolt |
| MW | molecular weight |
| Nav | voltage-gated sodium channel |
| NCKX | Sodium calcium potassium exchanger |
| NCX_Mj | NCX from *Methanococcus jannaschii* |
| NCX1 | Sodium Calcium Exchanger |
| NEM | N-ethylmaleimide |
| NMDA | *N*-Methyl-D-aspartic acid |
| OMe | farnesyl carboxymethylester |
| P/S | Penicillin/Streptomycin |
| pA | picoampere |
| PAGE | polyacrylamide gel electrophoresis |
| PANTHER | Protein Analysis Through Evolutionary Relationship |
| PATs | protein acyl transferases |
| PBS | Phosphate Buffered Saline |
| PBS-T | Phosphate Buffered Saline Tween-20 |
| PCR | polymerase chain reaction |

| | |
|---|---|
| PFA | paraformaldehyde |
| Pfa | Protein fatty acyltransferase |
| Pfu | plaque forming units |
| PI-PLC | phosphatidylinositol |
| $PIP_2$ | Phosphatidylinositol 4,5-Bisphosphate |
| PKA | Protein Kinase A |
| PKC | Protein Kinase C |
| PLM | phospholemman |
| PMSF | phenylmethanesulfonylfluoride |
| PPT | Palmitoyl-protein thioesterase |
| PSD | post synaptic density |
| PTP | permeability transition pore |
| PVDF | polyvinylidene difluoride |
| RDA | RNA Dilution Buffer |
| RLA | residual luminal area |
| RLA | RNA Lysis Buffer |
| RNA | Ribonucleic Acid |
| RT | room temperature |
| RV | right ventricular |
| RWA | RNA Wash Solution |
| s | second |
| SDS | Sodium Dodecyl Sulphate |
| SEA0400 | 2-[4-[(2,5-difluorophenyl)methoxy]phenoxy]-5-ethoxyaniline |
| SERCA | Sarcoplasmic Reticulum $Ca^{2+}$ ATPase |
| SFV | Semliki Forest virus |
| SH | SRC Homology |
| Shh | Sonic Hedgehog |
| SHR | spontaneous hypertensive rats |
| SILAC | stable isotope labeling by/with amino acids in cell culture |
| siRNA | small interfering RNA |
| SLC8 | Solute Carrier 8 |
| SM | starting material |
| SNAP | Soluble NSF Attachment Protein |
| SNARE | Soluble NSF Attachment Protein Receptor |
| SOC | Super Optimal broth with Catabolite repression |

| | |
|---|---|
| SR | Sarcoplasmic Reticulum |
| STREX | stress-axis-regulated insert sulfonate |
| Swf | Spore wall formation |
| TEMED | Tetramethylethylenediamine |
| TMDs | transmembrane domains |
| TMS | Transmembrane Segments |
| UB | unbound |
| UF | unfractionated |
| UK | United Kingdom |
| $V_m$ | membrane potential |
| WK | Wistar-Kyoto |
| WT | wild type |
| w/v | weight/volume |
| X-gal | 5-bromo-4-chloro-3-indolyl-β-D-galactopyranoside |
| XIP | Exchanger Inhibitory Peptide |
| YFP | Yellow Fluorescent Protein |

**Acknowledgements**

First and foremost, I would like to thank my supervisors Dr Will Fuller and Professor Mike Ashford for giving me the opportunity to do my PhD with them. I am hugely grateful for all the support that Will has given me throughout my 3 years in his lab. I know I've been hard work at times, but I am thankful he stuck with me! And hey, he got a hand knitted scarf out of it! I am also thankful for time and advice that Mike has given me throughout this very demanding project. Their time, patience and invaluable input into my project are very much appreciated.

I am very thankful indeed for the best post doc a PhD student could ask for, Dr Jacquie Howie. She has been an absolute pleasure to work with over these last 3 years, and I am going to miss her when I leave. I will take everything she taught me and use it to torture other poor defenseless PhD students. Seriously, thank you for calming me down when I was on the verge (or in the middle of!) a full meltdown for one reason or another. As always, she was right and helped me stay focused and carry on with my PhD. Jacquie has been a huge source of information over the years. I will miss our tea times.

I would like to thank all the members of the Fuller lab, past and present. Each one of them has been there to listen to my rants about this experiment not working or writing not happening for me. We have tormented each other and had a lot of laughs a long the way. I hope our paths will cross again in the future. A big thank you to all my CVDM colleagues and friends, we made it out alive!

A huge thank you to Professor Donald Hilgemann for teaching me how to patch clamp. All the help and advice you have given me over the last year has been invaluable. I only wish we had gotten to work together for longer. Thank you to Dr Michael Fine and Dr Mei-Jung Lin for being so welcoming during my time in Dallas. Especially to Mei-Jung for keeping me stocked up on food!

I would obviously like to thank both of my parents and their partners for their continued support. Even if I have remained a student far longer than I had originally anticipated, thank you for sticking with me. The advice and life skills they taught have helped shaped the person I am today. Both of them were there when I needed them, all that a

child asks of their parents. Thank you for showing interest and support not just the last 3 years but my entire scientific career.

I would like to thank all of my friends. Each one of them, in their own way, has given me support and advice over the last 3 years. Either just by giving me a brief hug or telling me to man up and get on with it, there is no way I could of done it without all of you. I am especially thankful for my knitting group at Fluph. Without the support of them, I definitely would have given up. Always there with a sympathetic ear and a cuppa, the knit group saw me through. We'll not mention that one time I cried at knit night!

Without a doubt, I would have gone crazy without the support of my partner, Jeremy. Always straight-talking and supportive when I needed it most, he provided me with the most support. Thank you for being patient, sympathetic and understanding and for pointing out when I was being ridiculous. For always making me feel loved, special and appreciated. Thank you for all the laughs we've had.

**Declaration**

I declare that the following thesis is based on the results of experiments carried out by myself, and that this thesis is of my own composition. Work other than my own is clearly indicated in the text by reference to the relevant researchers or their publications. This dissertation has not been accepted or previously submitted in whole, or in part, for a higher degree.

Louise Reilly

**Supervisors Declaration**

I certify that Louise Reilly has completed nine terms in experimental research in the Division of Cardiovascular and Diabetes Medicine, Medical Research Institute, University of Dundee. She has fulfilled the conditions of the Ordinance General No. 39 of the University of Dundee and is qualified to submit this thesis in application for the degree of Doctor of Philosophy.

Dr William Fuller

Professor Michael Ashford

**Abstract**

The cardiac sodium/calcium exchanger (NCX1) regulates intracellular $Ca^{2+}$ in cardiac muscle. Inappropriate NCX1 function contributes to cardiac contractile abnormalities and heart failure; reduced NCX1 activity reduces Ca removal therefore impairing relaxation, whereas overactive NCX1 unloads intracellular Ca stores and impairs systolic function. Although the structure-function relationship is well characterised, dynamic regulation of NCX1 function by post-translational modifications is controversial.

The dynamic reversible post-translational modification of cysteine residues with the 16-carbon fatty acid palmitate in proteins is an important and common post-translational modification in a variety of tissues. The cardiac palmitoyl proteome is largely uncharacterised. Few proteins have been identified as palmitoylated, for example the sodium pump regulator, phospholemman (Tulloch et al. 2011).

Palmitoylation of NCX1 was investigated in isolated adult rat ventricular myocytes (ARVM), using site-specific resin assisted capture (Acyl Rac). Acyl rac purified 100% of the constitutively palmitoylated protein, caveolin-3 from ARVM lysates, and 60% of NCX1, indicating a biologically meaningful fraction of NCX1 is palmitoylated in ventricular muscle. Mutagenesis of selected cysteine residues revealed that Cys739, which is located in the large intracellular loop domain, is the principal palmitoylation site in NCX1. Palmitoylation is required to anchor this domain to membranes, and occurs in the secretory pathway. Co-immunoprecipitation of NCX1 with Golgi resident DHHC-containing enzymes revealed DHHC5, DHHC9, DHHC12 and DHHC18 are associated with NCX1 in HEK293 cells. Mutation of the active cysteine in DHHC5, 9, 12 and 18 to serine revealed that DHHC9 and DHHC18 are important for NCX1 palmitoylation.

Measurement of NCX1 cell surface localisation using membrane impermeable biotinylation reagents revealed that palmitoylation was not required for trafficking of NCX1 to the cell surface membrane. The effect of palmitoylation on NCX1 exchange activity was measured using whole cell electrophysiology. Measurement of the current-voltage relationship of NCX1 revealed that palmitoylation significantly reduced outward current measured at positive membrane potentials. Finally, NCX1

palmitoylation was not significantly changed in *in vivo* models of left ventricular heart failure and cardiac hypertrophy. In conclusion, palmitoylation of NCX1 influences its transport function and occurs in the secretory pathway.

# Chapter 1 Introduction

## 1.1 Cardiac Ion Transport

The appropriate regulation of the ion transporters present in cardiac muscle is vital for the maintenance of normal electrical activity, ion gradients and thus cardiac output. There are several ion transport systems present in cardiac tissue that contribute to the maintenance of ion gradients. The $Na^{+}$-$Ca^{2+}$ exchanger is just one of these transport systems.

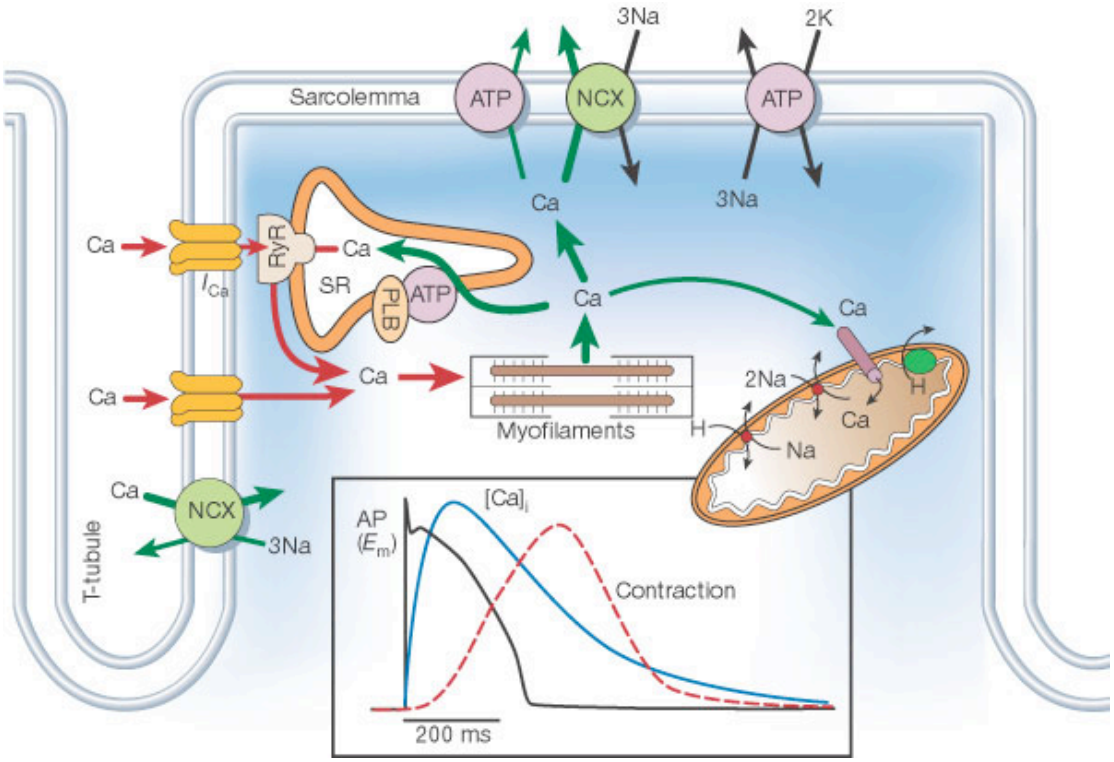


***Figure 1.1: The Transport Of $Ca^{2+}$ In Ventricular Myocytes.*** *Membrane depolarisation due to the influx of $Na^{+}$ via voltage-gated $Na^{+}$ channels, results in the influx of $Ca^{2+}$ via the activation of voltage-senstive $Ca^{2+}$ channels. This triggers $Ca^{2+}$ release from intracellular stores, which binds to the contractile machinery to initiate contraction. This $Ca^{2+}$ is then exported out of the cell by the $Na^{+}$-$Ca^{2+}$ exchanger, into the SR by the sarcoplasmic reticulum $Ca^{2+}$ ATPase and into the mitochondria by the mitochondrial $Ca^{2+}$ uniporter. The inset shows the action potential, $Ca^{2+}$ transient and contraction in a rabbit myocytes at 37˚C. Modified from (Bers 2002).*

As shown in figure 1.1, the contraction cycle of the cardiac myocyte is a complex process, depending entirely on the unique interaction of a variety of ion transporters and channels to maintain correct $Ca^{2+}$ homeostasis during the action potential and

afterwards to initiate relaxation. The $Na^+$-$Ca^{2+}$ exchanger is predominantly involved in extruding $Ca^{2+}$ from the cell following a rise in cytoplasmic levels after an action potential. The action potential initiates in the sinoatrial node and propagates through the atria then to the ventricles. This activates $Na^+$ channels and the influx of $Na^+$ results in membrane depolarisation, thus activating voltage-gated $Ca^{2+}$ channels and allowing $Ca^{2+}$ to enter the cell. $Ca^{2+}$ binds to ryanodine receptors located on the sarcoplasmic reticulum, and yet more $Ca^{2+}$ is released into the cytoplasm. This free $Ca^{2+}$ binds to the contractile machinery within the myocytes and initiates contraction. The $Na^+$/Ca2+ exchanger works together with the sarcoplasmic reticulum $Ca^{2+}$-ATPase (SERCA) to remove $Ca^{2+}$ from the cytoplasm triggers relaxation. $Na^+$ brought in by the exchanger is removed via the $Na^+$ pump.

### 1.1.1 SLC8 – $Na^+$-$Ca^{2+}$ Exchanger Family

The $Na^+$-$Ca^{2+}$ exchanger, NCX1, present in cardiac cells, is a member of the $Na^+$-$Ca^{2+}$ exchanger family. All members of this family share a large percentage of homology, particularly in the transmembrane domains (Philipson & Nicoll 2000). There is 68% identity between NCX1 and 2, 73% between 1 and 3 and 75% between 2 and 3 (Nicoll, Quednau, et al. 1996b). There are 3 known mammalian $Na^+$-$Ca^{2+}$ exchangers, collectively known as SLC8 (Philipson et al. 2004). The family members, NCX1, NCX2 and NCX3 are products of distinct, separate genes (Nicoll, Quednau, et al. 1996b). Despite not showing any major differences in functionality, the expression of these three family members is quite distinct (Linck et al. 1998). NCX1 mRNA is found in virtually all cell types, whereas NCX2 and 3 have only been detected in brain and skeletal muscle (Linck et al. 1998).

In cardiomyocytes, NCX1, is expressed on surface and T-tubular sarcolemma (Philipson et al. 2004). In the rat brain, NCX1 is expressed in a regional pattern and is localised to discrete sites on the plasmalemma, some of which are in close proximity with intracellular $Ca^{2+}$ stores (S. L. Lee et al. 1994; Philipson et al. 2004). In addition, NCX1, 2 and 3 proteins are expressed in a cell-specific fashion, to distinct regions of the rat brain (Quednau, Nicoll & Philipson 1997a; Thurneysen et al. 2002). NCX1 and 3 are expressed in the sarcolemma of rat skeletal muscle, in a way that is muscle fibre-specific (Deval et al. 2000; Fraysse et al. 2001). Differences in contractile responses between slow-twitch and fast-twitch muscle fibres was demonstrated by Léoty, in which

slow-twitch fibres displayed contraction in the absence of $Na^+$, unlike the fast-twitch fibres (Léoty 1984; Deval et al. 2000). This suggests that contraction within fast-twitch fibres is dependent upon NCX1. It is unclear whether NCX1, 2 and 3 have unique functions in each of the cell types in which they are expressed.

### 1.1.2 Structural Features Of NCX

The first $Na^+$-$Ca^{2+}$ exchanger to be extensively studied was NCX1, which was isolated from cardiac sarcolemma (Nicoll et al. 1990). NCX1 was first proposed to have 12 transmembrane domains, however subsequent analysis revealed that the first 32 amino acids, which form a hydrophobic segment, is a signal peptide that is cleaved during processing in the endoplasmic reticulum (Durkin et al. 1991; Hryshko et al. 1993). This first model of the exchanger was based on hydropathy analysis and was not confirmed experimentally. It was subsequently proposed by Nicoll and colleagues that the mature protein contains 9 transmembrane segments (TMS) (Figure 1.2) (Nicoll et al. 1999). These transmembrane segments are arranged into two sets, separated by a large intracellular loop of approximately 550 amino acids (Nicoll et al. 1990; Nicoll et al. 1999) located between transmembrane segments 5 and 6. At the N terminus, there are 5 hydrophobic TMS, whereas at the C terminus, there are 4 hydrophobic TMS.

Interestingly, there are regions of NCX1 that show intramolecular homology. The sequence that extends between TMS 2 and 3 shares homology with the sequence that extends between TMS 7 and the non-transmembrane segment (see figure 1.2) (Shigekawa & Iwamoto 2001; Schwarz & Benzer 1997). The regions of similarity are the α-repeats, termed α1 and α2 respectively. These repeat regions are conserved in all members of the SLC8 family, suggesting functional importance (Shigekawa & Iwamoto 2001). The large intracellular loop also contains repeated regions, which are termed the β repeats, β1 and β2, being regions of approximately 70 amino acids. Strikingly, these β repeats share homology with the cytoplasmic region of β4 integrin (Schwarz & Benzer 1997). In addition to the β repeats, the intracellular loop contains other areas that contribute to the regulation of the exchanger. At the N-terminal end of the loop, there is an autoinhibitory region consisting of approximately 20 amino acids, termed the endogenous exchanger inhibitory peptide (XIP) region (Li et al. 1991). Close to the C-terminal end of the XIP region, there is a region of approximately 135 amino acids, which has been shown to confer a high affinity $Ca^{2+}$ binding site (Levitsky et al. 1994)

(this will be discussed in more detail in following sections). Also contained within the intracellular loop is a region that undergoes alternative splicing (S. L. Lee et al. 1994). This region is encoded by six small exons (labelled A to F), which are expressed in different combinations in a tissue specific manner (Dipolo & Beaugé 2006). Exon A or B, which are essential to maintaining an open reading frame, must be included in all splice variants. Excitable tissues, such as the heart, generally have exchangers that contain exon A, whereas exon B is present in virtually all other tissues. The cardiac splice variant, NCX1.1 contains exons ACDEF. Finally, between TMS 7 and 8 there is a hydrophobic domain that is proposed to form a re-entrant membrane loop, similar to the pore-forming region of ion channels (Nicoll et al. 1990; Dipolo & Beaugé 2006; Bers 2002; Nicoll et al. 1999). In the centre of the sequence, there is a GIG sequence, showing resemblance to the GYG motif that is found in $K^+$ channels.

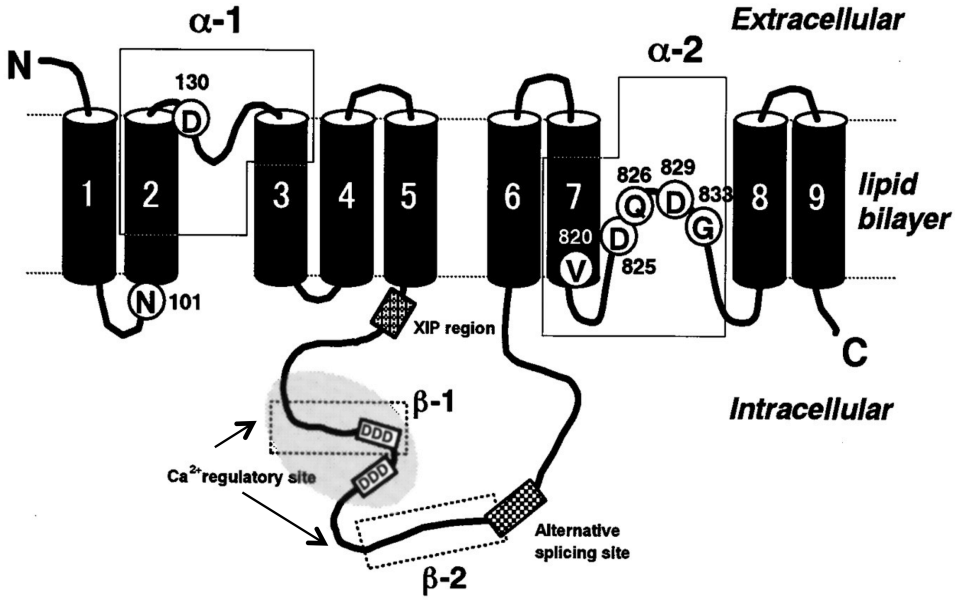


***Figure 1.2: Schematic Structure Of $Na^+$-$Ca^{2+}$ Exchanger.*** *The current topological model for the structure of the $Na^+$-$Ca^{2+}$ shows 9 transmembrane segments, separated by a large intracellular loop. The α1- and α2-repeat regions are shown, forming reentrant loops between TMS 2 and 3 and TMS 7 and 8 respectively. Also shown is the XIP region. The β-1 and β-2 repeats are now known to contain the $Ca^{2+}$ binding sites followed by the region where alternative splicing occurs. Modified from (Shigekawa & Iwamoto 2001).*

Difficulties in producing large amounts of pure functional protein and crystallising membrane proteins in general mean that there is no crystal structure for mammalian

NCX as yet. However, studies from Philipson's group investigating the helix packaging of the exchanger have revealed some interesting insights into the possible 3D structure of this protein. In the first of 3 studies from this group, utilising cysteine mutagenesis and oxidative cross-linking, the proximity of the TMS to one another was investigated. Cysteine pairs were re-introduced into a cysteine-less exchanger, one in the N-terminal half and one in the C-terminal half, then expressed in HEK293 cells and spontaneous disulphide bond formation examined by gel mobility shifts (Qiu et al. 2001). This revealed that mutants S117C/V804C, A122C/Y892C, A151C/T815C and A151C/A821C shifted from 120kDa to 160kDa under non-reducing conditions, indicating the presence of a disulphide bond between the cysteines. These cysteine residues are located in TMS 2, 3, 7 and 8 (now thought to be TMS 9, see following section) (see figure 1.3 for further details), indicating that TMS7 is close to TMS3 near the intracellular side of the membrane and is also in close proximity to TMS2 near the extracellular side (Qiu et al. 2001). They also propose that TMS2 must form a disulphide bond with TMS8 in their mutant exchangers, suggesting that these two TMS are in close proximity in the native exchanger. These results indicate that the α-repeats are close to each other, pointing towards a role in ion translocation. Figure 1.3 shows the proposed packing of the TMS in the exchanger based on these experiments.

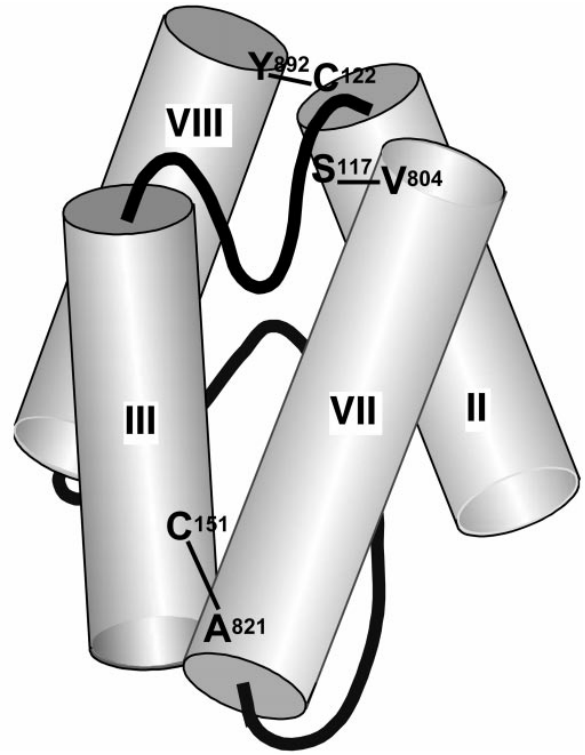


***Figure 1.3: Helix Packing Of TMS 2, 3, 7 And 8 In The Cardiac $Na^+$-$Ca^{2+}$ Exchanger.*** *Proposed model of the proximity of TMS of NCX based on cross-linking data by Qiu et al. Also shown are the reentrant loops of the α-repeats, which are modelled to be in close proximity and would face one another. The cytoplasmic surface is at the bottom of the model. Modified from (Qiu et al. 2001).*

A follow up study by the same group sought to elucidate the position of the other TMS segments with reference to the already proposed helix packing of TMS 2, 3, 7 and 8 (Figure 1.4). Using a similar method to the previous study, cysteine mutations were introduced into TMS 1 or 2 and paired with cysteine 768, which is located in TMS6. Mutants were expressed in insect High Five cells, then using thiol-specific cross-linkers containing spacer arms of known lengths, mobility shifts on SDS-page was examined (Ren et al. 2006). The study showed that TMS 1 and 2 are in close proximity to TMS6. Interestingly, cysteine 768 was able to form cross-links with residues that are proposed to be near intra- and extracellular surfaces of TMS1 and 2, with cysteine 768 thought to lie roughly in the middle of TMS6. This suggests that TMS1 and 2 are not continuous α-helices, because if they were then residues that interact with Cys-768 would be separated by a distance of about 27 Å, meaning that any interaction would require a cross-linker that is longer than 10 Å (Ren et al. 2006). However, an interaction is observed with a cross-linker of only 6.4 Å. In addition, in the wild-type receptor,

cysteines 122 and 768 have also been shown to interact. Cys122 is located between the extracellular end of TMS2 and the reentrant loop of the α-1 repeat, which is suggested to be functionally important (Ottolia et al. 2005). Ren and colleagues found an interaction between these 2 cysteine residues, supporting a functional importance for TMS6 (Ren et al. 2006). An updated helix packing model was proposed based on these findings (Figure 1.4). One must bear in mind that the positions of the TMS are not fixed and must move on binding of regulatory $Ca^{2+}$ in order to facilitate the exchange of $Na^{+}$ for $Ca^{2+}$, however, such structural data has not yet been published. TMS movement during the NCX reaction cycle may account for the reported proximity of multiple residues in TMS1 and 2 to Cys768 in TMS6.

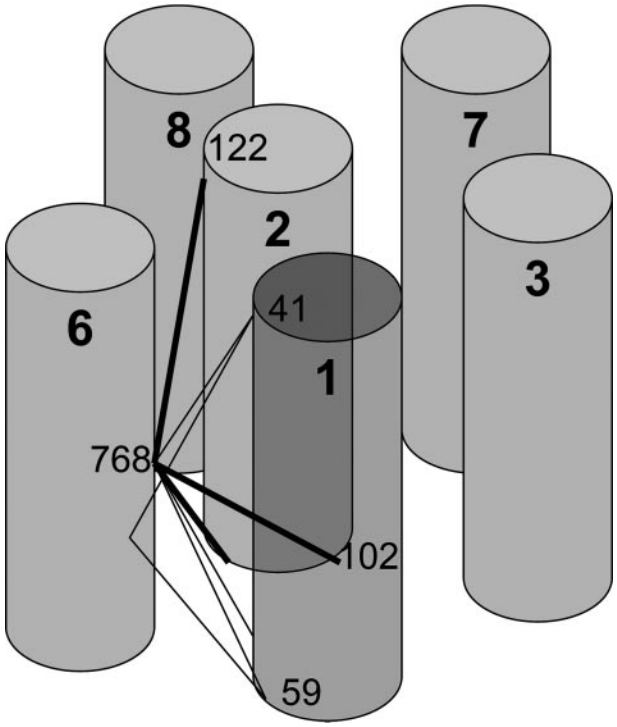


***Figure 1.4: New Helix Packing Model Of Cardiac $Na^{+}$-$Ca^{2+}$ Exchanger.*** *Proposed updated helix packing model, incorporating previous data from (Qiu et al. 2001) coupled with new data on TMS 1, 2 and TMS6. Heavy lines represent cross-links between TMS6 and TMS2 and light lines represent cross-links between TMS6 and TMS1. Modified from (Ren et al. 2006).*

In a study by Ren and colleagues, the position of the remaining TMS were investigated using the same experimental procedure as previously described. Based on all cross-linking data obtained to date, it suggests that each of the N-terminal TMS forms a cross-

link with at least 2 of the C-terminal TMS and vice versa (Ren et al. 2010). Shown in figure 1.5 is the proposed helix packing of NCX in 2010.

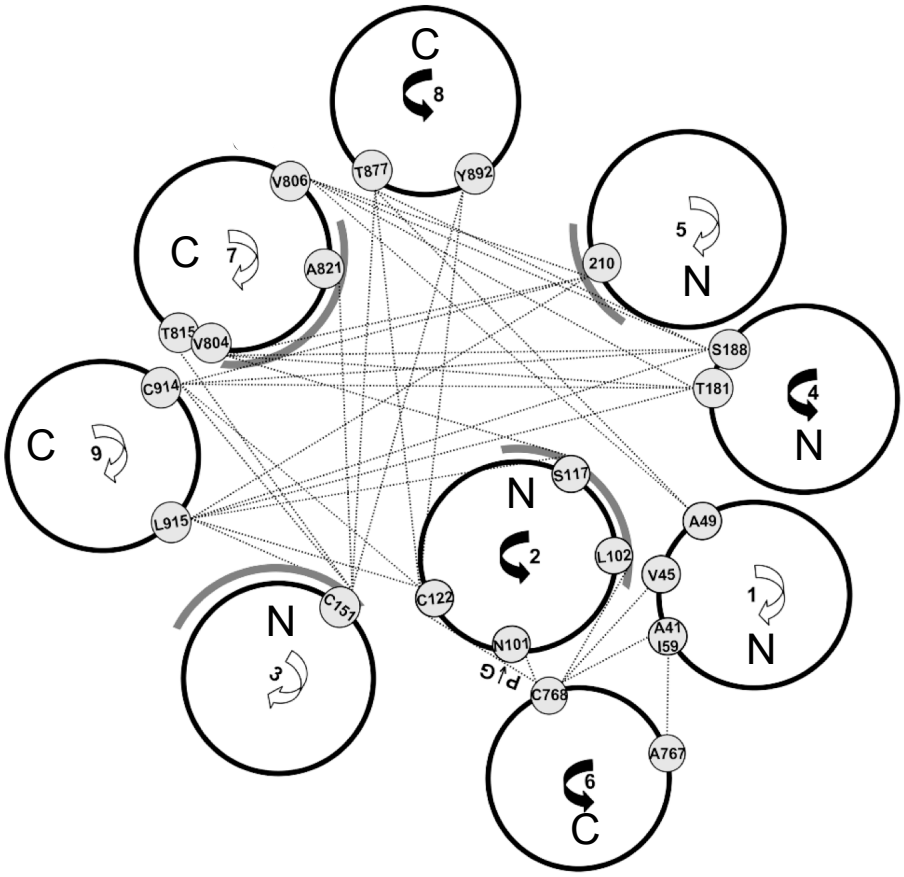


***Figure 1.5: Computer-Generated Model Of NCX Helix Packing.*** *Current work from (Ren et al. 2010) put together with previous work (Ren et al. 2006; Qiu et al. 2001) are combined to generate a working model of NCX. Lines are indicative of cross-link interactions. The grey arcs indicate residues that, upon mutation, alter the activity of the exchanger. Annotation of C and N within the TMS indicates at which end of the exchanger the TMS is located. Modified from (Ren et al. 2010).*

Recently, a prokaryotic homolog of mammalian NCX, NCX_Mj was found to have $Na^+/Ca^{2+}$ exchange activity and it was subsequently crystallised (figure 1.6) (Liao et al. 2012). NCX_Mj consists of 10 transmembrane helices, which form two structural repeats of 5 transmembrane helices with opposing topology (Liao et al. 2012). The crystal structure revealed 8 of the helices, TMD 2 to 5 and TMD 7 to 10 form a tightly packed core perpendicularly embedded in the membrane. This part of the model fits with the predicted helix packing model proposed by Ren et al (Ren et al. 2010). Interestingly, TMD6 and TMD1 are long, with approximately 35 residues in each helix.

They are orientated at a 45° to the surface membrane and are loosely packed against the core (figure 1.6) (Liao et al. 2012). The conserved α-repeat domains are bundled in the centre of the protein, surrounded by the helices. α-repeat helices are bent in two or three segments, creating space in the middle where $Ca^{2+}$ and $Na^{+}$ bind.

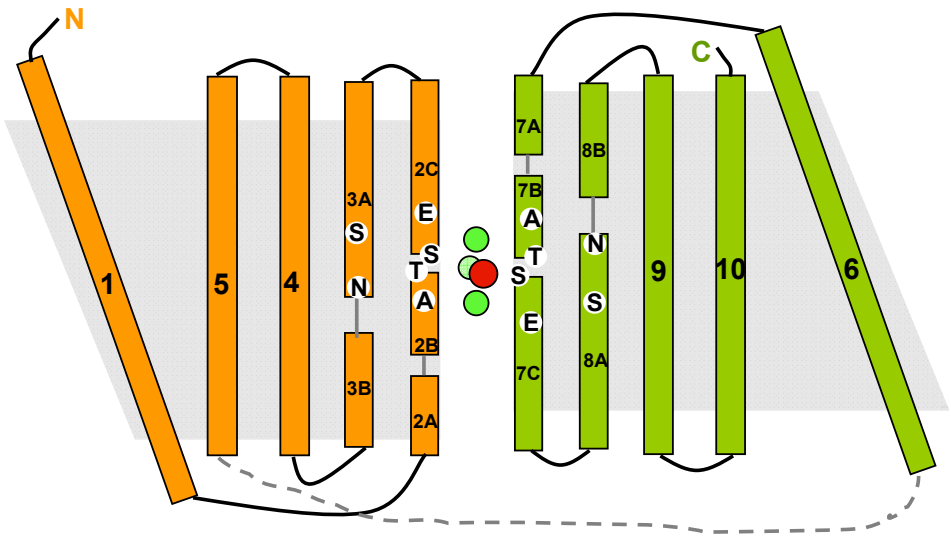


***Figure 1.6: Topology Of NCX_Mj.*** *Schematic representation of NCX_Mj topology based on crystal structure. Residues involved in ion binding shown in white circles. Green circles – $Na^{+}$, red circles – $Ca^{2+}$. Modified from (Liao et al. 2012).*

The N-terminal half of the protein shares structural similarity with the C-terminal half but with opposite topology. The authors propose the two halves are related by a molecular dyad (Liao et al. 2012). Based on this structure, Philipson and colleagues were prompted to re-examine the propose topology for mammalian NCX1 (Ren & Philipson 2013). NCX_Mj shares sequence homology to NCX1 in the α-repeat regions, with no homology outwith this region. Using a cross-linking approach, the topology of the C-terminal half of mammalian NCX1 was reinvestigated, as this was the region of discrepancy. $Cys^{20}$ is on the extracellular side and $Leu^{102}$ on the intracellular side of TMD2 have been verified in previous studies (Iwamoto et al. 1999; Nicoll et al. 1999; Doering et al. 1998) and is consistent with NCX_Mj. $Cys^{20}$ or $Leu^{102}$ mutated to cysteine were reintroduced into a cysteine-less exchanger. Additional cysteine residues were introduced in the C-terminal half of the exchanger at specific locations; 825, 897 and 938. Cysteine at 897 crosslinked with the internal $Cys^{102}$ but not with $Cys^{20}$, suggesting it is located on the intracellular side of NCX1 (Ren & Philipson 2013). The opposite result was obtained for cysteine at 938, which crosslinked with $Cys^{20}$ but not

$Cys^{102}$, suggesting its extracellular location. Taken together, the results indicate the presence of an additional TMD 8 and an extracellular C-terminus, consistent with NCX_Mj (figure 1.7) (Ren & Philipson 2013). Based on these results, the topology of NCX1 was revised to include 10 TMDs, in line with NCX_Mj crystal structure.

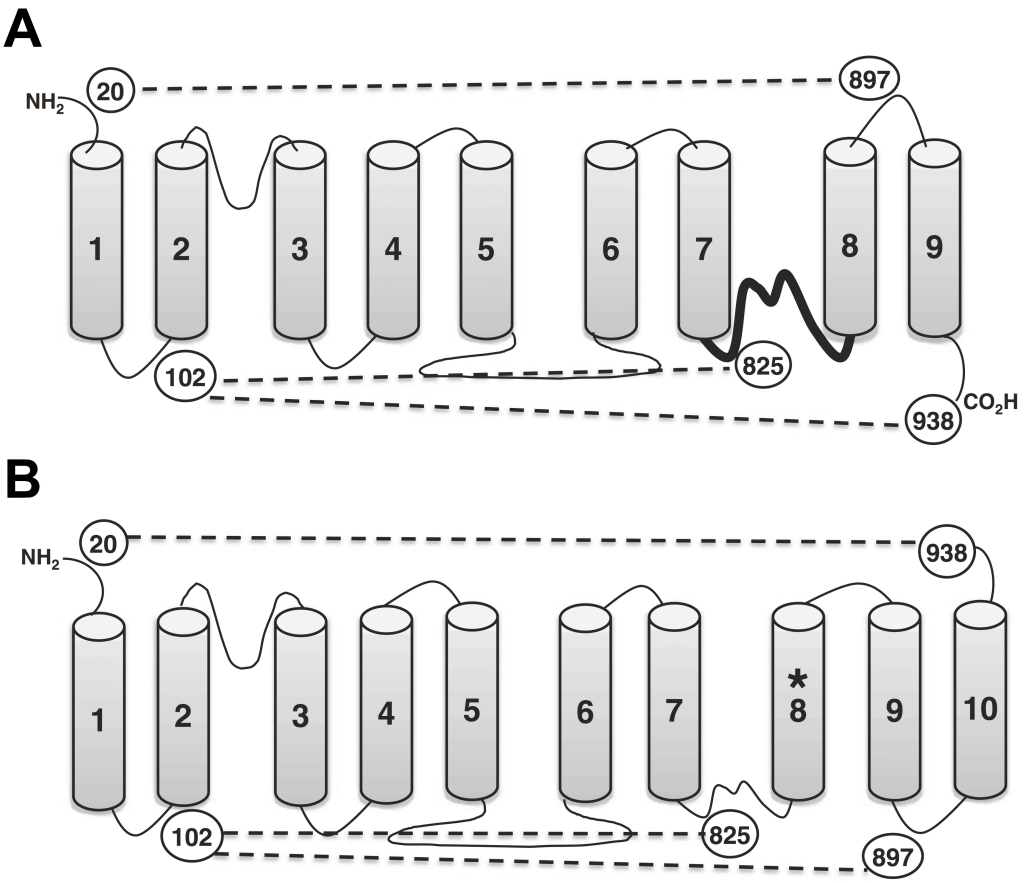


***Figure 1.7: Schematic Of Alternative NCX1 Topologies.*** ***A.*** *The currently accepted topology of NCX1 showing 9 TMDs.* ***B.*** *Predicted topology of NCX1 based on NCX_Mj crystal structure. Circled residues show location of cysteine used to confirm NCX1 topology. The bold section in panel A forms the new TMD8 in panel B. Modified from (Ren & Philipson 2013).*

### 1.1.3 Function Of NCX1

The predominant role of NCX1 in cardiac tissues is the extrusion of $Ca^{2+}$, however it can also function in a way that allows $Ca^{2+}$ influx into the cell, depending on the electrochemical gradients of $Na^{+}$ and $Ca^{2+}$ (Blaustein & Lederer 1999). However, under physiological conditions, NCX1 predominantly functions in forward mode, i.e. the

extrusion of 1 $Ca^{2+}$ and the influx of 3 $Na^{+}$. To date, 4 modes of operation of NCX1 have been described (Blaustein & Lederer 1999; Dipolo & Beaugé 2006),

1) forward mode, responsible for $Ca^{2+}$ extrusion ($Na^{+}_{o}/Ca^{2+}_{i}$ exchange),
2) reverse mode, responsible for $Ca^{2+}$ entry ($Na^{+}_{i}/Ca^{2+}_{o}$ exchange),
3) homologous $Ca^{2+}_{o}/Ca^{2+}_{i}$ exchange,
4) homologous $Na^{+}_{o}/Na^{+}_{i}$ exchange.

### 1.1.4 Modes Of Function

#### i Forward Mode

The mode in which NCX functions is dependent on a variety of factors. The first of the four modes, is defined as external $Na^{+}$-dependent $Ca^{2+}$ efflux and internal $Ca^{2+}$-dependent ouabain and tetrodotoxin insensitive $Na^{+}$ influx (Blaustein & Lederer 1999). This mode of transport is capable of being activated by internal monovalent cations (P. F. Baker et al. 1969; Blaustein & Christie Ector 1976; Gadsby et al. 1991; Fontana et al. 1995) and is inhibited by a high concentration of intracellular $Na^{+}$ ($[Na^{+}]_i$) (Dipolo & Beaugé 1990). In addition, it is also activated by non-transported intracellular $Ca^{2+}$ (Hilgemann, Collins & Matsuoka 1992a), however this mode of exchange does not require extracellular $Ca^{2+}$ to be activated (Dipolo & Beaugé 1990). Unlike other forms of ion exchange, the $Na^{+}/Ca^{2+}$ exchanger does not require hydrolysis of ATP to fuel $Ca^{2+}$ efflux, as demonstrated by experiments showing that $Na^{+}/Ca^{2+}$ exchange still occurs in ATP-depleted cells (Dipolo & Beaugé 1990). Although $Ca^{2+}$ efflux does not require ATP hydrolysis, ATP has a profound effect on the regulation of the exchanger, will be discussed in detail in following sections.

#### ii Reverse Mode

The second of the four modes, reverse mode, is defined as internal $Na^{+}$-dependent $Ca^{2+}$ influx and external $Ca^{2+}$-dependent ouabain-insensitive $Na^{+}$ efflux. An important feature of this mode of operation, which is shared by the forward mode, is the requirement for intracellular $Ca^{2+}$. The concentration of normal resting $Ca^{2+}$ within the cell is approximately 100nM, however the concentration for half-maximal activation of this mode is approximately 1μM under physiological conditions, deeming that only a

small number of exchangers are active (Blaustein & Lederer 1999). However, low micromolar concentrations of intracellular $Ca^{2+}$ are capable of activating the exchanger, suggesting that it only contributes to significant $Ca^{2+}$ entry when cytoplasmic $Ca^{2+}$ is high, although this is not thermodynamically favourable unless there is a positive membrane potential. As with forward mode, reverse mode of operation is also activated by low concentrations of external monovalent cations, including $Na^{+}$ (Fontana et al. 1995), which are not transported. High concentrations of extracellular $Na^{+}$ decrease the level of $Ca^{2+}$ influx mediated by the exchanger.

The final 2 modes of operation, homologous $Ca^{2+}$ exchange and homologous $Na^{+}$ exchange are difficult to investigate, as there is no net movement of charge across the membrane, unlike the previous two modes of transport. Like the reverse mode, homologous $Ca^{2+}$ exchange is activated by external monovalent cations and inhibited by external $Na^{+}$. A unique feature of this mode of transport however is that internal monovalent cation is needed for activation and high intracellular levels of $Na^{+}$ inhibits this mode of exchange (Blaustein & Santiago 1977). The homologous $Na^{+}/Na^{+}$ exchange shares similarity in activation requirements with the reverse mode of operation, in that it also dependent on internal $Ca^{2+}$ for activation. Additional activation parameters required include internal alkalinisation and internal ATP. This mode of operation can be inhibited by both internal $Mg^{2+}$ and external $Ca^{2+}$ (Blaustein & Lederer 1999).

As mentioned previously, $Na^{+}$-$Ca^{2+}$ exchange plays an important role in extruding excess $Ca^{2+}$ following an action potential. During the cardiac action potential, $Ca^{2+}$ enters the cell through depolarisation-activated $Ca^{2+}$ channels (Bers 2002). This influx of $Ca^{2+}$ stimulates ryanodine receptors located on the sarcoplasmic reticulum (SR), stimulating further $Ca^{2+}$ release. The rise in free intracellular $Ca^{2+}$ is able to bind to the contractile machinery within cardiomyocytes and initiate contraction. In order for the myocytes to relax, the level of intracellular $Ca^{2+}$ must decrease in order to stimulate the dissociation of $Ca^{2+}$ from the contractile machinery (Bers 2002). There are four major pathways that are involved in moving $Ca^{2+}$ out of the cytoplasm, the sarcoplasmic reticulum $Ca^{2+}$ ATPase, sarcolemmal $Na^{+}/Ca^{2+}$ exchanger, sarcolemmal $Ca^{2+}$ ATPase and the mitochondrial $Ca^{2+}$ uniporter. The sarcoplasmic reticulum $Ca^{2+}$ ATPase pump removes around 70% of the intracellular $Ca^{2+}$ for storage in the SR, whereas the $Na^{+}/Ca^{2+}$ exchanger removes approximately 28% (Bers 2002) in humans. This leaves

only 2% to be dealt with by the sarcolemmal $Ca^{2+}$ ATPase and the mitochondrial $Ca^{2+}$ uniporter. The $Na^+$ that enters the cell via the $Na^+/Ca^{2+}$ exchanger is removed from the cell by the $Na^+$ pump.

### 1.1.5 Structure-Function Of NCX1

#### i Function Of The α-repeats

As previously discussed, there are 2 domains that show intramolecular homology, termed the α-repeats. One of these repeats, α1, is located at the N-terminal half of the exchanger, between TMS 2 and 3, the second is located in the C-terminal half in a region now known to form TMS8. It is proposed that α1 repeat forms a reentrant loop, similar to that which has been described for several ion channels (Nicoll et al. 1999; Iwamoto 2000). It is possible that these repeats are involved in the translocation of $Na^+$ and $Ca^{2+}$ across the plasma membrane. This is a rather plausible function of these domains, given that recent structural data suggests that these repeats are in proximity to one another (Qiu et al. 2001; X. Ren et al. 2006; X. Ren et al. 2010). However there is some debate as to the specific region of the α-repeat that is involved in the translocation of ions. In a study conducted by Iwamoto and colleagues, it was suggested that mutating specific residues in the sequence of the α-repeats alters the affinity of the exchanger for extracellular $Ca^{2+}$ (Iwamoto et al. 2000). Of the 44 α-repeat residues that were mutated to cysteines, 6 showed an increase in $K_{m\,(Ca)}$ for $Ca^{2+}{}_o$ when compared to the wild-type exchanger. They proposed that these residues may not necessarily be involved with the translocation of the ions themselves but may be in close proximity to the binding site, suggesting that mutations could indirectly alter the structure of this site and therefore affinity (Iwamoto et al. 2000). In addition, they also examined the role of 3 conserved aspartate residues in exchanger function, hypothesising that acidic residues could be important for binding and transport of ions. Mutations of Asp130 (in α1) and Asp829 (in α2) to Gln or Asn resulted in a decrease of affinity for extracellular $Ca^{2+}$, whereas mutations of Asp825 had no effect (Iwamoto et al. 2000) (sites of these mutations are shown in figure 1.2). It is predicted that the size of the side chains and charge of carboxylates in residues 130 and 829 are possibly important for maintaining normal $K_{m\,(Ca)}$. These mutations affected the $Na^+{}_o$ affinity to a much lesser extent than $Ca^{2+}{}_o$. It appears that these conserved aspartate residues may not be directly involved with ion

transport, however they could line the ion translocation pathway, providing negative charges that promote through-space electrostatic interactions (Iwamoto et al. 2000).

Much of the mutational analysis to date has focused on the α1-repeat of the exchanger. To this end, Ottolia and colleagues investigated its role in the binding and transport of ions, specifically what residues of the repeat are important for function (Ottolia et al. 2005). Investigating the reentrant loop, mutations were introduced at residues H124N, N125C, F126C, T127H and D130C and the biophysical properties investigated. All mutations introduced generated active exchangers. H124N and D130C mutations resulted in an increase in $Na^+$ affinity of these mutants, whereas affinity decreased for F126C, and N125C had no measureable effect (Ottolia et al. 2005). Mutants expressing H124N, F126C and T127H and D130C also displayed a decrease in the Hill coefficient. There were no significant changes in the affinity for $Ca^{2+}$ in any of the mutated exchangers. Overall, the authors propose that the α1-repeat is not involved in the cytoplasmic affinity for ions but does play a role in the cooperativity of $Na^+$ binding rates (Ottolia et al. 2005), as the affinity was only modestly affected by mutations introduced into the reentrant loop. To further validate this finding, a squid chimera exchanger was generated, given that the α1-repeat is conserved between the 3 mammalian exchangers but not in the squid neuronal exchanger. Replacement of this repeat does not disrupt ion transport, but similar to the previous mutational data, effects on intracellular $Na^+$ affinity and cooperativity of $Na^+$ binding are observed. As previously described, the α1-repeat encompasses part of TMS 2, followed by the reentrant loop, then part of TMS 3. Ottolia and colleagues (2005) also examined the effect of mutations in TMS 3 of the exchanger. Mutations were introduced at 137-145 and 147. Previously examined by Nicoll and colleagues, a mutation of G138A displayed moderate effects on activity, whereas mutation to serine resulted in a reduction in activity of the exchanger (Nicoll, Hryshko, et al. 1996a). Expression of a N143V mutant resulted in an inactive exchanger. However, when N143D, a functional exchanger results, that displays normal $Na^+$ affinity and activity (Ottolia et al. 2005). In addition, mutations of residues 140, 145 and 147 displayed an alteration in the affinity for intracellular $Na^+$ (Ottolia et al. 2005). Mutation of 140 and 147 resulted in a decrease of affinity for $Na^+$ whereas mutations at 145 resulted in an increase affinity. These results suggest that TMS3 has a more critical role in both ion binding and translocation function of the exchanger than the reentrant loop. Through this work, Ottolia and colleagues challenge the widely held view that the reentrant loops form part of the ion

pore of the exchanger, as the only change observed when mutations are introduced in the α1 repeat is a change in the binding of $Na^+$ on the opposite side of the membrane from the reentrant loops (Ottolia et al. 2005). Their conclusions are supported by the identification of ion binding sites in TMS 2 and 3 and TMS 7 and 8.

There is some mutational data available for the α2-repeat, suggesting it also plays a role in exchanger activity. Mutations at Ser811, Asp814, Ser818 and Ser838 all resulted in exchangers with no exchanger activity (Nicoll, Hryshko, et al. 1996a). A reduction in exchanger activity was observed with mutations at Gly809, Gly837 and Asn842, whereas an altered current-voltage relationship was recorded for Gly837. The profound effect of mutations in the α-repeats suggests that they do in fact play an important role in regulating the binding and translocation of ions dealt with by the exchanger (Nicoll, Hryshko, et al. 1996a).

### ii Function Of The XIP Region

A sequence of basic and hydrophobic amino acids, termed the XIP region, is located at the N-terminal end of the large intracellular loop of NCX. This sequence stretches from 219-238 (Li et al. 1991). A peptide corresponding to this region was generated and shown to be a potent inhibitor of NCX exchange activity when applied to the intracellular surface of the exchanger, using the giant excised patch technique (Li et al. 1991). This points towards a role for the endogenous XIP region to regulate exchanger activity. Mutagenesis revealed that exchanger mutants lacking residues 562-679 fails to be inhibited by exogenously applied XIP, suggesting that this region is involved in exchanger regulation by XIP (Maack et al. 2005). If the XIP binding site is on the intracellular loop, the structure and conformation of this region may be important for interaction (Ottolia et al. 2001). Utilising split exchangers, where the exchanger is split into its N-terminal and C-terminal halves then co-expressed in oocytes, Ottolia and colleagues demonstrated that the split exchanger retains sensitivity to XIP (Ottolia et al. 2001).

Further mutational analysis of the XIP region itself revealed that XIP plays a role in the $Na^+$-dependent inactivation and $Ca^{2+}$ regulation of the exchanger (Matsuoka et al. 1997). Nine mutants of the XIP region were constructed (F223E, Y224T, K225Q, Y226T, R230Q, K229Q, Δ229-232, 229(QQTQ)232 and Δ229*237) and based on

electrophysiological properties, were sub-divided into two distinct groups (see figure 1.8 for position of mutations in XIP sequence). Group 1 mutants (F223E, Y224T, K225Q, Y226T, R230Q), $Na^+$-dependent inactivation was still apparent, but displayed a faster rate of inactivation compared to the wild-type exchanger. In contrast, group 2 mutants (K229Q, Δ229-232, 229(QQTQ)232, Δ229*237) display a complete abolition of $Na^+$-dependent inactivation (Matsuoka et al. 1997). As well as an effect on the kinetics of $Na^+$-dependent inactivation, group 1 mutants display a reduced inhibition of $Na^+$-dependent inactivation by $Ca^{2+}$ compared to the wild-type exchanger (Matsuoka et al. 1997). Group 2 mutants do not show any alteration in the affinity for regulatory $Ca^{2+}$. Therefore, these results suggest that XIP is involved in the regulation of $Na^+$-dependent inactivation. In addition, it appears that XIP may regulate $Na^+$-dependent inactivation via an interaction with phosphatidylinositol 4,5-bisphosphate ($PIP_2$) (Z. He et al. 2000). It was demonstrated that XIP binds with high affinity to $PIP_2$, which is also proposed to modulate $Na^+$-dependent inactivation, as high membrane levels of $PIP_2$ stimulates exchange activity by decreasing inactivation. The location of XIP is suited to an interaction with $PIP_2$.

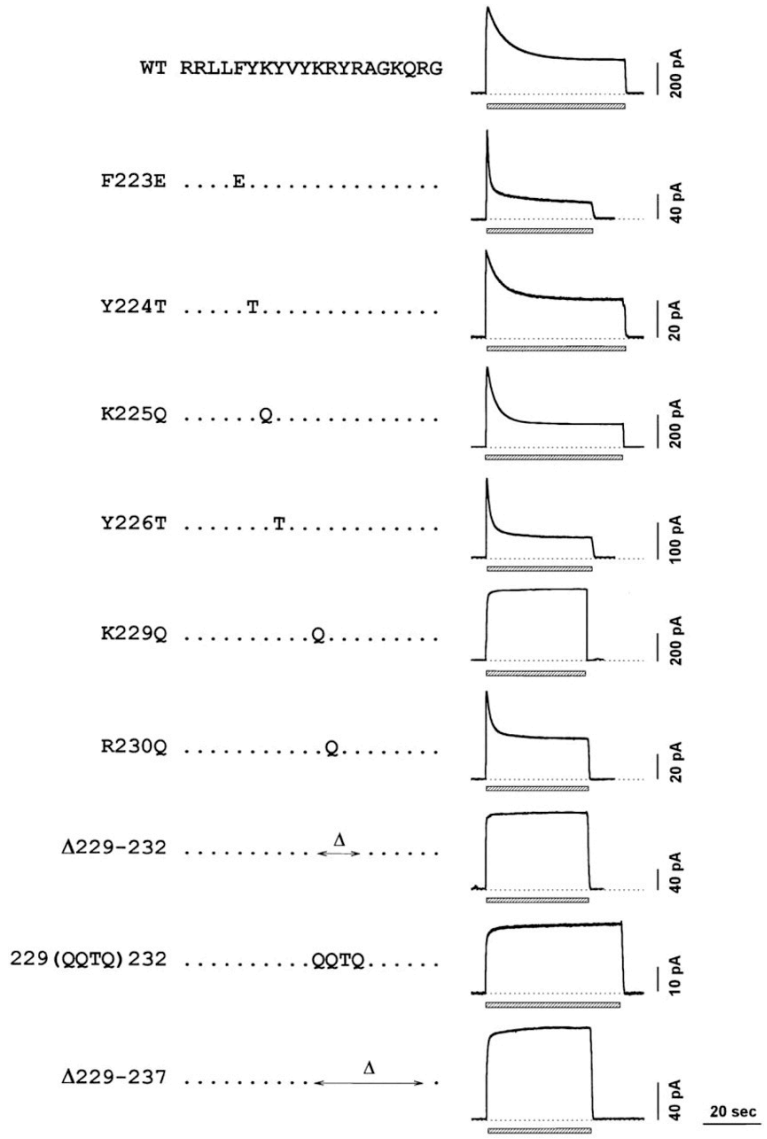


***Figure 1.8: Mutations Of The XIP Region Of NCX Have Different Effects On Outward Exchange Current.*** *The WT sequence for the XIP region is shown as one letter abbreviations. Mutations are shown, where dots indicate unchanged residues. Outward exchange current was induced by replacing 100 mM Cs with 100 mM Na at the cytoplasmic face of the patch (bars). Extracellular and cytoplasmic* $Ca^{2+}$ *were 8 mM and 1M, respectively. Dotted lines indicate 0 current level. Modified from (Matsuoka et al. 1997).*

### iii Function Of The $Ca^{2+}$ Regulatory Domain

As mentioned previously, there is a region of the large intracellular loop that confers a high affinity $Ca^{2+}$ binding site. The β-repeats, a pair of domains with high sequence similarity, were shown to be involved in the binding of regulatory $Ca^{2+}$, as mutations of these regions resulted in the affinity for regulatory $Ca^{2+}$ being lowered (Matsuoka et al.

1995; Ottolia et al. 2010). Discovery of the crystal structure coupled with NMR data on the β-repeats revealed that both are involved in the binding of regulatory $Ca^{2+}$. As such, the β-repeats were renamed CBD1 and CBD2 ($Ca^{2+}$ binding domain 1 and 2 respectively). CBD1 and CBD2 both possess an immunoglobulin fold, similar to that found in the cadherins and fibronectins (Hilge et al. 2006). Each of the domains is a 7-strand antiparallel β-sandwich, containing $Ca^{2+}$ binding sites at the head and unstructured loop F-G at the tail (see figure 1.9 for a schematic representation). The connection between the two domains is short, therefore it has been assumed that they are arranged in a head-to-tail configuration (Ottolia et al. 2010). Both sites are capable of binding $Ca^{2+}$, however the number of ions they bind and the affinity with which the ions bind is different for each of the 2 domains.

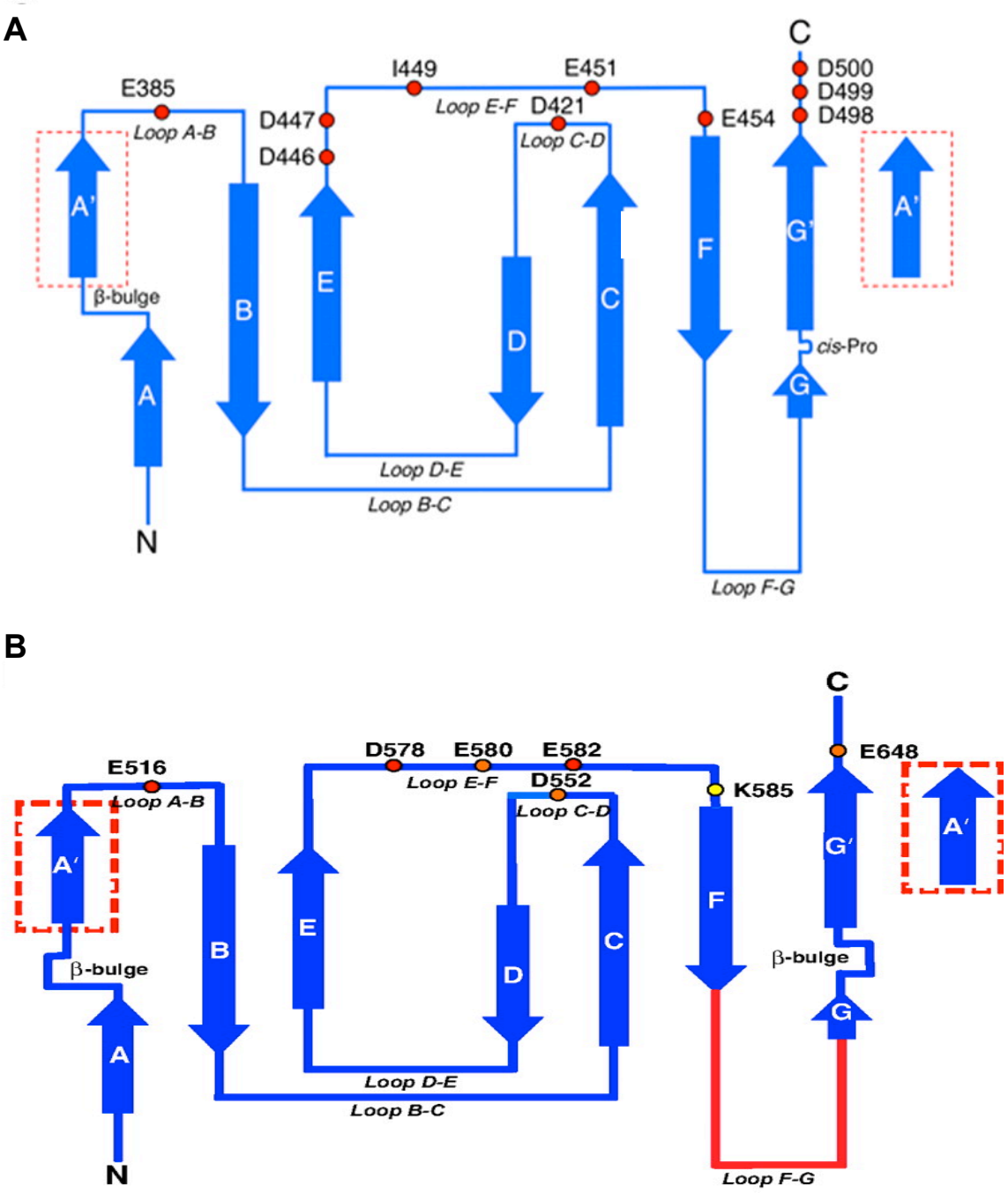


***Figure 1.9: Schematic Representation Of $Ca^{2+}$ Regulatory Domains.*** *A depicts the structure of CBD1, blue arrows represent the β-strands, residues involved in coordination of $Ca^{2+}$ are shown as red circles. The red box around strand A' shows the break in hydrogen bonding between strand A and B caused by the β-bulge. B depicts the structure of CBD2, blue arrows represent the β-strands, the disordered F-G loop is shown in red, Lys585 is shown as a yellow circle, orange circles show residues involved in $Ca^{2+}$ coordination and Lys585 stabilisation. Again, the red box around strand A' indicates the break in hydrogen bonding between strand A and B. Modified from (Nicoll et al. 2006; Besserer et al. 2007).*

CBD1 binds 4 $Ca^{2+}$ ions, which are coordinated by an extensive network of amino acid residues (Nicoll et al. 2006). The sites in which $Ca^{2+}$ binds are termed Ca1, Ca2, Ca3 and Ca4. This extensive network connects the 4 $Ca^{2+}$ ions that are clustered in the distal loops of the β-sandwich. The 4 binding sites are suggested to be arranged in a parallelogram-like configuration, which are coordinated by aspartic and glutamic acid residues, that form polydentate interactions between 2 or 3 of the $Ca^{2+}$ ions (Nicoll et al. 2006). The residues involved in the coordination of the $Ca^{2+}$ are predominantly located in the C terminus (Asp498, Asp499, Asp500) and in loop E-F (Asp446, Asp447, Ile449, Glu451, Glu454). There are also additional interactions that take place between Glu385 in the A-B loop, Asp421 in the C-D loop and 3 water molecules (Nicoll et al. 2006). Of these residues, Glu451, Asp421 and Asp500 are suggested to be key residues that help coordinate the 4 $Ca^{2+}$ ions into a tightly bound cluster. It appears that this complex coordination scheme involves carboxylate groups from aspartic acid and glutamic acid residues to form interactions with the $Ca^{2+}$ ions. The $Ca^{2+}$-free form of CBD1, shows a loss of structural integrity in the upper half of the molecule (Hilge et al. 2006). Residues that form $Ca^{2+}$ binding sites become unstructured following the release of $Ca^{2+}$. This is thought to be due to the lack of basic residues in the binding sites, which therefore are not able to counter the repulsive forces between the glutamate and aspartate residues.

In contrast to CBD1, CBD2 only binds 2 $Ca^{2+}$ ions, at sites Ca1 and Ca2. The first $Ca^{2+}$ binding site (Ca1) is octacoordinated with carboxylate groups from 3 acidic residues, a carbonyl backbone and 2 water molecules (Besserer et al. 2007). Glu516 from the A-B loop and Glu648 from the C-terminal end of the binding site, form bidendate interactions with the $Ca^{2+}$, and together with Asp578 and Glu580, coordinate the primary $Ca^{2+}$ in its binding site. The second $Ca^{2+}$ binding site (Ca2) is heptacoordinated by 5 water molecules, Asp552 and Asp578 (Besserer et al. 2007). Two of the water molecules are coordinated to a lysine residue at position 585, which forms a salt bridge with Glu582. Asp578 is involved in the coordination of both primary and secondary $Ca^{2+}$ ions, through a bridging bidentate ligand, which connects the primary and secondary binding sites. In the $Ca^{2+}$-free form of CBD2, there are no major conformational changes, except a slight shift in the loops that coordinate the $Ca^{2+}$ ions (Besserer et al. 2007). The E-F loop shifts towards the C-D loop and the C-terminus is shifted away from the E-F loop. This shifts Lys585 to the same position that was occupied by the $Ca^{2+}$ ion in the secondary binding site, enabling this residue to form salt

bridges with Asp552 and Glu648, with the oxygen from the carbonyl group of Glu580 hydrogen-bonded to Lys585. This series of interactions between these residues prevents the CBD2 from unfolding in the same manner as CBD1, allowing the primary site in CBD2 to aid rapid binding of $Ca^{2+}$ (Besserer et al. 2007). The role of these two binding sites in the regulation of the exchanger will be discussed in more detail in following sections.

### 1.1.6 Regulation Of NCX

The Na+/$Ca^{2+}$ exchanger is subject to various modes of regulations, which are predominantly regulated through specific regions in the large intracellular loop. Below, the different modes of regulation are discussed.

#### i $Na^+$-dependent Inactivation

As described previously, the $Na^+/Ca^{2+}$ exchanger exchanges 3 $Na^+$ for 1 $Ca^{2+}$, activated by a rise in intracellular $Ca^{2+}$ during the action potential. Not only is it capable of transporting these ions but is also regulated by them. Hilgemann described a decrease in exchange current, which occurs during activation by cytoplasmic $Na^+$ (Hilgemann 1990). This is termed $Na^+$-dependent inactivation. It is proposed that this inactivation is induced by the binding of $Na^+$ ions to cytosolically disposed translocation sites (Hilgemann, Matsuoka, Nagel & Collins 1992c). This was supported by 4 findings in Hilgemann's study, application of $Na^+$ to the cytoplasmic side induces inactivation of the outward current, a reduction in extracellular $Ca^{2+}$ decreases the extent of the inactivation, depolarisation does not affect inactivation and finally application of $Na^+$ to the extracellular side in outside-out patches induced an inward current that did not show signs of decaying (Hilgemann, Matsuoka, Nagel & Collins 1992c). $Na^+$-dependent inactivation is time-dependent, showing a decline of 80% in the outward current in giant excised patches with a time constant of approximately 1s (Hilgemann 1990). Treatment of the exchanger with chymotrypsin, which proteolyses the large intracellular loop of the exchanger, decreases the level of $Na^+$-dependent inactivation observed, suggesting a role for the intracellular loop in this process (Hilgemann 1990; Hilgemann, Matsuoka, Nagel & Collins 1992c).

In an extensive study by Hilgemann and colleagues, it was demonstrated that $Na^+$-dependent inactivation is sensitive to a number of regulatory factors. Addition of $Ca^{2+}$ to the cytoplasmic side of the membrane results in activation of an outward current and inhibition of $Na^+$-dependent inactivation (Hilgemann 1990; Hilgemann, Matsuoka, Nagel & Collins 1992c). Temperature and pH are also factors that affect $Na^+$-dependent inactivation. A higher pH of 7.8 resulted in a much reduced decay of the outward current, suggesting that no to little inactivation is occurring (Hilgemann, Matsuoka, Nagel & Collins 1992c), whereas at pH 6.8, current decayed by approximately 85%. An increase in temperature alters the peak current and increases the rate of inactivation, resulting in a faster decay of the current (Hilgemann, Matsuoka, Nagel & Collins 1992c). $Na^+$-dependent inactivation of exchange activity can be reversed by addition of Mg-ATP to giant excised patches (Hilgemann & Ball 1996), which is also capable of increasing the current observed in these patches. This effect is also mimicked by addition of $PIP_2$ and inhibited when membranes were treated with a phosphatidylinositol-specific phospholipase C, indicating a role for $PIP_2$ in the regulation of $Na^+$-dependent inactivation (Hilgemann & Ball 1996; Reeves & Condrescu 2008). In addition to regulation of $Na^+$-dependent inactivation by pH, temperature, cytoplasmic $Ca^{2+}$ and ATP, the endogenous XIP region is also capable of regulating this process. As discussed previously (see Structure-Function of XIP section), Matsuoka and colleagues demonstrated that mutations in the endogenous XIP region of the exchanger alters the kinetics or completely abolishes $Na^+$-dependent inactivation, supporting a role for the intracellular loop in its regulation (Matsuoka et al. 1997).

In terms of physiological relevance, the role of $Na^+$-dependent inactivation is subject to debate. A study by Chernysh and colleagues utilising Chinese Hamster Ovary (CHO) cells expressing the canine NCX demonstrate that at physiological concentrations of intracellular $Na^+$ (10mM), there is very little $Na^+$-dependent inactivation observed (Chernysh et al. 2008). They postulate that while $Na^+$-dependent inactivation is probably not relevant under normal physiological conditions, under ischemic conditions, when $[Na^+]_i$ is high, there is low ATP/$PIP_2$, and low $pH_i$, this would promote $Na^+$-dependent inactivation, resulting in a reduction in the level of influx and thus reducing the possibility of $Ca^{2+}$ overload (Chernysh et al. 2008). While this study confirms results from giant patch studies, there are also significant differences. For example, the authors find that in CHO cells the wild-type NCX1 exchanger is

remarkedly resistant to $Na^+$-dependent inactivation, even at high levels of intracellular $Na^+$, which contrasts to data from other groups (Hilgemann, Matsuoka, Nagel & Collins 1992c; Chernysh et al. 2008; Hryshko 2008). These differences observed in exchanger regulation and activity could be caused by the different approaches used by these groups, some employing giant patch clamping and the others cell-based fluorescence techniques. The exact contribution of $Na^+$-dependent inactivation to the regulation of the exchanger in normal physiological conditions is still unknown, however it has been shown that in ischemia-reperfusion injury, reverse mode of $Na^+/Ca^{2+}$ exchange contributes to the $Ca^{2+}$ overload (C. Lee & Hryshko 2004; Imahashi et al. 2005; Wang et al. 2007; Hryshko 2008). It appears that the pharmacological agents, SEA0400 and KB-R7943 result in an apparent transport mode selectivity (C. Lee et al. 2004), as pharmacological interventions appear to stablise the $Na^+$-dependent inactivation of the exchanger, reducing the cardiac injury observed under these settings. More work is needed to elucidate the exact role of $Na^+$-dependent inactivation in a physiological setting.

### ii $Ca^{2+}$ Regulation

NCX is capable of not only transporting $Ca^{2+}$, it is also regulated by it. It is important to understand that transported $Ca^{2+}$ is distinct from regulatory $Ca^{2+}$, i.e. $Ca^{2+}$ that regulates NCX is not transported and vice versa. In a complementary study to their work on $Na^+$-dependent inactivation, Hilgemann and colleagues sought to characterise the role of $Ca^{2+}$ in the regulation of the exchanger. $Na^+$-dependent inactivation is strongly regulated by cytoplasmic $Ca^{2+}$, increasing concentrations of $Ca^{2+}$ increases the rate of recovery from the $Na^+$-dependent inactive state (Hilgemann, Collins & Matsuoka 1992a). $Ca^{2+}_i$ is also capable of activating the exchanger, as there is no activation of outward current by $Na^+$ in the absence of $Ca^{2+}_i$ (Hilgemann 1990). It was proposed that $Na^+$ and $Ca^{2+}$ regulated the exchanger at distinct sites as they argued that high $Na^+_i$ would displace $Ca^{2+}_i$ from its regulatory site, resulting in a bell-shaped concentration-current relation, which was not observed (Hilgemann, Collins & Matsuoka 1992a). In addition, it was demonstrated that while both $Ca^{2+}$ and ATP applied at the intracellular surface are both capable of activating an exchange current, they do this by separate mechanisms (Hilgemann 1990). Similar to $Na^+$-dependent inactivation, regulation by $Ca^{2+}$ is abolished by chymotrypsin treatment, indicating the regulatory domain for $Ca^{2+}$ lies within the intracellular loop (Hilgemann 1990).

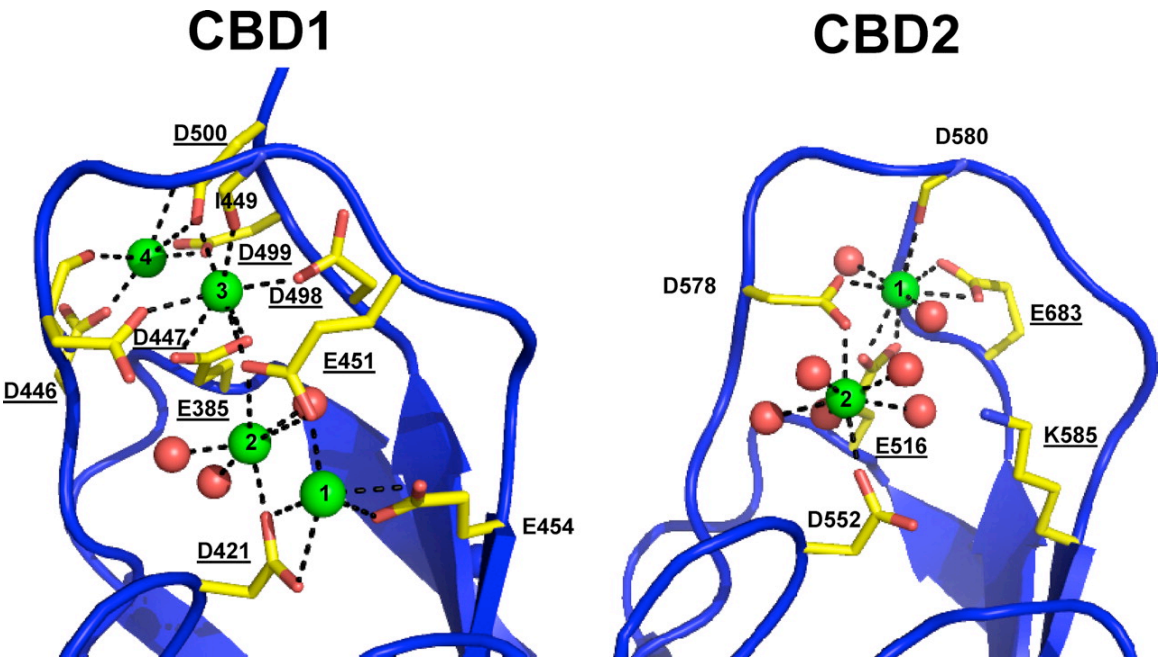


***Figure 1.10: Structure Of CBD1 And CBD2.*** *The residues involved in coordination of $Ca^{2+}$ into each of the binding sites in the CBDs are shown. Notes that CBD1 has 4 binding sites and CBD2 has 2. The residues underlined are those that were mutated in (Ottolia et al. 2009) and water molecules are shown as red spheres. Modified from (Ottolia et al. 2009).*

It is indeed in the intracellular loop of the exchanger where the 2 CBDs lie (see figure 1.10 for structure of both CBDs). The exact role of each of the domains in $Ca^{2+}$ regulation is only beginning to be elucidated via mutational studies (Besserer et al. 2007; Ottolia et al. 2009; Ottolia et al. 2010; John et al. 2011). Mutational analysis of the CBD2 domain revealed that it is important for the regulation of NCX by regulatory $Ca^{2+}$, as regulation is lost when key residues in each of the two binding sites, Ca1 and Ca2 are mutated (Besserer et al. 2007). E516L, D552V, D578V and E683V contribute a carboxylate group to the binding of regulatory $Ca^{2+}$, hence why they were selected for mutational analysis. In addition, K585E, involved in providing a positive charge to prevent unfolding of the protein in the absence of $Ca^{2+}$, was also chosen. Effect of mutations was assessed by electrophysiological techniques, using wild-type or mutant exchangers injected into *Xenopus oocytes* and biophysical properties studied by using the giant patch technique (Besserer et al. 2007). Exchange current was generated by application of 100mM $Na^{+}$ to the intracellular surface in the presence of 8mM $Ca^{2+}$ in the pipette (which represents the extracellular surface), as well as submicromolar regulatory $Ca^{2+}$ at the intracellular surface. The wild-type exchanger behaves as

expected, in the absence of regulatory $Ca^{2+}$, very little exchange current is observed in response to application of $Na^{+}$, however in the presence of regulatory $Ca^{2+}$, $Na^{+}$ results in a current that partially inactivates to a steady state over a few seconds (Besserer et al. 2007). At high regulatory $Ca^{2+}$ concentrations, peak current is enhanced and $Na^{+}$-dependent inactivation is reduced. In contrast to the wild-type, mutations of the residues involved in coordinating $Ca^{2+}$ to the primary site of CBD2 abolishes the sensitivity to regulatory $Ca^{2+}$ (Besserer et al. 2007). E516L, D578V and E683V are located in the primary site, and in response to regulatory $Ca^{2+}$, peak current or $Na^{+}$-dependent inactivation are unaffected, showing the same result in the absence of regulatory $Ca^{2+}$. Based on this result, the primary site of CBD2 is essential for maintaining regulation of NCX by $Ca^{2+}$.

D552V, located in the secondary site of CBD2, is the one residue that is involved in coordination of $Ca^{2+}$ binding to the secondary site only. The effect of a rise in regulatory $Ca^{2+}$ results in an increase in the peak current and a decrease in $Na^{+}$-dependent inactivation in wild-type exchanger responses (Besserer et al. 2007). When comparing the results from wild-type and D552V mutant exchangers, there are no significant changes in the response to regulatory $Ca^{2+}$. This indicates that the secondary site in CBD2 is not necessary for regulation of NCX by $Ca^{2+}$. Mutations were also introduced in $Lys^{585}$, which is involved in maintaining tertiary structure in the absence of regulatory $Ca^{2+}$ binding. K585E displayed full regulation by $Ca^{2+}$, but with lower affinity compared to the wild-type exchanger (Besserer et al. 2007). $Na^{+}$-dependent inactivation was more decreased in K585E mutant. Therefore, $Lys^{585}$ is not essential for NCX to retain regulatory function (Besserer et al. 2007).

The roles of the individual $Ca^{2+}$ coordination sites of CBD1 were also examined by mutational analysis. Mutations introduced at sites coordinating $Ca^{2+}$ to Ca1 and Ca2, D421A and E451A, resulted in outward currents that peaked rapidly and then decayed over several seconds due to $Na^{+}$-dependent inactivation (Ottolia et al. 2009), which was similar to results obtained for the wild-type exchanger. Raising intracellular $Ca^{2+}$ concentrations resulted in an increased in peak currents from both wild type and mutant exchangers. Similar to wild type, mutant exchangers show the same reduction in $Na^{+}$-dependent inactivation in response to increasing intracellular $Ca^{2+}$ concentrations. These results indicate that Ca1 and Ca2 of CBD1 do not play a major role in the regulation of NCX by regulatory $Ca^{2+}$ (Ottolia et al. 2009).

Mutational analysis of the residues coordinating sites Ca3 and Ca4 yielded more interesting insights into the contribution of each binding site to $Ca^{2+}$ regulation. Previous work showed that mutants D447V, D498I and D500V altered the affinity of the exchanger for cytoplasmic $Ca^{2+}$, which are involved in coordinating $Ca^{2+}$ at both Ca3 and Ca4 (Matsuoka et al. 1995). Therefore, biophysical properties of E385A and the double mutant D446A/D447A were characterized and the effects of D500V were further investigated (Ottolia et al. 2009). E385A is involved in the coordination of Ca3, whereas the double mutant D446A/D447A and D500V will interfere with Ca3 and Ca4. All 3 mutants required higher concentrations of $Ca^{2+}_i$ compared to wild-type exchanger to initiate exchanger currents. In addition, the affinity of the mutants for $Ca^{2+}_i$ was decreased by approximately 5-fold (Ottolia et al. 2009). This points towards Ca3 and Ca4 having a significant role in the regulation of NCX by $Ca^{2+}$. In addition to creating mutants with residues mutated that affect individual sites, a mutant, with 7 of the 10 amino acid residues that are involved with coordination of $Ca^{2+}$ into the binding sites of CBD1 mutated, was generated (designated M7, mutations introduced E385A, D421A, D446A, D447A, D498A, D499A and D500A). The M7 mutant retained $Ca^{2+}$ regulation, however the affinity was undetermined due to lack of saturation, indicating a role for CBD2 in the regulation of the exchanger (Ottolia et al. 2009). As well as still retaining $Ca^{2+}$ regulation, all mutants displayed a reduction in $Na^{+}$-dependent inactivation. Furthermore, the $Ca^{2+}$-dependence of the steady-state current was investigated for E385A and D500V. In wild-type exchangers, steady-state current has a higher dependence on $Ca^{2+}$ than peak current, whereas in E385A, the sensitivity of peak current to $Ca^{2+}$ has decreased. In D500V, the steady-state current was demonstrated to be saturable and displays a similar affinity for $Ca^{2+}$ as the peak current. The peak current is reduced and the sensitivity of steady-state current to $Ca^{2+}_i$ is increased (Ottolia et al. 2009). These results indicate that Ca3 and Ca4 have important roles in exchanger regulation mediated by $Ca^{2+}_i$.

Further to the work carried out in this study, Ottolia and colleagues introduced mutations within CBD2, to better understand its role in the regulation of the exchanger by $Ca^{2+}$. As discussed previously, it demonstrated that mutations E516L, D578V and E638V abolished $Ca^{2+}$ regulation of the exchanger. These residues are located in Ca1 of CBD2. Given the obvious importance of Ca1 in maintaining $Ca^{2+}$ regulation of NCX, it was hypothesised that introduction of positive charges at these residues may simulate a

positive charge and "trick" the exchanger that $Ca^{2+}$ is bound at Ca1 (Ottolia et al. 2009). With this in mind, E516R and E683R were investigated in the presence and absence of $Ca^{2+}$. D578R has previously been shown to be regulated by $Ca^{2+}$ (Dunn et al. 2002). In the absence of $Ca^{2+}$, both mutants display outward current, which is further raised by increasing $Ca^{2+}$ concentrations, indicating that both mutants are still partially regulated by $Ca^{2+}$ (Ottolia et al. 2009). Introduction of neutral amino acid residues at the same sites do not show the same biophysical properties. In addition, mutation K585E, which results in the introduction of a negative charge, slightly decreases the $Ca^{2+}$ sensitivity of the peak outward current, and $Na^{+}$-dependent inactivation is abolished at much lower $Ca^{2+}$ concentrations than compared to the wild-type exchanger. Therefore, introduction of a negative charge at $Lys^{585}$ increases the affinity for $Ca^{2+}$ to relieve $Na^{+}$-dependent inactivation. As previous discussed, this residue is involved in maintaining tertiary structure of CBD2 in the absence of regulatory $Ca^{2+}$ binding. Furthermore, using this mutation on the M7 mutant background, it was predicted that this would increase the affinity of CBD2 for regulatory $Ca^{2+}$ and may rescue the low affinity for $Ca^{2+}$ of the M7 mutant (Ottolia et al. 2009). This in fact turned out to be the case, as an increase in affinity of the peak current for $Ca^{2+}$ was observed. Taken together, these results suggest that CBD1 regulates $Ca^{2+}$ regulation of the exchanger and CBD2 is required for $Ca^{2+}$ regulation to occur.

To determine if any conformational changes occur in the CBDs in response to $Ca^{2+}$ regulation of the exchanger, FRET analysis was used to determine structural changes. Both the full-length exchanger and isolated CBD peptides were used in the analysis. Full length $Na^{+}/Ca^{2+}$ exchanger, labeled with a single fluorophore, was expressed in *Xenopus laevis* oocytes then subjected to FRET measurements (John et al. 2011). FRET was observed for these exchangers, demonstrating that they are close enough to generate a signal, supporting previous data that NCX exists as oligomers (X. Ren et al. 2008b; John et al. 2011). Analysis of changes in FRET as a function of fluorophore concentration, NCX was determined to exist as a dimer in the plasma membrane. The authors suggest that dimerisation may be important for trafficking of NCX to the plasma membrane, as it was previously shown that co-expression of a tagged WT-NCX and a mutant NCX resulted in the tagged NCX remaining in the endoplasmic reticulum (Ottolia et al. 2007). Addition of $Ca^{2+}$ to the cytoplasmic surface of giant patch clamp experiments, revealed an increase in FRET, suggesting that the distance between the intracellular loops of the exchangers decreases in response to $Ca^{2+}$ (John et al. 2011). To

determine which CBD is involved in initiating the conformational change, mutagenesis techniques were employed. Residues that are involved in $Ca^{2+}$ binding to either CBD1 or CBD2 were mutated. D421A, E451A and D500V were introduced into the exchanger, which interfere with the binding of $Ca^{2+}$ to all four binding sites in CBD1. These mutations completely abolish $Ca^{2+}$ induced movement of NCX. In stark contrast, mutation E516L in CBD2 does not have a significant effect on FRET observed in response to $Ca^{2+}$ (John et al. 2011). However, although it appears that CBD1 is responsible for the conformational changes in response to $Ca^{2+}$, it is still not sufficient to regulate NCX if CBD2 is nonfunctional.

To further elucidate the role of $Ca^{2+}$ binding to the 2 domains, 3 peptides were generated, CBD1 (residues 371-501), CBD2 (residues 501-689) and CBD12 (residues 371-689), which were linked to CFP and YFP at their N and C terminal ends respectively. Addition of $Ca^{2+}$ to the peptides, resulted in a decrease in $FRET_E$ (FRET efficiency) values, with the largest decrease in CBD1 (John et al. 2011). Consistent with results obtained for full-length NCX, mutations of residues 421, 451 and 500 resulted in loss of $Ca^{2+}$-dependent movements of CBD12, further supporting a role for CBD1 in initiating these movements. Despite these results suggesting that CBD1 initiates conformational changes in response to $Ca^{2+}$, this does not prove that CBD2 does not also play a role. The authors admit that the placement of the fluorophores may not be in the best position to detect movements in CBD2 and are currently investigating this.

### iii ATP Regulation

The role of ATP in the regulation of the $Na^+/Ca^{2+}$ exchanger has also been investigated. In the study examining the regulation of the exchanger by cytoplasmic $Ca^{2+}$, the effect of ATP was also examined (Hilgemann, Collins & Matsuoka 1992a). ATP demonstrated a similar inhibitory effect on $Na^+$-dependent inactivation as cytoplasmic $Ca^{2+}$. Application of 10mM ATP to excised patches resulted in an increased outward current, with a decreased inactivation phase, suggesting that ATP causes an acceleration of the recovery from $Na^+$-dependent inactivation (Hilgemann, Collins & Matsuoka 1992a). The rate of recovery upon removal of $Na^+$ in the presence of ATP increases, and the decay of current generated during $Na^+$ application is slower, indicating that ATP slows the transition of the exchanger into an inactivated state. Current decay induced by removal of $Ca^{2+}$ was also decreased in response to ATP, as the outward current decayed

by approximately 80% in response to $Na^+$, however after application of ATP, current only decayed by 10% (Hilgemann, Collins & Matsuoka 1992a). Interestingly ATP also protects against inhibition of the exchanger induced by lowering the cytoplasmic pH (Dipolo & Beaugé 2002). The authors hypothesise that these effects of ATP may be important in cardiac ischemia where a combination of acidosis and a rise in cytoplasmic $Na^+$ occurs. However, there is further evidence that the effect of ATP can be inhibited by applying a phospholipase C that specifically hydrolyses phosphatidylinositol (PI-PLC) to membrane patches (Hilgemann & Ball 1996). Indeed, this effect of PI-PLC on ATP can be attenuated by application of $PIP_2$ to the patch, suggesting that ATP acts upstream of $PIP_2$, which is responsible for the stimulation of the current.

### iv $PIP_2$ Regulation

Since the realisation that ATP exerts its effects upon the exchanger via $PIP_2$, Hilgemann's group focused their efforts on elucidating the effects of $PIP_2$ on exchanger function as well as surface expression, proposing that $PIP_2$ has a role in endocytosis of the exchanger (Hilgemann & Ball 1996; Yaradanakul et al. 2007; Shen et al. 2007). As discussed the previous section, $PIP_2$ can alleviate the inhibitory effect of PI-PLC on ATP stimulation of exchanger current (Hilgemann & Ball 1996). $PIP_2$ application results in an increase of peak outward current as well as increasing the steady-state current in mouse myocyte and Baby Hamster Kidney (BHK) cell patches, with no effect on the inward current in the absence of cytoplasmic $Na^+$ (Yaradanakul et al. 2007). Inactivation processes are also ablated by application of $PIP_2$, such that removal of cytoplasmic $Ca^{2+}$ does not result in current inactivation, therefore suggesting an effect on the CBDs. These effects are easily reversed following washout of $PIP_2$.

In CHO cells expressing the M1 muscarinic acetylcholine receptor, M1, and NCX, treatment with carbachol, a muscarinic agonist results in rapid inhibition of outward exchange current, coupled with a small rise in capacitance that slowly decays over 3 minutes, suggesting exocytosis of the exchanger (Yaradanakul et al. 2007). Capacitance of a cell is usually indicative of a change in the size of the cell, suggesting a rise in endocytosis or exocytosis of exchangers, as fusion of vesicles containing exchangers would increase the surface area of the cell membrane. The authors suggest that this effect is due to a direct effect of M1-receptor induced $PIP_2$ depletion on exchanger function.

The effect of carbachol on inward NCX current in this model is different to the effect previously described for outward exchange current. Application of carbachol potentiates inward NCX current with an initial decrease in capacitance followed by an increase (Yaradanakul et al. 2007). However, at high cytoplasmic $Ca^{2+}$, carbachol is unable to potentiate the current. It appears that the effect of carbachol and its ability to activate internalisation of the exchanger is dependent on cytoplasmic $Ca^{2+}$ concentrations. There are contradictions raised by this study. There is evidence pointing towards a role for $PIP_2$ in internalisation of the exchanger, however when depleted, internalisation rises. The authors explain this could be due to PIP and $PIP_2$ rebounding during continued activation of M1 receptors (Zaika et al. 2006). To investigate the significance of $PIP_2$ synthesis, wortmannin was applied in the presence of carbachol, resulting in an abolition of the internalisation of the exchanger (Shen et al. 2007), suggesting that synthesis of phosphoinositide is important in exchanger internalisation as this process is inhibited by wortmannin. Therefore it does appear that $PIP_2$ is important for exchanger internalisation (Yaradanakul et al. 2007; Shen et al. 2007).

Given the effects of $PIP_2$ on the exchanger, it was logical to try and elucidate where on the protein its binding site is located. In a study by He and colleagues, it was demonstrated that the XIP region is the most likely candidate for the binding site of $PIP_2$ (Z. He et al. 2000). Utilising $PIP_2$ loaded vesicles immobilized on PVDF membranes, they showed that radiolabelled-XIP bound strongly to very low concentrations of $PIP_2$. Unlabelled XIP is able to displace this binding, unlike other peptides of other regions of the exchanger, suggesting that binding between XIP and $PIP_2$ is specific. To further define the specificity of this interaction, wild-type and a mutant exchanger with 9 amino acids of the XIP region deleted were expressed in *Xenopus* oocytes (Z. He et al. 2000). In the deletion mutant, the response to $PIP_2$ is completely lost. In the wild-type exchanger, $Na^+$-dependent inactivation is reduced, increasing steady-state current as a result. $Na^+$-dependent inactivation is lost in the deletion mutant, with no different in current between control and $PIP_2$ stimulated patches.

Two mutants that were previously used that show disrupted $Na^+$-dependent inactivation, in which the XIP also plays a role (Matsuoka et al. 1997), were utilised to further support the role of the XIP region in the regulation of the exchanger by $PIP_2$. The

K229Q mutant lacks $Na^+$-dependent inactivation, whereas the F223E mutant shows enhanced $Na^+$-dependent inactivation. Application of $PIP_2$ to the K229Q mutant exchanger results in a small stimulation of exchange current, approximately 5% (Z. He et al. 2000). The authors propose that the inactivation process results in the exchanger having reduced affinity for $PIP_2$, and postulate that inactivation may indicate dissociation of $PIP_2$ from its binding site on the exchanger. In line with this, $PIP_2$ has no effect on the outward current produced by the F223E exchanger mutant (He et al. 2000). These results suggest that the XIP region binds to $PIP_2$, which is thus able to regulate the inactivation processes of the exchanger.

### v Phosphorylation Of NCX1

Evidence regarding the phosphorylation status of NCX1 is controversial. Despite a number of papers published on the issue, there is still no consensus on whether NCX1 is subject to direct phosphorylation (Morad et al. 2011; Ruknudin et al. 2007). Direct measurement of NCX1 phosphorylation has proven to be difficult (Wei 2003; Condrescu et al. 1995). Two groups have reported phosphorylation of NCX1 in vitro by PKA (Wei 2003; Schulze et al. 2003), with one group demonstrating in vitro phosphorylation of NCX1 by PKC (Iwamoto et al. 1996). The paucity of groups reporting in vitro and in vivo phosphorylation of NCX1 casts doubt on whether NCX1 is regulated directly by β-adrenergic signalling. The majority of evidence for NCX1 phosphorylation comes from PKA-mediated "back-phosphorylation". Back-phosphorylation gives an indirect measure of phosphorylation levels of proteins by determining if it can be further phosphorylated. Wei et al demonstrated that NCX1 immunoprecipitated from control and failing hearts showed decreased back-phosphorylation in failing hearts, leading to the conclusion that NCX1 is hyperphosphorylated (Wei 2003). However, high levels of phosphatase activity have been reported during maladaptive cardiac hypertrophy and failure (Cheng et al. 2010). Based on this, it would be predicted that control NCX1 would also be hyperphosphroylated, which is not the case (Wei 2003). Another study provided evidence detailing an increase in NCX1 activity and an increase in phosphorylation, however it is still reliant on back phosphorylation and not a true in vivo assay (Ruknudin et al. 2000). Although lines of evidence exist to support NCX1 phosphorylation, there is no direct measure.

In contrast to evidence supporting NCX1 phosphorylation, rigorous testing on the role of phosphorylation of NCX1 has been carried out. Hilgemann addressed whether ATP or ATP-dependent phosphorylation was capable of regulating NCX1. However, no functional changes in NCX1 current resulting from phosphorylation following application of PKA or PKC catalytic subunits to giant excised patches of cardiac myocytes or *Xenopus* oocytes expressing canine NCX1 were observed (Hilgemann & Ball 1996; Linck et al. 1998; Matsuoka & Hilgemann 1994). In addition, investigation of β-adrenergic stimulation on NCX1 current was performed in guinea pig, mouse and rat ventricular myocytes. Effect of isoproterenol on NCX1 current was attributed to contaminating $I_{CFTR\text{-}Cl}$, which is also sensitive to $Ni^{2+}$. In addition, no significant difference was observed in the $Ni^{2+}$-sensitive current following treatment with forskolin. It appears that frog heart NCX1 is modulated by PKA, which can be recapitulated in canine NCX1 by creating a chimera of canine NCX1 that contains exon X from frog NCX1 (He et al. 2003). This suggests that mammalian NCX1 is not directly regulated by PKA. A rather elegant approach to determine whether or not NCX1 is regulated by PKA was recently carried out (Wanichawan et al. 2011). Using bioinformatics analysis and peptide arrays, NCX1 was screened for putative PKA sites. Several NCX1 peptides were phosphorylated, however only one site was identified following mutational analysis (threonine 699). Upon expressing wild-type NCX1 or T699A NCX1 in HEK293 cells, no phosphorylation was observed, suggesting NCX1 is not a direct physiological substrate of PKA (Wanichawan et al. 2011). Although some groups have demonstrated changes in NCX1 activity following β-adrenergic stimulation, this may be due in part to differences in electrophysiological measurements. To answer whether NCX1 is directly regulated by PKA or indeed PKC, more sophisticated single molecule imaging techniques will be required to visualise direct interaction of these two molecular players.

### 1.1.7 Contribution Of NCX To Cardiovascular Disease

Given that the $Na^+/Ca^{2+}$ exchanger plays a pivotal role in $Ca^{2+}$ homeostasis in the heart, and the balance of $Ca^{2+}$ is important to maintenance of excitation-contraction coupling, it seems logical to discuss its role in cardiovascular disease. Cardiovascular disease is characterised by a mismanagement of $Ca^{2+}$ that leads to disrupted contraction and ultimately heart failure. The disrupted excitation-contraction coupling can be attributed to altered sarcoplasmic reticulum $Ca^{2+}$ accumulation and is proposed to contribute

significantly to heart failure pathophysiology (Schillinger et al. 2003). This altered SR $Ca^{2+}$ content in heart failure is proposed to be caused by 3 major factors, 1) an increase in the leak of $Ca^{2+}$ from ryanodine receptors, 2) reduced SERCA activity and 3) increased $Ca^{2+}$ extrusion mediated by NCX (Hasenfuss & Schillinger 2004). As discussed previously, in human cardiomyocytes, the balance of $Ca^{2+}$ removal from the cytoplasm by SERCA and NCX is approximately 70% to 28%. However, it has been demonstrated in several studies that this ratio shifts to 50:50 in heart failure (Pogwizd et al. 1999; Pieske et al. 1999). The proposed reason for this shift is that, in heart failure, NCX is upregulated both at the mRNA and protein levels (Pogwizd et al. 1999). This results in increased exchange activity, shifting the ratio in favour of NCX. However, the rate of exchange does not change, it is simply that there are more exchangers present at the sarcolemmal membrane. Pogwizd and colleagues propose that upregulation of NCX could contribute to the mechanical dysfunction and arrhythmogenesis observed in heart failure. Thus suggesting that upregulation of NCX could enhance $Ca^{2+}$ extrusion from myocytes in early heart failure, but may limit SR $Ca^{2+}$ loading and cellular $Ca^{2+}$ transients as the heart failure progesses (Pogwizd et al. 1999).

Due to these findings, recent work has focused on the effect of NCX inhibition in various models of heart failure. Hobai and colleagues demonstrated that partial inhibition of NCX is able to restore $Ca^{2+}$ handling in a canine model of heart failure induced by rapid pacing (Hobai et al. 2004). Application of the peptide, XIP, to myocytes from failing hearts, resulted in an increase in the cytoplasmic $Ca^{2+}$ transients, due to the aforementioned shift to $Ca^{2+}$ extrusion mediated by NCX being partially reduced. In addition, since NCX activity was reduced by XIP, myocytes were still able to autoregulate intracellular $Ca^{2+}$ by taking up and releasing more $Ca^{2+}$ from the SR, despite impaired basal SERCA function (Hobai et al. 2004). They postulate that lower SR rate of $Ca^{2+}$ uptake in heart failure, (accompanied by only a 28% downregulation of SERCA (O'Rourke et al. 1999)), could be a result of lower amplitude $Ca^{2+}$ transients and lack of $Ca^{2+}$ stimulation of SERCA, suggesting there may be a cycle between decreased SR $Ca^{2+}$ release and uptake which is interrupted by XIP (Hobai et al. 2004). Treatment of failing myocytes with XIP results in improved SR $Ca^{2+}$ load and improvement of the stimulus-dependent positive $Ca^{2+}$ staircase, as NCX is no longer able to extrude the excess $Ca^{2+}$ from the cytoplasm as effectively.

In support of these findings, using an opposite approach, Schillinger and colleagues demonstrated a similar effect using adenovirus to increase NCX expression in isolated rabbit myocytes (Schillinger et al. 2000). Overexpression of NCX resulted in a decrease of the $Ca^{2+}$ content of the SR, decrease myocyte shortening and blunted forced frequency relationship. Utilising the NCX inhibitor, SEA-0400, Ozdemir et al investigated the effect of this inhibitor on left ventricular myocytes from healthy pigs or mice and mice with heart failure (Ozdemir et al. 2008). They showed that inhibition of NCX could display adverse effects in heart failure, as resting $Ca^{2+}_i$ is raised and relaxation is slowed. However, SR load is increased, meaning that SR uptake is preserved, preventing excessive concentrations of cytoplasmic $Ca^{2+}$ (Ozdemir et al. 2008).

Knockout and single point mutations in vivo have also been performed on the $Na^+/Ca^{2+}$ exchanger to elucidate its role in normal healthy conditions and in heart failure. Global knockout of the exchanger leads to embryonic lethality by around E9 – E10.5 (Wakimoto et al. 2000; Cho et al. 2001; Koushik et al. 2001). However there is some controversy surrounding the exact role of NCX in the embryonic lethality observed. Henderson et al showed that cardiac-specific knock-out of NCX in mice, which ablates 80-90% of NCX expressed in the heart, develops to adulthood (Henderson et al. 2004). In addition, reintroduction of NCX1 into transgenic mice partially rescues the phenotype observed in total knockouts (Cho et al. 2003). The single amino acid substitution mutant, which substitutes an asparagine at position 874 to a lysine residue, generated by Wansleeben et al also results in embryonic lethality (Wansleeben et al. 2010). This whole body knock-in mutant was identified via a genetic screen of N-ethyl-N-nitrosourea (ENU) induced mutations as it affected development of embryos. This residue is located in the reentrant loop of the α2-repeat. These embryos die at approximately embryonic day E10.5 due to cardiac abnormalities, although expression of the exchanger is unchanged at this time compared to wild-type controls. However, cardiomyocytes isolated from mutant embryos at E9 display altered characteristics. These cells are found fibrillating and contracting randomly, compared to wild-type cells, which contracted normally and synchronously in small clusters (Wansleeben et al. 2010). In addition, $Ca^{2+}$ transients were smaller in amplitude and fewer in frequency, and the action potential was rarely detected and was not repetitive as in wild-types. This study also showed that mutants had defective placentation, lack of yolk-sac

vascularisations, abnormalities of heart development, culminating in impaired blood circulation (Wansleeben et al. 2010).

The model produced by Henderson and colleagues contradicts many of these findings as the mice survive to adulthood. Utilising Cre/loxP technology, they were able to generate a cardiac-specific ablation of NCX1. Exon 11 was selected as the group had previous evidence to suggest that this region was critical for exchange activity (Nicoll, Hryshko, et al. 1996a). Exon 11 encodes for amino acid residues 722-813, which corresponds to 2 TMS, see figure 1.11 for details. The model displays an 80-90% reduction in protein levels of NCX1, as measured by immunoblot. There is also a 110kDa band observed that corresponds to the exchangers that possess the deletion, but this band is reduced, which the authors propose indicates that it is degraded rapidly (Henderson et al. 2004). On the whole, the mice appear normal, however they do display reduced cardiac contractility. At 7-8 weeks of age there is no change in the thickness or chamber size, suggesting an absence of hypertrophy. Although mice have functional myocardium, they are unable to cope with stress as homozygous females cannot survive the stress of breeding (Henderson et al. 2004). Cardiac function of the knockouts also declined with age, and ultimately leads to death, presumably due to heart failure as post mortems revealed enlargement of the heart. In addition excitation-contraction coupling of the knockout myocytes appears normal. The major difference between knockout and control cells is the activity of the L-type $Ca^{2+}$ channels. The activity is decreased by approximately 50%, and perhaps demonstrates a coping mechanism by the myocytes to limit the level of $Ca^{2+}$ influx during the action potential (Henderson et al. 2004). The action potential of knockout cells is also altered, lacking the plateau following the upstroke that is displayed by control cells, caused by less L-type $Ca^{2+}$ current, which is responsible for the plateau. Taken together, the data outlined above demonstrate that complete loss of activity of NCX should be met with caution as it may lead to serious adverse cardiac effects.

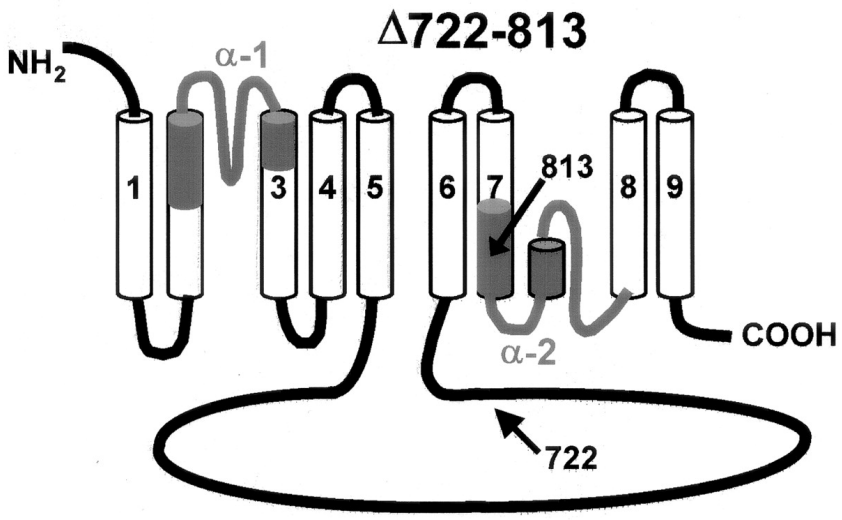


***Figure 1.11: Excision Of Exon 11 Deletes Amino Acids 722-813.*** *Topological model of NCX1 showing the domains eliminated by excision of exon 11 using Cre-loxP technology. Modified from (Henderson et al. 2004).*

## 1.2 Palmitoylation

### 1.2.1 Overview Of Palmitoylation Mechanism

Palmitoylation is a post-translational modification of a protein with a fatty acid. There are two forms of palmitoylation described to date, S-palmitoylation and N-palmitoylation. S-palmitoylation refers to the addition of palmitate (C16) to cysteine residues via a thioester linkage (Linder & Deschenes 2003) (see figure 1.12). However, it is not only palmitate that can be linked to proteins, other fatty acids such as saturated, monosaturated and polyunsaturated species can be linked to the protein via S-acylation (Smotrys & Linder 2004). These fatty acids that are linked in this way can have varying chain lengths, typically 14 carbon atoms or longer. N-palmitoylation on the other hand is slightly different from S-palmitoylation. N-palmitoylation was first described for Sonic Hedgehog (Pepinsky et al. 1998), where palmitate is added to the N-terminal cysteine residue via an amide link (see figure 1.12). When palmitate is added to this cysteine, a thioester intermediate is formed which is followed by the formation of a stable amide link (Linder & Deschenes 2007). The addition of palmitate to the cysteine residue is catalysed by palmitoyl-acyl transferases, although there is evidence to suggest that palmitoylation can occur spontaneously. Palmitoyl-CoA has been shown to be capable of S-acylating cysteine residues using peptides derived from palmitoylated proteins (Quesnel & Silvius 1994). Rhodopsin and G-protein α-subunits have also been

shown to undergo spontaneous S-acylation (O'Brien et al. 1987; Duncan & Gilman 1996; Mollner et al. 1998). Despite being possible *in vitro*, not all proteins are able to undergo spontaneous S-palmitoylation. Attempts to autoacylate proteins that are palmitoylated *in vivo* have proved unsuccessful (Duncan & Gilman 1996). Although autoacylation occurs *in vitro* for some proteins, so far whether this occurs *in vivo* has yet to be proven.

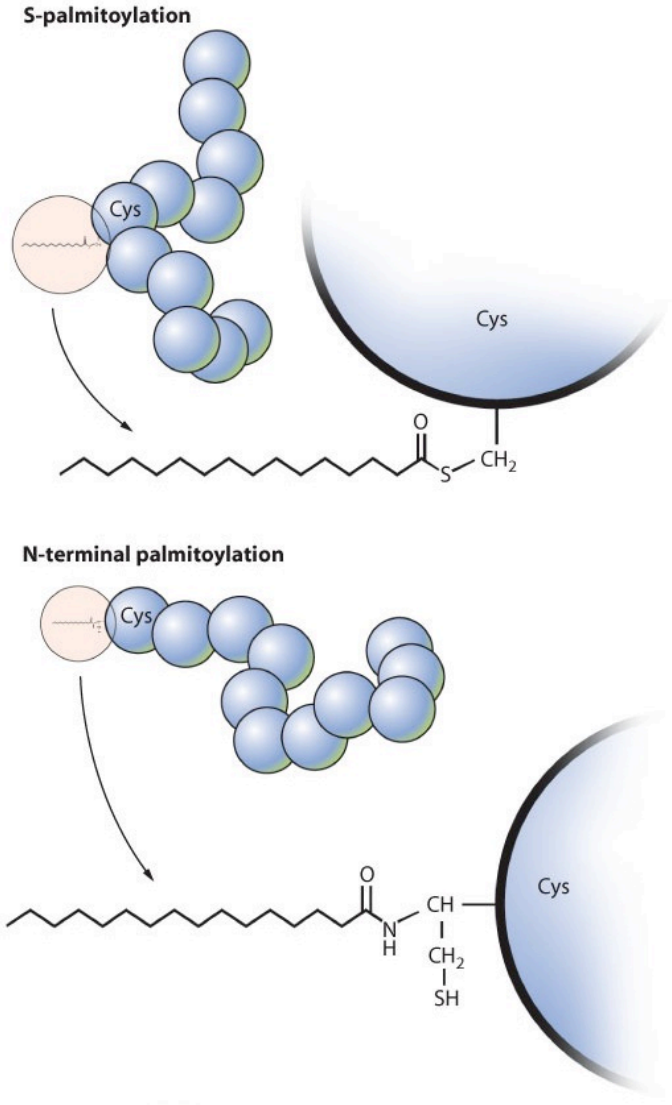


***Figure 1.12: Addition Of Fatty Acids To Cysteine Residues Via S-Palmitoylation And N-Palmitoylation.*** *S-palmitoylation is characterised by the addition of palmitate to a cysteine residue via a thioester linkage whereas N-palmitoylation occurs when a N-terminal cysteine is amide linked to palmitate. Modified from (Resh 2006).*

### 1.2.2 Control Of Palmitoylation

Protein palmitoylation has been shown to be either dynamic, (i.e. cycling through phases of palmitoylation and depalmitoylation throughout the lifetime of the protein) or stable. As mentioned previously, palmitate or other long chain fatty acid groups can be S-acylated to the protein via protein acyl transferases and palmitate is removed by thioesterases or hydrolases.

#### i Protein acyl transferases

Until recently, the enzymes responsible for catalysing the transfer of palmitate and other long chain fatty acids on to proteins were largely unknown. Largely, work carried out in *Saccharomyces cerevisiae* led the way for the discovery of yeast protein acyl transferases (PATs) and thus enabled identification of their mammalian counterparts. Using a genetic screen based on palmitoylation-dependent Ras proteins, the enzyme that palmitoylates Ras was identified (Bartels et al. 1999). However, trying to isolate the identified enzyme proved unsuccessful, which sparked the belief that palmitoylation occurs spontaneously (Mitchell 2006). This hypothesis was further enhanced by the instability of enzyme activity after solubilisation (Linder 2001). Another key identification led to the discovery of the genes involved in Ras palmitoylation, the identification of a palmitoylation-dependent Ras2 molecule (Mitchell et al. 1994). Possible enzymes responsible for palmitoylation were identified using mutagenesis of the yeast genome to identify lethal mutations in the presence of palmitoylation-dependent Ras2 protein. Using a palmitoylation-dependent Ras2 yeast strain, mutations that resulted in a decrease or inhibition of Ras2 palmitoylation were isolated (Bartels et al. 1999). These mutations were termed *ERF* (*Effectors of Ras Function*) (Mitchell 2006). Study of the Erf ezymes in yeast helped elucidate their structure and defining features, which have thus led to the identification of their mammalian counterparts. Deletion of Erf2, results in a reduction in palmitoylation of Ras2 and decreased membrane association (Bartels et al. 1999). A defining characteristic of Erf2 is the Asp-His-His-Cys (DHHC) domain located between TMD 2 and 3 (Mitchell et al. 2006). Scanning the yeast genome identified 7 other DHHC containing proteins, Akr1, Akr2, Pfa3, Swf1, Pfa4 and Pfa5. Akr1 (Roth et al. 2002), Erf2 (Lobo et al. 2002) and Pfa3 (Smotrys et al. 2005) have been demonstrated to catalyse palmitoylation. Identification of this conserved DHHC motif between yeast PATs led to the identification of DHHC-

containing proteins within mammals, insects and plants (Mitchell et al. 2006). There are 24 identified DHHC containing proteins within humans.

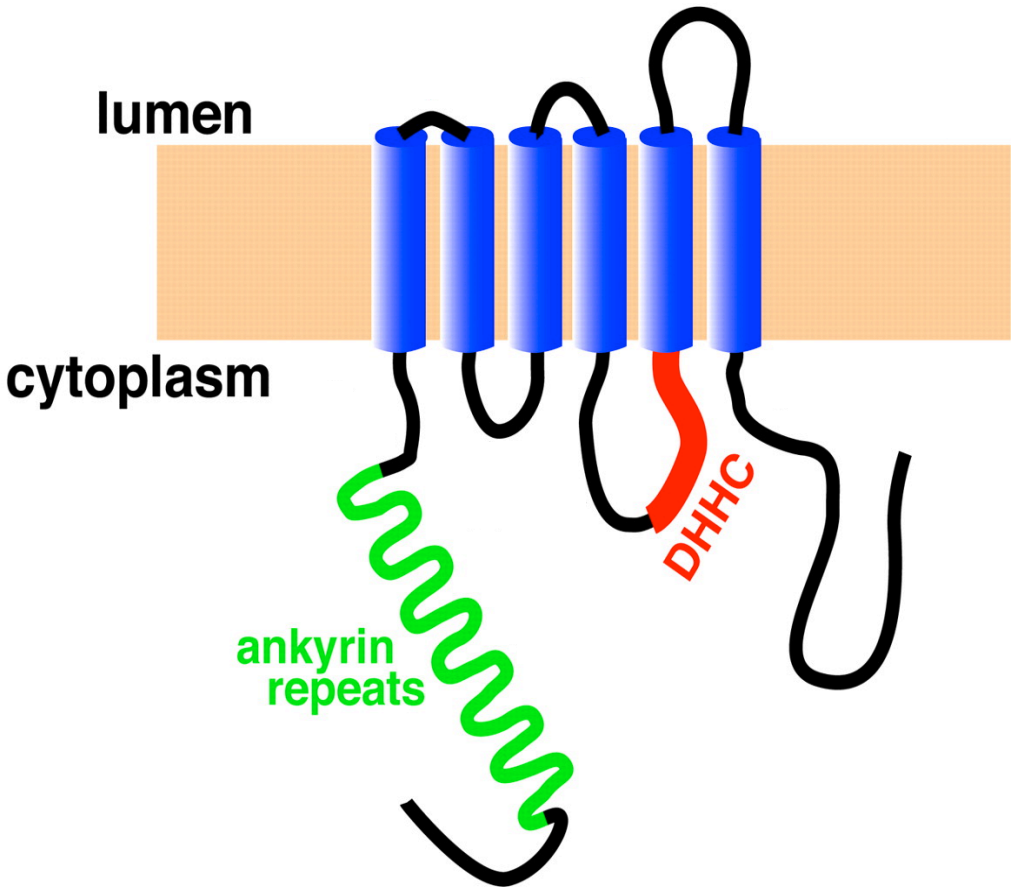


***Figure 1.13: DHHC-containing protein topology.*** *Proposed topology model of DHHC-containing protein acyl-transferases based on hydropathy analysis of yeast Akr1p. Modified from (Politis et al. 2005).*

DHHC proteins are predicted to be multi-pass membrane proteins, with between 4 and 6 transmembrane domains (Politis et al. 2005). The DHHC domain, which is predicted to mediate acylation, lies on the cytosolic side, which was confirmed experimentally for Akr1 (figure 1.11) (Politis et al. 2005). The majority of DHHC proteins have been found to localise to the secretory pathway, predominantly Endoplasmic Reticulum (ER) and Golgi Apparatus (Golgi) (Ohno et al. 2006; Korycka et al. 2012). Interestingly, some DHHC proteins are associated with the plasma membrane (Dipolo & Beaugé 2006; Ohno et al. 2006; Noritake et al. 2009; Greaves & Chamberlain 2010; Korycka et al. 2012). A large amount of effort has gone into investigating the mechanism of action

of DHHCs. It has long been known that DHHC proteins can be palmitoylated when incubated with palmitoyl-CoA (Mitchell et al. 2006). Additionally, mutation of the conserved cysteine residue within the DHHC motif abolishes palmitoyl transfer and autoacylation (Lobo et al. 2002; Roth et al. 2002). It is hypothesised that DHHC autoacylation is a transient intermediate with DHHC enzymes using a two-step ping-pong mechanism to catalyse transfer of palmitate. Using an HPLC, peptide-based PAT assay enabled kinetic constants for substrates to be determined (Jennings & Linder 2012). Single turnover assays confirmed that autoacylation represents a transient intermediate of the two-step ping-pong mechanism. In addition, this study also showed differences in preferences for available acyl-CoA between DHHC2 and DHHC3 to autoacylate with and transfer acyl chains longer than 16-carbon palmitate (Jennings & Linder 2012).

Recently, oligomerisation of DHHCs was described (Lai & Linder 2013). Formation of dimers and higher-order oligomers is a property of numerous membrane proteins including ion channels, transporters and receptors. Bioluminescence resonance energy transfer (BRET) uses *Renilla* luciferase (the luminescent energy donor) and its substrate coelenterazine, which transfers energy to a GFP variant (the energy acceptor) (Achour et al. 2011). Using BRET, homomultimerisation of DHHC2 and DHHC3 was demonstrated in intact cells as well as membrane preparations (Lai & Linder 2013). However, BRET suggested that these oligomers were not stable and were dynamic at the cell membrane. Interesting, mutation of the cysteine within the DHHC motif results in increased oligomerisation. Surprisingly, inhibition of enzyme activity resulted in increased oligomerisation, while in contrast, increasing palmitoyl-CoA availability decreased oligomerisation (Lai & Linder 2013). This suggests that when in an oligomeric state, DHHCs are inactive. However, convalently linked DHHC3 dimers are enzymatically active, although less so than the monomeric form.

One of the major questions surrounding the discovery of DHHCs is why are there 23 isoforms. 12 of the DHHCs are found to be expressed in the Golgi alone (Ohno et al. 2006). Co-expression studies in mammalian cells have revealed that DHHCs display substrate specificity (Fukata et al. 2004). In support of this, a study conducted in yeast confirmed that inactivation of specific DHHCs led to loss of palmitoylation of specific substrates (Roth et al. 2006). Several SNARE proteins showed reduced palmitoylation upon mutation of the ER-localised DHHC protein, Swf1. This study also showed that some DHHCs show preference to particular types of substrates: Swf1 targeted

transmembrane proteins with juxtamembrane cysteine residues, whereas most Akr1p substrates were soluble proteins (Roth et al. 2006). These data suggest that DHHCs do indeed display substrate specificity. It was shown that structural features regulate DHHCs substrate specificity. Huntingtin has been demonstrated to be palmitoylated by DHHC17 but not DHHC3 (Huang et al. 2009). DHHC17 possess several ankyrin repeats at its N-terminus and transfer of this region to the N-terminus of DHHC3 results in binding and palmitoylation of huntingtin to the same level as wild-type DHHC17 (Huang et al. 2009). Although transfer of the ankryin repeat allows DHHC3 to palmitoylate an non-target protein, there are targets known to be targets of both DHHC17 and DHHC3 (Greaves et al. 2008; Greaves et al. 2009).

Not only are structural features of DHHCs important for substrate specificity, but the substrates themselves also possess features that influence which DHHCs palmitoylates them. It has been demonstrated for SNAP25 that it is palmitoylated by DHHC3, DHHC7 and DHHC17 (Fukata et al. 2006). The sequence downstream of the palmitoylation site within SNAP25 is important for directing palmitoylation by DHHC17 (Greaves et al. 2009). Although this region is important for directing DHHC17, it is not required for palmitoylation by DHHC3 and DHHC7 of SNAP25. Supporting this data, Src homology 4 (SH4) domain purified from Vac8 was palmitoylated by not only Pfa3 but also by other DHHC proteins (Nadolski & Linder 2009), thus suggesting that regions outwith acylation sites contribute to DHHC substrate specificity. It is emerging that DHHC-substrate interactions involve palmitoylation of target cysteine residues in the substrate and the DHHC domain, as well as interactions between other sites/domains present within both proteins (Greaves & Chamberlain 2010).

### ii Thioesterases

In addition to enzymes that catalyse the addition of palmitate to target proteins, enzymes that remove it are involved in the control of palmitoylation. To date, relatively few proteins that are involved in depalmitoylation have been identified. Only a few acyl protein thioesterases (commonly referred to as thioesterases) have been identified to catalyse depalmitoylation (Hornemann 2014). Acylprotein thioesterase-1 (APT1) was originally isolated from rat liver as a lysophospholipase (Sugimoto et al. 1996), but it was later shown to have a preference for palmitoylated proteins (Duncan & Gilman

1998; Zeidman et al. 2009). APT1 is a cytosolic protein with widespread tissue distribution (Toyoda et al. 1999). It removes palmitate from proteins on the cytosolic surface of membranes (Linder & Deschenes 2007). APT1 has demonstrated lysophospholipase activity towards palmitoylated glycerol-3-phosphocholine (Sugimoto et al. 1996) and can remove palmitate from Giα, H-Ras and endothelial nitric-oxide synthase (Duncan & Gilman 1998; Yeh et al. 1999; Linder & Deschenes 2007; Duncan 2002). In yeast cell deficient in an APT1 homologue, deacylation of Giα is decreased (Duncan 2002). Infusion of APT1 protein caused 50% reduction in steady state palmitoylation and reduced $G\alpha_q$ palmitoylation and membrane association in permeabilised platelets (Sim et al. 2007). Co-expression of APT1 with eNOS results in increased levels of eNOS depalmitoylation compared to eNOS alone (Yeh et al. 1999). Dislocation of SNAP-23 from plasma membrane has been reported upon increasing APT1 levels in cells (Sim et al. 2007).

To date, no consensus motif has been described to target thioesterases (Zeidman et al. 2009). Based on data discussed previously, APT1 is promiscuous in the substrates it depalmitoylates. APT1 can depalmitoylate structurally different substrates, soluble intracellular proteins as well as integral membrane proteins (Zeidman et al. 2009). Despite its promiscuity, APT1 does display specificity towards substrates it depalmitoylates. Caveolin, an integral membrane protein which is palmitoylated on cysteine residues within its intracellular C-terminal domain (Dietzen et al. 1995), is not depalmitoylated by APT1 under conditions where eNOS depalmitoylation is reported (Yeh et al. 1999). Furthermore, substrates are not depalmitoylated with similar efficiencies. Rat APT1 has been reported to be 10-fold more efficient at depalmitoylating $G\alpha_{i1}$ compared to Ras (Zeidman et al. 2009), which is more pronounced in yeast APT1 (Duncan 2002). Activation status of substrates may influence catalytic efficiency of APT1; free $G\alpha_{i1}$ is more readily depalmitoylated than heterotrimeric $G\alpha_{i1}$ (Duncan 2002).

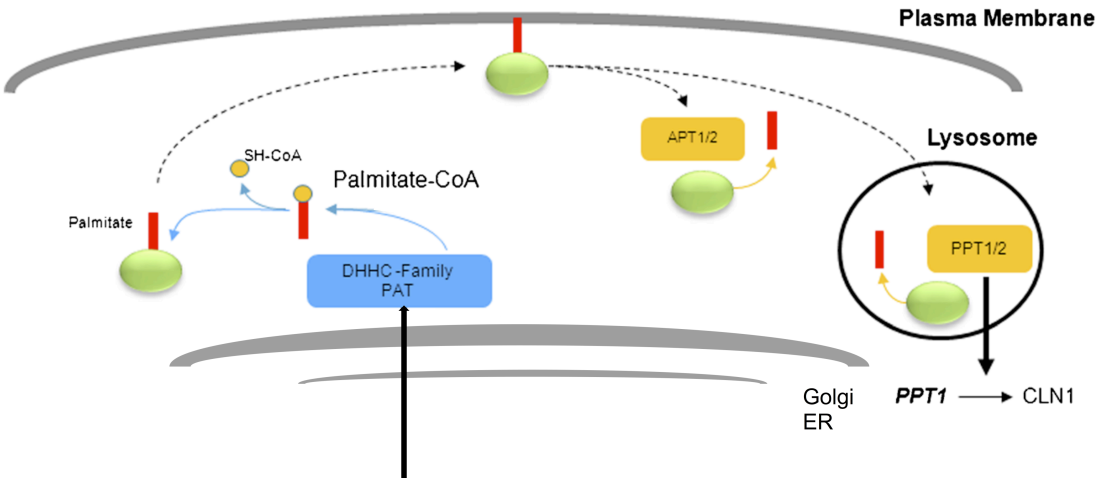


***Figure 1.14: Schematic Representation Of Thioesterases.*** *Schematic demonstrating interplay between DHHCs and acyl protein thioesterases. Modified from (Hornemann 2014).*

An alternative explanation for variation in substrate specificity of APT1 could be due to selectivity of fatty acids linked to substrates (Zeidman et al. 2009). Semliki Forest virus (SFV) protein E2 and influenza virus protein HEF are acylated with palmitic and stearic acid respectively, and are strong APT1 substrates. In contrast, SFV E1 protein, which is mainly modified with palmitate (Veit et al. 1996), is a poor APT1 substrate (Veit & M. F. G. Schmidt 2001). These results suggest that APT1 does not demonstrate preference for fatty acid chain length in order to depalmitoylate substrates. Recently, an APT1 inhibitor, palmostatin B was developed, shown to affect Ras localisation and signalling (Dekker et al. 2010). Following palmostatin B treatment, H- or N-Ras relocalise from the plasma membrane to endomembrane compartments and growth-factor induced activation of Ras on the Golgi is blunted. Palmostatin B could be useful for studying the role of APT1 in cells.

The crystal structure of APT1 has been solved (Devedjiev et al. 2000). This revealed that APT1 is a member of the large family of α/β hydrolases and has a classical triad composed of Ser114, His203 and Asp169 in APT1 (Devedjiev et al. 2000). A Blast search of APT1 sequence reveals homologues in a wide variety of species, including humans and other mammals as well as lower organisms (Zeidman et al. 2009). Thus, the conservation of APT1 throughout evolution indicates an essential role for this thioesterase.

APT2 is a homolog of APT1 and shows 64% amino acid sequence homology (Toyoda et al. 1999). Similar to APT1, APT2 mRNA has been reported in several different tissues, suggesting widespread, ubiquitous expression (Toyoda et al. 1999). APT2 has been reported to depalmitoylate GAP-43 (Tomatis et al. 2010). Singly acylated GAP-43 were deacylated faster than doubly acylated counterparts, which was not catalysed by APT1. APT2 has also been shown to depalmitoylate H-Ras (Rusch et al. 2011). Despite evidence showing that APT1 and APT2 are capable of depalmitoylating proteins, there is little data on the mechanism by which this is achieved. A recent study showed that APT1 and APT2 are themselves palmitoyated and inhibiting palmitoylation affected their membrane localisation as well as that of substrates (Kong et al. 2013). APT1 catalyses self-depalmitoylation, and that of APT2, thus promoting dynamic palmitoylation of both thioesterases. Inhibition of APT1 with palmostatin B results in increased membrane association of APT2. In constrast, inhibition or knockdown of ATP2 had no effect on APT1. It is likely that more thioesterases remain to be discovered and studied in depth.

Palmitoyl-protein thioesterase 1 (PPT1) has been reported to depalmitoylate proteins via thioesterase activity. PPT1 is located in lysosomes and depalmitoylates substrates during the process of protein degradation, therefore is unlikely to be involved in dynamic palmitoylation (Hellsten et al. 1996; Verkruyse & Hofmann 1996). PPT1 has been shown to interact with F(1)-complex of mitochondrial ATP synthase and levels of F(1) α and β subunits were increased in PPT1-deficient mice (Lyly et al. 2008). PPT1 was isolated from bovine brain extracts based on its ability to depalmitoylate [$^{3}$H]-palmitate-labeled H-Ras (Camp & Hofmann 1993). In addition to H-Ras depalmitoylation, PPT1 was shown to depalmitoylate Gα subunits and acyl Co-As *in vitro*, showing preference for carbon chain lengths between 14 and 18 (Soyombo & Hofmann 1997). Interestingly, mutations within the PPT1 gene were found to be associated with infantile neuronal ceroid lipofuscinosis (INCL) (Vesa et al. 1995). Accumulation of granular deposits inside cells is associated with INCL, and [$^{35}$S]cysteine-labeled lipid thioesters accumulated in immortalized lymphoblasts from INCL patients, which was reversed by adding recombinant PPT1 (Lu et al. 1996). Recombinant PPT1 was taken up by cells and trafficked to lysosomes (Hellsten et al. 1996), supporting the normal function of PPT1, which is to depalmitoylate proteins as they are degraded.

PPT2 is a homlog of PPT1 that shares 18% identity at the amino acid level (Soyombo & Hofmann 1997). PPT2 has comparable thioesterase activity to PPT1, and is also a lysosomal enzyme. Unlike PPT1, PPT2 does not remove palmitate from palmitoylated proteins that serve as substrates for PPT1. PPT2 shows specificity for palmitoyl-CoA, indicating a novel role in hydrolysis of lipid thioesters in lysosomes (Soyombo & Hofmann 1997).

### iii Hydrolases

APT1 is a member of the α/β-hydrolase domain (ABHD) family. The ABHD family contains at least 19 proteins and is part of a superfamily of proteins that contain an α/β-hydrolase fold (Ollis et al. 1992). The α/β-hydrolase fold is composed of 8 β-strands, with the second strand being anti-parallel (Lord et al. 2013). These β-strands form a core β-sheet, surrounded by helices and loops connecting the β-strands. The hydrolase activity is due to a catalytic triad of nucleophile-acid-histidine residues, located on loop regions. Nucleophilic residues, such as serine, cysteine or aspartic acid are located in a tight loop, known as the nucleophilic elbow following β5 strand. The nucleophilic elbow can be identified by a Sm-X-Nu-X-Sm consensus motif, where Sm is a small reside, X is any residue and Nu is the nucleophilic residue (Nardini & Dijkstra 1999). This motif is GXSXG in most ABHD members. The acidic residue is predominantly either a glutamate or aspartate, located after strand β7. The histidine residue within the catalytic triad is conserved between ABHD proteins (Nardini & Dijkstra 1999) and is located in a variable loop following the final β strand. The majority of ABHD proteins contain a conserved His-XXXX-Asp motif, which has previously been linked to acyltransferase activity (Ghosh et al. 2008; Montero-Moran et al. 2010). As a result, several ABHD have been predicted to have both hydrolase and acyltransferase activity. In a study to characterise dynamic protein palmitoylation, targets of hexadecyl fluorophosphonate (HDFP), a candidate probe for depalmitoylating enzymes, were identified. Several ABHD proteins were shown to interact with HDFP (Martin et al. 2011). The authors argue that interaction with HDFP identifies hydrolases that show preference for lipid substrates. However, ABHD show diverse function, therefore it is unlikely that all share similar functional activity. Further study will be required to determine substrates for these enzymes and whether they are truly involved in depalmitoylating palmitoylated proteins.

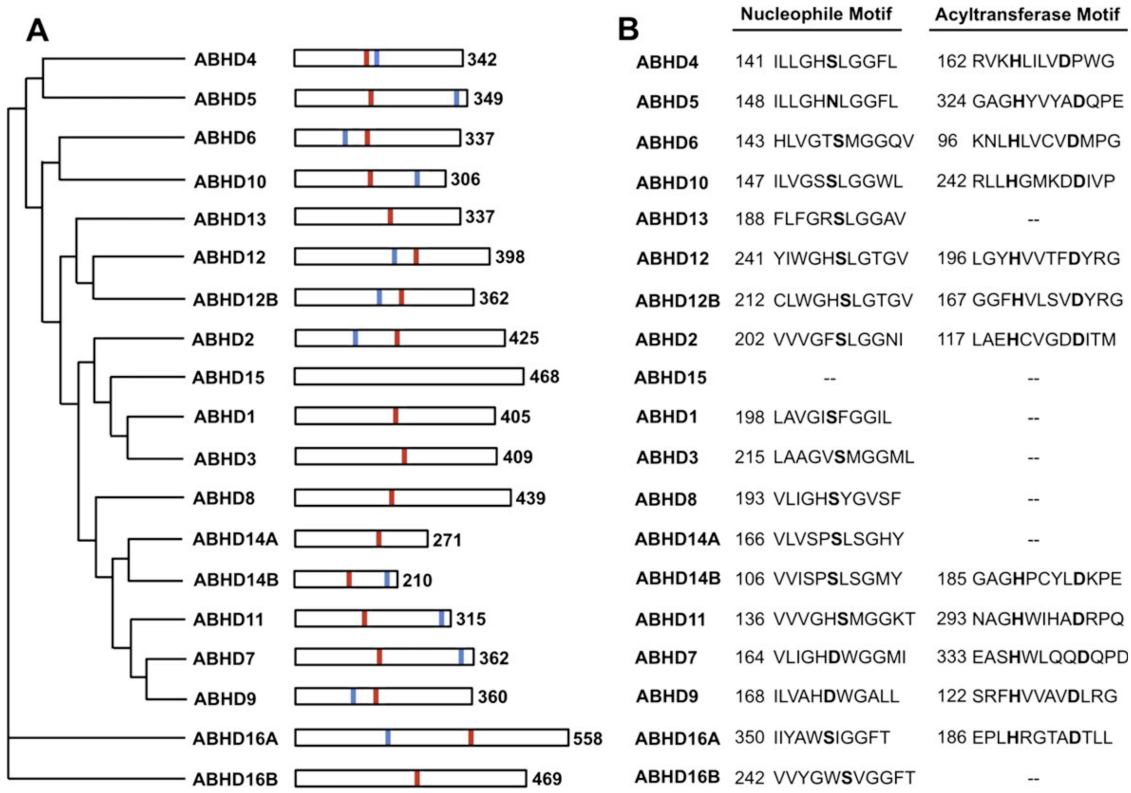


***Figure 1.15: Human ABHD Family. A.*** *Phylogenic relationship of ABHD proteins, based on Clustal W alignment. Numbers are indicative amino acid number in full-length protein. Red lines – predicted active site nucleophile, blue lines – predicted acyl transferase motif (HXXXXD).* ***B.*** *Conserved nucleophilic and acyltransferase motifs. -- indicates where the acyltransferase motif is absent. Modified from (Lord et al. 2013).*

### 1.2.3 Palmitoylation And Role In Control Of Protein Biology

Large-scale profiling studies revealed that the number of proteins that undergo palmitoylation varies from ~50 in yeast (Roth et al. 2006) to several hundred in mammals (Martin & Cravatt 2009; W. Yang et al. 2010). Palmitoylation has been reported for both soluble and transmembrane proteins, and the list of target proteins is expanding. A number of key cellular functions have shown to be affected by palmitoylation, such as membrane targeting, membrane cycling, regulation of activity and endocytosis.

#### i Membrane Targeting

Palmitoylation has been implicated in the trafficking of proteins between intracellular organelles and in the segregation or clustering of proteins within membrane

compartments (Linder & Deschenes 2007). Due to the localisation of DHHCs to membranes, palmitoylation must occur at membranes. Therefore, proteins that are palmitoylation targets must interact with the membrane at least transiently (Smotrys & Linder 2004). Following palmitoylation, stable membrane association is promoted. Palmitoylation is often found with N-myristoylation or prenylation to regulate membrane interactions of soluble proteins (Salaun et al. 2010). N-myristolylation or prenylation of target proteins acts to increase hydrophobicity and promote membrane association, however single lipid modifications are only sufficient for transient membrane interactions (Shahinian & Silvius 1995). Two closely positioned lipid modifications, however, promotes stable membrane association (Shahinian & Silvius 1995). Therefore, at the cellular level, myristolyation and prenylation may act to facilitate transient membrane association to enable interaction with membrane-bound DHHCs and allow palmitoylation to occur. As a result, palmitoylation is essential for stable membrane attachment of several proteins, such as farnesylated Ras and myristoylated Gα subunits (Hancock et al. 1990; Linder et al. 1993; Parenti et al. 1993). However, several soluble proteins are exclusively modified by palmitoylation. Therefore it has been suggested that these proteins rely on intrinsic weak membrane affinity for transient membrane association to enable interaction with DHHCs and thus palmitoylation.

For a number of proteins, palmitoylation appears to serve as a signal for rentention in the Golgi or ER or as a cue to traffic substrates to membranes (Greaves & Chamberlain 2007). In the case of AMPA receptors, in which all subunits are palmitoylated, palmitoylation at 1 site was enhanced by overexpressed of DHHC3, resulting in Golgi accumulation of the receptor and decreased cell surface expression (Hayashi et al. 2005). This suggests that preferential palmitoylation at this site promotes retention of the receptor in the Golgi. Interestingly, this effect of palmitoylation on targeting of proteins is not restricted to AMPA receptors. Palmitoylation of PSD-95 at 2 N-terminal cysteines is required for trafficking to the synaptic membrane (Craven et al. 1999; El-Husseini et al. 2000) and disruption of dual palmitoylation of PSD-95 blocks ion channel clustering mediated by PSD-95. Similarly, palmitoylation of γ2 subunit of $GABA_A$ receptors by DHHC3 has been demonstrated to regulate membrane trafficking (Keller et al. 2004). As with PSD-95 and γ2 subunit of $GABA_A$ receptors, human δ opioid receptor is palmitoylated at 2 sites and is dynamically regulated at one of these sites (Petaja-Repo et al. 2006). Inhibition of palmitoylation with 2-BP results in

decreased cell surface expression, suggesting that palmitoylation is required for efficient intracellular transport. These results suggest that palmitoylation is required for biosynthetic delivery of substrates to the plasma membrane. For mucin-like MUC1 protein, palmitoylation at 2 cysteine residues is not required for targeting to the cell surface, but is linked to trafficking from recycling endosomes to the plasma membrane (Kinlough et al. 2006). Utilising an ω-alkynyl fatty acid analogue, Wnt and Sonic Hedgehog (Shh) were shown to be palmitoylated and that membrane association of these proteins was promoted by palmitoylation (Gao et al. 2011). In a similar manner, palmitoylation of GAP43 is required for its membrane targeting (Gauthier-Kemper et al. 2014). Palmitoylation, in this instance, tags GAP43 for global sorting via exocytic vesicles. It was also demonstrated that phosphorylation of palmitoylated GAP43 regulates its mobility and plasma membrane targeting.

### ii Membrane Cycling

The best studied example of palmitoylation regulating membrane cycling are the Ras oncogenic proteins. Ras membrane targeting is dependent on the C-terminus of the protein, which includes the CaaX box and a hypervariable domain that contains a palmitoylation site or a polybasic residue (Wright & Philips 2006). N-Ras and H-Ras are palmitoylated following targeting to the ER (Linder & Deschenes 2007). The secretory pathway and a functional Golgi are required for plasma membrane localisation of N-Ras and H-Ras. Appropriate trafficking of N-Ras and H-Ras requires palmitoylation. N-Ras is palmitoylated on a single cysteine residue, which is sufficient for trafficking to the plasma membrane from the ER. H-Ras, however, can be palmitoylated on one or both of two cysteine residues, Cys181 and Cys184 (Roy et al. 2005). Palmitoylation of Cys184 results in Golgi localisation of H-Ras. In contrast, palmitoylation of Cys181 causes plasma membrane localisation to cholesterol-rich micro-domains (Linder & Deschenes 2007). These results suggest that site-specific palmitoylation of H-Ras can influence trafficking and microdomain localisation. In addition to microdomain localisation, differential palmitoylation of N-Ras and H-Ras governs distinct Golgi sub-compartment localisation (Lynch et al. 2014). Doubly-palmitoylated H-Ras is distributed throughout the Golgi, whereas singly palmitoylated N-Ras is confined to the *trans* Golgi. Singly palmitoylated H-Ras shows a similar Golgi localisation to that of singly palmitoylated N-Ras. Conversely, doubly palmitoylated N-Ras showed Golgi localisation similar to wild-type H-Ras (Lynch et al. 2014).

Palmitoylation of Ras proteins is highly reversible, with half life ranges from 20 minutes to 2 hours for H-Ras (Magee et al. 1987; Lu & Hofmann 1995; Baker et al. 2003). The role of dynamic palmitoylation was elegantly demonstrated using quantitative fluorescence microscopy and photobleaching techniques (Rocks et al. 2005; Goodwin et al. 2005). Palmitoylated Ras isoforms are found at the plasma membrane, whereas depalmitoylated forms are found predominantly at the ER and the Golgi (Apolloni et al. 2000; Choy et al. 1999). Using fluorescence recovery after photobleaching (FRAP), Golgi-localised Ras was repopulated by rapid exchange rather than by a vesicle mediate mechanism (Rocks et al. 2005). The rapid replacement of Ras by a non-vesicle mediated mechanism was reminiscent of nonpalmitoylated Ras, suggesting interconversion of Ras between palmitoylated and depalmitoylated states. In addition, fluorescently-labelled N-Ras coupled to farnesylated peptides with reversible palmitoyl thioester-linkage resulted in wild-type N-Ras associating with the Golgi and plasma membrane (Rocks et al. 2005). In contrast, N-Ras coupled to farnesylated peptides with non-cleavable hexadecyl group resulted in non-specific membrane association. These results suggest that palmitoylation is required for correct subcellular targeting of Ras, and that depalmitoylation is also required for Ras trafficking.

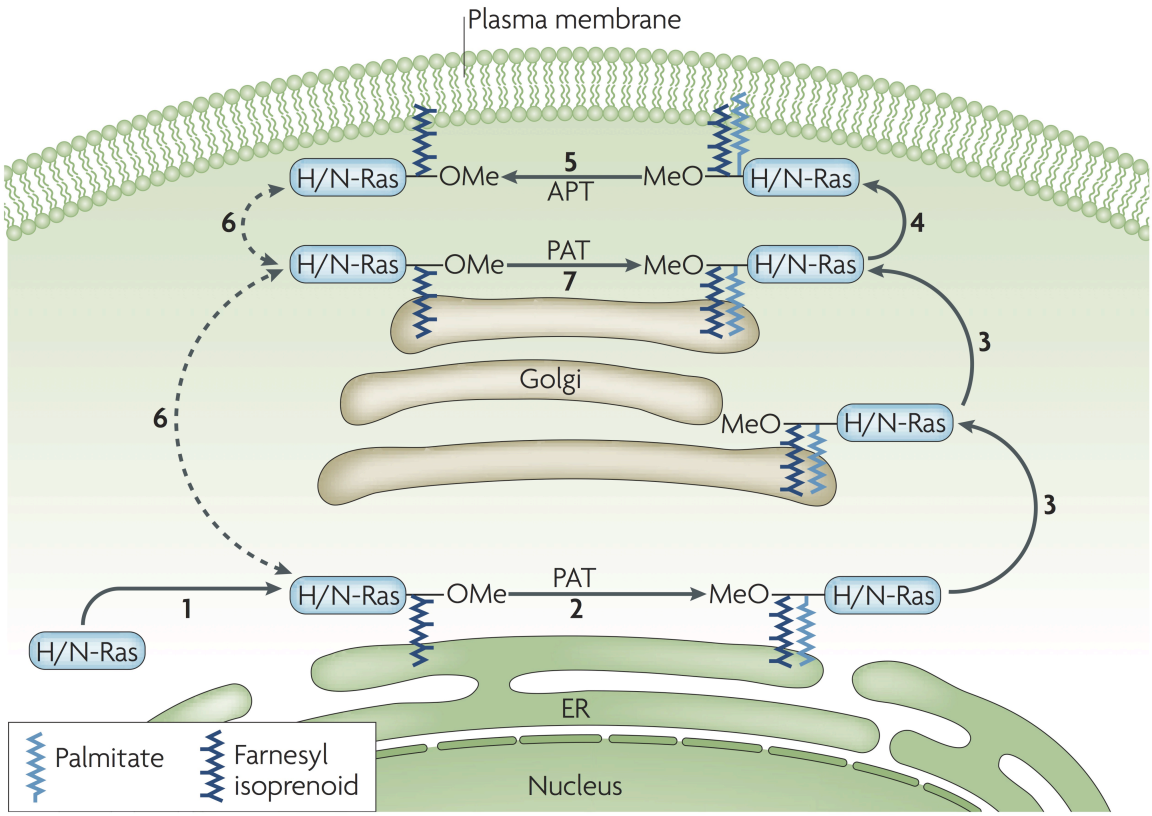


***Figure 1.16: Palmitoylation And Depalmitoylation Are Required For Ras Trafficking.*** *1: Farnesylation targets H/N-Ras to the ER. Post-prenylation processing of CaaX box results in C-terminal farnesyl carboxymethylester (OMe). 2: H/N-Ras is palmitoylated. Dual modified H/N-Ras can traffic to the Golgi (3) and the plasma membrane (4) via the classical secretory pathway. 5: H/N-Ras can be depalmitoylated by thioesterases at the plasma membrane, causing rapid non-vesicular exchange with endomembranes (6). 7: H/N-Ras may be trapped on the Golgi by another PAT. The palmitoylation cycling accounts for dynamic subcellular trafficking of Ras by vesicular (solid arrows) and non-vesicular (dashed arrows) pathways. Modified from (Linder & Deschenes 2007).*

### iii Regulation Of Ion Transport

Recent advances in proteomic approaches to characterise protein palmitoylation has revealed an important role for palmitoylation in the regulation of various ion channels and transporters (Shipston 2011). Plasma membrane localisation of ion channels is dependent on interplay between channel synthesis, trafficking to membrane and internalisation, recycling and degradation. Palmitoylation influences this cycle by acting at distinct stages of the trafficking pathway (Shipston 2011). For some channels, such as

voltage-gated Na (Nav1.2) (J. W. Schmidt & Catterall 1987) and potassium (Kv1.5) (Zhang et al. 2007), palmitoylation has been reported to occur early in the biosynthetic pathway and regulates channel maturation. In case of nicotinic acetylcholine receptors, palmitoylation is involved in formation of ligand binding sites (Alexander et al. 2009; Drisdel et al. 2004). Blocking palmitoylation with 2-bromopalmitate results in loss of ligand binding sites. Failure to form ligand binding sites in the absence of palmitoylation of $\alpha_4\beta_2$ and $\alpha_7$ subtypes suggests that palmitoylation occurs during subunit assembly and regulates formation of binding sites (Alexander et al. 2009). The role of palmitoylation on membrane targeting of ion channels varies from channel to channel. NMDA receptors, which have 2 distinct clusters of palmitoylation sites within their C-terminal region, are regulated in different ways depending on the site of palmitoylation (Hayashi et al. 2009). Palmitoylation within the first cluster of cysteine residues increases phosphorylation by Src protein tyrosine kinases, thus promoting stable membrane expression of NMDA receptors. In contrast, palmitoylation of the second cluster results in accumulation of receptors within the Golgi and thus reduces membrane expression. These results suggest that palmitoylation is capable of differential regulation of NMDA-receptor trafficking, which may be important for synaptic plasticity (Hayashi et al. 2009). Similarly, palmitoylation of AMPA receptors on TMD2 results in accumulation in the Golgi and decreased membrane expression (Hayashi et al. 2005), whereas palmitoylation on a C-terminal site decreases interaction with 4.1N protein and regulates AMPA- and NMDA-induced AMPA receptor internalisation. However, this is not the case for all ion channels. Palmitoylation of BK channels regulates cell-surface targeting but is not essential (Jeffries et al. 2010).

In addition to regulation of membrane trafficking of ion channels, palmitoylation also governs spatial organisation once at the plasma membrane. The mammalian water channel aquaporin-4 (AQP4) assemble into square arrays and mediate bidirectional water transport across membranes (Suzuki et al. 2008). However, only the shorter isoform forms these square arrays. The longer form AQP4M1 possesses 2 palmitoylation sites at its N-terminus. Mutation of these residues resulted in square array formation by AQP4M1, suggesting palmitoylation prevents it from forming square arrays (Suzuki et al. 2008). P2X7, an ATP-gated channel, requires palmitoylation to be targeted to lipid rafts (Gonnord et al. 2009). Abolition of P2X7 palmitoylation results in a decrease in cell surface expression and ER retention and promotes proteolytic degradation. In the case of P2X7, the palmitoylated form is found

in detergent-resistant membranes. This suggests that palmitoylation is involved in targeting P2X7 to lipid rafts (Gonnord et al. 2009). In neurons, palmitoylation has been shown to play a role in the synaptic clustering of ion channels, as well as their agonist-induced internalisation (Shipston 2011). Palmitoylation of γ2 subunit of neuronal $GABA_A$ receptors is involved in membrane targeting as well as synaptic clustering. Mutational or pharmacological inhibition of palmitoylation resulted in decreased synaptic clustering of $GABA_A$ receptors and steady-state membrane localisation (Rathenberg et al. 2004). As mentioned previously, palmitoylation regulates agonist-induced internalisation of AMPA receptors (Hayashi et al. 2005). The pool of palmitoylated GluR2 subunits increased in response to acute AMPA or NMDA treatment, but not GluR1 (G. Yang et al. 2009). Therefore, these results suggest that palmitoylation of AMPA receptors is a subunit-specific process that plays a role in its regulation and trafficking.

Despite a number of studies examining the effect of palmitoylation on membrane targeting and spatial organisation of a number of ion channels, few studies have elucidated the effect of palmitoylation on activity (Shipston 2011). Palmitoylation of voltage sensitive Kv1.1 channel revealed a role for palmitoylation in the regulation of channel activity (Gubitosi-Klug et al. 2005). Kv1.1 is palmitoylated within an intracellular linker domain between TMDs 2 and 3 at Cys243. Mutation of this cysteine results in a 20-mV leftward shift in the current-voltage relationship of the channel, compared to wild-type. The authors argue that this is due to palmitoylation modulating voltage sensing via protein-membrane interactions (Gubitosi-Klug et al. 2005). Palmitoylation was demonstrated to regulate epithelial $Na^+$ channels (Mueller et al. 2010). Abolition of palmitoylation of β subunits at Cys43 and Cys557 by mutagenesis showed significantly decreased amiloride-sensitive whole cell currents. In addition, $Na^+$-inhibition was enhanced and open probability was reduced compared to wild-type ENaC (Mueller et al. 2010). Finally, palmitoylation of β2a subunit of $Ca_v2.2$ channels is involved in the voltage-dependent inactivation of this channel. Blockade of palmitoylation via mutagenesis of palmitoylated cysteine residues reduces the voltage-dependent inactivation mediated by β2a subunit (Stephens et al. 2000). Thus, it appears that palmitoylation can regulate activity of target ion channels, presumably by either modulating their interaction with the membrane or by changing their structure thus impacting their activity.

Interestingly, for several ion channels and transporters, palmitoylation has been shown to influence regulation by other post-translational modifications. It was demonstrated in GluR6 kainate receptors that palmitoylation influenced regulation by phosphorylation (Pickering et al. 2005). Unpalmitoylated mutant GluR6 served as a better substrate for PKC-mediated phosphorylation. Similarly, palmitoylation inhibited PKC-mediated phosphorylation of GluR1 subunits of AMPA receptors (Lin et al. 2009). The disruption of phosphorylation in both cases is likely due to steric hindrance as the palmitoylated cysteine is adjacent to the consensus phosphorylation site. Conversely palmitoylation can promote phosphorylation. Fyn-dependent tyrosine phosphorylation of NR2A subunit of NMDA receptors is lost upon mutation of palmitoylated residues (Hayashi et al. 2009). As a result, NMDA receptors are prone to internalisation, which is prevented upon enhancement of phosphorylation by palmitoylation. In addition, the cardiac $Na^+/K^+$ ATPase is also regulated indirectly by palmitoylation of its accessory protein, phospholemman (PLM) (Tulloch et al. 2011). Palmitoylation of PLM results in inhibition of $Na^+/K^+$ ATPase. In addition, phosphorylation of PLM at Ser68 promotes its palmitoylation, which is lost upon mutation of Ser68. Phosphorylation of PLM has historically been reported to enhance $Na^+/K^+$ ATPase activity (Fuller et al. 2004; Fuller et al. 2009; Fuller et al. 2012). Therefore it is surprising that phosphorylation of PLM results in increased palmitoylation. It is hypothesised that phosphorylation enhances the mobility of the intracellular domain of PLM, thus making it more accessible to PATs (Tulloch et al. 2011). Cross-talk between phosphorylation and palmitoylation also occurs for the BK channel. Palmitoylation of a dicysteine motif in an alternative spliced C-terminal STREX domain, promotes association of this domain with the plasma membrane (Tian et al. 2008). PKA phosphorylation of a serine upstream from this region results in dissociation of STREX from the plasma membrane, thus leading to channel inhibition. Not only does palmitoylation influence ion channel targeting, but also activity and its regulation by other post-translational modifications.

### iv Massive Endocytosis (MEND)

Recently, a novel role for palmitoylation was described. A newly discovered form of endocytosis, termed massive endocytosis (MEND) was shown to be regulated by palmitoylation (Hilgemann et al. 2013; Lin et al. 2013). MEND was demonstrated to be initiated by excessive influx of $Ca^{2+}$ and to occur during cell wound healing response (Corrotte et al. 2013). The major characteristic of MEND is internalisation of large

portions of ordered plasma membrane, up to 50% (Lariccia et al. 2011). In response to stimulation of NCX1 outward exchange current (influx of $Ca^{2+}$ ions), resulting in mitochondrial membrane depolarisation, formation of permeability transition pores (PTPs) was initiated. As a result of mitochondrial PTPs opening, Coenzyme A is released into the cytoplasm (Hilgemann et al. 2013). Increases in cytoplasmic CoA results in synthesis of Acyl-CoA, providing substrates for DHHC enzymes. This increases palmitoylation of transmembrane proteins and promoting their clustering into ordered domains. Thus an increase in ordered domains to a critical size triggers MEND. In addition, metabolites that promote PTP opening rapidly initiate MEND. Depletion of cellular fatty acids by addition of fatty-acid free BSA suppressed MEND in BHK fibroblast cells. Surprisingly, inhibition of palmitoylation with 2-BP results in inhibition of MEND by ~70%, supporting a role for palmitoylation in the reaction pathway that triggers MEND (Hilgemann et al. 2013). In addition, siRNA knockdown of DHHC5 from BHK fibroblasts results in blockade of MEND. This suggests that generation of cytoplasmic acyl CoA promotes palmitoylation of substrates by DHHC5. However, addition of CoA alone was not sufficient to induce MEND, only when added in the presence of PKC activators or $H_2O_2$, both activated by $Ca^{2+}$ influx, in MEND observed. PKC activation or $H_2O_2$ release is predicted to increase palmitoylation site availability and thereby perpetuating MEND (Hilgemann et al. 2013).

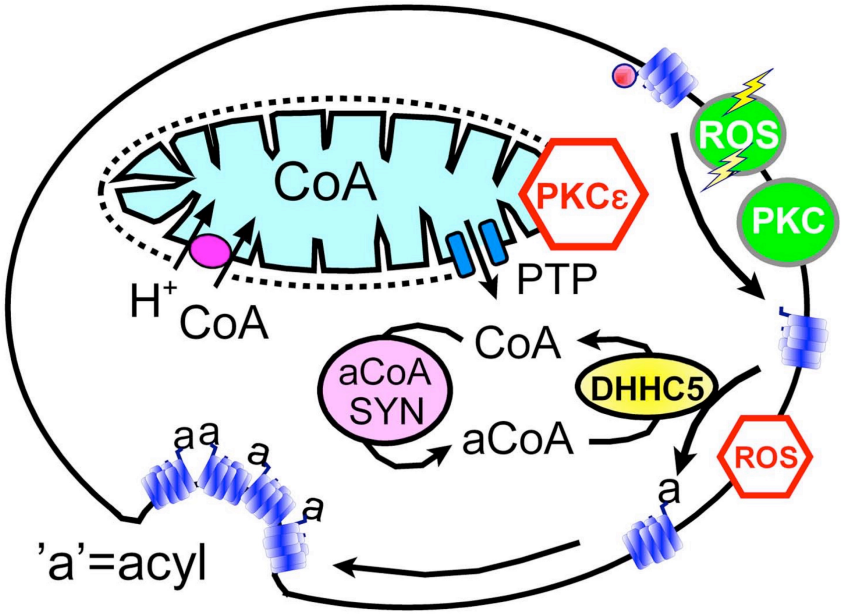


***Figure 1.17: Hypothetical MEND Pathway.*** *In response to membrane depolarisation, mitochondrial PTPs open and release CoA into the cytoplasm. CoA is metabolised to acyl CoA, which serves a substrate for DHHC5. This results in palmitoylation of transmembrane proteins, which causes them to cluster. Upon reaching a critical point, this clustering of proteins causes internalisation of the surface membrane via MEND. Modified from* (Hilgemann et al. 2013).

In addition to MEND in BHK fibroblasts, a physiological context was also examined (Lin et al. 2013). Acute ischemic events are becoming an increasingly prevalent cause of death. Surprisingly, most of the damage caused by ischemia occurs during reoxygenation of the tissue, as mitochondria generate reactive oxygen species (ROS) at an increased rate (Jennings 2013). A key characteristic of reperfusion injury is the swelling of mitochondria and opening of PTPs, ultimately leading to cell death. Given the evidence described above, the authors sought to determine whether MEND played a key role in reperfusion injury following ischemia. Using mouse right ventricular (RV) cardiac strips, MEND was initiated during reoxygenation of anoxic muscle (M. J. Lin et al. 2013). Additionally, MEND was accompanied by an increase in palmitoylation. MEND could be blocked in these experiments by treatment of cardiac tissue with agents that protect the heart from reperfusion injury, such as cyclosporine and adenosine. Furthermore, mouse RV strips from gene-trapped DHHC5 (DHHC5-GT) mice, in which DHHC5 expression is almost absent, subjected to ischemia-reperfusion show decreased MEND. This is associated with a decrease in palmitoylation of known DHHC5 targets, namely PLM and flotillin-2. Finally, DHHC5-GT mice show increased

contractile responses post ischemia, compared to WT controls. This suggests that down-regulation of palmitoylation may mimic preconditioning (Lin et al. 2013). Thus it appears that internalisation of sarcolemmal membrane during ischemia-reperfusion may contribute to acute death of cardiac function during such episodes.

## 1.3 Project Aims

Palmitoylation is becoming an increasingly important post-translational modification, regulating a wide variety of proteins and their activity. Currently, the cardiac palmitoyl proteome is uncharacterised and the effect of palmitoylation largely unexplored. Given the important role of ion homestasis within cardiac muscle to maintain efficient cardiac function, regulation of the molecular players involved merits further study. NCX1 is involved in the removal of $Ca^{2+}$ following contraction. Although regulation of NCX1 by the ion transporters as well as $PIP_2$ regulation has been well studied, regulation by post-translational modifications has not. To date, palmitoylation of NCX1 has not been documented, nor the effect on its activity.

This study examines palmitoylation of NCX1 and the functional consequences thereof. Palmitoylation of NCX1 in cardiac tissue will be verified, followed by mass spectrometry analysis to determine other palmitoylated proteins within cardiac muscle. Additionally, using mass spectrometry and site-directed mutagenesis, palmitoylation site(s) within NCX1 will be elucidated. In addition to determining the cardiac palmitoyl proteome, control of palmitoylation via expression of DHHCs within cardiac muscle will be investigated. As with all novel findings, a functional role must be established. Whether palmitoylation functionally affects NCX1 activity will be determined. Finally, given the role of NCX1 in cardiovascular disease, whether palmitoylation of NCX1 is differentially regulated in *in vivo* models of heart failure will be elucidated.

# Chapter 2: Materials and Methods

## 2.1 Chemicals And Reagents

All general chemicals were of highest grade available and obtained from Sigma Aldrich (Gillingham, Dorset, UK) and Fisher Scientific (Loughborough, Leicestershire, UK) unless otherwise stated.

## 2.2 Ethics Statement

All work involving animals was undertaken using a method designated Schedule 1 of the Animals (Scientific Procedures) Act 1986. Experiments approved by local ethical review board.

## 2.3 Adult Rat Ventricular Myocyte Isolation

### 2.3.1 Myocyte Isolation

Ventricular myocytes were isolated by retrograde perfusion in the Langendorff mode. Prior to cardiac excision, the Langendorff apparatus was switched on and water jacketed solution reservoirs were warmed to 37°C. Solutions in Table 2.1 were prepared and solutions 1, 2 and 3 (without collagenase) were added to individual solution reservoirs and allowed to equilibrate to 37°C. Additionally, 50 ml aliquots of solution 1 were stored at -20°C to allow the solution to cool, which is used following excision to preserve cardiac function.

Male adult Wistar rats, weighing 250g to 300g, were terminated in accordance with Schedule 1 procedures as set by the UK Home Office. Rats were terminated by cervical dislocation following intraperitoneal injection with 200mg/ml $Na^+$ pentobarbital (Euthatal, Merial, UK). Hearts were excised as quickly as possible to minimise ischemia. Following excision, hearts were immediately immersed in ice cold buffer 1 (See table 1) to lower oxygen demand. Hearts were cannulated via the aorta, with 3.5ml per minute of buffer 1 being pumped by a peristaltic pump. Once cannulated, the flow of buffer was increased to 10 ml per minute. Once the coronary circulation had cleared from remnants of blood, perfusion was continued with buffer 2, which contains EGTA. The function of the EGTA is to chelate the $Ca^{2+}$ in the heart and prevent contraction.

After 4 minutes, hearts were then perfused with buffer 3 (containing collagenase) for a further 8 minutes.

| **Buffer** | **Constituents** | **pH** |
|---|---|---|
| 10X Myocyte Isolation Buffer | 1300 mM NaCl<br>54 mM KCl<br>14 mM $MgCl_2$<br>4 mM $NaH_2PO_4$<br>42 mM HEPES | 7.3 |
| Base Buffer | 1:10 dilution of 10X MIB<br>10 mM Glucose<br>20 mM Taurine<br>10 mM Creatine | 7.3 |
| 1 | 1X Base Buffer<br>0.75 mM $CaCl_2$<br>0.001kU/ml Heparin | 7.3 |
| 2 | 1X Base Buffer<br>0.1 mM EGTA | 7.3 |
| 3 | 1X Base Buffer<br>0.1 mM $CaCl_2$<br>0.625 mg/ml Collagenase (Worthington, USA) | 7.3 |
| 4 | 1X Base Buffer<br>1% BSA<br>0.5 mM $CaCl_2$ | 7.3 |
| 5 | 1X Base Buffer<br>1 mM $CaCl_2$ | 7.3 |

***Table 2.1: Cardiac Myocyte Cell Isolation Buffers.*** *Buffers used in the isolation of cardiac myocytes by retrograde collagenase digestion using the Langendorff method.*

During perfusion, buffer 3 was recirculated to save collagenase. After 2 minutes, buffer 3 was collected into a weigh boat. Once 8 minutes had passed, ventricles were cut down and immersed in buffer 3. The heart was cut into small pieces and placed in a 50 ml Falcon tube which was incubated at 37°C, while being bubbled with oxygen for 5-10

minutes. This solution was triturated to assess digestion. Once sufficiently digested, the solution was filtered through 200μM count nylon mesh (Cadisch, UK) into a 50 ml centrifuge tube and left to settle in a water bath at 35°C for 8 minutes. The supernatant was removed and settled cardiac myocytes were slowly resuspended in buffer 4. Cells were allowed to settle in the water bath for 10 minutes, after which supernatant was removed and cells were gently resuspended in buffer 5. Finally, cells were allowed to settle for an additional 10 minutes before the supernatant was removed and fresh buffer 5 was added.

### 2.3.2 Assessment Of Healthy Viable Cells

Cells were assessed for quality and yield. Quality was assessed by eye under a microscope. If >70% of cells were rod-like in shape, it was considered a successful isolation (see Figure 2.1). Yield was assessed using a Bradford Assay measured on a spectrophotometer. Typical yields were approximately 30 mg of protein.

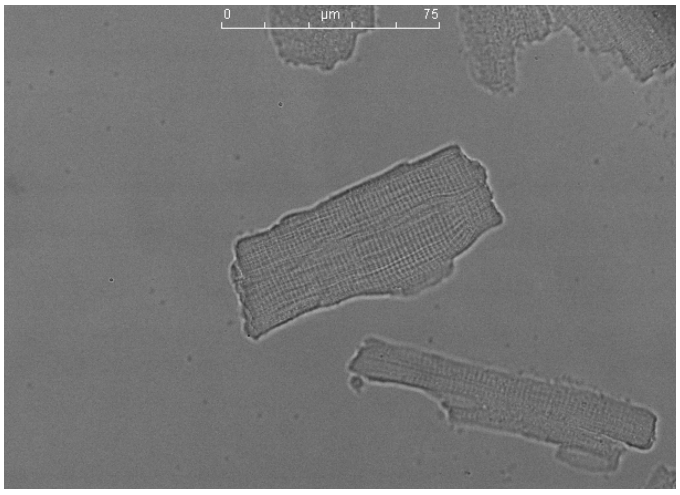


***Figure 2.1: Isolated Adult Rat Ventricular Myocytes (ARVM).*** *Isolated rat ventricular myocytes as assessed by light microscopy. Healthy, $Ca^{2+}$ tolerant myocytes have a straight, rod like morphology. Unhealthy cells are rounded in morphology. Image provided by Dr Jacqueline Howie.*

## 2.4 Cell Culture

### 2.4.1 Culture Conditions

Cell culture reagents were supplied by Gibco™ (Life Technologies, Paisley, UK) and all tissue culture plastics were supplied by Nunc. Cell lines were maintained in the appropriate growth media and supplemented as recommended by ATCC and Life Technologies. In addition, 1% Penicillin/Streptomycin (P/S) was added to culture media for maintenance of stock plates. Cells were grown in vented cap flasks in the presence of 5% $CO_2$ and maintained at 37°C in a water jacketde incubator. All tissue culture practices were carried out in a sterile class II biological safety cabinet. All reagents used were sterile and pre-warmed to 37°C. The cell lines used during the course of this research are indicated in Table 2.2.

### 2.4.2 Subculture Of Cells

All cell lines used were adherent and grown in 75$cm^2$ flasks. Once a monolayer reached ~90% confluency, cells were sub-cultured. Media was removed by aspiration and the cells washed with 5ml sterile Phosphate Buffered Saline (PBS) to remove all traces of growth media. Trypsin-EDTA (2ml) was added and the flask incubated at 37°C for 2-3 minutes until cells detached, visible by microscopy. Growth media (8ml) was added back to the flask and cell triturated to prevent clumping. A proportion of cell suspension was then removed to another flask and the final volume of growth media adjusted to 10ml.

### 2.4.3 Freezing And Revival Of Cell Stocks

Stocks of cells were frozen routinely at low passage (<25) for long-term storage in a liquid nitrogen store. Cells were grown to ~90% confluency and detached using trypsin as previously described (section 2.4.2). Growth media (5ml) was added to cells then transferred to a sterile 15ml centrifuge tube. Cells were pelleted by centrifugation at 1500rpm for 5minutes at room temperature. The supernatant was removed by aspiration and cell pellet resuspended in 6ml of freezing media (90% Fetal Calf Serum (FCS) and 10% of the cryoprotectant dimethyl sulphoxide (DMSO)). Appromixately 1.5ml of cell suspension was added per cryovial (Thermo Scientific, Cat.no.: 363401) and placed in a

cryo freezing vessel and stored at -80°C overnight. This allows cells to be cooled slowly to preserve cell viability. Cryovials were transferred to liquid nitrogen for long-term storage where available otherwise they were stored at -80°C. Upon cell revival, cryovials were thawed rapidly in order to minimise cell damage. Cells were thawed by addition of 5ml of pre-warmed media until cells were completely thawed. Cell suspension was transferred to a 25cm$^2$ vented cap tissue culture flask. Growth media was changed the following day to remove traces of DMSO.

| | Origin | Morphology | Media Composition | Source |
|---|---|---|---|---|
| HEK293 | Human embryonic kidney | Epithelial | DMEM + 10% FCS + 1% P/S | |
| HeLa | Human Cervix Adenocarcinoma | Epithelial | DMEM + 10% FCS + 1% P/S | |
| BHK | Baby Hamster Kidney | Epithelial | DMEM + 2mM L-glutamine + 10% FCS + 1% P/S (w/ sodium pyruvate) | |
| Flp-In™ -293 | Derived from HEK293 | Epithelial | DMEM + 2mM L-glutamine + 10% FCS + 1% P/S + 100ug/ml Zeocin™ | Life Technologies |
| FT293 WT NCX1 | Derived from HEK293 | Epithelial | DMEM + 2mM L-glutamine + 10% FCS + 1% P/S + 100ug/ml Hygromycin + 15ug/ml Blasticidin | |
| FT293 C739A NCX1 | Derived from HEK293 | Epithelial | DMEM + 2mM L-glutamine + 10% FCS + 1% P/S + 100ug/ml Hygromycin + 15ug/ml Blasticidin | |



***Table 2.2: Details Of Cell Lines.*** *Details of all cell line employed in this study, showing their origin, respective morphologies and their media composition.*

## 2.5 Cell Based Assays

### 2.5.1 Transient Transfection Of Cell Lines

Cells were seeded to 70-80% confluency in 6-well or 12-well dishes. In the case of cells for confocal microscopy, cells were seeded on to poly-L-lysine coated coverslips in a 12-well plate. When cells were to be used for biotinylation of cell surface proteins using sulfo-SS-NHS-biotin (see section 2.5.4), wells coated with poly-L-lysine. Briefly, 0.1% (w/v) poly-L-lysine (Invitrogen, UK) was diluted 1:10 with PBS and added to wells then incubated at room temperature for 15 minutes. Wells were washed 3 x with PBS and allowed to dry at room temperature for 10 minutes. Once seeded, cells were left to adhere overnight.

For transient transfection of cells, 1µg of DNA was mixed with 100µl (12-well) or 250µl (6-well) Opti-MEM (Life Technologies, Cat. No.: 31985070). Separately, 4µl (12-well) or 8µl (6-well) per well of Lipofectamine 2000 was added to a sterile tube for each transfection and mixed with 100µl (12-well) or 250µl (6-well) of Opti-MEM and incubated at room temperature for 5 minutes. The Opti-MEM/Lipofectamine 2000 mix was then added to each DNA/Opti-MEM mix, vortexed briefly and incubated at room temperature for 20 minutes. Following incubation, the transfection mix was added to each well and incubated overnight at 37°C. Cells were harvested 16-18 hours post transfection. For transfection experiments with DHHCs, provided by Professor Mike Shipston, see (M. Fukata et al. 2004). Hemagglutinin (HA)-tagged mammalian DHHC clones in pEFBOS-HA were used. DHHS clones were generated by site-directed mutagenesis as described in section 2.10. NCX-YFP clones were generated using the methods described in section 2.9.

### 2.5.2 Generation Of Stable Cell Lines

To generate stable cell lines, the Flp-In™ T-Rex™ System from Life Technologies, which generates a tetracycline inducible cell line, was used. When the pcDNA™5/FRT/TO inducible expression vector containing the gene of interest is cotransfected with pOG44 Flp recombinase expression plasmid into a Flp-In™ T-Rex™ mammalian host cell line, the pcFNA™5/FRT/TO plasmid containing the gene of

interest is inserted in a Flp recombinase-dependent manner into the genome of the target cell. The FRT/TO expression plasmid contains a hygromycin resistance gene, that after homologous recombination confers hygromycin resistance to the resultant cell line (see figure 2.2).

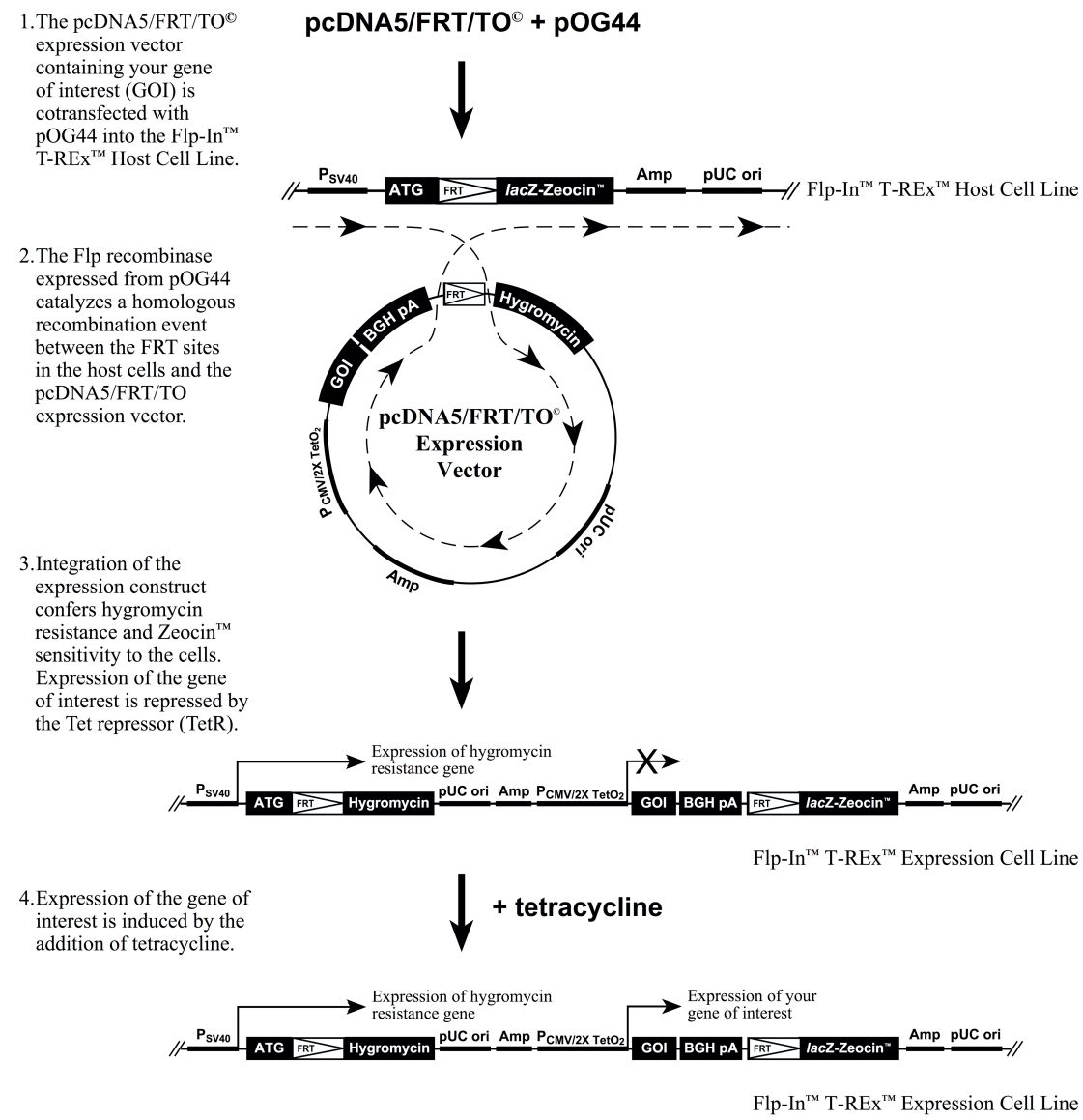


***Figure 2.2: Schematic Of Methodology For Generation Of Inducible Stable Cell Lines.*** *Detailed flowthrough of gene insertion using the Flp-In™ Inducible cell line system. Modified from Invitrogen.*

To generate inducible stable cell lines, Flp-In 293 cells were transfected with pcDNA5/FRT/TO expression vector containing the gene of interest in combination with the Flp recombinase plasmid, pOG44. To maximise success, 3 ratios of pOG44 to pcDNA5/FRT/TO were selected, 5:1, 9:1 and 12:1. Flp-In 293 cells were seeded at 70-80% confluency in a 6-well plate as previously described. The following day, wells

were transfected with the ratios of pOG44:pcDNA5/FRT/TO with Lipofectamine 2000 as previously described (Section 2.5.1). After transfection, cells were trypsinised briefly and transferred to a 25cm$^2$ flask. Growth media containing 15µg/ml Blasticidin was added to cells and left for 2-3 days for cells to acclimatise to the selection. Hygromycin at a concentration of 100µg/ml was then added to the cell culture. During this step, the majority of the cells die. Media was changed the following day to remove dead cells and cell debris and fresh growth media containing both antibiotics was added. Cell cultures were monitored until small colonies of resistant cells appeared. These resistant cells were cultured then tested for gene integration through induction with tetracycline and also for zeocin sensitivity to ensure efficient recombination (figure 2.3). The Flp-In 293 cells contain an integrated FRT site and express the lacZ-Zeocin fusion gene. Co-transfection of pcDNA5/FRT/TO and pOG44 results in Flp recombinase mediating a homologous recombination event between the FRT sites in the genome and the pcDNA5/FRT/TO plasmid (figure 2.2). This results in insertion of the gene of interest into the FRT site within the cell genome. As a result the SV40 promoter and the ATG start codon are brought within close proximity and frame, disrupting the lacZ-Zeocin fusion gene. Thus, this confers hygromycin resistance and zeocin sensitivity.

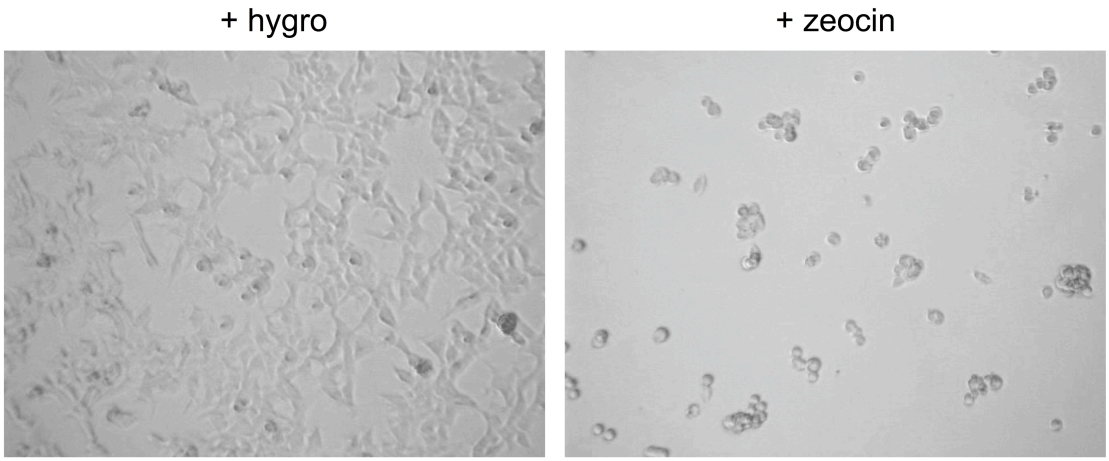


***Figure 2.3: Bright Field Images Comparing Effects of Hygromycin And Zeocin On Flp-In 293 Inducible Cell Lines.*** *Images show cells grow in the presence of hygromycin (Hygro) and in the presence of zeocin. Successful gene recombination is determined by hygromycin resistance and zeocin sensitivity.*

### 2.5.3 Treatment Of Cells With Global Palmitoylation Inhibitor, 2-Bromohexadecanoic Acid

In order to inhibit palmitoylation, a non-specific DHHC inhibitor was utilised. 2-bromohexadecanoic acid (2-BP) was prepared fresh before each treatment by dissolving in DMSO to a final concentration of 100mM. This was then aliquoted into sterile 1.5ml eppendorf tubes to give a final concentration of 100μM when added to wells. To ensure even distribution of 2-BP, 1ml of media was removed from the treatment well and added to the tube containing 2-BP. This mix was then triturated to mix the media with 2-BP then added back to the treatment well. Treatments of 2-BP were incubated with cells overnight and cells harvested for respective experiments.

### 2.5.4 Labelling Of Cell Surface Proteins With Biotin

Following transfection or induction of cells, where appropriate, cells were labelled with the cell-impermeable amine reactive biotinylation reagent sulfo-NHS-SS-biotin (Pierce), which binds to cell surface resident proteins. Cells were washed 3 x with PBS, being careful to avoid cell loss. Biotinylation solution was prepared by dissolving 1mg/ml sulfo-SS-NHS-biotin in PBS, which was then added to cells and incubated at 37°C for 10minutes. Cells were washed 3 x with PBS to remove traces of excess reagent. Cells were lysed in 1% Triton/PBS supplemented with protease inhibitor cockatil (Calbiochem, Cat.no.: 539134) then biotinylated proteins purified as described in section 2.6.3.

### 2.5.5 Confocal Microscopy Analysis Of Transiently Transfected Cell Lines

Cells for confocal microscopy were seeded on to glass coverslips. Following transfection, cells were washed 3 x with PBS. Cells were fixed with 4% paraformaldehyde (PFA) for 10 minutes at room temperature. After fixation, cells were washed 3 x with PBS. To stain for the Golgi apparatus, Grasp65, involved in stacking of Golgi cisternae (Barr et al. 1997), fused to mCherry (generously provided by Dr Jon Lane, University of Bristol) was transfected into cells at the same time as YFP-fusion constructs. To stain the endoplasmic reticulum (ER), a ER directed plasmid encoding the ER targeting sequence of calreticulin fused to the 5’ end of DsRed2 and the ER retention sequence KDEL fused to the 3’ end of DsRed2 (provided by Dr Chris

Connolly, University of Dundee), was transfected into cells at the same time as the YFP-fusion constructs. Cells were washed 3 x with PBS. Coverslips were mounted onto glass slides using 100µl Hydromount (National Diagnostics, Hull, UK) containing 1µl of 1µg/ml DAPI (Sigma, UK) and 1µl of 50mg/ml Dabco (Sigma, UK). Slides were covered and left to dry overnight. Coverslips were sealed with clear nail polish to ensure oil from the confocal oil objectives would not contaminate the cells. Fluorescence micrographs were produced using a Leica SP5 Confocal Microscope. Wavelengths used to detect YFP were 519nm to 542nm DSRED2-ER 575nm to 644nm and mCherryGrasp65 580nm to 700nm.

## 2.6 Protein Analysis

### 2.6.1 Bradford Assay

Total protein concentrations of cell lysates were determined using the Bio-Rad protein assay (Bio-Rad Laboratories, Hempstead, UK). The assay is based on measurement of a differential colour change of a dye in response to various protein concentrations. Bio-Rad reagent is supplied as a 5-fold concentrate and was diluted with ultrapure water prior to use. Disposable 1ml micro-cuvettes were filled with 995µl of diluted Bio-Rad reagent, to which 5µl of protein lysate was added and mixed with end over end agitation. Samples were incubated at room temperature for 2-3 minutes prior to analysis. The spectrophotometer (Jenway) absorbance was set to zero using a cuvette filled with 1ml of Bio-Rad reagent without protein. The spectrophotometer was pre-loaded with a concentration curve for determining protein concentrations. Absorbance of protein samples were analysed following incubation.

### 2.6.2 Purification Of Palmitoylated Proteins By Resin Assisted Capture

To purify palmitoylated proteins from cell lysates or tissues, resin assisted capture of acylated proteins (Acyl Rac) was used, based upon the method developed by Forrester and colleagues (Forrester et al. 2011). 2mg of protein from tissue or 1-well of cells from a cell culture dish was lysed in 300µl of blocking buffer (see Table 2.3) containing 1% methyl methanethiosulfonate (MMTS) or N-ethylmaleimide (NEM) where indicated. Lysates were incubated on a shaking heat block at 40°C at 1400rpm for 4 hours.

Following incubation, 3 volumes of acetone were added to precipitate proteins from sample, which were then incubated overnight at -20°C.

| **Chemical** | **Concentration** | |
|---|---|---|
| | ***Blocking Buffer*** | ***Binding Buffer*** |
| HEPES | 100mM | 100mM |
| SDS | 2.5% | 1% |
| EDTA | 1.0mM | 1.0mM |
| MMTS | 1% | - |

***Table 2.3: Buffer Compositions For Acyl Rac.*** *Details of buffers used to acyl rac and concentrations of their respective constituents. Note, MMTS is added fresh each time to blocking buffer prior to use.*

After precipitation of protein, samples were centrifuged at 17,000g for 5 minutes at room temperature. Once pelleted, proteins were washed vigorously 5 times with 70% acetone to remove residual MMTS. Pellets were air-dried following wash steps. Protein pellets were dissolved in 140µl of binding buffer by shaking at 1400rpm at 40°C until no pellet was observed. Samples were briefly centrifuged to collect the sample. A 20µl analytical sample, unfractionated (UF) was retained for analysis by SDS-PAGE. During resolubilisation, thiopropyl sepharose 6B (GE Healthcare, Cat.no.: 17-0420-01) was rehydrated for 15 minutes in ultrapure $H_2O$ at room temperature with end over end agitation. Following rehydration, sepharose was equilibrated into 1:1 volume of binding buffer. Additionally, a 2M stock of hydroxylamine (ha) was prepared fresh and adjusted to pH 7.5. In some cases, 2M NaCl was added to acyl rac reaction in place of ha to serve as a negative control.

Once samples were dissolved and UF removed, 50µl of sepharose slurry was added to each sample, to give approximately 5mg of sepharose per sample. Hydroxylamine was added to each sample to a final concentration of 200 mM. Samples were then incubated for 2.5 hours at room temperature with end over end agitation. Following incubation, samples were centrifuged at 17,000g for 1 minute. Where indicated, unbound (UB) fractions were retained for analysis. Sepharose was washed 5 times with 1ml of binding buffer, incubating with end over end agitation for 2-3minutes and centrifuging in between each wash. Following the final wash, wash buffer was removed and sepharose

was resuspended in 50µl of 2X SDS PAGE loading buffer containing 100mM DTT. Samples were heated at 37°C for 10 minutes to elute proteins.

### 2.6.3 Purification Of Biotin Labelled Cell Surface Proteins Via Streptavidin Affinity Capture

Proteins were solubilised by incubation at 4°C with gentle shaking for 30 minutes. Lysates were then scraped from wells into pre-chilled 1.5ml microcentrifuge tubes and then centrifuged at 17,000g for 5minutes at 4°C to remove insoluble material. The supernatant was transferred to a clean tube. A protein assay was performed to determine protein concentration and the protein content of all samples was normalised. A 50µl sample was taken as an analytical fraction prior to purification. Approximately 30µl of streptavidin sepharose which had been previously equilibrated with 1% Triton X-100/PBS was added to each cell lysate which were then incubated with end over end rotation at 4°C overnight. Following overnight incubation, samples were centrifuged at 4°C at 17,000g for 1 minute. A 50µl sample of the unbound fraction was taken prior to removal of the supernatant. The sepharose was washed 3 times with 1% Triton X-100/PBS. Proteins captured on the sepharose where then eluted by resuspending the sepharose in 100µl of 2X SDS Loading Buffer supplemented with 100mM DTT and incubated at 37°C for 10minutes.

### 2.6.4 Co-Immunoprecipitation

Protein-protein interactions were assessed using co-immunoprecipation. Anti-HA Affinity Matrix (Roche, Cat.no.: 11815016001) was equilibrated in 2mg/ml octaethylene glycol monododecyl ether (C12E10)/PBS with protease inhibitor cocktail (Calbiochem, Cat. no.: 539134) and 0.1M PMSF (co-IP lysis buffer) for 1 hour at room temperature. Cells transfected with DHHCs and WT NCX-YFP or empty vector were lysed in 300µl of co-IP lysis buffer. Lysates were scraped into 1.5ml microcentrifuge tubes and agitated at 4°C for 30 minutes to solubilise membrane proteins. Lysates were centrifuged at 17,000g for 5 minutes at 4°C to remove insoluble material. Supernatant was transferred to a clean, prechilled 1.5ml microcentrifuge tube. A 30µl sample was retained as IP input sample. The resulting pellet was dissolved in 600µl SDS PAGE buffer to assess efficiency of solubilisation. 200µl cell supernatant was used in the IP. HA-beads were given a final wash and resuspended in 100µl per IP reaction. 100µl of

slurry was added to each IP reaction, which were incubated overnight with end-over-end rotation at 4°C. The following day, 50µl of unbound supernatant was taken from each IP and mixed 1:1 with SDS PAGE buffer. Beads were washed 5 times with 1ml of 0.5mg/ml C12E10/PBS with protease inhibitor cocktail and PMSF (co-IP wash buffer) at 4°C. Proteins were eluted from HA-beads by resuspending in 20µl of 2x SDS PAGE sample buffer supplemented with 5% β-mercaptoethanol and 100mM DTT. Samples were heated at 65°C for 10 minutes, then centrifuged at 17,000g for 1 minute and analysed by western blotting.

### 2.6.5 Cell Fractionation

Briefly, cell media was removed and cells were lysed in 150µl of PBS containing 0.05% digitonin, protease inhibitor cocktail (Calbiochem, Cat. no.: 539134), 0.1µM PMSF. Cell lysates were then scraped and transferred to clean 1.5ml microcentrifuge tubes, a small analytical sample was taken and incubated at 4°C for 10 minutes with end over end rotation. Following incubation, cell lysates were centrifuged at 17,000g for 5 minutes. The supernatant was collected and mixed 1:1 with 2X SDS Loading buffer (cytosolic fraction). The pellet was then lysed in 150µl of PBS/1% Triton X-100 with protease inhibitors and PMSF as before. This lysate was then incubated at 4°C for 10 minutes with end-over-end rotation. Lysates were then centrifuged at 17,000g for 5 minutes. The supernatant was collected and mixed 1:1 with 2X SDS Loading buffer (membrane fraction). The remaining pellet was lysed directly in 300µl of 2X SDS Loading Buffer (insoluble material). Samples were then analysed by Western Blotting.

### 2.6.6 Sucrose Gradient Fractionation Of Caveolin-enriched Membranes

Caveolin-enriched buoyant membranes were prepared from isolated ARVMs as described in (Wypijewski et al. 2013). ARVMs were homogenised and sonicated in 500mM sodium biocarbonate, pH 11, supplemented with 1mM DTT, 1mM EDTA and protease and phosphatase inhibitors. Lysates were adjusted to 45% sucrose by addition of an equal volume of 90% (w/v) sucrose in 25mM MES, 150mM NaCl, pH 6.5. 4ml was transferred to an ultracentrifuge tube and overlaid with 4ml of 35% sucrose and 4ml of 5% sucrose. Sucrose gradients were centrifuged overnight at 270,000g. 1ml fractions were collected and each volumes of each were analysed by SDS-PAGE and

western blotting. Fractions 4 and 5 and 8 – 12 were pooled and palmitoylated proteins were captured using acyl rac.

## 2.7 Gel Electrophoresis

### 2.7.1 Gel Preparation

Solutions containing either 6% acrylamide or 20% acrylamide were prepared (See Table 2.4 for details).

| **Chemical** | **Percentage** | **Percentage** |
|---|---|---|
| | **6%** | **20%** |
| **$H_2O$** | 16ml | 1.6ml |
| **1.5M Tris.HCl pH=8.8** | 7.6ml | 6.3ml |
| **10% SDS** | 300µl | 250µl |
| **30% Acrylamide** | 6ml | 16.7ml |
| **10% APS** | 125µl | 80µl |
| **TEMED** | 12.5µl | 12.5µl |

***Table 2.4: Gradient Gel Recipe.*** *Respective volumes of buffer stocks required to prepare 6-20% gradient gels.*

| **Chemical** | | | | |
|---|---|---|---|---|
| | **8%** | **10%** | **12%** | **15%** |
| **$H_2O$** | To 10ml | To 10ml | To 10ml | To 10ml |
| **1.5M Tris.HCl pH=8.8** | 375mM | 375mM | 375mM | 375mM |
| **10% SDS** | 0.1% | 0.1% | 0.1% | 0.1% |
| **30% Acrylamide** | 8% | 10% | 12% | 15% |
| **10% APS** | 0.1% | 0.1% | 0.1% | 0.1% |
| **TEMED** | 0.6mM | 0.4mM | 0.4mM | 0.4mM |

***Table 2.5: Alternative Gel Recipe.*** *Respective constituents of alternative percentage gels.*

| Chemical | Stacking Gel |
|---|---|
| **$H_2O$** | to 5ml |
| **1M Tris.HCl pH=6.8** | 126mM |
| **10% SDS** | 0.05% |
| **30% Acrylamide** | 2.49% |
| **10% APS** | 0.05% |
| **TEMED** | 0.5mM |

***Table 2.6: Stacking Gel Recipe.*** *Volumes and constituents of stacking gels for polyacrylamide gels. Total volume is 5ml, which was scaled up for gradient gels.*

| Buffer | Chemical | Concentration | pH |
|---|---|---|---|
| 2x SDS PAGE Loading buffer | Tris<br>SDS<br>Glycerol<br>Bromophenol Blue<br>β-mercaptoethanol | 100mM<br>4% (w/v)<br>20% (w/v)<br>0.02% (w/v)<br>5% (v/v) | 6.8 |
| 10X Tris/Glycine | Tris<br>Glycine | 0.25M<br>1.92M | - |
| 1X Running Buffer | Tris<br>Glycine<br>SDS | 25mM<br>192mM<br>0.1% (w/v) | - |
| 1X Transfer Buffer | Tris<br>Glycine<br>SDS<br>Methanol | 25mM<br>192mM<br>0.01% (w/v)<br>20% (v/v) | - |

***Table 2.7: Buffers For Protein Gel Electrophoresis And Western Blotting.*** *Buffers and constituents for protein gel electrophoresis and western blotting.*

### 2.7.2 Sample Preparation

Prior to loading samples into the well for gel electrophoresis, samples were heated to 37°C for 10 minutes. Following incubation, samples were centrifuged at 17,000g for 1 minute. In the case of samples containing agarose beads, this collected at the bottom of

the tube, therefore not interfering with sample loading. Samples were allowed to cool to room temperature prior to loading.

### 2.7.3 Sodium Dodecyl Sulphate – Polyacrylamide Gel Electrophoresis (SDS-PAGE)

For casting gels, BioRad 0.75mm spacer plates (BioRad, Cat.no.: 1653310) and BioRad short plates (BioRad, Cat.no.: 1653308) were used. Gradient gels or 8% Acrylamide gels were used for experiments where indicated. Alternative percentage gels to gradient gels were cast according to the composition, shown in table 2.5. Following addition of the resolving gel to the plates, resolving gels overlaid with 80µl of water-saturated butan-1-ol. Butan-1-ol was then washed off after resolving gels had polymerised and stacking gel (Table 2.6) was added to each gel, with combs to form wells being added immediately after. 5µl of PageRuler Plus prestained protein ladder (Pierce, Cat.no.: 26619) was loaded. Running buffer was used according to the recipe outline in Table 2.7. All wells were loaded with 5ul of respective samples. Gels were run for 20 minutes at constant voltage of 120V. The voltage was then increased to 200V until the dye front was at the bottom of the gel.

### 2.7.4 Western Blotting

Following SDS-PAGE to separate proteins, proteins were transferred to a PVDF membrane. The following set-up was used, 1 sheet of extra thick blotting paper, PVDF membrane, SDS-Page gel, 2 x sheets of thin blotting paper, 1 sheet of extra thick blotting paper. Prior to transfer, PVDF membrane was equilibrated in methanol for 5 minutes at room temperature. The methanol was then removed and replaced with Transfer Buffer (see Table 2.7) for 5 minutes. The blotting paper was also equilibrated in Transfer Buffer prior to transfer. The SDS-Page gel was removed from the plate and placed on the PVDF, ensuring all bubbles were removed to enable even transfer. The sheets of thin blotting paper were then placed on top of the gel, and a roller used to remove an additional air bubbles. The final sheet of extra thick blotting paper was placed on top and the roller was used again to remove air bubbles. This sandwich was assembled in a BioRad Trans-Blot Turbo Transfer System (BioRad, Cat.no.: 170-4155) and transferred at 25V 1.0A for 30 minutes. Following transfer, membranes were

incubated in 5% milk/PBST for 1 hour. Membranes were incubated overnight at 4°C with primary antibodies (dilutions indicated in table 2.6).

The following day, membranes were agitated for up to 1 hour at room temperature with multiple changes of PBS-T. Secondary antibodies raised to the appropriate species for the primary antibody were then applied to the membrane and incubated at room temperature with shaking for 1 hour. Secondary antibodies were prepared in 5% milk/PBST. Following incubation with secondary antibodies, membranes were agitated for 1 hour and 30 minutes at room temperature with multiple PBS-T changes. To visualise the proteins on the membrane, Immobilon HRP Substrate (Millipore, Cat. No.: 11556345) was used. Solution A and Solution B were mixed 1:1 and applied to the membrane, which was placed on a stretch of saranwrap. The HRP substrate was incubated with the membranes for 5 minutes at room temperature, with membranes being flipped over after 2.5 minutes to ensure even coverage of the HRP substrate. Excess HRP substrate was removed from the blot, which was then placed between 2 sheets of plastic wrap before being exposed using chemiluminescence on a BioRad imaging system.

| **Antibody** | **Species** | **Manufacturer** | **Dilution Used** |
|---|---|---|---|
| NCX1 (R3F1) | Mouse | Swant | 1:1000 |
| Caveolin-3 | Mouse | BD Biosciences | 1:5000 |
| Flotillin-2 | Mouse | BD Biosciences | 1:5000 |
| SERCA2a | Mouse | Thermo Scientific | 1:5000 |
| GAPDH | Mouse | Sigma | 1:1000 |
| H-Ras | Rabbit | Santa Cruz | 1:300 |
| GFP | Rabbit | Abcam | 1:2000-1:5000 |
| Anti-mouse | | Pierce | Range: 1:2000-1:10,000 |
| Anti-rabbit | | GE Healthcare | Range: 1:2000-1:5000 |

***Table 2.8: Antibodies Used In Western Blotting Analysis.*** *Details of antibodies used in western blotting and their respective dilutions.*

### 2.7.5 Detection Of Total Protein Using SimplyBlue™ SafeStain Gel Stain

To detect all proteins from a given experiment, polyacrylamide gels were stained with SimplyBlue™. Following electrophoresis, gels were placed in 100ml of MilliQ water and heated on high for 1 minute in a microwave until the solution almost reached boiling point. Gels were agitated on an orbital shaker for 1 minute following heating. Gels were washed in this manner twice more. Following the last wash step, 20ml of SimplyBlue™ SafeStain was added and gels heated on high for 45 seconds to 1 minute until the solution approached boiling point. Gels were agitated on an orbital shaker for 5 minutes. Gels were washed with 100ml MilliQ water for 10 minutes on an orbital shaker. For storage, gels were stored in 20% NaCl solution. Gels were imaged using chemiluminescence on a BioRad imaging system.

## 2.8 mRNA Preparation And Quantitative PCR

### 2.8.1 Rat Heart Isolation

To identify DHHC gene expression in adult rat heart, mRNA was prepared. Hearts were excised as previously described (Section 2.3.1). In this instance, hearts were perfused briefly with buffer 1 to remove blood from the coronary circulation. Hearts were snap frozen in liquid nitrogen and stored at -80°C until required.

### 2.8.2 RNA Preparation

In order to extract RNA from rat heart, the whole heart was pulverised using mortar and pestle prechilled to minimise RNA degradation. A small volume of liquid nitrogen was added to the mortar, to which frozen whole heart was added. This was then crushed and pulverised to a fine powder, taking care to ensure that tissue remained frozen by adding more liquid nitrogen as needed. This procedure was repeated for a total of 4 hearts.

Following tissue preparation, RNA was prepared using the SV Total RNA Isolation System (Promega, Cat.no.: Z3101). Approximately 60mg of powder heart tissue was used to generate RNA. RNA was extracted as per the manufacturers instructions. Briefly, RNA Lysis Buffer (RLA) was added to the powdered tissue. The lysate was diluted by addition of RNA Dilution Buffer (RDA). Lysates were centrifuged for 10

minutes. Cleared lysates were transferred to clean microcentrifuge tubes and 95% ethanol was added to the lysate and transferred to Spin Basket Assembly and centrifuged to immobilise lysate on the filter. Lysates were washed with RNA Wash Solution (RWA) followed by DNase treatment for 15 minutes at room temperature. DNase treatment was stopped by addition of DNase Stop Solution (DSA) and centrifuged for 1 minute. RNA immobilised on filter was washed with RWA twice before elution with Nuclease-free water. RNA was snap-frozen in liquid nitrogen and stored at -80°C until required.

### 2.8.3 cDNA Preparation

Approximately 200ng of RNA was used to generate cDNA from adult rat hearts. The cDNA reaction was performed in the presence and absence of GoScript Reverse Transcriptase, to serve as positive and negative controls respectively. cDNA was prepared using GoScript Reverse Transcription System (Promega, Cat.no.: A5000) as per the manufacturers instructions. Briefly, RNA was mixed with random primers (0.5µg/reaction) and heated at 70°C for 5 minutes followed by 5 minute incubation in ice water. GoScript™ 5X reaction buffer, $MgCl_2$, PCR Nucleotide Mix, Recombinant RNasin® Ribonuclease Inhibitor, Nuclease-free water and GoScript™ Reverse Transcriptase were added to reactions. Reactions were annealed at 25°C for 5 minutes followed by 1 hour extension at 42°C. Reverse transcriptase was inactivated at 70°C for 15 minutes. cDNA was stored at -80°C until required.

### 2.8.4 Quantitative PCR

The resultant mRNA generated in section 2.8.3 was sent to Professor Mike Shipston's lab at University of Edinburgh for analysis. Briefly, mRNA expression for each DHHC was quantified relative to the geometric mean of β-actin and GAPDH using Fast Start Universal SYBR Green Mastermix (Roche, UK) in a 25µl reaction using an ABIPrism 7000 real-time PCR machine. Reactions were performed in 25µl volumes using 0.2µM primers. Between 55-115ng of cDNA generated from 4 independent heart samples was used per reaction. Cycling conditions were 50°C for 2 minutes, 95°C for 10 minutes, followed by 40 cycles of 95°C for 15s and 60°C for 1 minute. All primers used were previously validated with efficiencies calculated to be within 0.1 of the control using the equation $e = 10^{(-1/slope)} - 1$. Internal reference controls were endogenous β-actin and

GAPDH, amplified using primer sets Rn_Actb_1_SG QT00193473 and Rn_Gapd_1_SG QT00199633. DHHC primers were designed in house with the exception of DHHCs 6 (Rn_Zdhhc6_1_SG QT02382807), 19 (Rn_Zdhhc19_1_SG QT01575462) and 25 (RnZdhhc25_1_SG QT00436163), which were purchased from Qiagen.

## 2.9 Cloning Using TOPO® TA Cloning System

### 2.9.1 Amplification Of DNA For Cloning

In order to make stable expressing NCX1 cell lines, cDNA encoding NCX1 inserted into the appropriate expression vector for the Flp-In™ T-REx™ inducible expression system. Firstly NCX1 was amplified from adenovirus containing the sequence for canine NCX1.1 (kindly provided by Professor Godfrey Smith, University of Glasgow). A master mix containing $H_2O$, 10X Pfu Reaction Buffer, PCR Nucleotide mix, primers and Pfu DNA Polymerase was added to each sample. Pfu DNA Polymerase is a high fidelity enzyme resulting in fewer misreads in the final PCR product, designed for use in generating large PCR products. Primers used in this reaction are detailed in table 2.10. The amount of each reagent required was as follows,

For 1 sample,

31.1µl $H_2O$ (to 40µl)
4µl 10X Reaction Buffer
2µl PCR Nucleotide Mix (10mM each)
0.8µl NCX1 Canine Forward Primer (50µM stock)
0.8µl NCX1 Canine Reverse Primer (50µM stock)
0.8µl Pfu DNA Polymerase

---

39.5µl master mix per sample
+ 0.5µl NCX1 containing adenovirus

Samples were amplified on an Eppendorf Thermal Cycler on the following program,

1. 95°C for 2 minutes
2. 95°C for 1 minute
3. 50°C for 30 seconds
4. 72°C for 6 minutes
5. Go to 2 for 30 times
6. 72°C for 10 minutes
7. 4°C forever.

Following PCR, 0.5µl of GoTaq DNA Polymerase (Promega, Cat.no.: M3002) was added to each reaction and incubated at 72°C for 10 minutes. This was to add 5' overhangs on to PCR products as the Pfu DNA Polymerase does not do this and it is a requirement of the TOPO TA Cloning Kit (Invitrogen, Cat.no.: K4500-001).

### 2.9.2 Visualisation Of PCR Products By Agarose Gel Electrophoresis

Products from the PCR were analysed using gel electrophoresis. Agarose gels were prepared by dissolving 1% (w/v) of agarose in 1X TBE. Agarose was dissolved by heating in a microwave on high power until the agarose had dissolved. Liquid agarose was allowed to cool briefly, then approximately 1µl of ethidium bromide was added. The liquid agarose was then poured into a gel cast, ensuring all air bubbles were removed before a comb was inserted to form the wells. A 5µl sample of the PCR product was taken and mixed with Blue/Orange Loading Dye 6X (Promega, Cat.no.: G1881) then loaded onto the gel. A 1kb DNA ladder (Promega, Cat.no.: G2101) was loaded into an adjacent lane to verify PCR product size. The gel was run at a constant of 80V for 1 hour. Gels were analysed using the BioRad imager under UV light to visualise DNA bands on a gel.

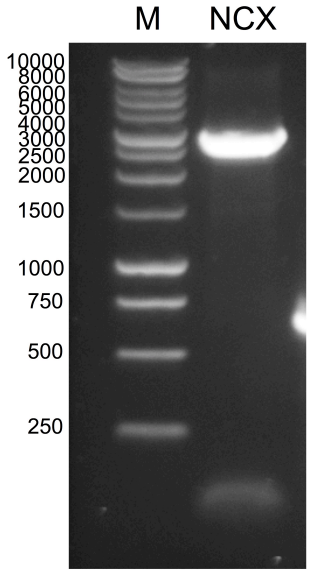


***Figure 2.4: Representative Image Of PCR Product Visualisation.*** *Agarose gel shows NCX1 PCR product following amplification. Successful PCR is indicated by a single product at approximately 3000bp.*

### 2.9.3 TOPO Reaction For Ligation Of DNA Into TOPO Vector

Once the PCR products had been analysed, the TOPO cloning reaction was set-up in the following manner,

4µl PCR Product
1µl Salt Solution
1µl TOPO vector
---
6µl final volume

This reaction was incubated at room temperature for 20 minutes.

### 2.9.4 Preparation Of Agar Plates

Agar plates were prepared by melting agar on high power in a microwave. Once melted, the agar was cooled to 55°C and ampicillin or kanamycin was added to a final concentration of 100µg/ml and 30µg/ml respectively. The antibiotic-containing agar was then poured into 10cm plates and allowed to set under a flame. If required, once dry

40µl of 40mg/ml X-gal in DMF was added and spread over the agar plate. Plates were prewarmed at 37°C or stored at 4°C.

### 2.9.5 Transformation Of Top10 Competent Cells

The TOPO ligation reaction was transformed into TOP10 cells that were supplied with the TOPO TA Cloning System. Cells were defrosted on ice. Once defrosted, 2µl of the TOPO cloning reaction was added to the cells and mixed gently. The transformation was incubated on ice for 30 minutes. Cells were then heat shocked at 42°C for 30 seconds. Following heat shock, 250µl of SOC media was added to the transformation and incubated at 37°C with 220rpm shaking for 1 hour. Following the incubation of the transformation reaction, this was plated onto the agar plates at 10% and 90% densities as recommended by the manufacturers. The plates were incubated inverted overnight at 37°C.

### 2.9.6 Extraction Of DNA From Positive Clones

TOPO® TA cloning utilizes blue/white screening, allowing rapid and efficient identification of recombinant *E.coli*. This technique relies on the activity of β-galactosidase, an enzyme present in bacteria, which cleaves lactose into glucose and galactose. The presence of lactose within the surrounding environment triggers the lacZ operon in *E.coli*, resulting in production of β-galactosidase. The TOPO® TA vector carries a short segment of the lacZ gene. The *E.coli* strain used contains a lacZΔM15 deletion mutation. As such, when the TOPO® TA vector is taken up by cells, functional β-galactosidase enzyme is produced via α-complementation. α-complementation serves as a marker for successful recombination of genes within the bacterial genome. A multiple cloning site (MCS) is present within the lacZ, into which foreign DNA can be inserted. Therefore, when *E.coli* takes up TOPO TA vector containing the gene of interest, α-complementation does not occur and functional β-galactosidase is not produced. Cells are plated on plates containing X-gal, which in the presence of functional β-galactosidase is hydrolysed to 5-bromo-4-chloro-indoxyl, which dimerises to produce insoluble blue pigment 5,5'-dibromo-4,4'-dichloro-indigo. As a result the colonies formed by non-recombinant cells appear blue in colour, while recombinant ones appear white. In cases where blue/white screening was not applicable, colonies were picked at random. Colonies were picked off the plate using a 200µl pipette tip and

placed in 50µg/ml ampicillin-containing LB Broth. These mini-preps were then incubated overnight at 37°C with 220rpm shaking to allow the E.coli to grow and replicate. The following day, DNA was extracted using a Qiagen QuickLyse Miniprep Kit as per the manufacturers instructions (Qiagen, Cat.no.: 27406). DNA concentration was determined using a NanoDrop 2000 Spectrophotometer.

### 2.9.7 Restriction Enzyme Digest Of DNA

Based on DNA concentrations, the highest yield from density plated (90% and 10%) was selected for restriction enzyme digest. At the same time as digesting the NCX1 products, the target expression vector FRT/TO was also digested. Restriction enzyme digests were set up in the following way,

| | |
|---|---|
| 6µg | TOPO containing NCX1 or FRT/TO vector |
| 3µl | 10X Buffer E |
| 0.3µl | 100X BSA |
| 1µl | HindIII |
| 1µl | BamHI |

This reaction was then incubated at 37°C for 1 hour. Following incubation, samples were separated on an agarose gel, as described previously. In the presence of correct products from the restriction enzyme digest, bands were excised from the gel. The DNA was extracted using Macherey-Nagel NucleoSpin® Gel and PCR Clean-up kit (Macherey-Nagel, Cat.no.: 740609) as per the manufacturers instructions.

### 2.9.8 Ligation Of DNA Into FRT/TO Expression Vector

Following DNA extraction, LigaFast (Promega, Cat.no.: M8221) was used to insert NCX1 into the FRT/TO vector. The reaction was set-up in the following way,

| | Vector | Insert | 2X LigaFast Buffer | T4 DNA Ligase | $H_2O$ |
|---|---|---|---|---|---|
| Vector only | 100ng | - | 5 | 1 | to 10µl |
| V + Insert | 100ng | 63ng | 5 | 1 | to 10µl |

***Table 2.9: Ligation Reaction Set-Up.*** *Details of the ratios of insert DNA to vector DNA in the ligation reaction.*

The ratio of insert to vector was calculated using the manufacturers recommendations. Ligation reactions were incubated for 15 minutes at room temperature. Following incubation, the ligation reactions were transformed into DH5α competent cells.

### i Transformation Of DH5α Competent Cells

DH5α competent cells were thawed gently on ice prior to transformation. 50µl of competent cells were added to 1µl DNA, 5X KCM (500mM KCl, 30mM $CaCl_2$, 50mM $MgCl_2$) and water to a final volume of 100µl. Transformation reactions were incubated on ice for 20 minutes, followed by 10 minutes at room temperature. Reactions were then spread on pre-warmed antibiotic-containing agar plates which were incubated overnight at 37°C. In the case of kanamycin resistant plasmids, before plating 1ml of LB was added and incubated at 37°C for 1 hour in an orbital shaker at 220rpm. Prior to plating transformed competent cells were recovered by centrifugation at 2000rpm for 5 minutes and supernatant removed. Approximately 100µl of LB was not removed and the cell pellet was resuspended and this suspension plated on pre-warmed agar plates and incubated at 37°C overnight.

Colonies were selected the following day for mini-preps. To ensure DNA extracted contained gene of interest, restriction enzyme digests were carried out. NCX1 was inserted into FRT/TO between two restriction sites, HindIII and BamHI. Restriction enzyme digest with HindIII alone or HindIII and BamHI verified resultant DNA. In the presence of HindIII alone, no insert will be removed from the plasmid, with the single digestion resulting in linearisation of the plasmid. In the presence of both HindIII and BamHI, NCX1 would be ‘cut’ out of the plasmid. This results in two distinct bands observed via agarose gel electrophoresis, one corresponding to the plasmid and the other, NCX1. Shown in figure 2.5, only when both restriction enzymes are used,

plasmids that have successfully ligated produce two distinct bands. Positively identified products were sequenced by The Genetics Core Services Unit, Ninewells.

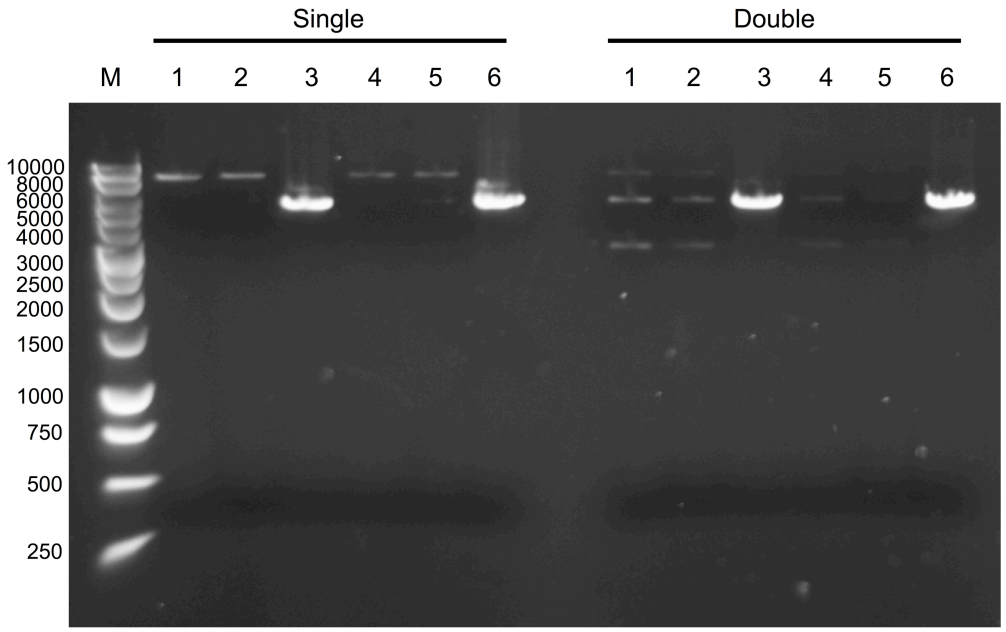


***Figure 2.5: Positive Clones Identified By Restriction Enzyme Digestion.*** *Representative gel showing a positively identified clone following digestion with restriction enzymes. Constructs were digested with one (single) or both (double) restriction enzymes. Positive clones defined as 2 distinct bands observed following double restriction enzyme digest.*

Following sequencing, correct constructs were selected and grown as maxi-preps by harvesting 1ml of mini-prep reaction and adding it to 200ml of LB Broth containing the appropriate antibiotic. Maxi-preps were incubated overnight at 37°C with 220rpm shaking. After incubation, a glycerol stock was made by mixing 250µl of the maxi-prep with 250µl of 50% glycerol and rapidly frozen. This glycerol stock was then stored at -80°C. DNA was extracted from the maxi-prep using a Qiagen HiSpeed Plasmid Maxi Kit (Qiagen, Cat.no.: 12663) as per the manufacturers instructions.

## 2.10 Mutagenesis

### 2.10.1 Single-Site Mutagenesis

To determine the palmitoylation site of NCX1, cysteine to alanine mutations were introduced into the FRT/TP/NCX1. A QuikChange Lightening Site-Directed

Mutagenesis kit was utilised, with primers designed to yield specific mutations throughout the NCX1 protein (see table 2.10). The mutagenesis reaction was prepared as follows,

2.5µl 10X Reaction buffer
0.5µl Forward primer (125ng)
0.5µl Reverse primer (125ng)
0.5µl dNTP mix
0.75µl QuikSolution reagent
---
100ng µl DNA

+ $H_2O$ to final volume of 25µl

then add 0.5 µl of QuikChange Lightning Enzyme

Reactions were then amplified using an Eppendorf Thermal Cycler using the following conditions,

1. 95˚C for 2 minutes
2. 95˚C for 20 seconds
3. 60˚C for 10 seconds
4. 68˚C for 30 seconds/kb of plasmid length
5. Go to 2 18 times
6. 68˚C for 5 minutes
7. 4˚C forever.

Once PCR reaction finished, 1µl of *Dpn* I restriction enzyme was added to each reaction and mixed thoroughly. This reaction was incubated at 37˚C for 5 minutes in order to digest any remaining non-mutated parental DNA. The resultant product was then transformed into XL-1 Blue supercompetent Cells provided with the kit.

**i Transformation Of XL-1 Blue Supercompetent Cells**

XL-1 Blue supercompetent cells were thawed gently on ice prior to transformation. For each reaction, 25µl was aliquoted into a pre-chilled 14-ml BD Falcon polypropylene round-bottom tube. 1µl of *Dpn* I-treated DNA from each reaction was added to separate

aliquots of the cells. The transformation reaction was mixed gently by swirling the tube and incubated on ice for 30 minutes. Reactions were heat pulsed at 42°C for 45 seconds then placed on ice for 2 minutes. 0.25ml of SOC media, preheated to 42°C was added to each transformation reaction and incubated at 37°C for 1 hour with shaking at 225rpm. Following incubation, transformation reactions were plated on to antibiotic-containing agar plates (See section 2.4.4). Agar plates were incubated overnight at 37°C. Resultant colonies were selected and grown as mini-preps as previously described and DNA extracted. Extracted DNA was then sent for sequencing.

### 2.10.2 Multiple-Site Mutagenesis

Following generation of single-site cysteine to alanine mutants of NCX1, mutants with multiple cysteine residues mutated to alanine were required. To achieve this, the QuikChange Multi-Site Directed Mutagenesis Kit was utilised, with primers designed to yield desired mutations (described in table 2.10). In the same way as the single-site mutants, multi-site mutant reactions were as follows,

2.5µl 10X Reaction buffer
0.2µl Forward primer (50ng of each primers used)
1µl dNTP mix
0.75µl QuikSolution reagent
---
100ng DNA

+ $H_2O$ to final volume of 25µl

then add 1µl of QuikChange Lightning Enzyme

Multi-site reactions were then amplified using an Eppendorf Thermo Cycler using the following conditions,

1. 95˚C for 1 minute
2. 95˚C for 1 minute
3. 55˚C for 1 minute
4. 65˚C for 2 minutes/kb of plasmid length
5. Go to 2 30 times
6. 4˚C forever.

Following the PCR reaction, multi-site reactions were incubated with 1µl of *Dpn* I restriction enzyme to digest non-mutated parental DNA. This reaction was then mixed briefly and incubated at 37°C for 1 hour. The resultant product was then transformed into XL-10 Gold ultracompetent Cells provided with the kit.

**i Transformation Of XL-10 Gold Ultracompetent Cells**

XL-10 Gold ultracompentent cells were gently thawed on ice prior to transformations. For each multi-site mutagenesis reaction, 22.5µl of ultracompetent cells were aliquoted into pre-chilled 14ml BD Falcon polypropylene round-bottom tubes. 1µl of β-ME mix provided with the kit was added to cells, then swirled gently. Cells were incubated on ice for 10 minutes, swirling every 2 minutes. 1.5µl of *Dpn* I-treated DNA from each multi-site reaction was added to each separate aliquot of cells. Transformation reactions were mixed gently then incubated on ice for 30 minutes. Reactions were heat pulsed at 42°C for 30 seconds followed by incubation on ice for 2 minutes. Following this incubation, XL-10 Gold ultracompetent cell transformation reactions were treated in the same way as XL-1 Blue supercompetent cells as previously described.

### 2.10.3 Generation Of NCX-YFP Fusion Construct

To determine how palmitoylation affects trafficking and anchoring of proteins, cDNA encoding YFP fused to the N terminus NCX1 large intracellular loop was generated. This allowed visualisation of protein localisation by confocal microscopy. First, the intracellular loop of wild-type, cysless or C739 containing NCX1 plasmids were amplified. These site mutants were previously generated during multi-site site directed mutagenesis reactions (section 2.10.2). Intracellular loops were amplified in the following way, with primer designed against the intracellular loop of NCX1 (see table 2.10 for details),

4µl 10X Reaction Buffer

0.8µl NCX Intra Forward Primer

0.8µl NCX Intra Reverse Primer

2µl PCR Nucleotide Mix (10mM each)

0.8µl Pfu DNA Polymerase

---

0.5µl FRT/TO NCX1.1 Plasmid

+ $H_2O$ to final volume of 40µl

Reactions were amplified on an Eppendorf Thermo Cycler under the following conditions,

1. 95˚C for 2 minutes
2. 95˚C for 1 minute
3. 60˚C for 30 seconds
4. 72˚C for 4 minutes
5. Go to 2 30 times
6. 72˚C for 10 minutes
7. 4˚C forever.

Following PCR reactions, clones were subjected to TOPO TA Cloning as previously described then subcloned into pEYFP-C1 expression plasmid as previously described (section 2.9) and transformed into DH5α competent cells.

| Primer | Sequence |
|---|---|
| NCX1 Canine Forward | ATAAGCTTGCCACCATGCTGCAGTTAAGACTATTACCTACC |
| NCX1 Canine Reverse | ATGGATCCTTAGAAGCCTTTTATGTGGCAGTAG |
| C383A Forward | CAAGGGACCTATCAGGCTCTGGAGAACTGTGGG |
| C383A Reverse | CCCACAGTTCTCCAGAGCCTGATAGCTCCCTTG |
| C387A Forward | CAGTGTCTGGAGAACGCTGGGACTGTAGCCC |
| C387A Reverse | GGGCTACAGTCCCAGCGTTCTCCAGACACTG |
| C383A/C387A Forward | GGGACCTATCAGGCTCTGGAGAACGCTGGGACTGTAGCC |
| C383A/C387A Reverse | GGCTACAGTCCCAGCGTTCTCCAGAGCCTGATAGGTCCC |
| C485A Forward | GTTTCTGCGCTCGCTGCCCTGGGATCTCCC |
| C485A Reverse | GGGAGATCCCAGGGCAGCGAGCGCAGAAAC |
| C557A Forward | GGACTTTGAGGACACTGCTGGAGAGCTCGAATTCC |
| C557A Reverse | GGAATTCGAGCTCTCCAGCAGTGTCCTCAAAGTCC |
| C731A Forward | GATGATGACGACGATGAAGCTGGAGAGGAGAAGCTG |
| C731A Reverse | CAGCTTCTCCTCTCCAGCTTCATCGTCGTCATCATC |
| C739A Forward | GGAGAAGCTGCCCTCCGCTTTCGATTATGTGATGC |
| C739A Reverse | GCATCACATAATCGAAAGCGGAGGGCAGCTTCTCC |
| C914A Forward | CAAGCTCCTCACATCCGCCCTCTTCGTGCTCCTATG |

***Table 2.10: PCR and Sequencing Primer Details.*** *Sequences of primers used in cloning of NCX1, mutagenesis reactions and sequencing.*

| Primer | Sequence |
|---|---|
| C914A Reverse | CATAGGAGCACGAAGAGGGCGGATGTGAGGAGCTTGG |
| NCX1 Intra Forward | ATAAGCTTCGGACAATTTCTTAGATGGTGCTCTG |
| NCX1 Intra Reverse | ACGGATCCGCCATTCCAGTATTCTGTCGG |
| NCX1 Sequencing Primer 1 | ATGCTGCAGTTAAGACTATTACCTACC |
| NCX1 Sequencing Primer 2 | TTACTTTCTTCTTCTTTCCTATCTGTG |
| NCX1 Sequencing Primer 3 | GACCCAGAAGGAAATCAGAGTT |
| NCX1 Sequencing Primer 4 | ACAAACAGCTGGAGAGAGCAG |



***Table 2.10 continued: PCR and Sequencing Primer Details.*** *Sequences of primers used in cloning of NCX1, mutagenesis reactions and sequencing.*

## 2.11 Mass Spectrometry

### 2.11.1 Filter Aided Sample Preparation

For protein samples to be analysed by mass spectrometry to identify palmitoylated proteins and respective palmitoylation sites, SDS was removed from samples. Since elution of palmitoylated proteins from thiopropyl sepharose cannot be achieved without the presence of SDS, a method to remove the SDS prior to mass spectrometry was sought. The Fingerprints Unit in the College of Life Sciences recommended Filter Aided Sample Preparation (FASP) (Liebler & Ham 2009). Samples for mass spectrometry were purified by acyl rac, which was scaled up to incorporate 90mg of protein from isolated ventricular myocytes (see section 2.3 for details). SDS-Loading buffer without bromophenol blue was prepared and used for elution (Table 2.8). Proteins were eluted in 100µl. A small analytical sample was retained, with the remaining sample mixed 1:5 with UA (see table 2.8). This was then loaded into a Microcon YM-10 (Millipore, Cat. No. number 42407) filtration unit and centrifuged at 14,000g for 40 minutes at 4°C. The flow-through was discarded after each wash except where indicated. The filtration unit was washed with UA and centrifuged at 14,000g for 40 minutes at 4°C. Previously palmitoylated cysteine residues were alkylated with iodoacetamide (IAA) to differentially alkylate these residues from non-palmitoylated residues. The sample was mixed with 100ul of IAA in a thermomixer at 37°C at 600rpm for 1 minute before being incubated for 5 minutes without mixing. Filtration units were centrifuged at 14,000g for 30 minutes.

| Buffer | Chemical | Concentration | pH |
|---|---|---|---|
| Tris/HCl | Tris | 0.1M | 8.5 |
| Tris/HCl | Tris | 0.1M | 8.0 |
| UA | Urea<br>Tris/HCl | 8M<br>0.1M | 8.5 |
| UB | Urea<br>Tris/HCl | 8M<br>0.1M | 8.0 |
| IAA Solution | Iodoacetamide<br>UA | 0.05M<br>8M | 8.5 |
| NaCl | NaCl | 0.5M | - |
| ABC | NH4HCO3 | 0.05M | - |
| SDS-Lysis Buffer | SDS<br>Tris/HCl<br>DTT | 4% (w/v)<br>0.1M<br>0.1M | 7.6 |

***Table 2.11: Buffers Used In FASP.*** *Details of buffers used during the FASP protocol to prepare proteins for mass spectrometry.*

Following centrifugation, 100µl of UB was added to the sample then centrifuged at 14,000g for 40 minutes. This step was repeated twice more. The proteins immobilized on the microcon YM-10 were digested using trypsin Gold (Promega). 100µl of UB was added to the sample, before 120µl ABC containing 1µl of 1µg/µl trypsin. Filtration units were then mixed in a thermomixer for 1 minute at 600rpm before being incubated overnight in a humidity chamber at 37°C. Filtration unit were then centrifuged at 14,000g for 40 minutes and flowthrough retained. Filtration units were washed with 50µl 0.5M NaCl and centrifuged at 14,000g for 20 minutes. Flowthrough from both centrifugation steps were combined and the sample sent to the FingerPrints Proteomic Facility for mass spectrometry analysis. Small aliquots of wash steps and final elution steps were retained and analysed by SDS-PAGE Gel electrophoresis and stained with SimplyBlue™ SafeStain to visualise proteins (Figure 2.6).

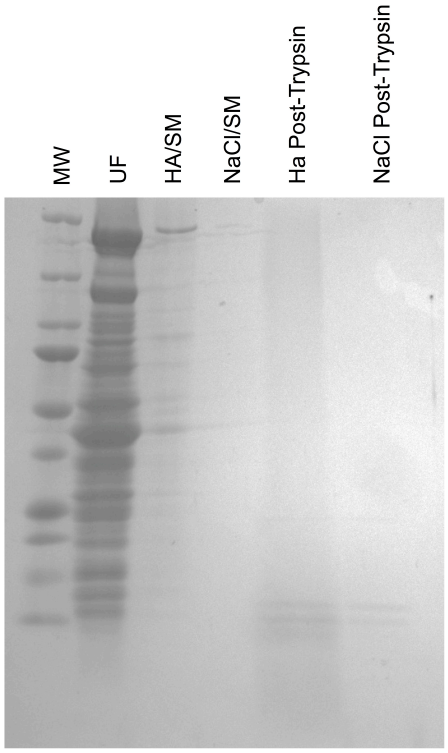


***Figure 2.6: SimplyBlue™ Stained SDS-PAGE Polyacrylamide Gel Of FASP Analysis.*** *Coomassie blue stained acrylamide gel of acyl rac following FASP prior to mass spectrometry. MW – molecular weight, UF – unfractionated, HA/SM – hydroxylamine/starting material, NaCl/SM – sodium chloride/starting material.*

## 2.12 Electrophysiology

Electrophysiology is the study of the electrical properties of biological cells and tissues. This technique can be used to record the electrical activity of ion channels, transporters and exchangers across the cell membrane. Depending on the configuration used, recordings can be from multiple (whole-cell configuration), single (cell-attached, outside-out excised patch, inside-out excised patch) ion transport mechanisms. In this work, whole-cell patch clamp was used, which is described below. Patch clamping set-ups range from simple rigs to elaborate arrangements, however there is a basic set of conditions that must be accounted for in all cases for successful patch clamping. Basic set-ups require a platform with minimal mechanical interference; microscope for visualisation of the preparation; manipulators to position micropipettes; electronics to perform stimulation, recording and analysis in an electrically clean environment.

Electrodes for electrophysiological recordings were produced from glass capillaries containing a filament with an outer diameter of 1.5mm and pulled using a

Flaming/Brown micropipette puller (Model P97, Sutter Instrument Co. USA). Once pulled, glass microelectrodes were fire polished to smooth and clean the tips using a Narishige microforge (MF-83, Japan). Electrodes were used on the day of preparation and kept in a container with a lid to prevent debris building up at the tip, which would prevent the establishment of a giga ohm seal. All experiments were carried out at 35°C, measured by heated perfusion tube (HPT-2A, Scientifica, UK). Cells were collected from the incubator and placed on the microscope stage. Excess growth media was removed by aspiration, then a custom made insert was put in the dish to reduce the bath volume to approximately 200µl. Perfusion of the bath was achieved using a 3-way stopcock perfusion system, allowing switching between different reservoirs. The perfusion was switched on and the HPT-2A enabled to heat the incoming solution to give a final bath temperature of 35°C. Cells were equilibrated for 5-10 minutes prior to experimental procedures.

| **Chemical** | **Extracellular** | **Intracellular** |
|---|---|---|
| NaOH | 120mM | 20mM |
| KOH | - | 5mM |
| $MgCl_2$ | 1mM | - |
| CsOH | - | 100mM |
| Ca-sulfamic | 1.5mM | 12mM |
| EGTA | - | 20mM |
| HEPES | 10mM | 10mM |
| D-glucose | 10mM | 8mM |
| Mg-ATP | - | 5mM |
| TEA-OH | - | 20mM |
| NMDG | 40mM | 25mM |

***Table 2.12: Composition Of Electrophysiology Buffers.*** *Details of buffers used in IV ramp recordings. pH of the extracellular solution was 7.0 and the intracellular solution was 6.8.*

### 2.12.1 Cell-attached configuration

Microelectrodes were filled with intracellular solution (see Table 2.12) and secured on a PatchStar micromanipulator (Scientifica, UK). Microelectrodes with resistance between

1.8-2.2MΩ were selected for experiments. A small amount of positive pressure was applied by mouth to the microelectrode, which was lowered into the bath, using PatchStar micromanipulator (Scientifica, UK). Square wave voltage perturbation (5mV) was used to assess pipette capacitance. Upon selecting a target cell, microelectrodes were positioned above the cell and lowered towards the cell membrane using the fine manipulator controls. Negative pressure was applied through gentle suction by mouth once the electrode was touching the cell membrane, as indicated by a small rise in resistance, typically about 1MΩ. This negative pressure aided the formation of a giga-ohm seal. After establishing the giga-ohm seal, microelectrode capacitance was compensated using the fast and slow controls until the input and output signals were equal.

### 2.12.2 Whole-cell configuration

Following microelectrode capacitance compensation, the holding potential of the cell was changed to the calculated NCX1 reversal potential -30mV, which is calculated as follows,

$$E_{Na/Ca} = 3E_{Na} - 2E_{Ca}$$

where,

$$E_{Na} \cong 60 \log \frac{[Na^+]_o}{[Na^-]_i}$$

$$E_{Ca} \cong \frac{60}{2} \log \frac{[Ca^{2+}]_o}{[Ca^{2-}]_i}$$

Thus, if membrane potential is equal to $E_{Na/Ca}$ then NCX1 is in equilibrium. Increasing, constant levels of negative pressure were applied by mouth until the membrane was ruptured and whole-cell configuration established. Cell capacitance and series resistance were adjusted until input and output signals were equal. The intracellular environment of the cell was allowed to dialyse with the microelectrode solution before commencing recordings.

### 2.12.3 IV Ramps

IV ramps were used to measure NCX1 currents (Ander et al. 2007). This allows the measurement of both inward and outward exchange currents in one protocol. Cell holding potential was ramped from +80mV to -100mV (Figure 2.7), as this allowed maximal outward and inward exchange currents to be recorded. Voltages used are approximate as liquid junction potentials were not compensated. Sequences of 5 sweeps were obtained for each cell during the ramp protocol. Following recording of NCX1 currents, the perfusion reservoir was switched to extracellular solution where $Na^+$ and $Ca^{2+}$ were replaced with equal concentrations of $Li^+$ and $Mg^{2+}$ respectively. $Li^+$ and $Mg^{2+}$-containing solution was allowed to enter the bath and cells were incubated for 5 minutes to ensure the bath solution had completely switched. IV ramps were repeated with the same cell in the presence of $Li^+$ and $Mg^{2+}$. Upon cessation of the $Li^+$ and $Mg^{2+}$ treatment, the dish was discarded and replaced with a new dish of cells. For analysis, all NCX1 IV ramps were normalised by subtracting the current remaining after $Li^+$ and $Mg^{2+}$ treatment. Cells with access resistance of 3-5MΩ were selected for analysis. Analysis of NCX1 IV ramps was performed using pClamp10 and GraphPad Prism 6. Calculation of retification index was performed by normalising current obtained at +80mV for each cell line to respective current at -80mV.

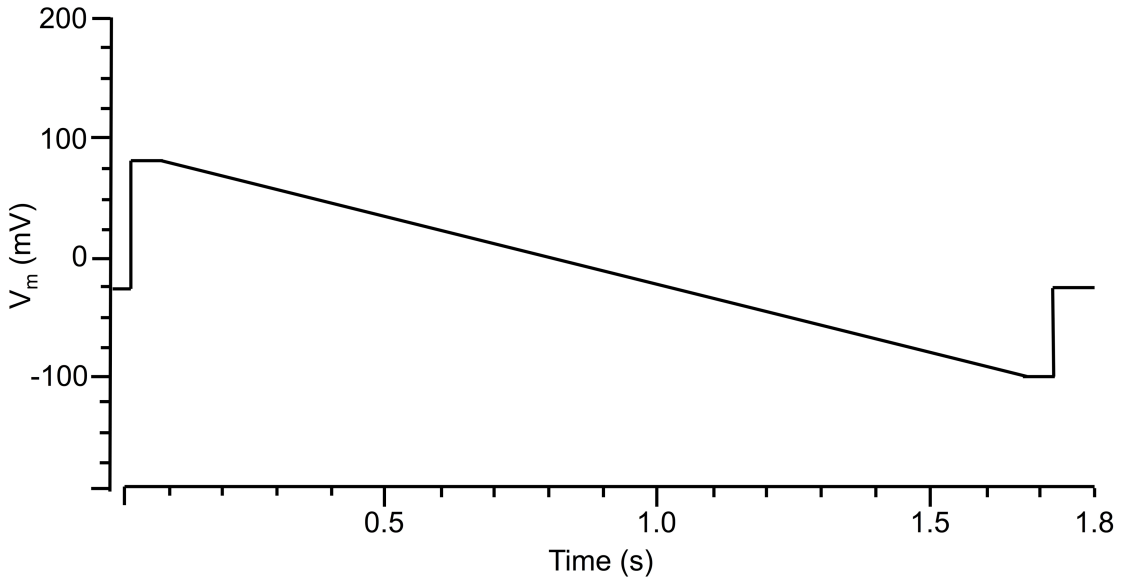


***Figure 2.7: IV Ramp Protocol For Electrophysiology.*** *Electrophysiological protocol used in the recording of NCX1 IV ramp protocol. $V_m$ – membrane potential, mV – millivolt, s – second.*

## 2.13 Left Ventricular Heart Failure

To assess the role of palmitoylation in cardiac failure, an aortic banding model of left ventricular (LV) failure in the rat was employed. To induce heart failure, a titanium clip (internal diameter 0.6 mm) was placed around the ascending aorta in animals at 5 weeks of age (60-80g). Control animals received sham surgery. The development of LV hypertrophy and subsequent failure was determined by echocardiography in rats under 2% isofluorane anaesthesia. LV structure and function were assessed using a GE Vivid 7 pro with 12 MHz transducer. Heart failure was defined as ejection fraction <45%. Changes in cardiac function were confirmed by direct measurement of LV pressure-volume relationships using Millar pressure-conductance catheters prior to tissue collection. Compensated hypertrophy was evidence at 16-20 weeks, which progressed to failure by approx. 25 weeks. This procedure was performed in the lab of Dr Sarah Calaghan at University of Leeds and the tissue kindly gifted for experiments. Approximately 3mg of tissue, as determined by Bradford protein assay, from each sham and banded animal was subjected to acyl rac followed by western blot analysis as described previously.

## 2.14 Cardiac Hypertrophy In Vivo Model

In addition to investigating the role of palmitoylation in heart failure, an in vivo model of cardiac hypertrophy was also analysed. The recently published method by Boguslavskyi et al was utilised to induce left ventricular hypertrophy in mice (Boguslavskyi et al. 2014). Briefly, hypertrophy was induced by pressure overload following suprarenal aortic constriction (banding) in 6-week-old C57BL/6J mice. Tissue was harvested 3 days, 14 days, 4 weeks and 8 weeks after surgery, to yield a full time course of disease progression. Heart excision was performed after terminal anaesthesia by i.p. injection of pentobarbital (Pentoject 200 mg/ml solution) at dose 300 mg/kg and heparin (150 U). Whole hearts were homogenised in PBS, and a small aliquot was shipped to our laboratory for experiments. Between 1-2mg of tissue (matched for each experimental group), as determined by Bradford Assay, palmitoylated proteins were purified by acyl rac from each experimental group and analysed by SDS-PAGE gel electrophoresis followed by western blotting.

# Chapter 3: Determining NCX1.1 Palmitoylation In Cardiac Muscle

### 3.1 NCX1.1 Displays Intramolecular Aggregation Following Prolonged Heating

Purification of acylated proteins by resin assisted capture (Acyl Rac) was used to assess palmitoylation of NCX1.1 in cardiac muscle. During this protocol, samples are heated for 4 hours at 40°C. Routinely, NCX1 would appear as two distinct molecular weight bands, 160kDa and 120kDa via western blot analysis after acyl rac (Figure 3.1). To investigate whether this was a product of the prolonged heating or due to the disulphide bond in NCX1.1 (Santacruz-Toloza et al. 2000), isolated ARVM were lysed in the presence and absence of DTT. During this protocol, ARVM were solubilised in blocking buffer and incubated with 50mM DTT for 30 minutes at 40°C, with analytical samples taken prior to and following incubation. Lysates were incubated for 4 hours at 40°C with NEM, after which proteins are precipitated overnight and resolubilised. Analytical samples were taken following incubation with NEM and following resolubilisation after precipitation. Samples were analysed by SDS-PAGE gel electrophoresis followed by western blotting. Membranes were incubated with NCX1 or caveolin-3 primary antibodies and visualised on a BioRad imaging system.

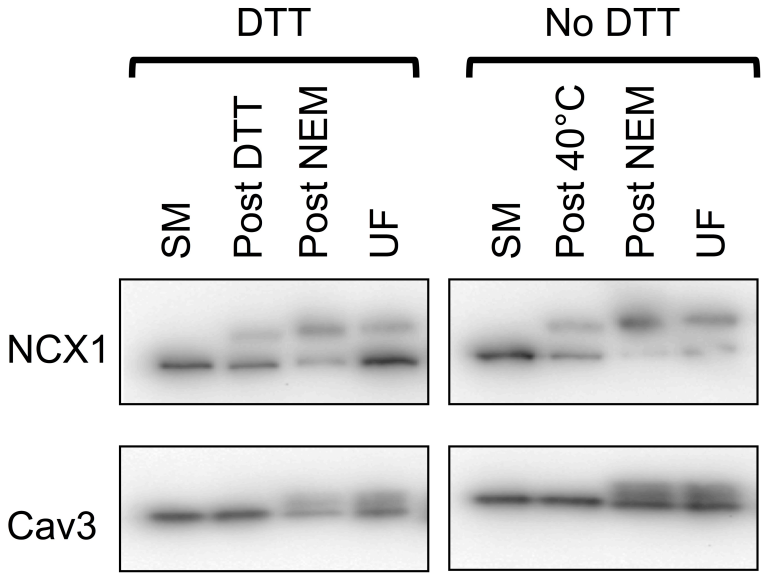


***Figure 3.1: NCX1 Displays Intramolecular Aggregation Following Prolonged Heating.*** *Following prolonged exposure to high temperatures, NCX1 appears as a double band on western blots. SM – starting material, DTT – Dithiothreitol, UF – unfractionated.*

Prior to heating, NCX1 migrates as a single 120kDa molecular weight band (figure 3.1) under non-reducing conditions. However, following exposure to 40°C for 30 minutes (Post-DTT lane in figure 3.1) in the presence and absence of DTT, NCX1 is observed a two molecular weight bands, 160kDa and 120kDa. The two distinct molecular weight bands are still seen following heating for 4 hours (Post-NEM lane, figure 3.1). The two molecular weight species are not affected by precipitation and resolubilisation (UF lane, figure 3.1). In contrast, caveolin-3 is unaffected by heating at any time during the heating protocol. Addition of NEM to caveolin-3 results in slightly smudged appearance on western blots, due to the size of the modification. These results suggest that NCX1 aggregates if unreduced prior to heating.

### 3.2 NCX1 Is Sensitive To Temperature And Reducing Agent

Heating NCX1 above 40°C alters electrophoretic mobility of NCX1. ARVM lysates were heated to different temperatures for 10 minutes. Room temperature (RT), 37°C and 60°C were selected to determine the effect of temperature on NCX1. In addition, the effect of routinely used reducing agents on detection of NCX1 by western blotting was investigated.

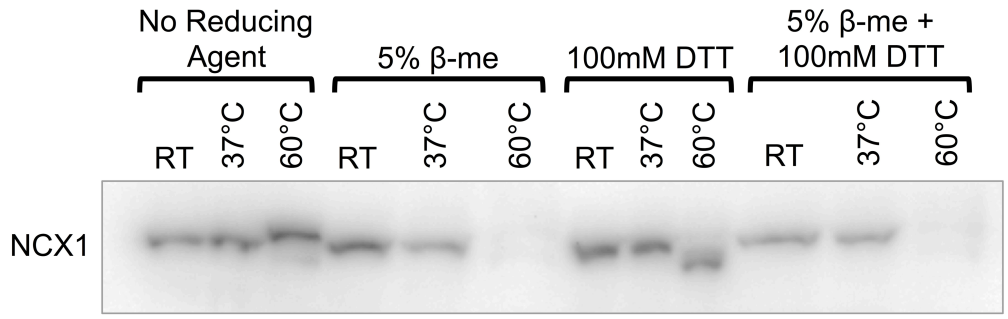


***Figure 3.2: NCX1 Is Sensitive To Temperature And Reducing Agent.*** *Following incubation for 10 minutes at various temperatures, in the presence and absence of reducing agent, visualisation of NCX1 via western blotting was reduced following heating above 37°C and further reduced by the presence of β-mercaptoethanol. RT – room temperature, DTT – Dithiothreitol, β-me - β-mercaptoethanol.*

2mg of ARVM were solubilised in 500µl 2 X SDS-Loading buffer (see Table 2.7), then subdivided into different treatment groups indicated in Figure 3.2. Samples were heated at the respective temperature for 10 minutes then subjected to SDS-PAGE gel

electrophoresis followed by western blotting. At RT, under all conditions, NCX1 was observed as 120kDa band (Figure 3.2). 37°C had no distinguishable effect on NCX1, regardless of reducing agent present. At temperatures above 60°C, NCX1 started to appear as a double band in samples without reducing agent (Figure 3.2), although a higher molecular weight band was more prominent. β-mercaptoethanol reduced visualisation of NCX1 on western blots at 60°C. This suggests that β-mercaptoethanol has an effect on aggregation of NCX1 or masks the epitope of antibody at high temperatures. At 60°C, in the presence of DTT, NCX1 was observed as 120kDa band. Despite NCX1 not adversely being affected by DTT, this was not sufficient to rescue the effect occurring in the presence of β-mercaptoethanol. Based on these results, NCX1 can only be heated to 37°C. Since a reducing agent is required for elution at the end of the acyl rac protocol, 100mM DTT was selected as β-mercaptoethanol had a detrimental effect on detection of NCX1.

### 3.3 NCX1 Is Palmitoylated In Adult Rat Ventricular Myocytes

Acyl rac was used to capture palmitoylated proteins from isolated ARVM in order to assess NCX1 palmitoylation. Two different alkylating agents to block free cysteine residues were evaluated. MMTS is a reversible alkylating agent, whereas NEM is an irreversible alkylating agent. These two different agents were compared to determine the most suitable agent to use in acyl rac protocol. In addition, the ability to use an irreversible alkylating agent at non-palmitoylated cysteine residues will allow differential labelling of previously palmitoylated cysteine residues once proteins are eluted from thiopropyl sepharose (see section 2.6.2 for details of acyl rac). Differential labelling of cysteine residues will allow identification of potential palmitoylation sites by mass spectrometry.

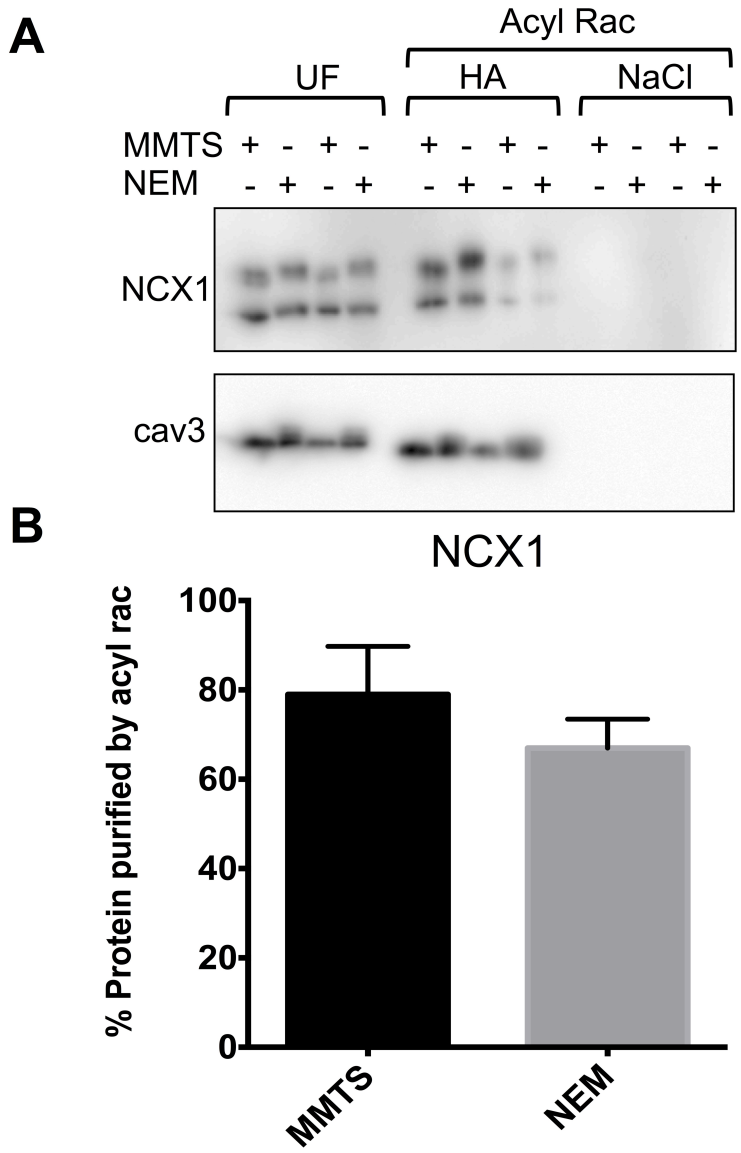


***Figure 3.3: NCX1 Is Palmitoylated In ARVM. A.*** *NCX1 can be purified by acyl rac from isolated ARVM. As a marker for the assay efficiency, the constitutively palmitoylated caveolin-3 (cav3) was also investigated.* ***B.*** *Mean data revealed no significant difference between NCX1 purification between MMTS (79% ± 10.7, n=6) and NEM (67% ± 6.5, n=6). UF – unfractionated, Ha – hydroxylamine, MMTS - S-Methyl methanethiosulfonate, NEM – N-Ethylmaleimide. Representative of 6 independent replicates.*

As shown in figure 3.3, NCX1 is palmitoylated, as it is observed in acyl rac fractions treated with hydroxylamine, which cleaves thioester bonds and reveals previously palmitoylated cysteine residues, allowing capture via thiopropyl sepharose. Additionally, caveolin-3 is a constitutively palmitoylated protein identified via acyl rac, confirming the effectiveness of this assay to capture palmitoylated proteins. Comparison of MMTS and NEM revealed that there is no significant difference using

either as a blocking agent prior to acyl rac to capture palmitoylated NCX1. The graph in figure 3.3 shows the mean palmitoylation data from 6 independent replicates for MMTS and NEM treated experiments. This is calculated as mean bound as a percentage of mean starting material. These results suggest that NEM is suitable for alkylating free cysteines, therefore making it a suitable alkylating agent for analysing palmitoylated proteins by mass spectrometry following acyl rac.

### 3.4 NCX1 Is Sub-Stoichiometrically Palmitoylated In ARVM

Caveolin-3 is known to be constitutively palmitoylated protein. This was utilised to estimate the extent of NCX1 palmitoylation. In addition to analysing the unfractionated (UF) and bound (B) fractions of the Acyl Rac protocol, the unbound (UB) fraction was analysed to determine if all NCX1 and caveolin-3 were being captured by the assay (figure 3.4). The double band corresponding to NCX1 was observed in UB fraction from acyl rac, suggesting acyl rac did not purify all of NCX1 present. Conversely, no caveolin-3 was observed in UB fractions, suggesting that acyl rac purified all of palmitoylated caveolin-3. Both NCX1 and caveolin-3 were observed in the bound fractions treated with hydroxylamine. This supports evidence suggesting caveolin-3 is 100% palmitoylated (Dietzen et al. 1995). In contrast, in the absence of hydroxylamine, NCX1 and caveolin-3 are not purified by acyl rac (bands present in UB NaCl fraction) confirming the specificity of capture. Normalised to caveolin-3 palmitoylation, acyl rac is able to purify approximately 60% of NCX1 from ARVM. This suggests that NCX1 is sub-stoichiometrically palmitoylated in ARVM.

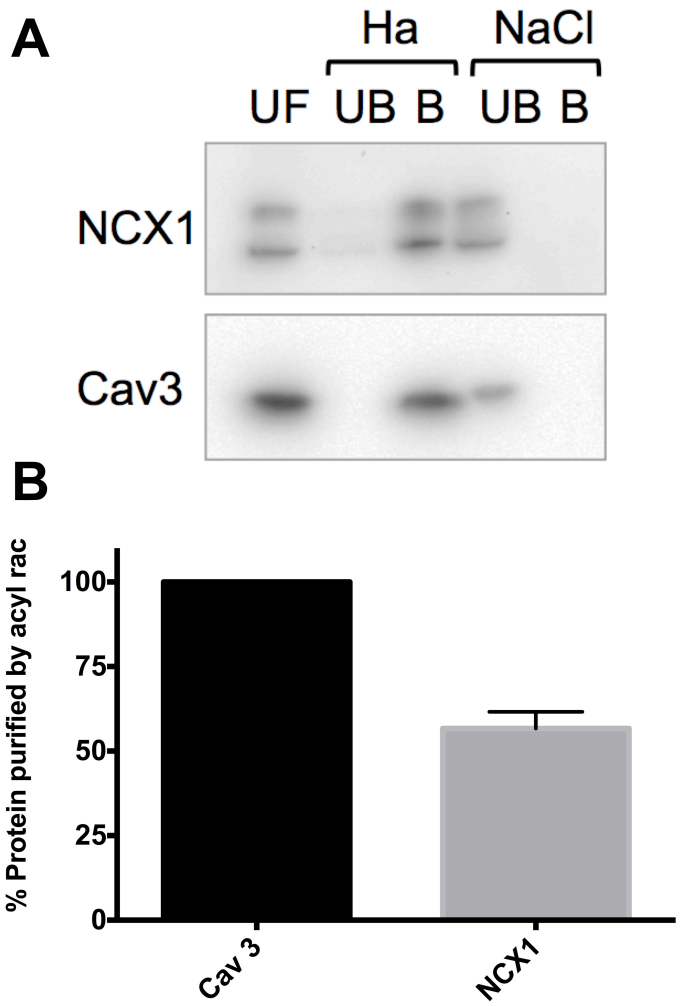


***Figure 3.4: NCX1 Is Sub-Stoichiometrically Palmitoylated In ARVM. A.*** *NCX1 was purified by acyl rac. Not all NCX1 was captured using this technique, suggesting it is not 100% palmitoylated. Acyl rac is able to purify all of palmitoylated caveolin-3.* ***B.*** *Estimating stoichiometry against caveolin-3, which is 100% palmitoylated, reveals NCX1 to be approximately 60% palmitoylated. Cav3, 100% ± 0, n=6, NCX1, 56.7% ± 4.9, n=6. UF – unfractionated, UB – unbound, B – bound, Ha – hydroxylamine, NaCl – sodium chloride. Representative of 6 independent replicates.*

### 3.5 Palmitoylation Of NCX1 Is Not Splice Variant Specific

As NCX1.1 can be purified by acyl rac, it was investigated whether this was specific to the cardiac splice variant. NCX1 is subject to alternative splicing within the intracellular loop, which are expressed in a tissue specific manner (Quednau, Nicoll & Philipson 1997b). To determine whether palmitoylation was confined to the NCX1.1 splice variant, whole brain or whole kidney lysates were subjected to acyl rac. The predominant splice variants in brain are NCX1.4, NCX1.5 and NCX1.6, whereas

NCX1.3 and NCX1.7 are predominant in kidney. The NCX1 monoclonal antibody, R3F1, was originally raised against the cardiac NCX1 (Porzig et al. 1993), however there is evidence to suggest that this antibody is capable of recognising other splice variants (Hurtado et al. 2006; Ander et al. 2007). Therefore NCX1 monoclonal antibody, R3F1, was used to detect brain and kidney NCX1 palmitoylation.

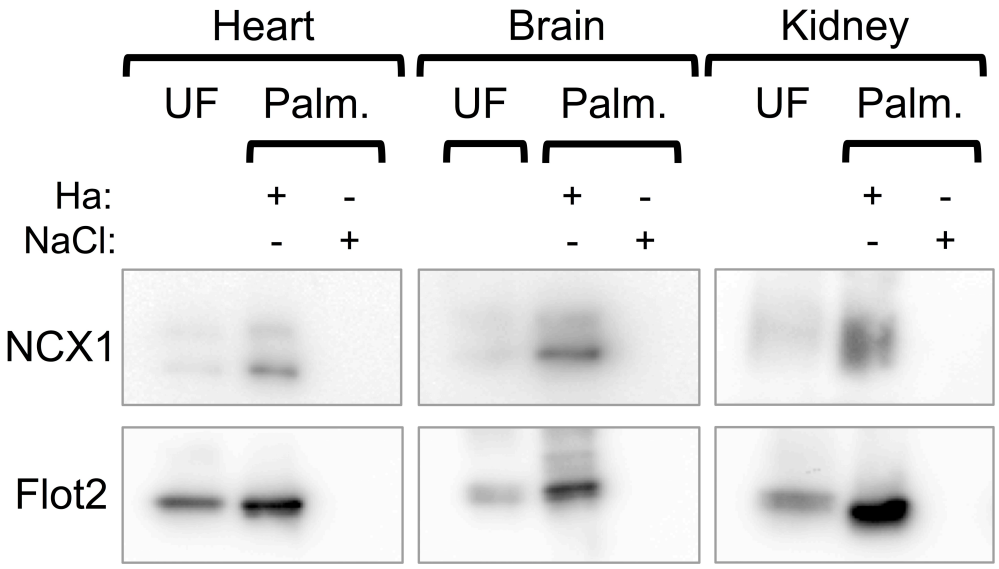


***Figure 3.5: Palmitoylation Is Not Specific To The Cardiac Splice Variant Of NCX1.*** *Splice variants of NCX1 expressed in brain and kidney are also targets of protein palmitoylation. NCX1 splice variants in these tissues are successfully captured by acyl rac. UF – unfractionated, Palm. – palmitoylated, Ha – hydroxylamine, NaCl – sodium chloride, Flot2 – flotillin 2. n=3.*

Shown in figure 3.5, NCX1 splice variants are detected by R3F1 NCX1 monoclonal antibody, bands corresponding to NCX1 are observed in UF samples from brain and kidney. Additionally, brain and kidney lysates reveal that NCX1 is palmitoylated in these tissues as NCX1 is purified by acyl rac in the presence of hydroxylamine. This interaction is specific since no NCX1 is detected when acyl rac is performed in the presence of NaCl. Flotillin-2 is also palmitoylated in all tissues examined, and is also captured during acyl rac in the presence of hydroxylamine. These results suggest that palmitoylation is not specific to the cardiac splice variant but occurs on other splice variants, regardless of expression within excitable and non-excitable cell types.

### 3.6 SDS Is Essential For Elution Of Palmitoylated Proteins Captured By Acyl Rac

Routinely, proteins captured by acyl rac were eluted using 2 X SDS-Loading Buffer containing 100mM DTT. In order to characterise the cardiac palmitoyl proteome, mass spectrometry was utilised to identify proteins captured during acyl rac. However, SDS is not compatible with mass spectrometry, therefore an alternative method of elution from the thiopropyl sepharose was required. Proteins are digested with trypsin prior to mass spectrometry. Digestion would be inhibited with SDS present, however urea is more compatible. Elution from thiopropyl sepharose was done using alternative reagents. Two different concentrations of urea were used to determine if proteins could be solubilised. Additionally, temperature was also investigated, with room temperature and 37°C since some proteins can be subject to temperature dependent aggregation effects (Section 3.2). Acyl rac was used to purify palmitoylated proteins from isolated ARVM. During the last wash step of acyl rac protocol, the sample was split into 3. Thiopropyl sepharose was recovered by centrifugation and proteins were eluted with 100mM DTT plus 2 X SDS-Loading Buffer lacking bromophenol blue, 0.8M Urea or 8M Urea. Samples were analysed by SDS-PAGE gel electrophoresis followed by western blotting. Membranes were probed for NCX1 and caveolin-3 to investigate efficiency of elution.

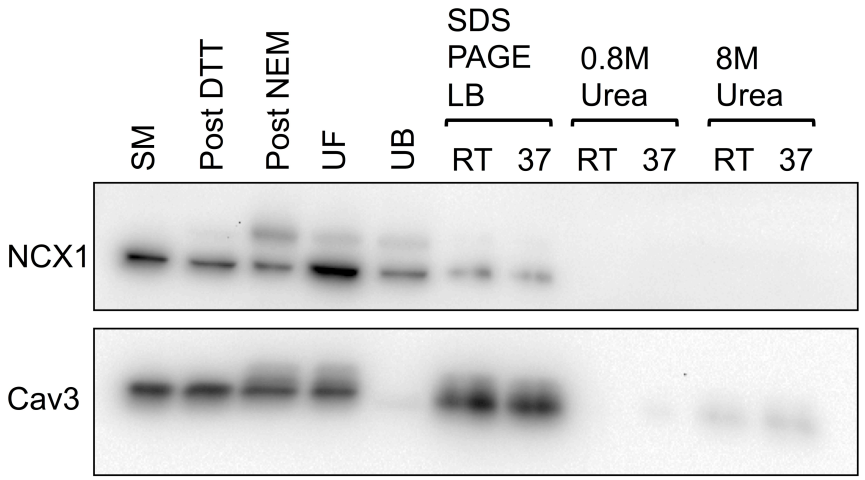


***Figure 3.6: SDS Is Essential For Elution Of Proteins From Thiopropyl Sepharose.*** *Samples taken and analysed throughout the acyl rac protocol then assessed for the ability of SDS and 2 different concentrations of Urea to solubilise proteins reveal that SDS is required to elute from sepharose. SM – starting material, DTT – Dithiothreitol, NEM – N- Ethylmaleimide, UF – unfractionated, UB – unbound, RT – room temperature. Representative of 3 independent experiments.*

NCX1 and caveolin-3 were detected in fractions eluted with SDS. There was no difference between level of proteins eluted between room temperature and 37°C. No bands corresponding to NCX1 or caveolin-3 were observed in samples eluted in the presence of 0.8M Urea, regardless of temperature used. Despite increasing the concentration of urea to 8M, NCX1 was not eluted to the same extent as with SDS. A small amount of caveolin-3 was eluted in the presence of 8M Urea, but not to the same level as SDS. Based on these results, proteins were solubilised with SDS, thus aiding elution with 100mM DTT, which was removed prior to mass spectrometry via filter aided sample preparation (FASP) (Section 2.11).

### 3.7 PANTHER Analysis Reveals Functions Of Proteins In Cardiac Palmitoyl Proteome

Mass spectrometry is capable of identifying large numbers of proteins through peptide recognition. To analyse a large data set, it is useful to determine functions of proteins identified. In order to generate a comprehensive overview of the cardiac palmitoyl proteome, 3 different data sets were pooled. Mass spectrometry data from acyl rac performed on isolated ARVM and whole heart were used. An additional data set from Dr Jacqueline Howie utilising acyl rac from isolated ARVM followed by iTRAQ, which determines amounts of proteins in a given sample via isobaric labelling followed by quantative proteomics by tandem mass spectrometry. Protein lists produced from the 3 experiments were compared and only high confidence candidates (appeared in 2 data sets or more) selected for further analysis. Mitochondrial proteins were removed from the list using MitoMiner. The remaining proteins were then analysed using **P**rotein **AN**alysis **TH**rough **E**volutionary **R**elationship (PANTHER) analysis, which classifies proteins and their genes (Mi et al. 2013). Resultant protein hits were classified according to family and subfamily, molecular function, biological process and pathway.

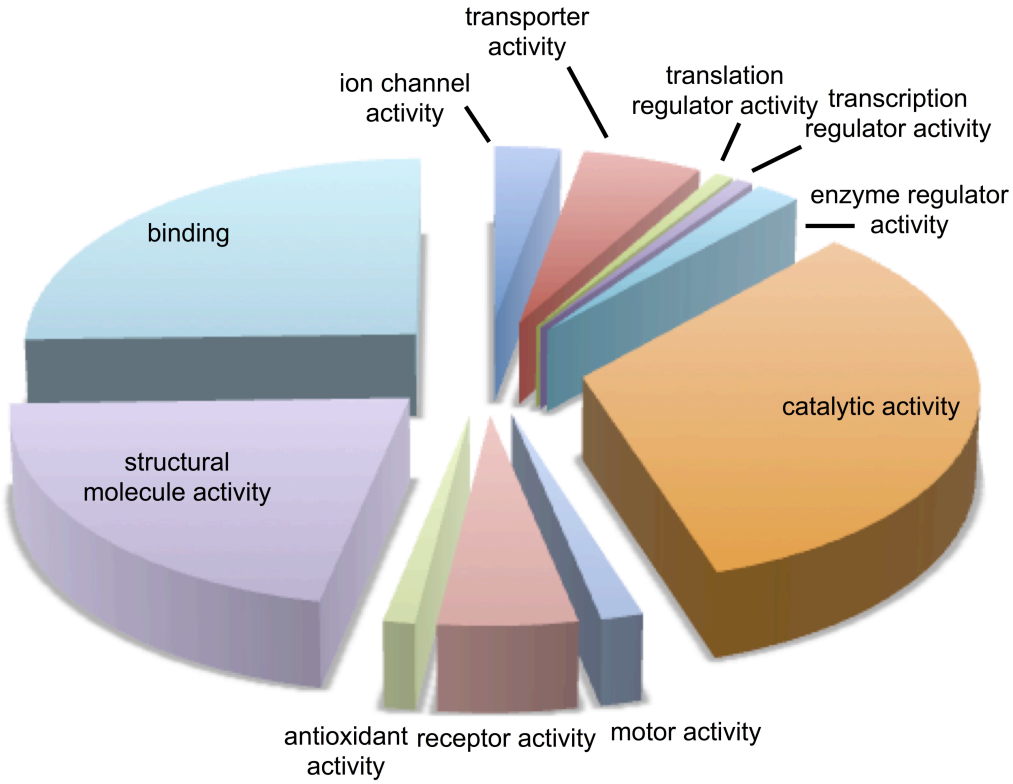


***Figure 3.7: PANTHER Analysis Reveals Respective Functions Of Palmitoylated Proteins Identified By Mass Spectrometry.*** *PANTHER analysis revealed that palmitoylated proteins in cardiac tissue have a variety of different functions.*

PANTHER analysis revealed that a large number of the proteins identified by mass spectrometry are associated with membranes. Shown in Figure 3.7, proteins possessing catalytic activity, structural molecule activity and binding activity are most abundant in this data set. Additional functions of proteins identified by mass spectrometry are ion channel, transporter activity, translation regulator activity, transcription regulator activity, enzyme regulator activity, antioxidant activity, receptor activity and motor activity. The functions of proteins identified by mass spectrometry are wide-ranging, indicating that palmitoylation is an important post-translational modification in cardiac tissue for a variety of different proteins. For a full list of proteins that were identified by mass spectrometry, see Appendix 1.

### 3.8 DAVID Analysis Indicates Functional Pathways That Are Palmitoylated In Cardiac Tissue

In addition to analysing the proteomic dataset identified by mass spectrometry using PANTHER analysis, DAVID analysis was also employed. DAVID bioinformatics resources are designed to enable users to extract biological meaningful data from large proteomic data sets (Huang et al. 2008). This analysis maps identified genes associated biological annotation (gene ontology terms) and then statistically determines the most represented (enriched) biological annotation out of thousands of linked terms and contents. The enrichment analysis allows users to identify biological processes that are most relevant to their biological phenomenon. The 287 UniProt Accession IDs remaining following MitoMiner analysis were uploaded to DAVID Bioinformatics Resources Version 6.7. Once generated, the results were functionally clustered at high classification stringency.

| Annotation Cluster 3 | Enrichment Score: 12.735748834017336 | | | | |
|---|---|---|---|---|---|
| Category | Term | Count | % | P Value | Genes |
| GOTERM_CC_FAT | GO:0005624~membrane fraction | 53 | 18.72791519 | 3.21E-13 | Q07065, P51636, Q6PIU2, Q03135, Q9Y512, O60716, P05023, P29992, O00161, O75955, P05556, Q92523, P11717, Q9Y4J8, Q9BTU6, O75323, Q92736, Q13813, P48751, P56539, Q9UIQ6, Q9Y277, P27105, Q15836, Q9UP95, P33121, P35222, P16615, P04899, O96008, P48509, P13929, P07947, P55072, Q14118, Q6NZI2, Q5JWF2, Q14254, Q13936, P14923, O43306, P28907, O14880, P20338, P32418, O43169, P09471, P53985, P16671, P11532, P01111, Q14108, P01112 |
| Annotation Cluster 5 | Enrichment Score: 10.132955758953933 | | | | |
| Category | Term | Count | % | P Value | Genes |
| GOTERM_BP_FAT | GO:0006096~glycolysis | 14 | 4.946996466 | 7.85E-13 | P04406, P40925, P60174, P18669, P04075, P06733, P00338, P06744, P07195, P19367, P08237, P13929, P00558, P14618 |
| Annotation Cluster 8 | Enrichment Score: 6.435714036308812 | | | | |
| Category | Term | Count | % | P Value | Genes |
| GOTERM_MF_FAT | GO:0003924~GTPase activity | 19 | 6.713780919 | 1.31E-08 | Q5JWF2, Q05639, P62070, Q9NP72, P08134, P68371, P04899, P11233, Q14344, P20338, P13639, P10114, P68366, P09471, Q9BQE3, P10301, P01111, P01112, P29992 |
| Annotation Cluster 12 | Enrichment Score: 4.710148595890581 | | | | |
| Category | Term | Count | % | P Value | Genes |
| GOTERM_BP_FAT | GO:0065003~macromolecular complex assembly | 27 | 9.540636042 | 9.28E-05 | P27105, P19022, Q8WZ42, Q15836, P51636, Q99714, P04040, P35222, Q03135, P35609, P68371, P02511, P17302, P68366, Q9Y512, Q6ZMU5, Q9BQE3, P11047, Q14118, P55072, O43920, Q6NZI2, P14923, P20671, P08237, P01112 |
| Annotation Cluster 14 | Enrichment Score: 4.325018055765178 | | | | |
| Category | Term | Count | % | P Value | Genes |
| GOTERM_BP_FAT | GO:0050801~ion homeostasis | 20 | 7.067137809 | 9.68E-05 | P02787, P12277, P21926, P50461, P02786, P26678, P00441, Q13936, P16615, Q03135, Q92736, P19429, P28907, Q14344, P11217, P32418, P56539, O00168, P29992, P23327 |

***Figure 3.8: DAVID Analysis Reveals An Array Of Biological Functional Clusters As Palmitoylated Within Cardiac Muscle.*** *Utilising DAVID analysis revealed 122 functional clusters as palmitoylated within cardiac muscle. Shown is a selection of functional clusters, highlighting the diverse range of functions found with the cardiac palmitoyl proteome. DAVID Bioinformatics Resources, version 6.7 was used.*

Figure 3.8 details a selection of functional clusters identified by DAVID analysis. As previously shown by PANTHER analysis, a wide variety of functions of proteins were identified by mass spectrometry. Functional clustering reveals proteins involved in membranes scaffolding, glycolysis, GTP binding, macromolecular complex assembly and ion homeostasis. 122 functional clusters were identified within cardiac muscle. A number of proteins found within each of these functional clusters have been described previously, in other tissues and cell types as being palmitoylated (Dietzen et al. 1995; Morrow et al. 2002; Linder et al. 1993; Howie et al. 2013). Identification of these proteins within the cardiac palmitoyl proteome confirms that mass spectrometry is capable of identifying palmitoylated proteins and the efficiency of acyl rac to capture palmitoylation proteins.

### 3.9 Verification Of Specific Targets Identified By Mass Spectrometry

A major disadvantage of using mass spectrometry to identify proteins within a sample is the possibility of false positives. Proteins that are abundant in the sample can contaminate the final sample. Due to their high abundance, these proteins may not be removed during wash steps completely and have a tendency to appear on mass spectrometry identification lists as positive hits. To ensure only positive hits were investigated further, we subjected isolated ARVM to acyl rac and analysed by SDS-PAGE gel electrophoresis followed by western blotting.

| Functional cluster | P Value (enrichment) |
|---|---|
| Membrane fraction | $3.2 \times 10^{-13}$ |
| UF + - 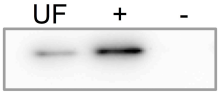 ***flotillin 1:*** | |
| GTPase activity | $1.3 \times 10^{-8}$ |
| UF + - 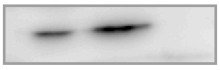 ***Giα:*** | |
| Glycolysis | $7.9 \times 10^{-13}$ |
| UF + - 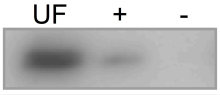 ***GAPDH:*** | |
| Macromolecular complex assembly | $9.3 \times 10^{-5}$ |
| UF UB+ B+ UB- B- 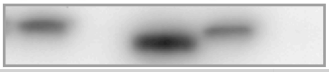 ***caveolin 3:*** | |
| Regulation of ion transport | $9.7 \times 10^{-5}$ |
| UF UB+ B+ UB- B-  ***NCX1:*** | |

***Figure 3.9: Verification Of Proteins Identified By Mass Spectrometry.*** *Acyl rac was performed on isolated ARVM and resultant samples immunoblotted for proteins of interest. Representative members of functional clusters identified by DAVID analysis were selected. UF – unfractionated, + - with hydroxylamine, - - without hydroxylamine, UB – unbound, B – bound.*

Representative members of select functional clusters identified by DAVID analysis (Section 3.8) were selected for investigation. Flotillin-1, the alpha subunit of $G_i$, GAPDH and caveolin-3 have been previously described to be palmitoylated (Morrow et al. 2002; Linder et al. 1993; Yang et al. 2005; Dietzen et al. 1995). Shown in Figure 3.9, flotillin-1, $G_i$alpha subunit, GAPDH, caveolin-3 and NCX1 were captured by acyl rac due to their visualisation in bound fractions following western blot analysis. Given that these targets have been previously described to be palmitoylated confirms the specificity of acyl rac in capturing palmitoylated proteins. Interestingly, the level of palmitoylation observed varies between targets, suggesting they are palmitoylated to differing levels. GAPDH, for instance, is much less palmitoylated compared to the constitutively palmitoylated caveolin-3 and flotillin-1. The P value shown is the

DAVID enrichment P value (Huang et al. 2008). Flotillin-1, $G_i$alpha subunit and GAPDH are well enriched in this sample, suggesting that acyl rac has captured a greater proportion of these proteins, or that they are simply more abundant in cardiac tissue compared to caveolin-3 and NCX1.

### 3.10 Mass Spectrometry Reveals Cys557 Is Not A Potential Palmitoylation Site

As previously described, non-palmitoylated cysteine residues were alkylated with NEM, and following elution from thiopropyl sepharose, palmitoylated proteins were differentially alkylated with iodoacetamide. All proteins captured were digested with trypsin and analysed using mass spectrometry. Differential alkylation of cysteine residues allows identification of previously palmitoylated cysteine residues and non-palmitoylated residues (Forrester et al. 2011). Mascot was used to match peptides identified by mass spectrometry to proteins and produce a coverage map of proteins identified.

```
  1 MLRLSLPPNV SMGFRLVTLV ALLFTHVDHI TADTEAETGG NETTECTGSY
 51 YCKKGVILPI WEPQDPSFGD KIARATVYFV AMVYMFLGVS IIADRFMSSI
101 EVITSQEKEI TIKKPNGETT KTTVRIWNET VSNLTLMALG SSAPEILLSV
151 IEVCGHNFTA GDLGPSTIVG SAAFNMFIII ALCVYVVPDG ETRKIKHLRV
201 FFVTAAWSIF AYTWLYIILS VSSPGVVEVW EGLLTFFFFP ICVVFAWVAD
251 RRLLFYKYVY KRYRAGKQRG MIIEHEGDRP ASKTEIEMDG KVVNSHVDNF
301 LDGALVLEVD ERDQDDEEAR REMARILKEL KQKHPDKEIE QLIELANYQV
351 LSQQQKSRAF YRIQATRLMT GAGNILKRHA ADQARKAVSM HEVNMDVVEN
401 DPVSKVFFEQ GTYQCLENCG TVALTIIRRG GDLTNTVFVD FRTEDGTANA
451 GSDYEFTEGT VIFKPGETQK EIRVGIIDDD IFEEDENFLV HLSNVRVSSE
501 VSEDGILDSN HVSAIACLGS PNTATITIFD DDHAGIFTFE EPVTHVSESI
551 GIMEVKVLRT SGARGNVIIP YKTIEGTARG GGEDFEDTCG ELEFQNDEIV
601 KIITIRIFDR EEYEKECSFS LVLEEPKWIR RGMKALLLNE LGGFTLTGKK
651 MYGQPVFRKV HARDHPIPST VISISEEYDD KQPLTSKEEE ERRIAEMGRP
701 ILGEHTKLEV IIEESYEFKS TVDKLIKKTN LALVVGTNSW REQFIEAITV
751 SAGEDDDDDE CGEEKLPSCF DYVMHFLTVF WKVLFAFVPP TEYWNGWACF
801 IVSILMIGLL TAFIGDLASH FGCTIGLKDS VTAVVFVALG TSVPDTFASK
851 VAATQDQYAD ASIGNVTGSN AVNVFLGIGV AWSIAAIYHA ANGEQFKVSP
901 GTLAFSVTLF TIFAFINVGV LLYRRRPEIG GELGGPRTAK LLTSSLFVLL
951 WLLYIFFSSL EAYCHIKGF
```

***Figure 3.10: Coverage Map Of NCX1.*** *Coverage map produced by Mascot following mass spectrometry. Residues shown in red were covered by mass spectrometry. Resultant coverage was approximately 27%.*

Since NCX1 is a large protein, achieving full coverage by mass spectrometry is difficult. As a result, coverage of NCX1 was approximately 27%. Of this 27%, only 1 cysteine residue out of a possible 15 was covered (Figure 3.10). Nevertheless, despite

the poor coverage of cysteine residues, Cys557 was identified as not being a palmitoylation site. Shown in Figure 3.11, the presence of N-ethylmaleimide on Cys557 (highlighted by the black box) suggests that this cysteine residue was not previously palmitoylated. Since NCX1 is not 100% palmitoylated, palmitoylation sites could be labelled with both NEM and IAA, making site identification tricky.

| Start - End | Observed | Mr(expt) | Mr(calc) | ppm | Miss | Sequence |
|---|---|---|---|---|---|---|
| 55 - 71 | 633.3283 | 1896.9631 | 1896.9622 | 0 | 0 | K.GVILPIWEPQDPSFGDK.I (Ions score 38) |
| 55 - 71 | 949.4891 | 1896.9637 | 1896.9622 | 1 | 0 | K.GVILPIWEPQDPSFGDK.I (Ions score 50) |
| 270 - 283 | 770.3827 | 1538.7508 | 1538.7511 | -0 | 1 | R.GMIIEHEGDRPASK.T (Ions score 46) |
| 386 - 405 | 743.3607 | 2227.0603 | 2227.0613 | -0 | 1 | R.KAVSMHEVNMDVVENDPVSK.V (Ions score 46) |
| 430 - 442 | 720.8605 | 1439.7064 | 1439.7045 | 1 | 0 | R.GGDLTNTVFVDFR.T (Ions score 42) |
| 443 - 470 | 998.1296 | 2991.3671 | 2991.3622 | 2 | 1 | R.TEDGTANAGSDYEFTEGTVIFKPGETQK.E (Ions score 47) |
| 474 - 496 | 1344.6596 | 2687.3045 | 2687.3079 | -1 | 0 | R.VGIIDDDIFEEDENFLVHLSNVR.V (Ions score 74) |
| 474 - 496 | 896.7764 | 2687.3075 | 2687.3079 | -0 | 0 | R.VGIIDDDIFEEDENFLVHLSNVR.V (Ions score 42) |
| 474 - 496 | 896.7769 | 2687.3088 | 2687.3079 | 0 | 0 | R.VGIIDDDIFEEDENFLVHLSNVR.V (Ions score 54) |
| 474 - 496 | 896.7775 | 2687.3106 | 2687.3079 | 1 | 0 | R.VGIIDDDIFEEDENFLVHLSNVR.V (Ions score 52) |
| 474 - 496 | 896.7790 | 2687.3153 | 2687.3079 | 3 | 0 | R.VGIIDDDIFEEDENFLVHLSNVR.V (Ions score 36) |
| 580 - 601 | 1278.5406 | 2555.0667 | 2555.0646 | 1 | 0 | R.GGGEDFEDTCGELEFQNDEIVK.T Nethylmaleimide (C) (Ions score 46) |
| 618 - 627 | 604.8192 | 1207.6239 | 1207.6237 | 0 | 0 | K.TFFIEIGEPR.L (Ions score 58) |
| 653 - 676 | 900.4526 | 2698.3359 | 2698.3337 | 1 | 1 | R.DHPIPSTVISISEEYDDKQPLTSK.E (Ions score 40) |
| 653 - 681 | 843.6588 | 3370.6059 | 3370.6052 | 0 | 2 | R.DHPIPSTVISISEEYDDKQPLTSKEEEER.R (Ions score 70) |
| 683 - 696 | 776.4191 | 1550.8237 | 1550.8239 | -0 | 1 | R.IAEMGRPILGEHTK.L (Ions score 51) |
| 914 - 926 | 465.2602 | 1392.7587 | 1392.7586 | 0 | 2 | R.RRPEIGGELGGPR.T (Ions score 39) |
| 914 - 926 | 697.3867 | 1392.7588 | 1392.7586 | 0 | 2 | R.RRPEIGGELGGPR.T (Ions score 36) |
| 915 - 926 | 619.3360 | 1236.6574 | 1236.6575 | -0 | 1 | R.RPEIGGELGGPR.T (Ions score 58) |

***Figure 3.11: Cys557 Is Not Palmitoylated In NCX1.*** *Mass spectrometry revealed that Cys557 is palmitoylated as designated by the presence of Nethylmaleimide (NEM) to the peptide (highlighted by the black box).*

The ion score of Cys557 is 46. In Mascot, the ion score is based on calculated probability, P, that the observed match between the experimental data and the database sequence is a random event. Therefore, if 1500 peptides fall within the tolerance window about precursor mass, and the significance level was 0.05, this would translate as an ion score of 45 or greater. Based on this, Cys557 is a genuine hit. However, Cys557 is 1 of 15 possible sites, therefore mass spectrometry has only eliminated one potential site. This is disappointing, given the high number of cysteines present, it was hoped that mass spectrometry could have eliminated more than 1 site.

## 3.11 Discussion

One of the major aims from this work was to determine NCX1 palmitoylation status and stoichiometry in cardiac muscle. As described previously, NCX1 plays an important role in the removal of $Ca^{2+}$ from the cytosol during diastole (Bers 2002). Although the structure-function relationship of NCX1 is well studied, less is known about its post-translational regulation. An appreciation is growing that palmitoylation is important in the regulation of protein function (Linder & Deschenes 2007). Of particular interest is recent evidence to suggest a role for palmitoylation in the regulation of ion transport (Shipston 2011; Howie et al. 2013).

### Temperature Sensitivity Of NCX1

During the course of this work, it became evident that NCX1 appeared as a double band when analysed by SDS-PAGE gel electrophoresis followed by western blotting. Philipson and colleagues previously described that NCX1 forms a disulphide bond between Cys 14 or 20 and Cys792 (Santacruz-Toloza et al. 2000). They report that under reducing conditions NCX1 appears as two bands of 120kDa and 70kDa molecular masses respectively following SDS-PAGE gel electrophoresis. Conversely under non-reducing conditions, NCX1 appears as a higher molecular weight band of 160kDa. Band shifts occurring in the presence and absence of reducing agents is suggestive of the presence of a disulphide bond. Given that DTT reduces the disulphide bond, samples were pre-reduced prior to cysteine alkylation. Prior treatment with DTT had no effect on the appearance of NCX1 as a double band. This suggests that the appearance of NCX1 as a double band is not dependent on the presence of a disulphide. Previous publications from Philipson and colleagues indicate that molecular mass of NCX1 varies dependent on SDS-PAGE conditions (Philipson et al. 1988). Interestingly, the double band only appears after heating at temperatures above 37°C, indicating that NCX1 forms aggregates as a result of heating. This would indeed result in a molecular weight band shift, as the higher molecular weight species would not migrate as easily through polyacrylamide gels.

Inclusion of different routinely used reducing agents had an effect on the appearance of NCX1 analysed by SDS-PAGE gel electrophoresis and western blotting (Figure 3.2). Without reducing agent, NCX1 appears as a higher molecular weight species following

exposure to 60°C. Including DTT in the sample prior to SDS-PAGE gel electrophoresis reduced this species to a lower molecular weight. Interestingly, β-mercaptoethanol has a profound detrimental effect on visualisation of NCX1 by western blotting by almost reducing its appearance completely. This suggests that β-mercaptoethanol facilitates temperature dependent aggregation of NCX1 at temperatures above 37°C. Furthermore, DTT appears to be more efficient at maintaining protein stability at higher temperatures. Despite being more efficient at stabilising NCX1 at higher temperatures, DTT did not prevent the detrimental effect of β-mercaptoethanol. DTT was used at 100mM, whereas β-mercaptoethanol was used at 700mM. This may explain why the effect of β-mercaptoethanol on NCX1 visualisation was not rescued by adding DTT as β-mercaptoethanol is in excess.

**NCX1 Palmitoylation Status In Cardiac Muscle**

Enriching palmitoylated proteins from isolated ARVM revealed that NCX1 is palmitoylated. Additionally, the constitutively palmitoylated caveolin-3 was captured by acyl rac. This confirms the specificity of this assay to capture palmitoylated proteins as caveolin-3 has previously been shown to be palmitoylated (Dietzen et al. 1995). Assessing compatibility of different alkylating agents revealed no significant difference between each agent for use in acyl rac as palmitoylated proteins can be purified to approximately the same extent. To estimate NCX1 palmitoylation stoichiometry, i.e. how much of NCX1 is palmitoylated, enrichment of NCX1 following acyl rac was compared to the constitutively palmitoylated caveolin-3 (Dietzen et al. 1995). As a result, NCX1 palmitoylation stoichiometry was estimated to be approximately 60%. Therefore NCX1 is sub-stoichiometrically palmitoylated in cardiac muscle. If NCX1 was 100% palmitoylated, this may suggest that palmitoylation is obligatory for cellular functions of NCX1 (e.g. membrane targeting), which is an established regulatory mechanism (Linder & Deschenes 2007). Given that NCX1 palmitoylation is estimated to be 60%, this suggests that palmitoylation may play a role in the regulation of NCX1, potentially in a dynamic way. There is increasing evidence for dynamic palmitoylation of targets, in contrast to the historical opinion that palmitoylation was a stable modification (Martin et al. 2011).

**Palmitoylation Status Of Alternatively Spliced Variants Of NCX1**

The canine sarcolemmal NCX1 was first cloned in 1990 and designated NCX1.1 (Nicoll et al. 1990). Since this point, NCX1 has been cloned from multiple species and tissues (Komuro et al. 1992; Low et al. 1993; Schulze et al. 1996). The wide expression profile of NCX suggests that it plays an important physiological role in various cell types. NCX1 is most abundant in the heart but is found in many other tissues and cells, such as brain, kidney, skeletal muscle, smooth muscle, lung and spleen(Quednau, Nicoll & Philipson 1997b). The C-terminus of the large intracellular loop domain contains a variable region of 110 amino acids that is subject to alternative splicing. The genomic structure within this region contains a cluster of 6 exons, designated A, B, C, D, E and F (Quednau, Nicoll & Philipson 1997b). Exons A and B are mutually exclusive, whereas C, D, E and F are cassette exons (Kofuji et al. 1994). Presently, there are 12 known splice variants of NCX1 (Quednau, Nicoll & Philipson 1997b), which are thought to convey functional diversity amongst the different splice variants. To investigate whether palmitoylation was restricted to the cardiac splice variant, NCX1.1, we subjected brain and kidney lysates to acyl rac. Brain predominantly expresses NCX1.4, 1.5 and 1.6, whereas kidney expresses NCX1.3 and 1.7 (Quednau, Nicoll & Philipson 1997b). The results revealed that NCX1 splice variants expressed in brain and kidney are palmitoylated. This is unsurprising, given that alternative splicing of NCX1 does not remove any cysteine residues (Figure 3.12).

```
NCX1.1    EPVTHVSESIGIMEVKVLRTSGARGNVIIPYKTIEGTARGGGEDFEDTCGELEFQNDEIV     600
NCX1.3    EPVTHVSESIGIMEVKVLRTSGARGNVIIPYKTIEGTARGGGEDFEDTCGELEFQNDEIV     600
NCX1.4    EPVTHVSESIGIMEVKVLRTSGARGNVIIPYKTIEGTARGGGEDFEDTCGELEFQNDEIV     600
NCX1.5    EPVTHVSESIGIMEVKVLRTSGARGNVIIPYKTIEGTARGGGEDFEDTCGELEFQNDEIV     600
NCX1.6    EPVTHVSESIGIMEVKVLRTSGARGNVIIPYKTIEGTARGGGEDFEDTCGELEFQNDEIV     600
NCX1.7    EPVTHVSESIGIMEVKVLRTSGARGNVIIPYKTIEGTARGGGEDFEDTCGELEFQNDEIV     600
          ************************************************************

NCX1.1    KTISVKVIDDEEYEKNKTFFIEIGEPRLVEMSEKKALLLNELGGFTLTEGKKMYGQPVFR     660
NCX1.3    KTISVKVIDDEEYEKNKTFFIEIGEPRLVEMSEKKG-------GF--------------     638
NCX1.4    KIITIRIFDREEYEKECSFSLVLEEPKWIRRG-MK-------GGFTL------TGQPVFR     646
NCX1.5    KIITIRIFDREEYEKECSFSLVLEEPKWIRRG-MK-------GGFT--------------     638
NCX1.6    KIITIRIFDREEYEKECSFSLVLEEPKWIRRG-MK-------GGFTLT-GKKMYGQPVFR     651
NCX1.7    KIITIRIFDREEYEKECSFSLVLEEPKWIRRG-MKALLLNELGGFTLT-GKKMYGQPVFR     658
          * *::::::* *****: :* : : **: :. .  *        **

NCX1.1    KVHARDHPIPSTVISISEEYDDKQPLTSKEEEERRIAEMGRPILGEHTKLEVIIEESYEF     720
NCX1.3    --------------TLTEEYDDKQPLTSKEEEERRIAEMGRPILGEHTKLEVIIEESYEF     684
NCX1.4    KVHARDHPIPSTVISISEEYDDKQPLTSKEEEERRIAEMGRPILGEHTKLEVIIEESYEF     706
NCX1.5    ---------------LTEEYDDKQPLTSKEEEERRIAEMGRPILGEHTKLEVIIEESYEF     683
NCX1.6    KVHARDHPIPSTVISISEEYDDKQPLTSKEEEERRIAEMGRPILGEHTKLEVIIEESYEF     711
NCX1.7    KVHARDHPIPSTVISISEEYDDKQPLTSKEEEERRIAEMGRPILGEHTKLEVIIEESYEF     718
                       ::*****************************************

NCX1.1    KSTVDKLIKKTNLALVVGTNSWREQFIEAITVSAGEDDDDDECGEEKLPSCFDYVMHFLT     780
NCX1.3    KSTVDKLIKKTNLALVVGTNSWREQFIEAITVSAGEDDDDDECGEEKLPSCFDYVMHFLT     744
NCX1.4    KSTVDKLIKKTNLALVVGTNSWREQFIEAITVSAGEDDDDDECGEEKLPSCFDYVMHFLT     766
NCX1.5    KSTVDKLIKKTNLALVVGTNSWREQFIEAITVSAGEDDDDDECGEEKLPSCFDYVMHFLT     743
NCX1.6    KSTVDKLIKKTNLALVVGTNSWREQFIEAITVSAGEDDDDDECGEEKLPSCFDYVMHFLT     771
NCX1.7    KSTVDKLIKKTNLALVVGTNSWREQFIEAITVSAGEDDDDDECGEEKLPSCFDYVMHFLT     778
          ************************************************************
```

***Figure 3.12: Clustal Alignment Of NCX1 Splice Variants.*** *Comparison of sequences of 6 splice variants of NCX1. Alignment performed using Clustal Omega.*

The alternative splicing of NCX1 only results in changes C terminal to the $Ca^{2+}$ binding domains (CBDs). Shown in figure 3.12 is a clustal alignment of NCX1 splice variants expressed in heart (NCX1.1), brain (NCX1.4, 1.5 and 1.6) and kidney (NCX1.3 and 1.7). Alternative splicing results in dramatic differences in amino acid sequences, but regulation of NCX1 by alternative splicing is largely uninvestigated to date. Expression of the cardiac splice variant and a kidney splice variant in oocytes revealed differential sensitivities to regulation by voltage, intracellular $Ca^{2+}$ and phosphorylation (Ruknudin et al. 2000). In addition, isoform-specific regulation by protein kinase A (PKA) has also been demonstrated (S. He et al. 1998). Investigation into the ionic regulatory properties of splice variants of NCX1 may provide insight into whether NCX1 is tailored for specific $Ca^{2+}$ handling requirements in different tissues. $Na^{+}$-dependent inactivation is more pronounced in NCX1.3 than NCX1.4 (Dyck et al. 1999). Furthermore, regulatory $Ca^{2+}$ only modestly affected Na-dependent inactivation of NCX1.3, whereas inactivation of NCX1.4 could be completely overcome by intracellular $Ca^{2+}$.

Although differences exist in the regulation of NCX1 splice variants, given that no cysteine residues are removed as a result of splicing suggests that palmitoylation still occurs. Interestingly, alternative splicing of NCX1 results in introduction of a new cysteine residue in NCX1.4, 1.5, 1.6 and 1.7. However, whether this cysteine is a site of palmitoylation within these different splice variants is beyond the scope of this investigation. Palmitoylation may potentially contribute to the differential regulation of splice variants by $Na^{+}$, $Ca^{2+}$, voltage and phosphorylation.

**Requirement Of SDS For Elution Of Palmitoylated Proteins**

Somewhat surprisingly, proteins captured during the acyl rac protocol cannot be eluted from thiopropyl sepharose in the absence of SDS in the elution buffer. Substituting urea at two different concentrations did not result in elution. However a small amount of caveolin-3 was observed following elution with 8M urea, but not same amount as SDS. The mode of binding of SDS to proteins and how the protein is denatured is dependent upon the concentration of SDS used (Bhuyan 2010). At submicellar concentrations of SDS, below 1mM, SDS monomers bind to proteins via hydrophobic interactions and causing unfolding of the tertiary structure. This would allow DTT access to bond between the protein and the thiopropyl sepharose, thus allowing elution of the proteins. In contrast, although high concentrations of urea are capable of denaturing proteins to a similar extent as SDS, this has shown to be dependent on heating the sample to temperatures above 60°C (Bennion & Daggett 2003). Since NCX1 does not tolerate high temperatures, samples were not heated above 37°C. If the denaturing effect of urea largely depends upon heating to higher temperatures; this may explain why proteins could not be eluted. To try and ensure high coverage of NCX1 by mass spectrometry, temperature dependent aggregation was avoided; hence samples were not exposed to high temperatures.

**Functional Analysis Of Palmitoylated Proteins In Cardiac Muscle**

Mass spectrometry is capable of generating a large amount of information regarding proteins present in a particular sample. Therefore, to extract meaningful data from lists of protein IDs generated, the ability to analyse a large dataset is important. Two methods of analysing the data were used, PANTHER analysis and DAVID analysis.

PANTHER analysis groups proteins into their respective functions to facilitate high-throughput analysis. This is particularly useful as it allows the functions of identified proteins to be determined. PANTHER is a comprehensive system that combines gene function, ontology, pathways and statistical analysis allowing analysis of large scale dataset (Mi et al. 2013). Functions of identified genes are classified in different ways; families and subfamilies annotated with ontology terms and sequences assigned to PANTHER pathways. Using genes classified into families and subfamilies allows an overview of functions identified within the dataset. The palmitoylated proteins identified by mass spectrometry revealed a plethora of functions of proteins identified. Unsurprisingly, a number of these proteins are associated with functions that are typically carried out at the cell membrane such as ion channel activity, transport activity, binding, structural membrane activity and catalytic activity. A role in membrane targeting is a well-established role for protein palmitoylation, as well as direct regulation of activity (Linder & Deschenes 2007; Linder & Deschenes 2003; Blaskovic et al. 2013; Blaskovic et al. 2014).

DAVID Analysis was also used to generate information regarding the functions of proteins identified by mass spectrometry. DAVID bioinformatics resources consists of an integrated biological knowledge database and analytical tools that extract biological meaning from large protein/gene lists (Huang et al. 2008). Proteins analysed by DAVID analysis can be functionally clustered into bio-pathways, giving information regarding biological pathways that proteins identified may play a role in. As a useful addition, enriched functionally related gene groups and enriched annotation terms can be identified by this analysis. This provides information regarding how well represented particular proteins are within the protein list. Analysing protein lists in this manner, supports the activities of proteins identified by PANTHER analysis. A number of proteins identified as palmitoylated in cardiac muscle are involved in the same signalling cascades, as shown by the functional clusters such as membrane fraction, glycolysis, GTPase activity, macromolecular complex assembly and ion homeostasis. Functional clusters group proteins involved in the same biological pathway together, providing insight into pathways potentially regulated by protein palmitoylation. Proteins involved in scaffolding of proteins or are integral to the membrane were identified as being palmitoylated, such as flotillin-1 and caveolin-3. Based on the emerging evidence that a number of ion transport mechanisms are regulated by protein palmitoylation, it is not surprising that a diverse range of ion transporters and channels were identified by

mass spectrometry (Shipston 2011). Somewhat surprisingly, all major routes of $Ca^{2+}$ and $Na^{+}$ entry and exit across the sarcolemmal membrane were identified as palmitoylated. This suggests that palmitoylation could be as important as phosphorylation in the regulation of excitation-contraction coupling and thus cardiac function. The regulation of these ion transport mechanisms by palmitoylation is relatively unexplored. One transport mechanism that has been studied with regards to protein palmitoylation is the cardiac $Na^{+}/K^{+}$ ATPase and its accessory protein, phospholemman (Howie et al. 2013; Tulloch et al. 2011). Palmitoylation of phospholemman inhibits the $Na^{+}/K^{+}$ ATPase, which is relieved by the non-specific DHHC inhibitor, 2-BP. In addition, phosphorylation of phospholemman, which activates $Na^{+}/K^{+}$ ATPase, promotes palmitoylation. The interaction between these two post-translational modifications on the ability of phospholemman to modulate $Na^{+}/K^{+}$ ATPase remains to be investigated fully.

**Verification Of Targets Identified By Mass Spectrometry**

A drawback of using affinity chromatography followed by mass spectrometry to identify proteins within a given sample is the possibility of false positives. The datasets shown as a result of this work have had all mitochondrial proteins removed, as cysteine thioesters exist within mitochondria as a result of fatty acid metabolism. Mitochondrial proteins were abundant in the samples analysed, due to the relative abundance of mitochondria within cardiac tissue. Evident from proteins identified by mass spectrometry were large structural proteins that may not be palmitoylated but are highly abundant in cardiac tissue. Large proteins will also generate large numbers of peptides, resulting in high MASCOT scores. To verify that other proteins within the sample that were relatively abundant are true positive hits, a small selection were verified by performing acyl rac followed by SDS-PAGE gel electrophoresis and western blotting. Representative members from different functional groups that had well characterised antibodies raised against them were selected for analysis. All protein targets selected for verification were identified by acyl rac, supporting the proteins identified by mass spectrometry. Additionally, not all targets selected were palmitoylated to the same extent. Given the diverse range of functional effects of palmitoylation on protein function, differential levels of palmitoylation would potentially regulated proteins in different ways, depending on their respective functions. For instance, structural and scaffolding proteins such as flotillin-1 and caveolin-3 are palmitoylated to a high

degree, suggesting that their palmitoylation is involved in anchoring these proteins to the membrane or targeting them to membrane compartments (Dietzen et al. 1995; Morrow et al. 2002). GAPDH, whose palmitoylation has been described previously (Yang et al. 2005), is only palmitoylated to a low extent, as acyl rac captured a small amount of the protein. GAPDH has a reactive cysteine residue within its active site, which plays a role in its activity. This could potentially generate a false positive as acyl rac relies on thioesters to purify palmitoylated proteins (see following section for discussion). Additionally, $G_i\alpha$ subunit was also identified in the mass spectrometry screen as well as verified by acyl rac analysis. This supports evidence previously described that G-protein subunits are subject to protein palmitoylation (Linder et al. 1993). For all proteins analysed, NaCl treated fractions revealed no bands, suggesting that none of these proteins bind to the thiopropyl sepharose used in the acyl rac protocol non-specifically. The positive verification of selected targets supports that proteins identified by mass spectrometry are genuine hits. Additionally, analysing high confidence targets from the pooled data from 3 separate experiments further supports the authenticity of identified proteins.

**Identification Of Palmitoylation Sites By Mass Spectrometry**

During the acyl rac protocol, irrelevant or non-palmitoylated cysteine residues are alkylated. This can be exploited to determine palmitoylation sites by mass spectrometry. Non-palmitoylated cysteine residues were labelled with N-ethylmaleimide (NEM), an irreversible alkylating agent as part of the acyl rac protocol. Following elution of captured proteins, during the FASP protocol used to remove the SDS from the sample previously palmitoylated cysteine residues were labelled with iodoacetamide. Peptides were digested with trypsin and submitted for mass spectrometry analysis. Peptides identified by mass spectrometry are matched to proteins via MASCOT. A coverage map is generated resulting from the number of peptides mapped to its respective sequence. Peptides containing amino acids with modifications are shown as a list following the coverage map. Cysteine residues labelled with NEM are designated as non-palmitoylated, given that NEM was used prior to thioester bond cleavage to label irrelevant cysteine residues. Conversely, peptides labelled with iodoacetamide (shown in MASCOT list as Carbamidomethyl) identify cysteines previously palmitoylated. Unfortunately, despite using an inclusion list for proteins of interest, mass spectrometry generated poor coverage of NCX1. As a result, the majority of the cysteine residues

present within NCX1 were not represented. Nevertheless, one cysteine residue was mapped within the sequence. Cys557 showed the addition of NEM, which suggests that this cysteine residue is not palmitoylated. Cys557, is located close to $Ca^{2+}$ binding domain 2 (CBD2) of NCX1 (Besserer et al. 2007). Palmitoylation of this residue would lead to a large change in secondary structure, presumably altering the $Ca^{2+}$ sensitivity and binding of these domains. NCX1 possesses 14 other cysteine residues. Two of these residues are known to be involved in forming a disulphide bond (Santacruz-Toloza et al. 2000). The precise location within the protein of the other cysteines is predicted but not proven. At present, there is no crystal structure available for mammalian NCX1.

**Summary**

Taken together, these results suggest that NCX1 is palmitoylated within cardiac muscle, and acyl rac captured approximately 60% of NCX1. NCX1 cannot tolerate prolonged exposure to temperatures above 37°C without aggregating. This aggregation is not caused by the presence of the disulphide within NCX1. In addition to palmitoylation of NCX1, vast arrays of proteins were identified as palmitoylated within cardiac tissue by mass spectrometry. This suggests that palmitoylation has the potential to regulate many different cellular processes. With a number of ion transport mechanisms across the sarcolemmal membrane found to be palmitoylated, this points toward palmitoylation being a significantly important post translational modification within cardiac muscle.

# Chapter 4: Mapping Palmitoylation Site(s) In NCX1.1

## 4.1 Comparison Of NCX1 Palmitoylation In BHK, HeLa and HEK293 Cell Lines

Culturing of cardiac myocytes can be challenging. In culture following isolation, myocytes isolated show gradual loss of subcellular structure (Pavlovic et al. 2010). In addition, ability to maintain contractile responses is diminished. Transfection of isolated ARVM is difficult using routine transfection techniques, with transfection rates varying between 0-15% (Djurovic et al. 2004). Using isolated cardiac myocytes would provide physiological palmitoylation stoichiometry of NCX1, but this would be extremely labor intensive. As a result, cell lines were selected for ease of use and transfection. As NCX1 is approximately 60% palmitoylated in cardiac tissue, the following cell lines were analysed for NCX1 palmitoylation; Baby Hamster Kidney (BHK), HeLa and Human Embryonic Kidney (HEK) 293 cell lines. These cell lines express no endogenous NCX1. Cell lines were transfected with canine NCX1. Palmitoylated proteins were purified from cell lysates using acyl rac followed by SDS-PAGE gel electrophoresis and western blotting to analyse degree of palmitoylation of transfected NCX1.

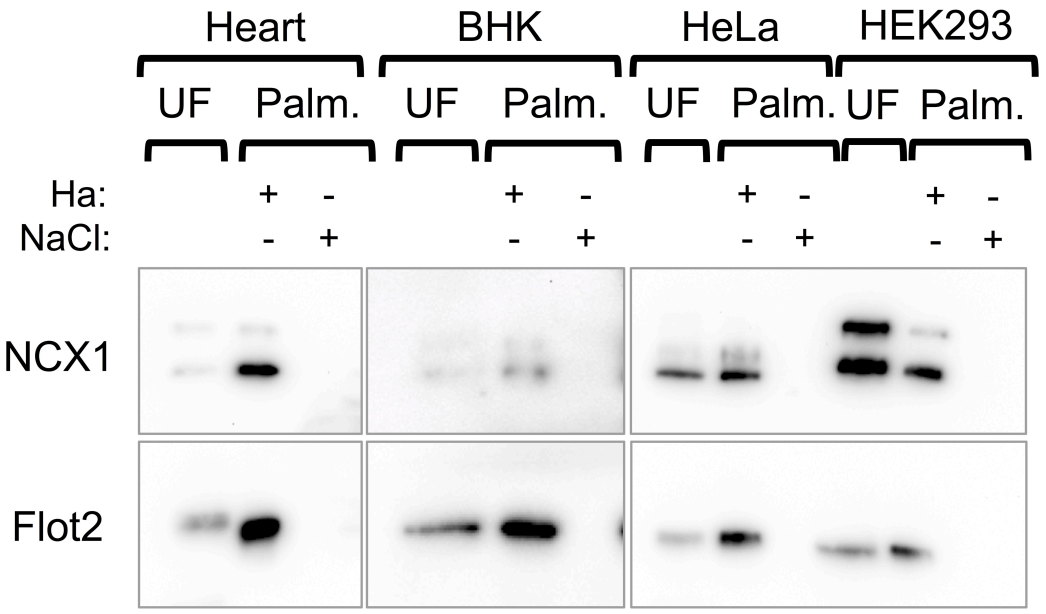


***Figure 4.1: NCX1 Is Palmitoylated To A Greater Extent In HeLa And HEK293 Cell Lines.*** *Comparison of acyl rac performed on NCX1 transfected BHK, HeLa and HEK293 cell lines revealed that HeLa and HEK293 cell lines show the highest palmitoylation.*

NCX1 palmitoylation in transiently transfected cells was compared to cardiac lysates. NCX1 palmitoylation is variable between cell lines. BHK cell line transfected with NCX1 show the lowest extent of palmitoylation (figure 4.1). NCX1 is palmitoylated to a greater level in transfected HeLa cells. In addition, NCX1 shows significant palmitoylation in transfected HEK293 cells. Flotillin-2 is palmitoylated in all cell lines investigated, however BHK cells show the lowest level of palmitoylation. These results suggest that HeLa and HEK293 cell lines palmitoylate NCX1 to a higher level, compared to BHK cell lines. However, HeLa and HEK293 cell lines do not palmitoylate NCX1 to the same extent as cardiac myocytes. Therefore, HeLa and HEK293 cell lines were used to investigate NCX1 palmitoylation.

## 4.2 Expression And Palmitoylation Of NCX1 Site Mutations In HeLa And HEK293 Cell Lines

As mass spectrometry did not definitively elucidate site(s) of palmitoylation on NCX1, a mutational approach was adopted. Mass spectrometry showed C557 was not palmitoylated, however given that NCX1 is not 100% palmitoylated in ARVM, this does not rule it out, as NCX1 exists in palmitoylated and non-palmitoylated states. A number of cysteine residues were excluded based on their predicted location. Cysteines at position 20 and 792 are experimentally determined to form a disulphide bond (Santacruz-Toloza et al. 2000). Additionally, recent reexamination of NCX1 predicted topology excluded C938 as it is predicted to lie on the extracellular side of the membrane. As a starting point, cysteine residues located within the large intracellular loop domain, which is known to be involved in regulation, were selected for mutational analysis. Using site-directed mutagenesis, cysteines at positions 383, 387, 485, 557, 731, 739 were mutated to alanine. In addition, cysteine at position 914, located within an intracellular loop domain between transmembrane domains 9 and 10, was also mutated to alanine. Single and double-site mutations were engineered to increase the probability of mapping the palmitoylation site(s). Following confirmation by DNA sequencing, mutant NCX1 constructs were transfected into either HeLa or HEK293 cell lines. Wild-type NCX1 and an empty vector control were transfected alongside.

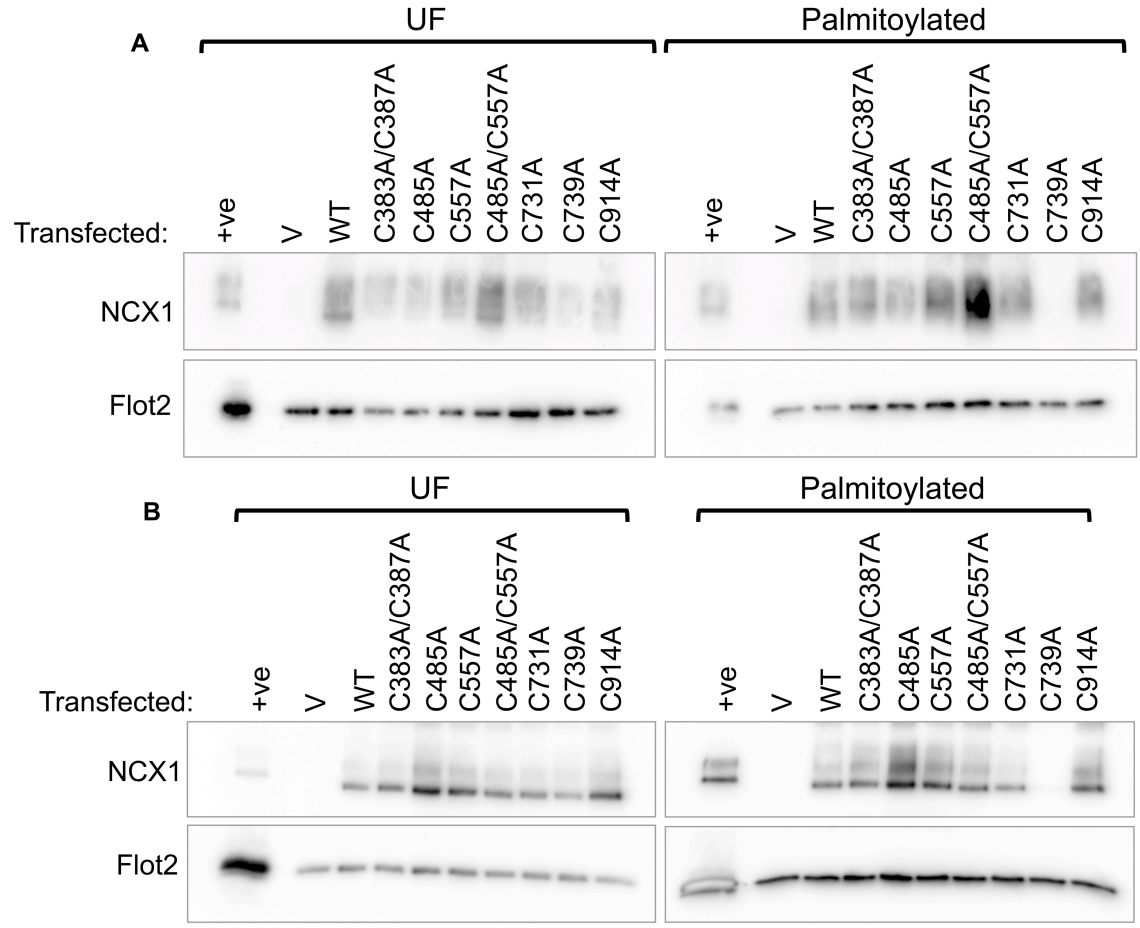


***Figure 4.2: Site-directed Mutagenesis Reveals Cys739 As The Principal Palmitoylation Site In NCX1. A.*** *NCX1 mutants C383A, C387A, C485A, C557A, C731A and C914A are palmitoylated when expressed in HEK293 cell lines. Mutation of Cys739 to alanine results in complete abolition of NCX1 palmitoylation.* ***B.*** *Mutation of Cys739 to alanine results in abolition of NCX1 palmitoylation in HeLa cell lines, consistent with HEK293 cell line data.*

Following transfection and expression of cysteine to alanine mutant NCX1 constructs, palmitoylation was assessed using acyl rac. Analysis of UF analytical samples taken during the acyl rac protocol revealed that all mutant NCX1 proteins express and are the expected size, compared to a positive control (Figure 4.2). Measuring palmitoylation of NCX1 mutants reveals that all constructs are palmitoylated, except C739A. Flotillin-2 was analysed as a quality control for acyl rac. Flotillin-2 was present in the absence of NCX1 C739A palmitoylation, suggesting acyl rac has captured palmitoylated proteins. Flotillin-2 is evenly expressed therefore differences in palmitoylation of NCX1 mutants result from differences in expression. This suggests that Cys739 is not palmitoylated when mutated to alanine. Inability to visualise C739A suggests that it is the principal

palmitoylation site. Both HeLa and HEK293 cell lines yield the same results, confirming that there is no difference in the processing and expression of NCX1 mutants between cell lines of different origins.

### 4.3 Expression And Palmitoylation Of NCX1 Intracellular Loop Site Mutants In HeLa And HEK293 Cell Lines

As a proof of principal approach, additional mutagenesis was performed to further verify the palmitoylation site of NCX1. A cysless intracellular loop was engineered using site-directed mutagenesis, to replace 6 endogenous cysteine residues within the large intracellular loop domain of NCX1 with alanine. Each cysteine residue was re-introduced one by one into the cysless intracellular loop background. This resulted in 7 different NCX1 mutant constructs, as follows,

1 Cysless
2 C383 Only
3 C387 Only
4 C485 Only
5 C557 Only
6 C731 Only
7 C739 Only.

All mutants were transfected alongside wild-type NCX1, as well as an empty vector control.

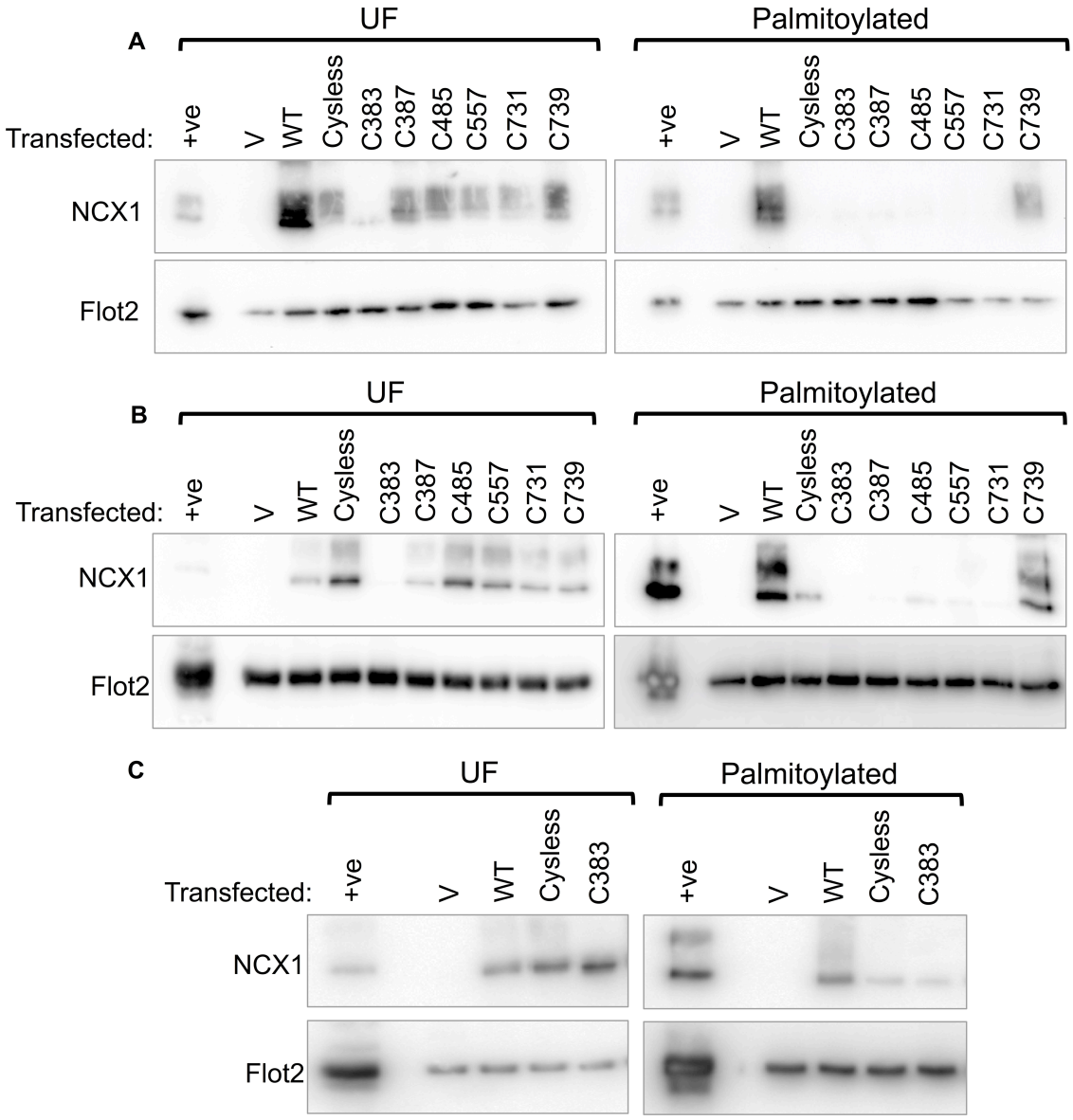


***Figure 4.3: Cys739 Is Necessary And Sufficient For Palmitoylation Of NCX1. A.*** *Mutational analysis revealed that only when Cys739 is present is NCX1 palmitoylated in HEK293 cell line.* ***B.*** *C739 is required for NCX1 palmitoylation in HeLa cell line.* ***C.*** *C383 has not expressed well in representative blots shown, but is palmitoylated to the same degree in other experiments.*

Palmitoylation of mutant NCX1 was assessed by acyl rac. Visualisation of NCX1 in UF suggests that all constructs are processed and expressed normally, regardless of cell line. Acyl rac reveals that when Cys739 is present, NCX1 is palmitoylated. In the absence of Cys739, NCX1 is poorly palmitoylated. These results support previous data that Cys739 is the principal palmitoylation site. Additionally, the results suggest that the presence of Cys739 is sufficient for NCX1 palmitoylation. When Cys739 is absent, palmitoylation does not occur at another cysteine residue. Analysis of flotillin-2

confirms the efficiency of acyl rac. Flotillin-2 is evenly expressed across both cell lines, suggesting differences observed are due to differences in NCX1 expression. C383 only has not expressed well in the experiments shown, however it has expressed in other experiments and is palmitoylated to the same level (panel C, figure 4.3) as other mutant NCX1 proteins in the absence of C739.

## 4.4 Expression And Palmitoylation Of NCX-YFP Fusion Mutants In HEK293 Cell Line

To elucidate the role of palmitoylation in NCX1, cDNAs encoding only the intracellular loop constructs were cloned into a YFP expression vector to generate YFP fusion proteins. The 3 constructs selected for further study were wild type (WT), cysless and C739 only containing NCX1 intracellular loop mutants. This results in fusion proteins with an N-terminal YFP tag. Fusion to YFP would allow visualisation by confocal microscopy to determine cellular localisation, providing insight into enzymes responsible for NCX1 palmitoylation. The impact of YFP tag on palmitoylation of NCX1 intracellular loop was addressed by acyl rac. Full length NCX1 containing cDNAs with wild type, cysless or C739 intracellular loops (Section 4.3) were amplified by PCR and cloned into pEYFP-C1 expression vector. Following verification by sequencing and restriction enzyme digest, constructs were transfected into HEK293 cell line. Palmitoylation was assessed by acyl rac followed by SDS-PAGE gel electrophoresis and western blotting.

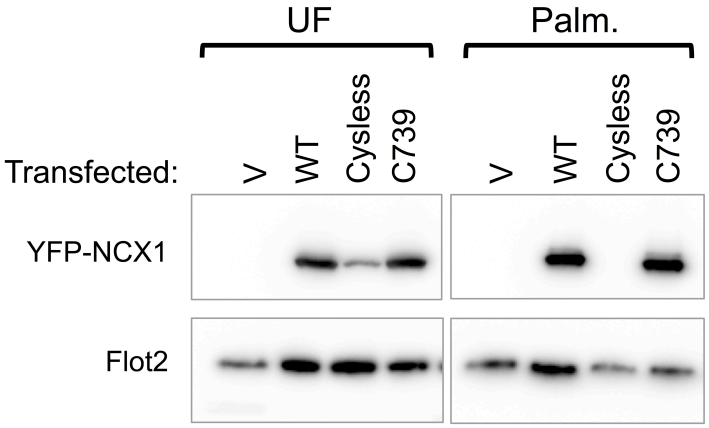


***Figure 4.4: NCX-YFP Fusion Proteins Are Palmitoylated In HEK293 Cell Line.*** *Acyl rac revealed that only wild type and C739 intracellular loop YFP-fusion proteins are palmitoylated in HEK293 cell lines. Cysless, containing no cysteine residues within its intracellular loop, is not palmitoylated.*

The presence of cysteine residues within intracellular loop domains is important for capture by acyl rac. WT-YFP and C739$^{ONLY}$-YFP are captured by acyl rac in the presence of hydroxylamine, suggesting they are palmitoylated. Conversely, Cysless-YFP is not captured by the thiopropyl sepharose in the presence of hydroxylamine, suggesting that it is not palmitoylated. Cysless-YFP consistently expressed less well compared to WT-YFP and C739$^{ONLY}$-YFP. These results suggest that a single cysteine residue is sufficient for NCX1 palmitoylation within the intracellular loop domain. Flotillin-2 was used as a loading control. Shown in figure 4.4, flotillin-2 expression and palmitoylation is consistent across different samples, suggesting differences observed are due to NCX1-YFP processing and expression.

## 4.5 Localisation Of WT NCX, Cysless And C739 Intracellular Loop Domains Fused to YFP

To address localisation of YFP-fusion proteins, cells were fractionated into membrane and cytosolic fractions based on detergent solubility. WT, Cysless or C739$^{ONLY}$ NCX-YFP fusion constructs were transfected into HEK293 cells. Cell lysates were fractionated into membrane and cytosolic fractions. Fractions were analysed by SDS-PAGE gel electrophoresis and western blotting. Anti-GFP antibodies were used to detect NCX-YFP mutants. Additionally, to confirm each fraction contained membranes and cytosol, samples were probed for $Na^+/K^+$ ATPase and GAPDH respectively.

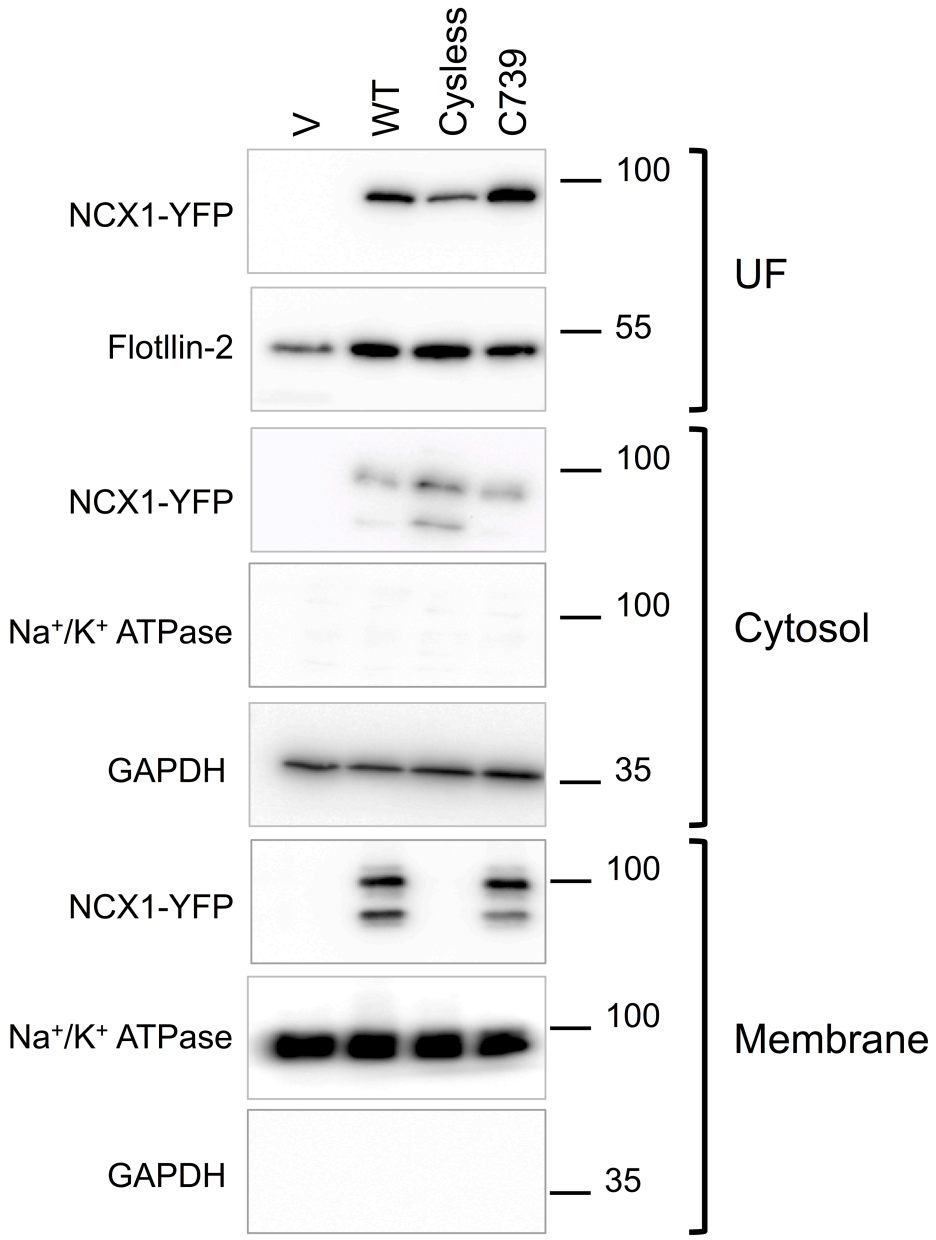


***Figure 4.5: WT And C739$^{ONLY}$ YFP Fusion Proteins Are Anchored To Membranes In HEK293 Cell Line.*** *Fractionation of cellular membranes and cytosolic components reveal that WT and C739$^{ONLY}$ YFP fusion proteins are anchored to membranes. Conversely, cysless YFP fusion protein is not anchored to membranes and remains in the cytosol. Numbers represent molecular weights in kDa.*

Analysis of cystosolic fractions reveal that all 3 YFP-fusion proteins are present, but WT-YFP and C739$^{Only}$-YFP are less abundant than Cysless-YFP (figure 4.5). Only WT-YFP and C739$^{ONLY}$-YFP are present in the membrane fraction. This suggests that palmitoylation anchors the intracellular loop to membranes. GAPDH is present within cytosolic fractions, confirming that cytosolic proteins were purified successfully. In addition, the membrane fraction was probed for α1 $Na^+/K^+$ ATPase subunit, which is

resident at the plasma membrane. $Na^+/K^+$ ATPase was successfully identified in membrane containing fractions, confirming the validity of the fractionation protocol used.

The crude fractionation protocol does not distinguish between plasma membrane and membranes from intracellular compartments or organelles. Direct visualisation of YFP-fusion protein localisation was investigated. WT-YFP, Cysless-YFP and $C739^{ONLY}$-YFP were co-transfected into HEK293 cell lines grown on glass coverslips with either DSRED-ER or Grasp65-mCherry constructs, which label the Endoplasmic Reticulum (ER) and Golgi apparatus (Golgi) respectively. Following transfection, cells were fixed and stained with DAPI, a nuclear marker, mounted on glass slides and analysed by confocal microscopy.

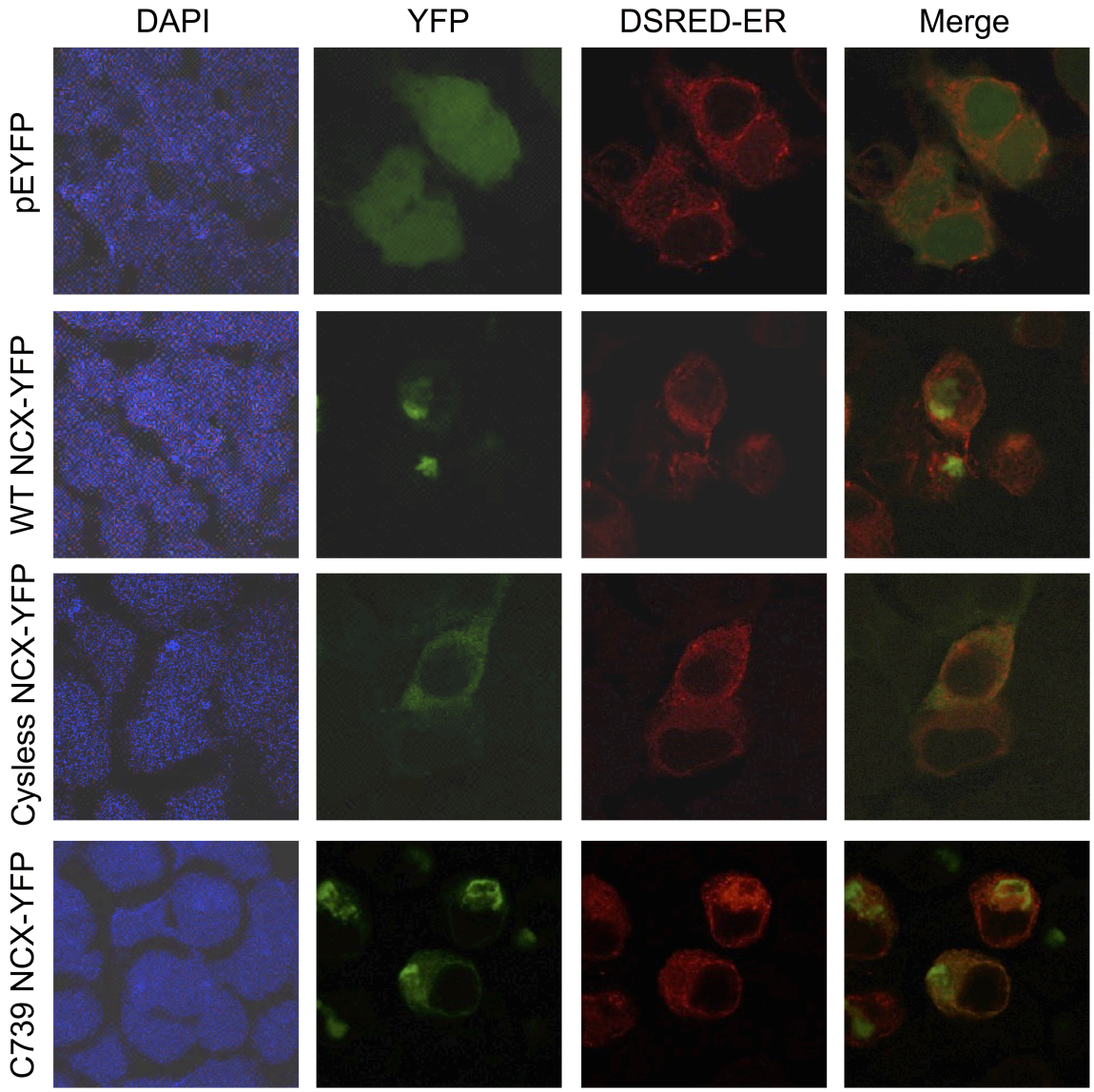


***Figure 4.6: Confocal Microscopy Of YFP-Fusion Proteins Do Not Localise To The ER.*** *Co-staining of YFP-fusion proteins with DSRED-ER, an ER marker, show that all 3 of the fusion proteins do not localise to the ER.*

WT-YFP shows distinct staining, which appears to be compartmentalised to an intracellular region. $C739^{ONLY}$-YFP shows a similar pattern, suggesting that it is localised to an intracellular region similar to WT-YFP. Cysless-YFP in contrast shows diffuse cytoplasmic staining. Cell nuclei are depicted in blue following DAPI staining (Figure 4.6). DSRED-ER, which visualises the ER in living cells, shows little co-localisation with YFP fusion proteins (Figure 4.6, merged images). This suggests that these proteins do not localise to the ER. As this is transient transfection, some staining observed may be an overexpression artifact.

To further determine the intracellular localisation of WT-YFP and C739$^{ONLY}$-YFP, co-localisation studies were performed using Grasp65-mCherry, which labels the Golgi apparatus in living cells. WT-YFP shows the same distinct staining, as well as C739$^{ONLY}$-YFP (Figure 4.7). Cysless-YFP shows diffuse cytoplasmic staining, as before. Interestingly, WT-YFP and C739$^{ONLY}$-YFP show co-localisation with Grasp65-mCherry (merged image, figure 4.7). Co-localisation with Grasp65-mCherry suggests WT-YFP and C739$^{ONLY}$-YFP localise to the Golgi apparatus in HEK293 cells. Cysless-YFP shows no co-localisation with Grasp65-mCherry, the staining pattern is diffuse, indicating that Cysless-YFP is present throughout the cytoplasm.

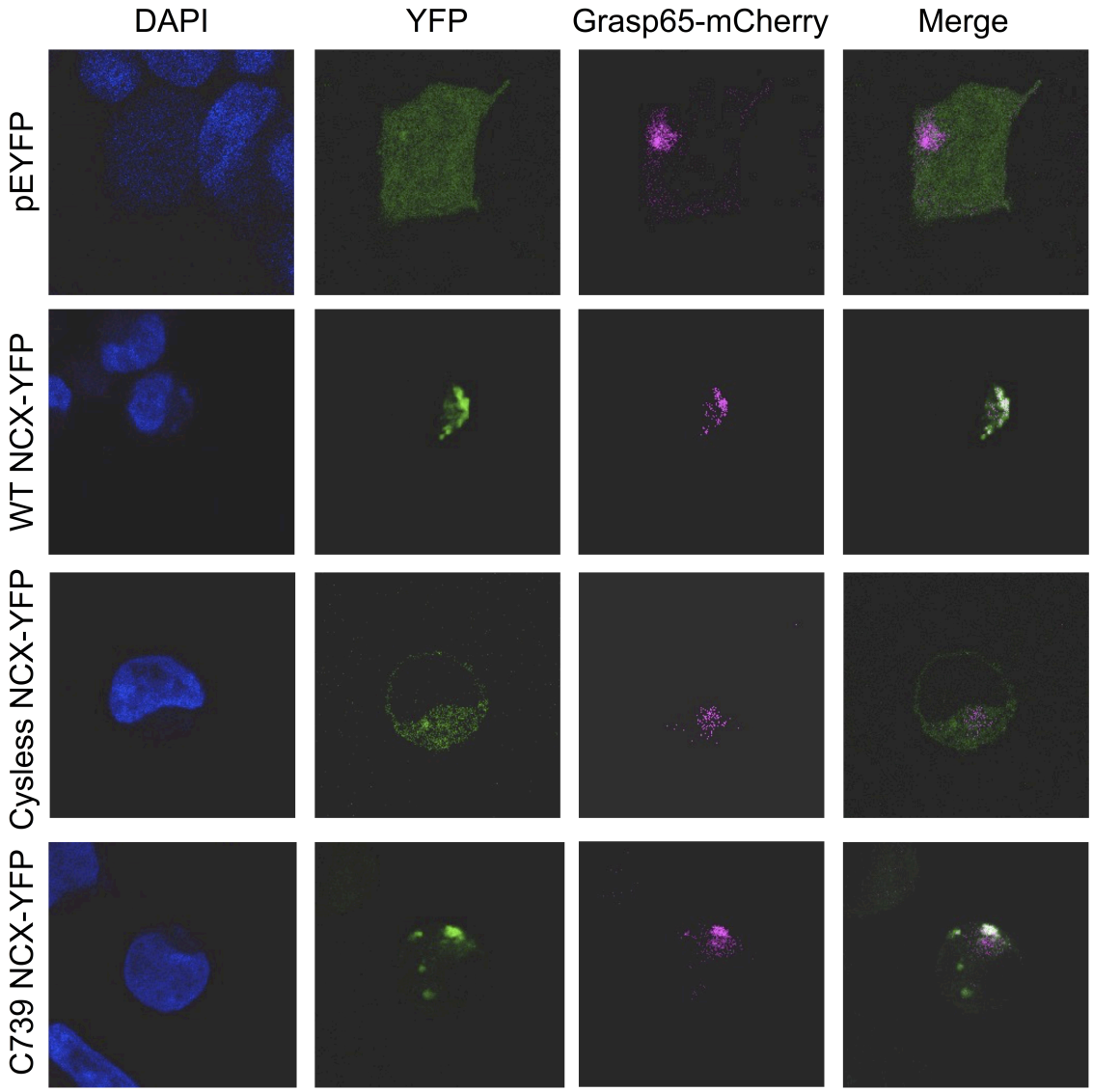


***Figure 4.7: Confocal Microscopy Of YFP-Fusion Proteins Reveal Localisation To The Golgi.*** *Co-transfections of NCX-YFP fusion proteins with Grasp65-mCherry, a Golgi resident protein, reveal that WT-YFP and C739$^{ONLY}$-YFP localise to the Golgi in HEK293 cells.*

## 4.6 Discussion

In order to identify and determine the functional effects of palmitoylation it was necessary to use genetic approaches. For many proteins that undergo palmitoylation, target cysteine residues are often located close to transmembrane domains (TMDs) (Bijlmakers & Marsh 2003). In some instances, the TMD has been shown to influence palmitoylation (Ponimaskin & M. F. G. Schmidt 1998). Mutation of non-hydrophobic residues within the TMD/cytoplasmic domain boundary of haemagglutinin to hydrophobic residues results in decreased palmitoylation. Additionally, palmitoylated cysteine residues are predominantly present within 10 residues of the TMD boundary, however this is not mutually exclusive as there is evidence for select proteins that their palmitoylation site(s) lie further than 10 amino acids away from the TMD boundary (Shipston 2014; Bijlmakers & Marsh 2003). Predicting site(s) of palmitoylation has been difficult, given there is no consensus sequence for directing palmitoylation towards particular residues. Prediction algorithms exist, such as CSS Palm 3.0 and the recently developed PalmPred (J. Ren et al. 2008a; Kumari et al. 2014). Historically, palmitoylation site(s) were identified using site-directed mutagenesis, which is time consuming and labour intensive. The development of techniques to analyse palmitoylation site(s) by mass spectrometry is becoming more prevalent, however sufficient coverage to provide bona–fide palmitoylation site information is difficult. Therefore, there is an urgency to develop *in silico* prediction algorithms, which will be of great use to the palmitoylation field.

### Mapping The Site(s) Of Palmitoylation In NCX1

As mass spectrometry did not yield definitive palmitoylation site(s), a site-directed mutagenesis approach was adopted. Prior to commencing mutagenesis, CSS Palm 3.0 was used to determine if any cysteine residues were predicted to be palmitoylated. CSS Palm 3.0 predicted 3 residues to be targets of palmitoylation, Cys 14, Cys 122 and Cys 768 with scores of 1.289, 0.371 and 1.364 respectively (J. Ren et al. 2008a). Since the completion of this work, a new prediction algrorithm was developed, PalmPred, which correctly identified the site determined here (Kumari et al. 2014). Cys14 was eliminated as it is predicted to be on the extracellular side of the membrane and is involved in formation of a disulphide (Santacruz-Toloza et al. 2000). Additionally, Cys122, located in TMD2 is predicted to be close to the extracellular membrane, furthest from the

cytoplasm, making it an unlikely target for palmitoylation. Finally, Cys768 is located within TMD6, which immediately follows the large intracellular loop domain (Figure 4.8). TMD6 is predicted to begin at 762, with Cys768 modelled to be at the centre of TMD6 (X. Ren et al. 2006). Therefore, cysteine residues present within the large intracellular loop domain were selected for mutational analysis, with the addition of Cys914 which is predicted to lie within the intracellular loop joining TMD 9 and 10 (X. Ren & Philipson 2013).

A single cysteine residue is the main palmitoylation site within NCX1. Cys739, located at the C-terminal end of the intracellular loop domain. In addition to being the principal palmitoylation site within NCX1, when Cys739 is unavailable, no other cysteine residue becomes palmitoylated. The abolition of palmitoylation in the absence of C739 suggests that there is a reason that this cysteine is preferentially palmitoylated. As mentioned previously, PalmPred, correctly predicts this residue as a palmitoylation site (Kumari et al. 2014). It is possible that it is simply the presence of the cysteine itself that is responsible for directing DHHCs. Further mutational analysis of residues surrounding C739 is required to determine which additional residues are important for palmitoylation.

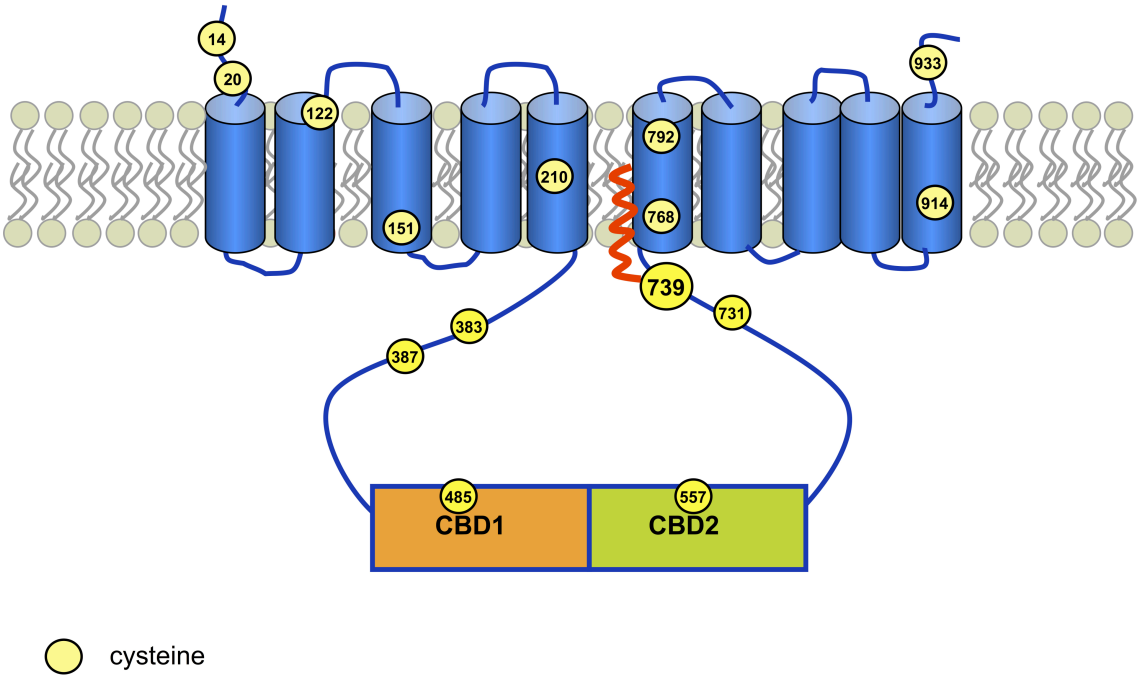


***Figure 4.8: Schematic Of NCX1 Predicted Topology.*** *Schematic showing positions of cysteine residues within NCX1. Generously provided by Dr Michela Ottollia.*

**NCX-YFP Localisation**

Using YFP-tagged fusion proteins of WT, Cysless and C739$^{ONLY}$ containing NCX1 intracellular loops and determining their localisation, palmitoylation was found to anchor this domain to membranes. One palmitoylation site is sufficient to target and anchor this domain to the membrane, as C739$^{ONLY}$-YFP fusion protein is present within membrane fractions. In the absence of cysteine residues, the intracellular loop domain is confined to the cytoplasm of the cell. These results suggest that a single cysteine residue is sufficient to anchor protein domains to membranes. It has been previously described that two lipid modifications lead to stable membrane association (Shahinian & Silvius 1995; Salaun et al. 2010). Therefore, a single palmitoylation site could result in transient association of the intracellular loop domain with membranes. It is unlikely that a single palmitoylation site is required for targeting of a 10 TMD protein to the plasma membrane. Interestingly, this cysteine residue is preceded by a stretch of negatively charged amino acids (figure 4.9), which will repel the negatively charged inner face of the lipid bilayer. The addition of a palmitate moiety to this region will drastically alter the microenvironment surrounding those residues and force it into the membrane. As a result, this will induce a large change in secondary structure, due to the negatively charged residues wishing to point away from the membrane.

```
720    VSAGEDDDDDECGEEKLPSCFDYVMHFLTVFWKVLFAFVPPTEYWNG
```

***Figure 4.9: Sequence Surrounding C739 Is Negatively Charged.*** *Sequence from 720 to 762, which is the start of TMD6, reveals negatively charged amino acids surrounding the palmitoylation site.*

As there is no crystal structure for the entire intracellular loop, determining how accessible C739 is to DHHCs is tricky. Using secondary structure prediction software can provide insight into accessible residues (Cole et al. 2008). The intracellular loop was analysed using Jpred 3, which can provide information on secondary structure and solvent accessibility. Shown in figure 4.10 is the secondary structure prediction of the intracellular loop of NCX1. C739 is predicted to be less than 25% solvent accessible, suggesting that it is not completely freely accessible, however it is must be still accessible. It is perhaps accessible enough to be palmitoylated by DHHCs. Residues upstream are completely free, which may play a role in interaction with DHHCs to

allow palmitoylation of C739. Downstream of the palmitoylation site, residues vary in their availability, with some residues completely buried. The role in which the relative accessibility of residues play in palmitoylation remains to be determined.

```
501-------511-------521-------531-------541----- :
TVSAGEDDDDDECGEEKLPSCFDYVMHFLTVFWKVLFAFVPPTEYWNG : OrigSeq

BB-B---------------BBBBBBBBBBBBB-BBBBBBBB--BB-B : Jnet_25
-B-------------------B-BB--B-----BBB-B-------- : Jnet_5
------------------------------------BB---------- : Jnet_0
74367777667777777763111104321442301122467777899 : Jnet Rel
```

***Figure 4.10: JPred3 Secondary Structure Prediction Of NCX1 Intracellular Loop.*** *Secondary Structure Prediction of NCX1 intracellular loop domain from Residue 721 to the beginning of TMD6. C739 is less than 25% solvent accessible, as designated by the B (burial) in Jnet_25. This suggests that C739 shows some accessibility. Jnet_25 – less than 25% solvent accessibility, Jnet_5 – less than 5% exposure, Jnet_0 – 0% exposure, Jnet Rel – reliability prediction accuracy (Cole et al. 2008). Run using Jpred 3 on Human NCX1 sequence.*

Recently, a crystal structure for a prokaryotic NCX1 homolog was established (Liao et al. 2012). This prompted reexamination of mammalian NCX1 topology, originally proposed to have 9 TMDs. As a result, the predicted topology of NCX1 was revised based on cross-linking studies to contain 10 TMDs, the same as its prokaryotic homolog, NCX_Mj (Ren & Philipson 2013). Examination of the crystal structure of NCX_Mj revealed that TMD 6 is longer than the remaining 8 TMDs, with the exception of TMD1. Additionally, TMD6 is modeled to lie at a 45° angle to the membrane surface (Liao et al. 2012). TMD6 moves dramatically between outward-facing and inward-facing conformations (Figure 4.10). C739 is located upstream of the start of TMD6, which starts at 762. Palmitoylation, anchoring this region to the membrane, may restrict the movement of TMD6. TMD6 is tilted compared in the outward-facing conformation, compared to the rest of the TMDs. During the inward-facing conformation, TMD6 moves dramatically, becoming perpendicular to the membrane. Addition of a palmitoyl moiety to C739, which is located upstream of the beginning of TMD6 (which starts at 762), may significantly impact the conformation changes of NCX1 during the exchange process. The effect of palmitoylation on the conformation of NCX1 during the reaction cycle remains to be examined.

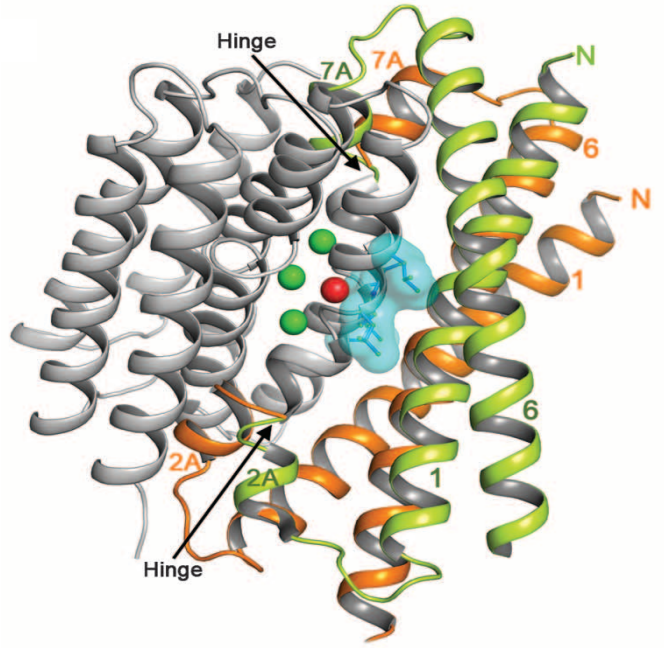


***Figure 4.11: Structural Comparison Of Outward-Facing And Inward-Facing Conformations.*** *Outward-facing NCX_Mj (orange) and inward-facing NCX_Mj (green) structural comparisons reveal conformation changes during the reaction cycle. Core portion (grey) does not change between conformations. Modified from (Liao et al. 2012).*

Confocal microscopy was used to elucidate where WT-YFP, Cysless-YFP and C739$^{ONLY}$-YFP are localised within the cell. As the engineered intracellular loop constructs are tagged with YFP, this enables visualisation via microscopy. In addition, markers for different cellular components can be employed to determine the precise localisation of the YFP-fusion proteins. Based on initial confocal microscopy data, WT-YFP and C739$^{ONLY}$-YFP showed a distinct staining pattern, in contrast to the diffuse, cytoplasmic staining of Cysless-YFP. It appeared that WT-YFP and C739$^{ONLY}$-YFP are localised to an intracellular compartment, within the secretory pathway. As result, two different cellular components were investigated, the ER and Golgi. Co-localisation studies of WT-YFP and C739$^{ONLY}$-YFP with DSRED-ER revealed that these proteins are not anchored to ER membranes. This suggests that the intracellular loop domain is not palmitoylated in the ER. Additionally, a number of the PATs, the enzymes responsible for palmitoylation, reside within ER membranes, suggesting that this subset of DHHCs are not involved in the palmitoylation of Cys739. Given that there are 24 known PATs, this narrows down the possible PATs that palmitoylate NCX1. Conversely, co-localisation studies with a Golgi marker revealed co-localisation with

Grasp65-mCherry, a Golgi marker. Based upon these results, it appears that WT-YFP and C739$^{ONLY}$-YFP are anchored to membranes within the Golgi. Cysless-YFP shows weak co-localisation with Grasp65-mCherry, however the staining pattern is more diffuse throughout the cytoplasm. However, Cysless-YFP may still interact with DHHCs but is no longer palmitoylated. Co-immunoprecipitation studies would determine whether Cysless-YFP interacts with DHHCs that palmitoylated NCX1. This suggests that palmitoylation of C739 occurs within the Golgi. There are a number of Golgi located PATs (Ohno et al. 2006), making them likely candidates as responsible for NCX1 palmitoylation. Following the identification of responsible PATs, comparing the region of NCX1 and known substrates of those PATs could possibly elucidate a potential consensus sequence for proteins. To date, no consensus sequence has been found for palmitoylation (Salaun et al. 2010). Suggested characteristics of palmitoylated cysteine residues such as proximity to myristoylation and prenylation sites, basic or hydrophobic amino acids surrounding site and location to cytoplasmic regions flanking transmembrane domains have been suggested (Salaun et al. 2010; Shipston 2014). However, C739 only fulfills one of these criteria, proximity to a transmembrane domain.

**Summary**

This work has identified that NCX1 has a single palmitoylation site, located within the large intracellular loop domain. Removal of the palmitoylation site, through site-directed mutagenesis, does not result in palmitoylation at another site, suggesting that PATs are directed to this site preferentially. Palmitoylation at this site anchors this domain to the membrane. Therefore, palmitoylation at this site will result in a large change in secondary structure. Given that this domain is involved in the regulation of NCX1 (Hilgemann, Collins & Matsuoka 1992b; Matsuoka & Hilgemann 1992; Hilgemann, Matsuoka, Nagel & Collins 1992d; Nicoll et al. 2006; Besserer et al. 2007), palmitoylation within this domain could potentially influence the activity of the exchanger. This may be achieved by changing the local microenvironment that the $Ca^{2+}$ binding domains are exposed to, or influencing the $PIP_2$ regulation or tilt of TMD6 of NCX (Shen et al. 2007; Yaradanakul et al. 2007). The effect of palmitoylation on NCX1 requires further investigation.

# Chapter 5: Identification Of Protein Acyl Transferases That Palmitoylate NCX1.1

## 5.1 Expression Profile Of PATs In Adult Rat Heart

To date, the expression profiles of the PATs or DHHCs within different tissues and cells have not been extensively studied. Shipston and colleagues published information regarding the expression profile of DHHCs expressed within the mammalian HEK293 cell line (Tian et al. 2010). This only provides information regarding DHHC expression at the mRNA level, as antibodies against all 24 isoforms are not commercially available. To investigate DHHCs that may be functionally relevant to cardiac palmitoylation, Total RNA was extracted from cardiac tissue of 4 male adult Wistar rats. cDNA was synthesized from the resulting RNA and expression was quantified relative to the geometric mean of β-actin and GAPDH using Fast Start Universal SYBR GreenTaqMAN with primers specific for the 24 known DHHCs in Real-Time PCR machine.

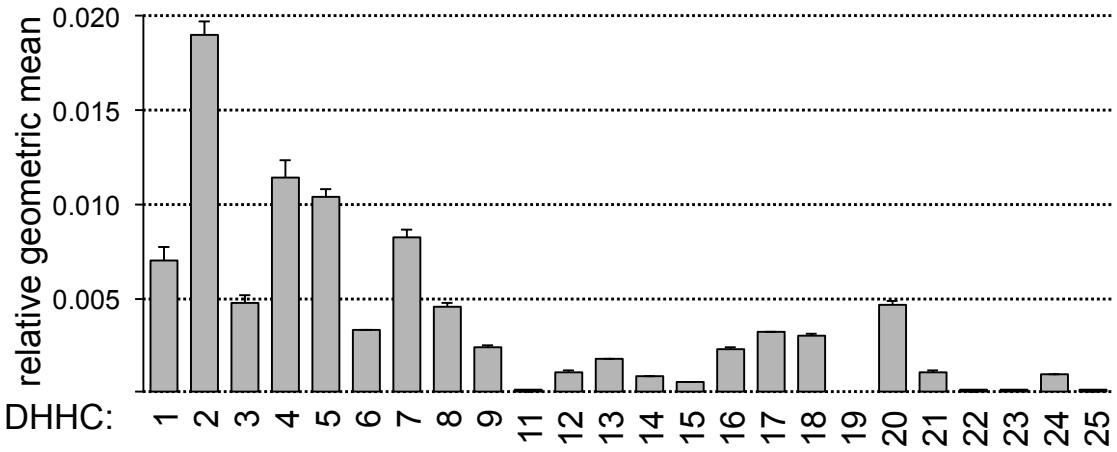


***Figure 5.1: DHHC Expression Profile In Cardiac Muscle.*** *The expression profile of DHHCs in cardiac muscle is expressed as the geometric mean relative to β-actin and GAPDH (n=4). Each measured in duplicate.*

Figure 5.1 shows the expression profile of DHHCs expressed in cardiac muscle. DHHC2 was the most abundant in cardiac muscle. DHHCs 4, 5 and 7 are also expressed at a high level. DHHCs 1, 3, 8 and 20 are expressed at a similar level. DHHCs 11, 23 and 25 are expressed at low levels. DHHCs 19 and 22 were undetectable by this assay. Expression levels of DHHCs are expressed as geometric mean relative to β-actin and GAPDH.

## 5.2 Co-Immunoprecipitation Of Candidate DHHCs With NCX1.1

Confocal microscopy data (Figure 4.6 and 4.7) revealed that the intracellular loop of NCX1 is localised to the Golgi apparatus in HEK293 cells. This suggests that palmitoylation of this region occurs within the secretory pathway, most likely the Golgi. Thus, DHHCs that are expressed in cardiac muscle were cross-referenced with known Golgi-resident DHHCs. This generated a list of 8 DHHCs that are expressed in cardiac muscle, within the Golgi apparatus. DHHCs 3, 4, 7, 8, 9, 12, 17 and 18 were selected for protein-protein interaction analysis with NCX1. In addition, DHHC5, a cell surface resident DHHC, and DHHC6, an ER resident DHHC, were selected as controls for co-immunoprecipitation experiments (Korycka et al. 2012). DHHCs were co-transfected into HEK293 cells with WT-YFP NCX1. Following transfection, HA-tagged DHHCs were immunoprecipitated and copurification of WT-YFP NCX1 assessed by immunoblotting for YFP.

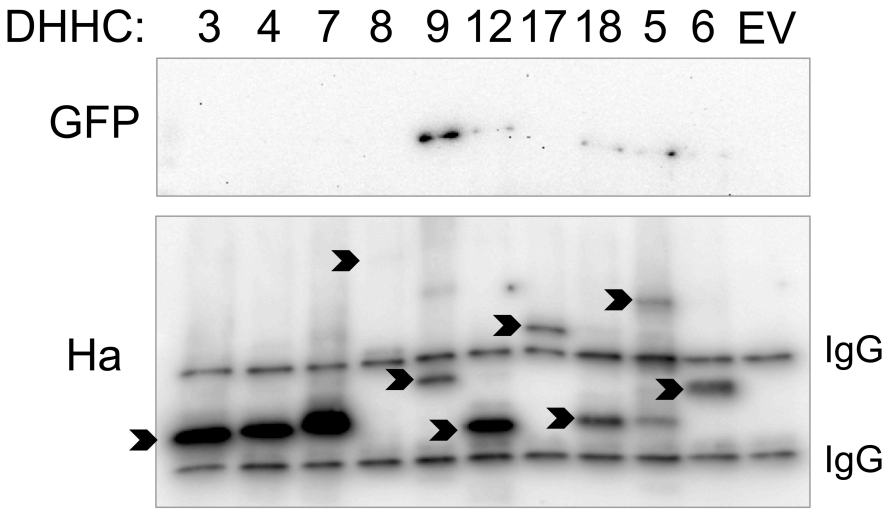


***Figure 5.2: Co-Immunoprecipiation Of Candidate DHHCs With WT–YFP NCX1.*** *Protein-protein interactions were assessed by co-immunoprecipitation with anti-HA affinity matrix. DHHCs 5, 9, 12 and 18 co-immunoprecipitated with WT-YFP NCX1. Arrowheads indicate DHHC proteins.*

Following co-immunoprecipiation, captured proteins were analysed by SDS-PAGE gel electrophoresis and western blotting. Figure 5.2 shows a representative blot from co-immunoprecipitation experiments. DHHC constructs used all possess a haemagglutinin (HA) tag, enabling purification using Anti-HA affinity matrix (Section 2.6.4). DHHC9 showed the highest interaction with WT-YFP NCX1. DHHC12 and DHHC18 show

weak interaction with WT-YFP NCX1 as shown by the faint bands detected. DHHC5 co-purified a small amount of NCX, suggesting a weak interaction. Results were variable between co-immunoprecipitation experiments. Only high confidence candidates were selected for further study with full length NCX1 (Table 5.1). High confidence candidates are classified as DHHCs purified with WT-YFP NCX1 in at least 3 experiments out of 4.

| DHHC | Exp 1 | Exp 2 | Exp 3 | Exp 4 | 3/4 |
|---|---|---|---|---|---|
| DHHC3 | - | - | + | - | x |
| DHHC4 | - | - | - | + | x |
| DHHC5 | + | + | - | + | ✓ |
| DHHC6 | - | + | - | + | x |
| DHHC7 | - | - | + | - | x |
| DHHC8 | - | - | - | - | x |
| DHHC9 | + | - | + | + | ✓ |
| DHHC12 | + | - | + | + | ✓ |
| DHHC17 | - | + | - | + | x |
| DHHC18 | + | + | - | + | ✓ |

***Table 5.1: Summary Of DHHCs Purified By Co-Immunoprecipitation.*** *DHHCs found to interact with NCX-YFP, assessed by co-immunoprecipitation experiments.*

### 5.3 Effect Of Candidate DHHCs On Full Length NCX1 Palmitoylation.

Based on the data obtained from co-immunoprecipitation experiments, DHHCs 5, 9, 12 and 18 were transfected into HEK293 cell lines stably expressing either full length WT NCX1 or C739A NCX1. DHHC8 and an empty vector control were transfected alongside as negative controls. Following transfection, palmitoylated proteins were purified from cell lysates by acyl rac and analysed by SDS-PAGE gel electrophoresis and western blotting.

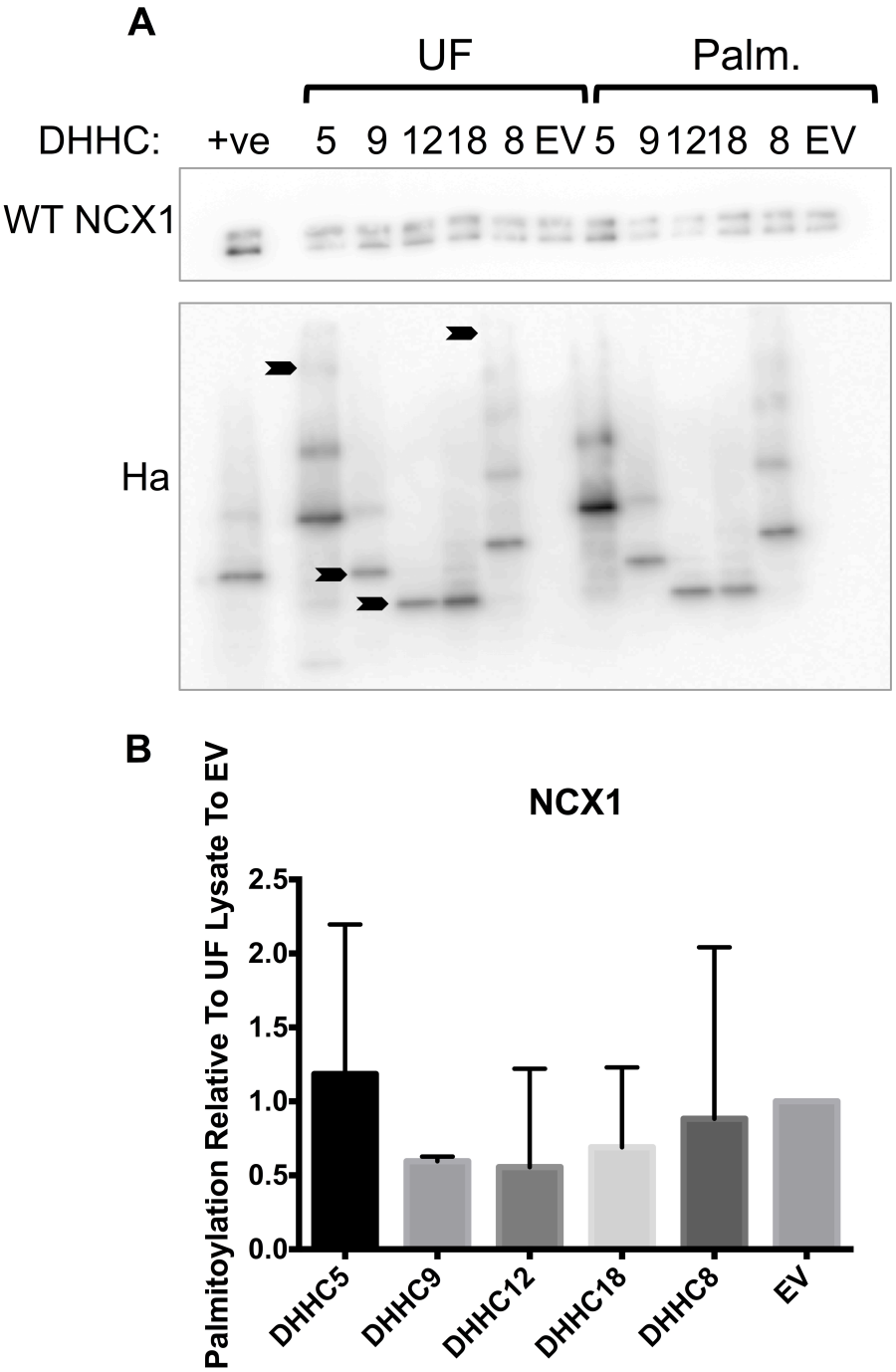


***Figure 5.3: Candidate DHHCs Have No Effect On Palmitoylation Of WT NCX1. A.*** *Representative blot from DHHC overexpression in FT293 cells stably expressing WT NCX1.* ***B.*** *Mean data from acyl rac experiments show no significant changes in WT NCX1 palmitoylation. Analysis by one way ANOVA with post hoc Dunnett correction. UF – unfractionated, Palm. – palmitoylated, EV – empty vector, Ha – haemagglutinin.*

Shown in panel A of figure 5.4, WT NCX1 is expressed in all cell lysates analysed. DHHCs 5, 9, 12 and 18 are each expressed following transfection of the cell lines.

DHHCs are detected in bound fractions following acyl rac in the presence of hydroxylamine. This suggests that DHHCs are palmitoylated as well as palmitoylating specific targets. Shown in panel B of figure 5.3, compared to EV, there was no significant difference in WT NCX1 palmitoylation following transfection of candidate DHHCs. These results suggest that WT NCX1 palmitoylation is principally controlled by thioesterase activity, as palmitoylation is not increased with DHHC overexpression.

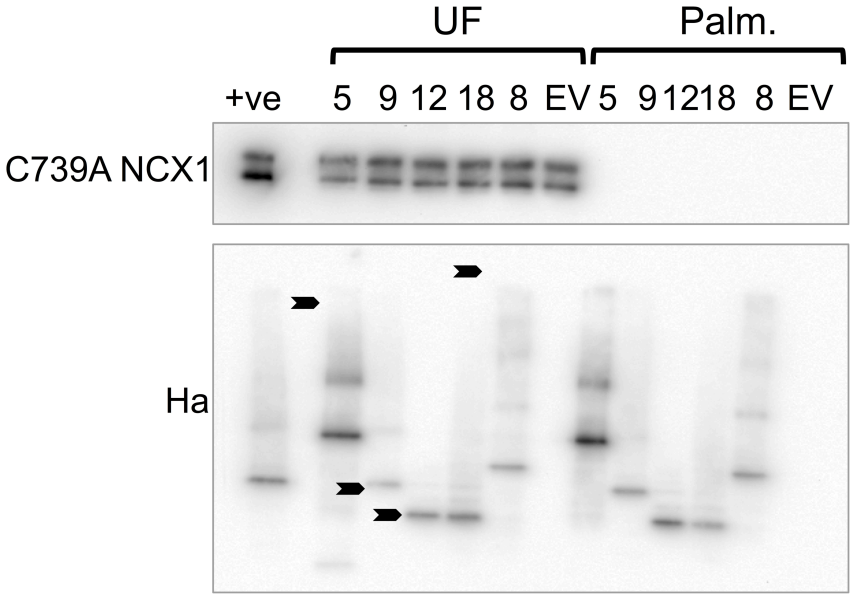


***Figure 5.4: Candidate DHHCs Do Not Increase C739A NCX1 Palmitoylation. A.*** *Representative blot from DHHC overexpression revealing no palmitoylation of C739A NCX1. UF – unfractionated, Palm. – palmitoylated, EV – empty vector, Ha – haemagglutinin.*

Based on previous data, mutation of Cys739 to alanine abolishes palmitoylation of NCX1. To determine if DHHCs are able to palmitoylate alternative cysteine residues in the absence of C739, candidate DHHCs were transfected into HEK293 cells engineered to stably express C739A NCX1. Shown in figure 5.4, C739A NCX1 is expressed in cell lysates (UF samples). Interestingly, regardless of DHHC expressed, C739A NCX1 is not palmitoylated. All DHHCs examined expressed and were also found to be palmitoylated. These results suggest that DHHCs will only palmitoylate NCX1 when C739 is available.

The effect of candidate DHHCs was assessed on known substrates, flotillin-2 and Ras. Shown in panel A of figure 5.5, overexpression of DHHC5 did not increase flotillin-2

palmitoylation. Mean flotillin-2 palmitoylation, expressed as fold change compared to EV show no significant increases in flotillin-2 palmitoylation. Panel B of figure 5.5, overexpression of DHHC9 did not increase Ras palmitoylation compared to EV. Mean data of Ras palmitoylation expressed as fold change compared to EV showed no statistical significant change in Ras palmitoylation. These results suggest that DHHC overexpression is not reliable as changes in palmitoylation of known substrates were unchanged.

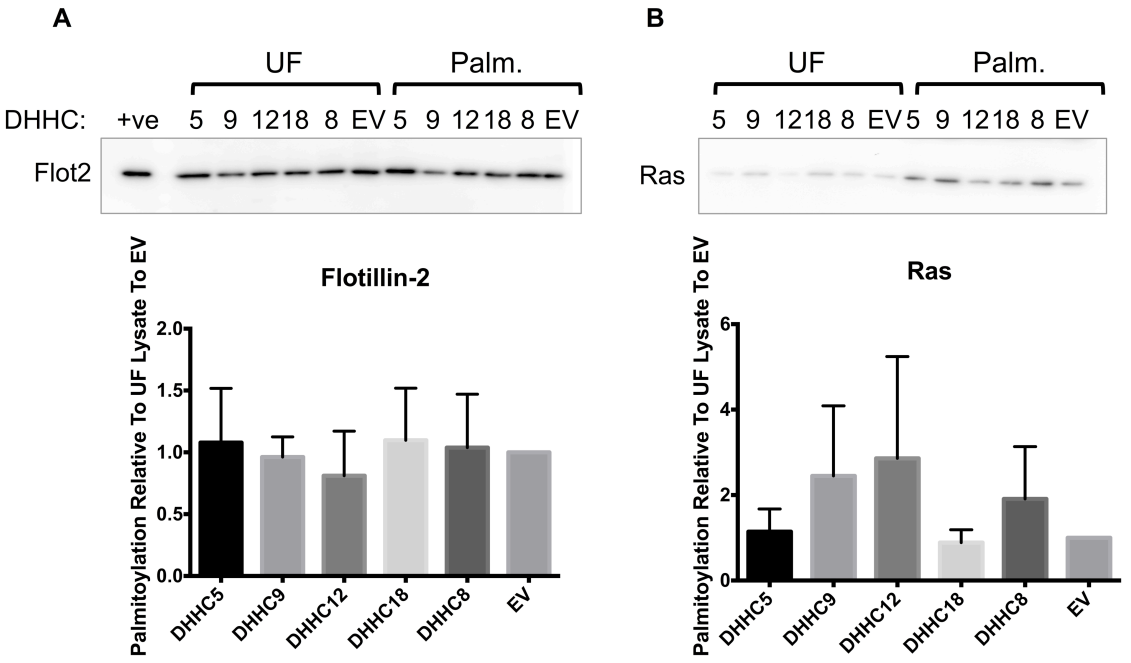


***Figure 5.5: Flotillin-2 And Ras Palmitoylation In Response To DHHC Overexpression.*** ***A.*** *Impact of DHHC overexpression on flotillin-2 palmitoylation. No significant differences observed.* ***B.*** *Impact of DHHC overexpression on Ras palmitoylation. No significant differences observed. Analysed by one-way ANOVA with post hoc Dunnett correction. UF – unfractionated, Palm. – palmitoylated, EV – empty vector, Flot2 – flotillin-2.*

## 5.4 Effect Of DHHS Mutants On Full Length NCX1 Palmitoylation.

As DHHCs 5, 9, 12 and 18 did not increase full-length NCX1 palmitoylation, site-directed mutagenesis was used to generate DHHC mutants, where cysteine residues within the conserved DHHC motif had been mutated to serine residues. The resultant DHHS proteins are predicted to be catalytically inactive (Mitchell et al. 2006) and act in a dominant negative manner. DHHS mutants of DHHC 5, 9, 12 and 18 were expressed

in FT293 WT NCX1 cell lines, palmitoylated proteins were purified from cell lysates by acyl rac then analysed by SDS-PAGE gel electrophoresis and western blotting.

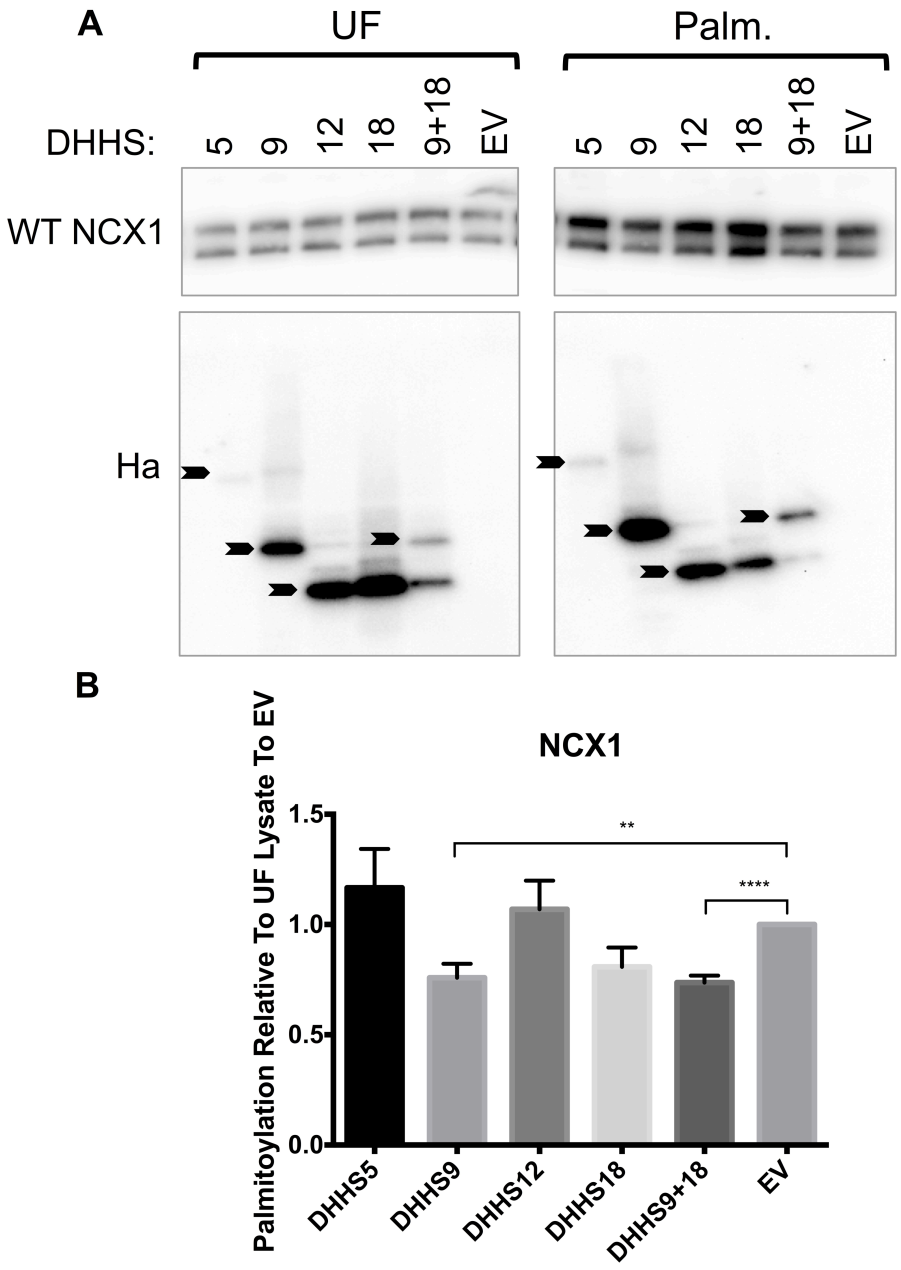


***Figure 5.6: DHHS9 Significantly Decreases WT NCX1 Palmitoylation.*** ***A.*** *Impact of DHHS overexpression on WT NCX1 palmitoylation.* ***B.*** *Mean data shows that DHHS9 significantly decrease WT NCX1 palmitoylation. In addition, co-expression of DHHS9 and 18 also results in decreases. DHHS9 mean, 0.71 ± 0.06, $p<0.01$, DHHS9+18 mean, 0.74 ± 0.04, $p<0.001$, $n=4$. UF – unfractionated, Palm. – palmitoylated, EV – empty vector, Bds – beads, Ha – hemagglutinin. Analysed by one-way ANOVA with post hoc Dunnett correction.*

Shown in panel A of figure 5.6, WT NCX1 is expressed in all cell lysates analysed. In addition, DHHS mutants express in FT293 cell line. The amount of palmitoylated NCX1 captured is decreased when DHHS9 is expressed. In addition, expressing DHHS9 and DHHS18 together also decreased NCX1 palmitoylation to a similar level as DHHS9 only transfections. Surprisingly, despite the lack of cysteine within the DHHC domain, DHHS mutants analysed are palmitoylated. This suggests that they are palmitoylated at cysteine residues outwith the DHHC domain. Panel B of figure 5.6 shows mean palmitoylation data. DHHS9 significantly reduced NCX1 palmitoylation compared to EV. In addition, co-expression of DHHS9 and DHHS18 significantly decreased NCX1 palmitoylation compared to EV. Reduction of NCX1 palmitoylation following co-expression of DHHS9 and DHHS18 was not additive suggesting the decrease in palmitoylation is due to DHHS9.

In order to determine whether DHHS mutants have an effect on established targets of DHHC proteins, acyl rac experiments were also examined for flotillin-2 and H-Ras. Panel A of figure 5.7 shows flotillin-2 palmitoylation detected by western blotting. Flotillin-2 palmitoylation was significantly decreased when co-expressed with DHHS9+18 compared to EV. Panel B of figure 5.7 shows Ras palmitoylation. Ras palmitoylation was decreased when cells were transfected with DHHS9, DHHS18 and DHHS9+18 compared to EV. DHHS18 decreased Ras palmitoylation to a greater degree than DHHS9. This suggests that DHHS proteins act in a dominant negative manner in this cell line, proven by their ability to negatively regulate palmitoylation of known targets.

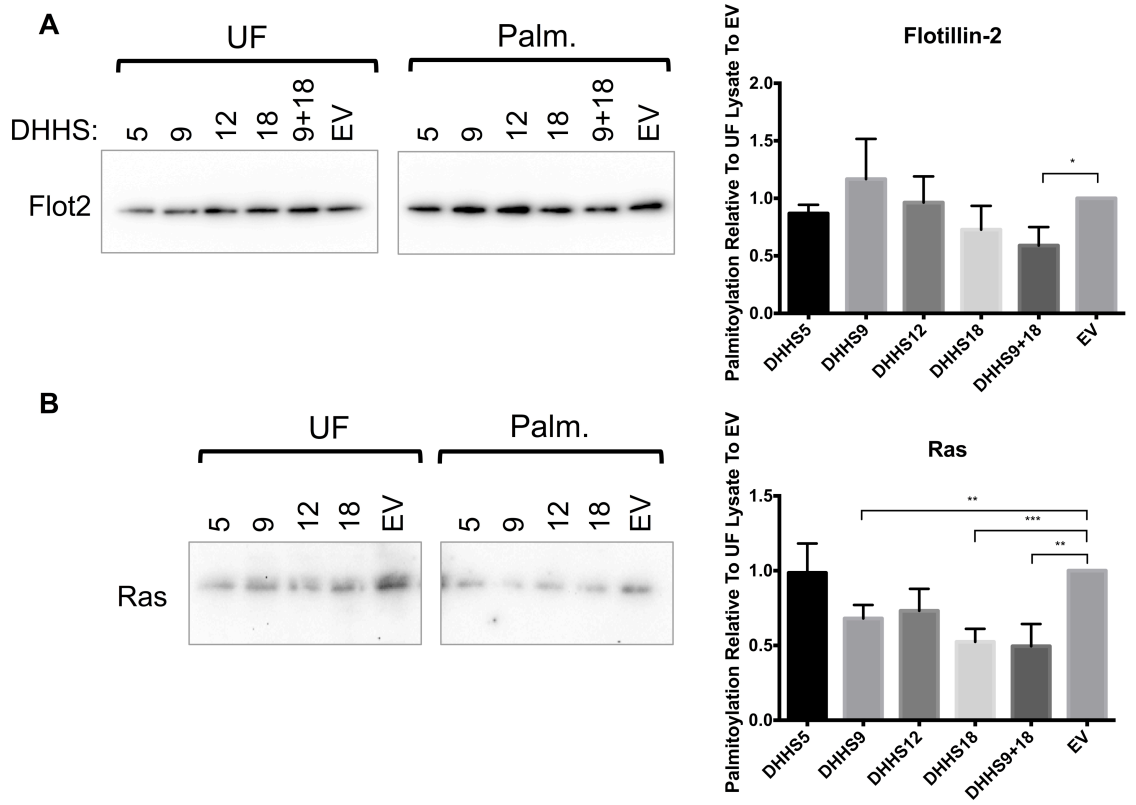


***Figure 5.7: Effect Of DHHS Overexpression On Flotillin-2 And Ras Palmitoylation.*** ***A.*** *Representative blot of impact of DHHS overexpression on flotillin-2 palmitoylation. Significant decreases in flotillin-2 were observed in DHHS 9 + DHHS18.* ***B.*** *Impact of DHHS overexpression on Ras palmitoylation. Mean data shows significant decrease in Ras palmitoylation with DHHS9, DHHS18 and DHHS9+18 compared to EV. DHHS9 mean 0.68 ± 0.09, $p<0.01$, DHHS18 mean 0.52 ± 0.09, $p<0.001$, DHHS9+18 mean 0.49 ± 0.15, $p<0.01$. UF – unfractionated, Palm. – palmitoylated, EV – empty vector.*

## 5.5 Discussion

In order to gain insight into the regulation of NCX1, determining which DHHCs are responsible for NCX1 palmitoylation was a key aim of this work. The 24 mammalian DHHCs localise to different intracellular regions, with the majority localised to the Golgi apparatus or the Endoplasmic Reticulum (ER) (Korycka et al. 2012). Presently, there are only 2 DHHCs known to localise to regions out with these intracellular compartments, DHHC2 which has been shown to localise to plasma membrane, endosomes and other vesicular structures (Greaves et al. 2011). DHHC5 was also shown to localise to the plasma membrane (Ohno et al. 2006). Determining the DHHC protein responsible for palmitoylation of NCX1 will give insight into the location of NCX1 palmitoylation and when during its processing this occurs.

### DHHC Expression Profile In Cardiac Muscle

To date, there are no commercial antibodies available to detect all 24 mammalian DHHCs. This makes determining relative protein levels of each DHHC difficult. Recently, the DHHC expression profile of HEK293 cell line was determined (Tian et al. 2010). cDNA was synthesised from mRNA generated from adult rat heart and DHHC expression profiles were analysed by quantitative PCR. β-actin and GAPDH were used as internal reference controls. The results revealed that DHHC2 was the highest expressed in adult rat heart. DHHC4, 5 and 7 were expressed at relatively high levels. Recent data suggests that palmitoylation can be dynamic as well as stable (Martin et al. 2011). The high expression of DHHC2 and DHHC5 in cardiac muscle may indicate that palmitoylation is occurring in a dynamic way at the sarcolemmal membrane. DHHCs that are expressed throughout the Golgi and ER are also expressed in cardiac muscle, such as DHHCs 1, 4, 7, 8 and 20. The expression profile of DHHCs within cardiac muscle varies from that found in HEK293 cell line. There is some evidence to suggest that DHHC proteins vary in expression level in a tissue-specific manner (Ohno et al. 2006). To date, very few DHHCs have established substrates. To address this question, pulse-chase experiments, similar to that performed previously (Martin et al. 2011), will be required to address palmitoylation turnover within cardiac muscle.

**DHHCs That Palmitoylate NCX1**

Based on confocal microscopy data, NCX-YFP localises to the Golgi apparatus within HEK293 cell line. DHHCs that are expressed within the Golgi apparatus and are abundant within cardiac muscle were selected to determine protein-protein interactions with NCX-YFP. DHHCs 3, 4, 7, 8, 9, 12, 17 and 18 were selected for co-immunoprecipitation experiments. DHHCs 5 and 6 were transfected alongside as additional controls, as they localise to the plasma membrane and ER respectively (Korycka et al. 2012; Ohno et al. 2006). Co-immunoprecipitation experiments were used to detect protein-protein interactions that may occur. DHHC9 was found to interact with NCX-YFP in HEK293 cell line. DHHCs 12, 18 and 5 also showed weak interaction. These results suggest that the intracellular loop of NCX1 is palmitoylated within the Golgi apparatus by DHHC9. These experiments assume NCX1 forms a stable complex with its palmitoylating enzyme, which has recently been questioned (Lemonidis et al. 2014).

**Effect Of DHHS Mutants On WT NCX1 Palmitoylation**

Given the high level of WT NCX1 palmitoylation observed, catalytically inactive DHHC mutants were engineered. Mutation of cysteine within the DHHC domain to alanine or serine blocks enzymatic activity and is essential for function (Mitchell et al. 2006). DHHS mutants of DHHC 5, 9, 12 and 18 were generated using a site-directed mutagenesis approach. Mutants were expressed in FT293 WT NCX1 cell line and palmitoylation of NCX1 was analysed by acyl rac followed by SDS-PAGE gel electrophoresis and western blotting. The results revealed that DHHS9 decreased WT NCX1 palmitoylation. Combining both DHHS 9 and 18 did not have an additive effect on decreasing NCX1 palmitoylation. Therefore, of those studied DHHC9 is the main palmitoylation enzyme responsible for the palmitoylation of NCX1. There is little to no information regarding the precise location of DHHCs within the Golgi apparatus, whether they are located in cis-, medial-, endo- or trans-Golgi regions. Depending on the precise location within the Golgi apparatus of these DHHCs, NCX1 may encounter different DHHCs depending on whether it is the full-length or fusion protein that is being processed and palmitoylated.


***Figure 5.8: Clustal Alignment Of Human NCX1, H-Ras and N-Ras.*** *Clustal alignment of intracellular loop region of NCX1, H-ras and N-Ras reveal sequence homology upstream of palmitoylation sites. Palmitoylation sites are highlighted in red. Alignments were performed using ClustalOmega.*

Sequence alignment of NCX1 with two known substrates of DHHC9, H-Ras and N-Ras (Swarthout et al. 2005) shows significant sequence homology. Examination of the sequence immediately surrounding the palmitoylation sites shows that the residue immediately preceding are small amino acids (serine in the case of NCX1 and glycine in the case of H-Ras and N-Ras (Figure 5.8)). Palmitoylation sites are on the C terminal side of negatively charged amino acids, glutamate and aspartate. These amino acids will be repelled by the phospholipid head groups of the lipid bilayer, as well as the negative membrane potential generated by $K^+$ movement across the cell membrane. Interestingly, from position 660 to 720, NCX1 shares a large amount of homology with H-Ras and N-Ras. There are a number of conserved residues (indicated by * underneath residues) as well as similarity in sequence (indicated by : underneath residues). This suggests that this region may be important for substrate recognition of DHHC9, given that 2 known substrates that share homology with a region of NCX1, demonstrated here to be palmitoylated by DHHC9. There is evidence that domains and residues distant from palmitoylation sites can influence specificity of substrate:DHHC interactions. Mutation of a proline residue 25 residues downstream of the palmitoylated cysteine-rich domain in SNAP25 results in its palmitoylation by DHHC3 and not DHHC17 (Greaves et al. 2009). In addition, regions outwith the palmitoylated domain of yeast substrates are important for governing interactions with DHHCs. Presence of SH4 domain within yeast proteins does not confer preferential palmitoylation by specific DHHCs (Nadolski & Linder 2009). Vac8, Meh1 and Yg1108 palmitoylation specificity was lost when SH4 domains were analysed in isolation. Collectively, these results indicate that regions outwith the palmitoylated region of substrates may contribute to recognition by specific DHHCs and thus confer substrate specificity.

The way in which DHHCs interact with and recognise their substrates is only becoming apparent for a limited number of proteins. Regions outwith the CRD-DHHC domain are involved in recognition of substrates. Huntingtin is palmitoylated by DHHC17 but not by DHHC3 (K. Huang et al. 2009). It was demonstrated that the ankyrin repeat domain of DHHC17 interacts with huntingtin (Singaraja et al. 2002). Chimeras of DHHC3 that contain the ankyrin repeat domain of DHHC17 is capable of palmitoylating huntingtin. In agreement with this, DHHC5 confers substrate recognition via its cytoplasmic tail (Howie et al. 2014). Truncation mutants of DHHC5, which lack the cytoplasmic tail, cannot palmitoylate its substrates flotillin-2 and phospholemman. These results suggest

that regions outwith the DHHC domain are important for governing substrate interactions.

In a recent study in which DHHC9 was depleted, intracellular localisation of H-Ras was unchanged (Rocks et al. 2010). In addition, replacement of amino acids surrounding palmitoylation sites in Ras with their D-amino acid counterparts did not affect Golgi localisation of micro-injected proteins, which is used as a measure of efficient palmitoylation. Furthermore, depletion of five DHHCs from yeast resulted in a reduction in Vac8 palmitoylation (Hou et al. 2009). Overexpression of each individual DHHC in this yeast strain results in Vac8 palmitoylation, suggesting DHHCs have overlapping activity. Thus it remains unclear and more work is required to determine the specificity of DHHC-substrate interactions.

**DHHC Overexpression**

DHHCs 5, 9, 12 and 18 were selected for overexpression experiments based on the co-immunoprecipiation with NCX-YFP. In addition to co-expression with WT NCX1, candidate DHHCs were co-expressed with C739A NCX1. This was to determine whether DHHCs are capable of palmitoylating other available cysteine residues. Surprisingly, no significant increases in WT NCX1 palmitoylation were observed (figure 5.5). DHHC9, DHHC12 and DHHC18 significantly decreased WT NCX1 palmitoylation. This was somewhat surprising, given palmitoylation would be expected to increase in response to DHHC overexpression. It may be that overexpression of specific DHHCs negatively regulates endogenous DHHCs or activates thioesterases and leads to decreased palmitoylation. Overexpression may result in high levels of binding to common sites, thus overcoming regulation in terms of where they are expressed, preventing endogenous DHHC actions. The level of NCX1 palmitoylation may be controlled by thioesterase activity, rather than DHHCs. WT NCX1 is likely to be palmitoylated in the secretory pathway as it is processed, it would only be in proximity to DHHCs as it traffics through the biosynthetic pathway but will likely be continuously exposed to thioesterases, therefore thioesterase activity is likely to be the main determinant in NCX1 palmitoylation. The turnover rate of NCX1 palmitoylation has not been addressed, however it is entirely possible that blocking thioesterase activity by siRNA knockdown or pharmacological inhibition would reveal whether depalmitoylation of NCX1 is the major factor in determining palmitoylation. In

addition, as WT NCX1 is likely to be palmitoylated in the secretory pathway as it is processed, it would only be in proximity to DHHCs as it traffics through the biosynthetic pathway. Surprisingly, flotillin-2 and Ras palmitoylation was unchanged by overexpression of DHHC5 and DHHC9 respectively. In the case of DHHC9, it could be due to limiting levels of GCP16. DHHC9 requires GCP16 for acyltransferase activity and protein stability (Swarthout et al. 2005). In the model used in this thesis, DHHC9 could be unstable when overexpressed in the absence of GCP16, which may account for why Ras palmitoylation is unchanged. However, DHHC5 has not been shown to require a co-factor for acyltransferase activity. Therefore, why DHHC5 overexpression does not result in increase flotillin-2 palmitoylation is unknown and unaccounted for in this model.

**Summary**

DHHCs 2, 4, 5 and 7 are the most abundantly expressed DHHCs within cardiac muscle, demonstrated by quantitative PCR. Co-immunoprecipitation experiments revealed protein-protein interactions between NCX-YFP and DHHCs 5, 9, 12 and 18. However, overexpression of candidate DHHCs identified by co-immunoprecipitation decrease full-length NCX1 palmitoylation. This may be due to an effect on the thioesterase activity. However, overexpression of one DHHC may adversely affect endogenous DHHCs and thus impact NCX1 palmitoylation. Finally, using DHHS mutants of DHHCs 5, 9, 12 and 18, DHHC9 was found to be responsible for NCX1 palmitoylation. Alignment of NCX1 with known substrates of DHHC9 revealed significant sequence homology upstream of palmitoylation sites, which may be important for DHHC9 substrate recognition. Further study is required to determine regions of NCX1 that may be important for conferring DHHC specificity.

# Chapter 6: Effect Of Palmitoylation On NCX1 Function

## 6.1 Effect Of Pharmacological And Mutational Inhibition Of Palmitoylation On WT NCX1

Few palmitoylation inhibitors exist, with 2-bromopalmitate (2-BP) commonly used to inhibit palmitoylation (Quednau, Nicoll & Philipson 1997b; Webb et al. 2000; B. C. Jennings et al. 2008). 2-BP has recently been documented to have off-target non-specific effects, making its use less desirable (Davda et al. 2013). As a result, to assess functional effects of palmitoylation on NCX1, mutational and pharmacological inhibition of palmitoylation were used. FT293 cell lines stably expressing WT NCX1 or C739A NCX1 were engineered and treated with 2-BP (100μM, overnight treatment). Lysates were used in acyl rac followed by SDS-PAGE gel electrophoresis and western blotting to assess palmitoylation.

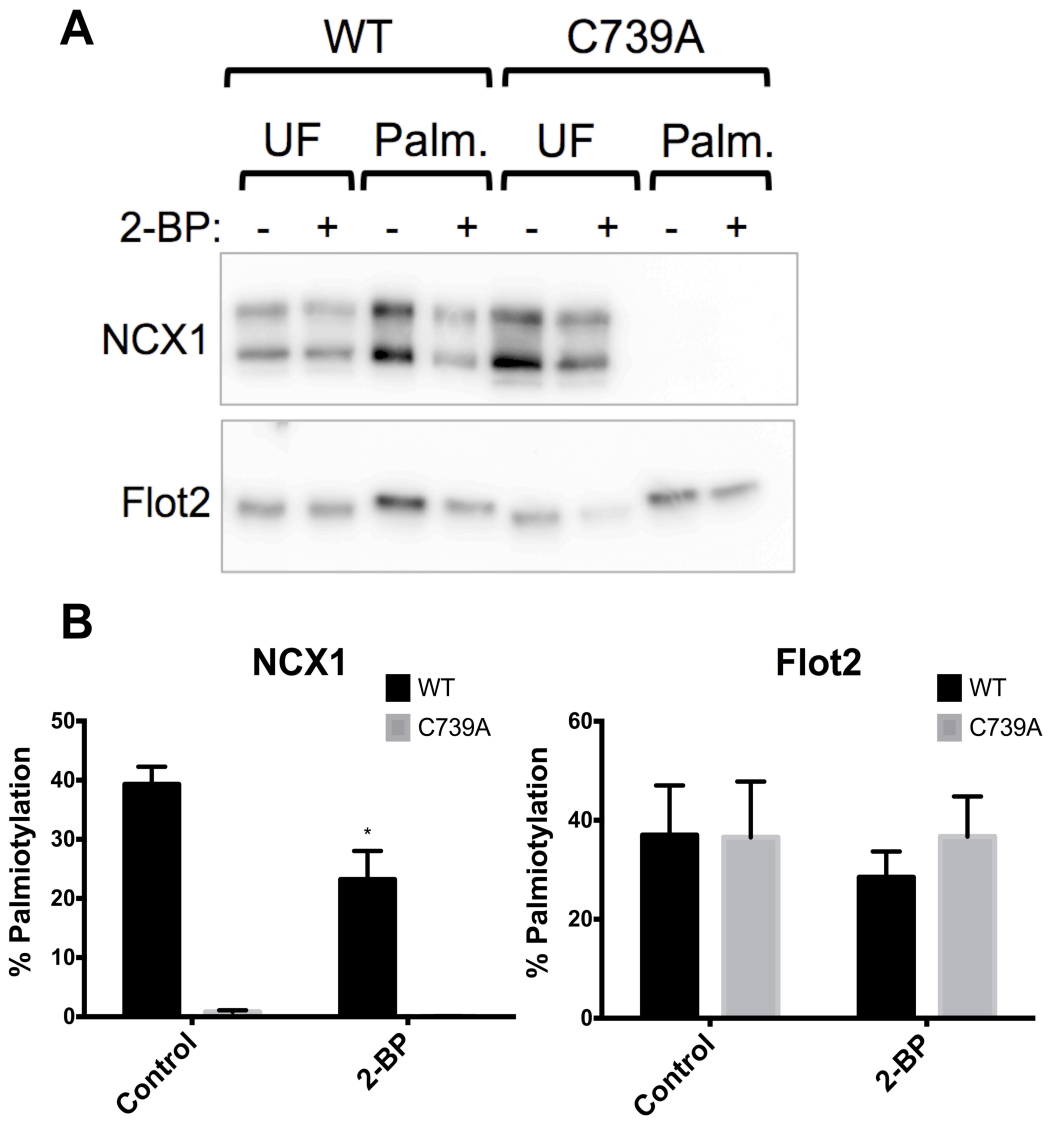


***Figure 6.1: 2-BP Decreases WT NCX1 Palmitoylation. A.*** *Treatment of FT293 WT NCX1 cells with 100μM 2-BP decreases WT NCX1 palmitoylation. No palmitoylation is observed in C739A NCX1 expressing cells.* ***B.*** *2-BP significantly decreased WT NCX1 palmitoylation. Flotillin-2 palmitoylation was unchanged by 2-BP treatment. C739A NCX1 was also not effected by 2-BP treatment.*

Shown in panel A of figure 6.1, WT NCX1 palmitoylation was reduced by 2-BP treatment. 2-BP had no effect on C739A NCX1 palmitoylation, which is completely abolished by mutation of C739. In addition, 2-BP did not reduce palmitoylation of flotillin-2. As previously shown, flotillin-2 is palmitoylated in both WT NCX1 and C739A NCX1 lysates, verifying the efficiency of acyl rac. The graph in panel B displays the mean data, showing that 2-BP significantly decreased WT NCX1 palmitoylation, with no effect on C739A NCX1. There was no significant effect on flotillin-2 palmitoylation following 2-BP treatment. These results suggest that 2-BP

inhibits NCX1 palmitoylation. The lack of effect on flotillin-2 palmitoylation, this suggests that flotillin-2 palmitoylation turns over slower than NCX1 palmitoylation.

## 6.2 Effect Of Pharmacological And Mutational Inhibition Of Palmitoylation On WT NCX1 Cell Surface Localisation

It is well documented that palmitoylation targets proteins to subcellular compartments (Linder & Deschenes 2007). To measure WT NCX1 that is localised to the cell membrane, a cell surface labelling assay, cell surface biotinylation, was used. Incubating cells with cell impermeable amine reactive biotinylation reagent sulfo-NHS-SS-biotin labels cell surface membrane resident proteins with extracellular primary amines (N-terminus or lysine residues). Biotinylated proteins were purified from cell lysates using streptavidin beads. Samples were analysed by SDS-PAGE gel electrophoresis and western blotting.

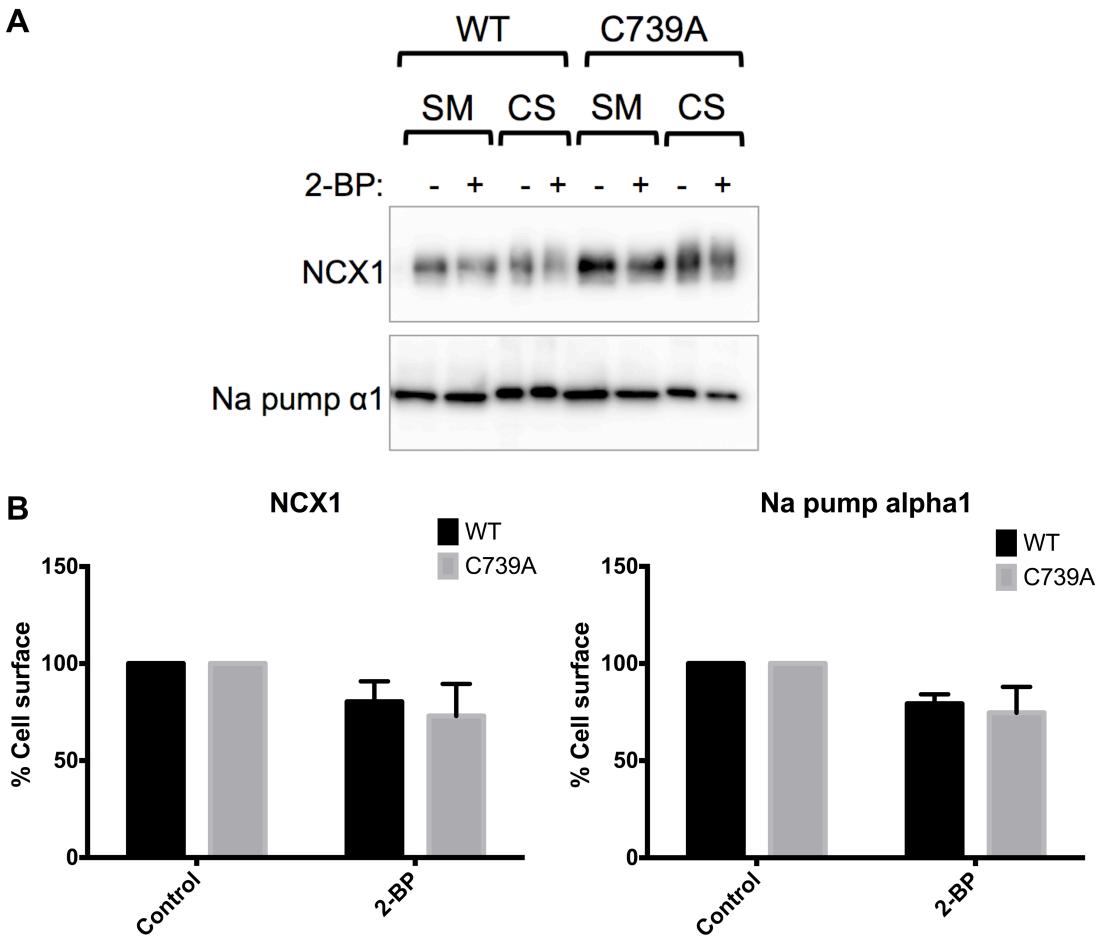


***Figure 6.2: NCX1 Cell Surface Localisation Is Not Decreased By Inhibiting Palmitoylation.*** ***A.*** *WT NCX1 cell surface localisation is not decreased by inhibiting palmitoylation with 2-BP. C739A NCX1 is also expressed at the cell surface membrane, which is not effected by 2-BP treatment. 2-BP also had no effect on Na pump cell surface localisation.* ***B.*** *Mean data shows no significant difference in WT NCX1, C739A NCX1 or Na pump cell surface localisation after 2-BP treatment. WT NCX1, 2-BP 80.3 ± 10.5, n=3, $Na^+/K^+$ ATPase 79.3 ± 4.8, n=3, C739A NCX1, 2-BP 73.0 ± 16.52 n=3, $Na^+/K^+$ ATPase 2-BP 74.7 ± 13.28 n=3.*

WT NCX1 was purified using cell surface biotinylation, shown in panel A of figure 6.2. Inhibition of palmitoylation using 2-BP did not decrease the amount of NCX1 localised to the cell membrane. As a control, samples were blotted for $Na^+$-$K^+$-ATPase α1 subunit, whose localisation is not regulated by palmitoylation (Tulloch et al. 2011). The amount of $Na^+$-$K^+$-ATPase captured was not affected by 2-BP treatment. Mean data revealed that 2-BP did not significantly decrease the amount of NCX1 localised to the cell surface. Additionally, the level of $Na^+$-$K^+$-ATPase was not significantly changed by

2-BP treatment. These results suggest that palmitoylation is not required for targeting of WT NCX1 to the cell membrane.

As 2-BP was recently shown to have non-specific and off-target effects (Davda et al. 2013), mutational inhibition of palmitoylation is a more elegant method of determining its role in membrane targeting of NCX1. FT293 C739A cell line was used to determine if non-palmitoylatable NCX1 is trafficked to the membrane. In addition, cells were treated with 2-BP to inhibit palmitoylation. Biotinylation of cell surface proteins was performed as previously described and samples analysed by SDS-PAGE gel electrophoresis and western blotting.

Shown in panel A of figure 6.2, C739A is present in cell surface fractions, indicating it is trafficked to the cell membrane. In addition, 2-BP has no effect on the amount of C739A NCX1 that is present at the cell membrane. The α1 subunit of $Na^+/K^+$ ATPase was purified using cell surface biotinylation, confirming the effectiveness of this assay to purify cell surface resident proteins. The amount of $Na^+/K^+$ ATPase at the cell membrane was not affected by 2-BP. The mean data (panel B, figure 6.2) shows that localisation of C739A NCX1 to the cell surface membrane is not significantly decreased by treatment with 2-BP. $Na^+/K^+$ ATPase shows no significant difference in the amount at the cell membrane after 2-BP treatment compared to control. These results suggest that for full-length NCX1, palmitoylation is not required to target the protein to the cell surface membrane.

## 6.3 Targeting Of NCX1 To Ventricular Myocyte Caveolae By Palmitoylation

There is evidence that suggests a role for palmitoylation in targeting proteins to microdomains within the cellular membrane (Brown 2006; Melkonian et al. 1999). Caveolae are flask-shaped invaginations of the plasma membrane (Stan 2005), which are rich in cholesterol and sphingolipids and present in multiple cell types. There is evidence to suggest various ion channels, exchanger and transporters, as well as other cell signalling molecules are concentrated in caveolae in cardiac muscle (Balijepalli & Kamp 2008). To determine whether palmitoylation is involved in targeting NCX1 to caveolae, acyl rac was used to assess amount of palmitoylated NCX1 present in sucrose gradient fractions of caveolin-enriched membrane prepared from ARVM.

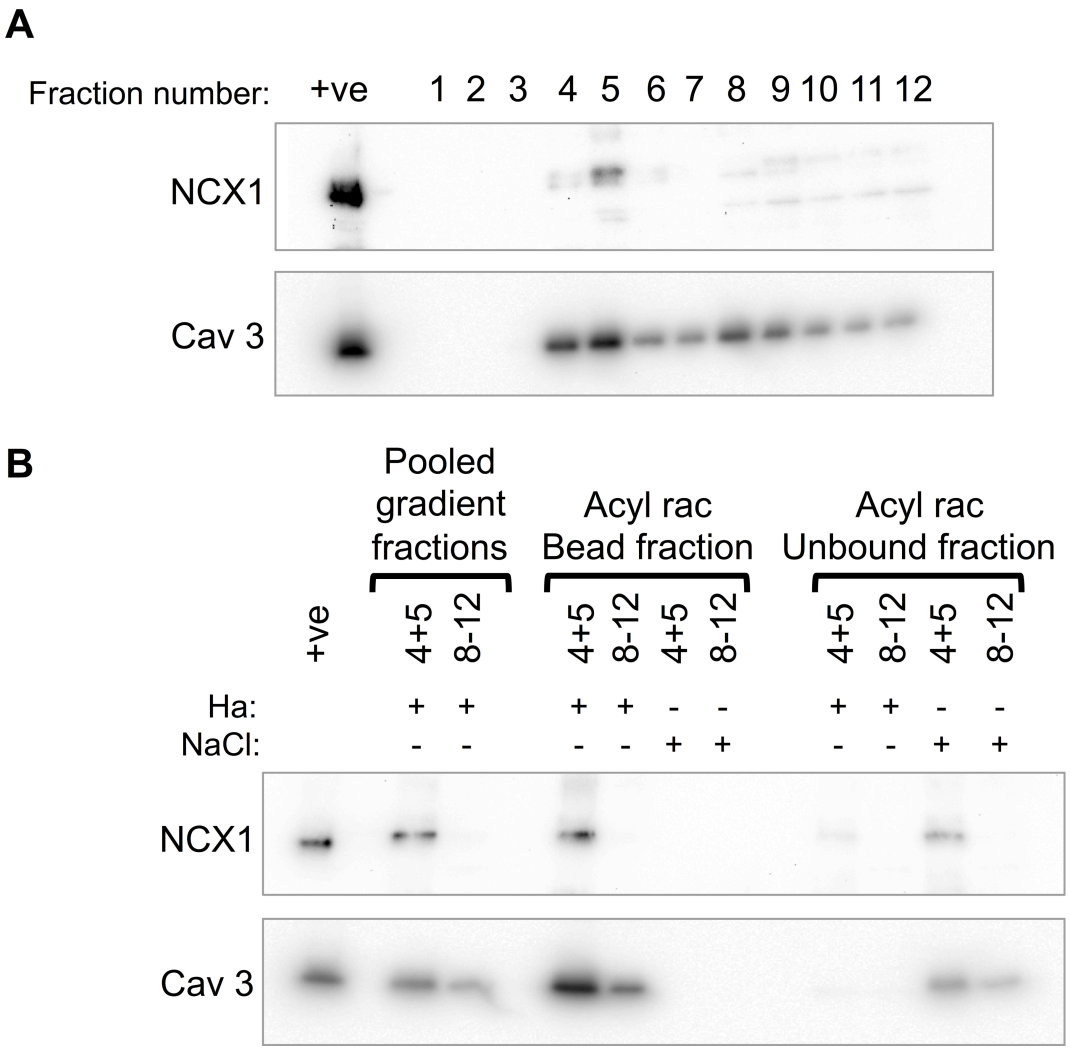


***Figure 6.3: Palmitoylation Is Not Involved In Targeting NCX1 To Caveolae. A.*** *Representative sucrose gradient. NCX1 is found in fractions 4 and 5, as well as caveolin-3, consistent with purification of caveolar membranes.* ***B.*** *Palmitoylated NCX1 is present in pooled fractions 4 and 5. However, NCX1 is also present in unbound fractions in the presence of hydroxylamine. Ha – hydroxylamine.*

Panel A of figure 6.3 shows a representative sucrose gradient. Using floatation on a discontinuous sucrose gradient, which isolates buoyant caveolin-enriched membranes from isolated cardiac myocytes, NCX1 was detected in buoyant membranes (fractions 4 and 5). In addition, caveolin-3, involved in the formation of caveolae, was detected within the same fractions, suggesting that NCX1 and caveolin-3 are both present in caveolae within cardiac myocytes. Fractions following 8-12 represent bulk sarcolemmal membrane, indicated by the presence of clathrin heavy chain within these fractions (Howie et al. 2014). There is a low level of NCX1 present within these fractions. This suggests that in cardiac myocytes, NCX1 predominantly localises to caveolar domains. As previously discussed, fractions 4 and 5 of the sucrose gradient represent caveolae-

enriched fractions, whereas fractions 8 – 12 represent non-caveolar membranes. Analysis of pooled fractions by acyl rac revealed palmitoylated NCX1 localised to caveolar domains with caveolin-3. NCX1 is not detected in pooled fractions from 8 – 12. Analysis of unbound fractions from acyl rac from pooled sucrose gradient fractions revealed NCX1 in pooled 4 and 5 fractions, in the presence of hydroxylamine. This suggests that not all NCX1 that localises to caveolae is palmitoylated. All of caveolin-3 present in fractions 4 and 5 is palmitoylated, as it was not detected in unbound fractions from acyl rac assays using pooled 4 and 5 fractions. Since non-palmitoylated NCX1 is found in buoyant membranes, these results suggest that palmitoylation is not required to target NCX1 to caveolar domains within cardiac myocytes.

## 6.4 NCX1 Exchange Current In HEK293 Cell Line

FT293 cell line expressing WT NCX1 and C739A was used to measure NCX1 current-voltage (IV) relationships via whole cell electrophysiology. Following establishment of whole cell mode, cells were held at the calculated reversal potential (-30mV). IV ramps were performed by stepping the membrane potential from -30mV to +80mV followed by decreasing membrane potential to -100mV over 1800ms.

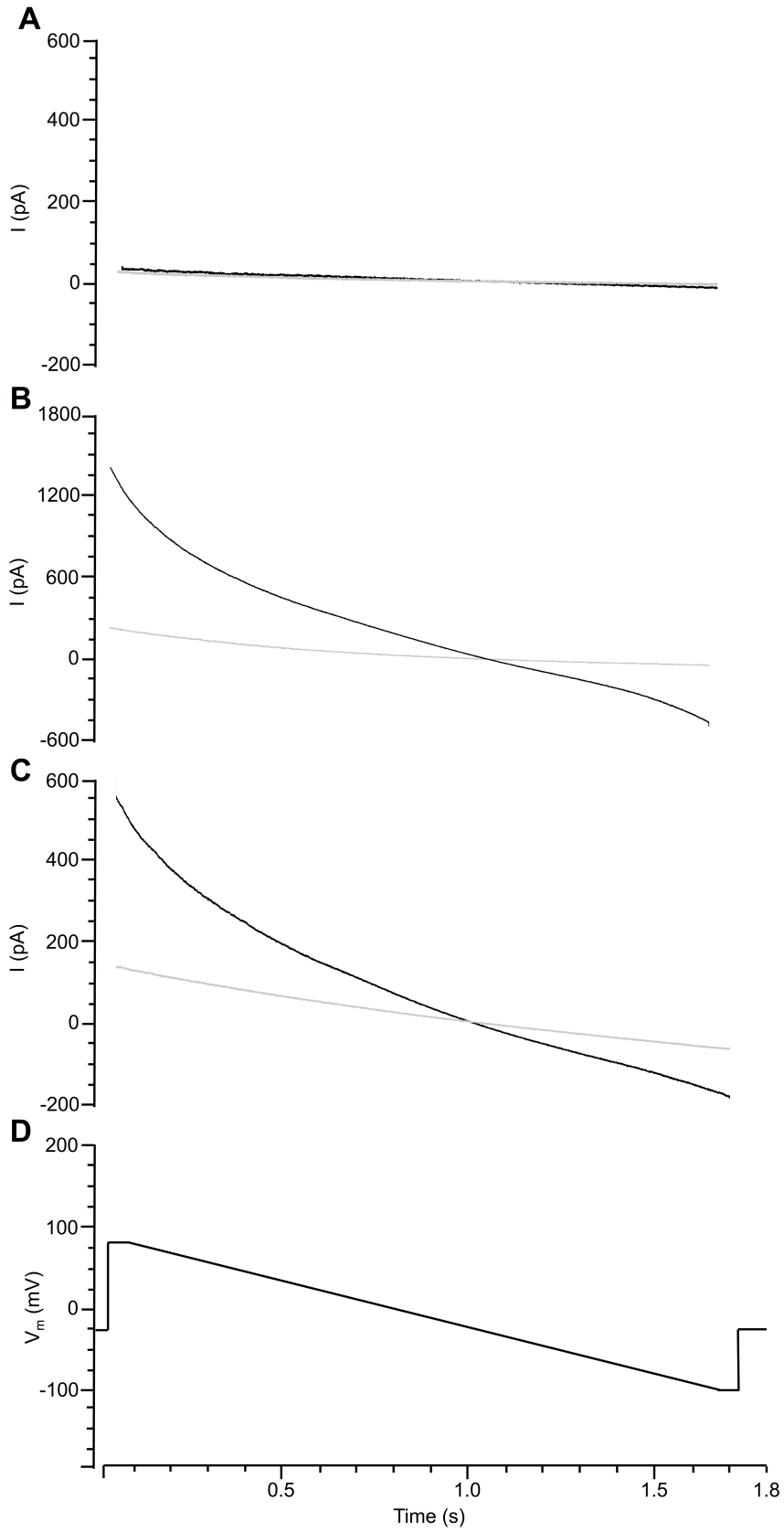


***Figure 6.4: WT NCX1 And C739A NCX1 IV Relationship In FT293 Cell Line. A.*** *Representative whole cell current (black trace) recorded from non-transfected HEK293 cell line with no sensitivity to replacement of $Na^+$ and $Ca^{2+}$ with $Li^+$ and $Mg^{2+}$ respectively (grey trace), which block NCX1 current. Current was measured from the*

*same cell prior to and following $Li^+$ & $Mg^{2+}$ treatment* ***B.*** *Representative whole cell current (black trace) recorded from FT293 cell lines expressing WT NCX1 shows sensitivity to replacement of $Na^+$ and $Ca^{2+}$ with $Li^+$ and $Mg^{2+}$ respectively (grey trace), which block NCX1 current. Current was measured from the same cell prior to and following Li & Mg treatment.* ***C.*** *Representative whole cell current (black trace) recorded from FT293 stable cell lines expressing C739A NCX1 also shows sensitivity to application of Li and Mg (grey trace). Current was measured from the same cell prior to and following treatment.* ***D.*** *Voltage ramp protocol over 1800 milliseconds from +80mV to -100mV. I – current, pA – picoampere, $V_m$ – membrane potential, mV – millivolt, s – seconds.*

Panel A of figure 6.4 shows whole cell current from the average of 5 consecutive ramps from +80mV to -100mV over a 1800ms protocol from a single non-transfected HEK293 cell (black trace). Replacement of $Na^+$ and $Ca^{2+}$ with $Li^+$ and $Mg^{2+}$ respectively resulted in little to no change in current recorded, demonstrating the absence of NCX1 current within non-transfected cells. Panel B of figure 6.4 shows whole cell current from a single FT293 cell stably expressing WT NCX1 (black trace). Following measurement of WT NCX1 current, extracellular $Na^+$ and $Ca^{2+}$ were replaced with $Li^+$ and $Mg^{2+}$ respectively to determine current remaining following replacement (grey trace). FT293 WT NCX1 cells showed large NCX1 currents, which were $Li^+$ and $Mg^{2+}$ sensitive. Panel C of figure 6.4 shows C739A NCX1 current from FT293 cells. C739A NCX1 current is also sensitive to replacement of $Na^+$ and $Ca^{2+}$ with $Li^+$ and $Mg^{2+}$ respectively. These results show that NCX1 proteins stably expressed in FT293 cells are active and are sensitive to $Li^+$ and $Mg^{2+}$.

Current from endogenous voltage gated ion channels and leak current can contaminate currents generated by voltage ramp protocols. To correct for this, $Li^+$ and $Mg^{2+}$ sensitive current, which represents NCX1 only current was calculated by subtracting current remaining after $Li^+$ and $Mg^{2+}$ treatment from the total measured current. Shown in figure 6.5 is comparison of corrected current from WT NCX1 and C739A NCX1 expressing cells. The reversal potential was not significantly different between WT NCX1 and C739A NCX1 expressing cells, -28.9 ± 1.7 mV and -35.9 ± 2.9 mV respectively, p value = 0.6 (panel A, figure 6.5). Normalising for cell capacitance, there was a significant difference in the amplitude of recorded current between WT NCX1 and C739A NCX1 (panel B, figure 6.5). C739A NCX1 current was significantly

decreased at positive voltages, +80, +70 and +60mV compared to WT NCX1. These results suggest that inhibition of palmitoylation results in decreased NCX1 outward mode exchange current. Calculation of the rectification index (inset in panel B, figure 6.5) showed that there was no significant difference between WT NCX1 and C739A NCX1 expressing cells, suggesting that differences observed may be due to subtle differences in expression levels between cells. Expression was normalised wherever possible by analysing expression levels between cells by western blotting.

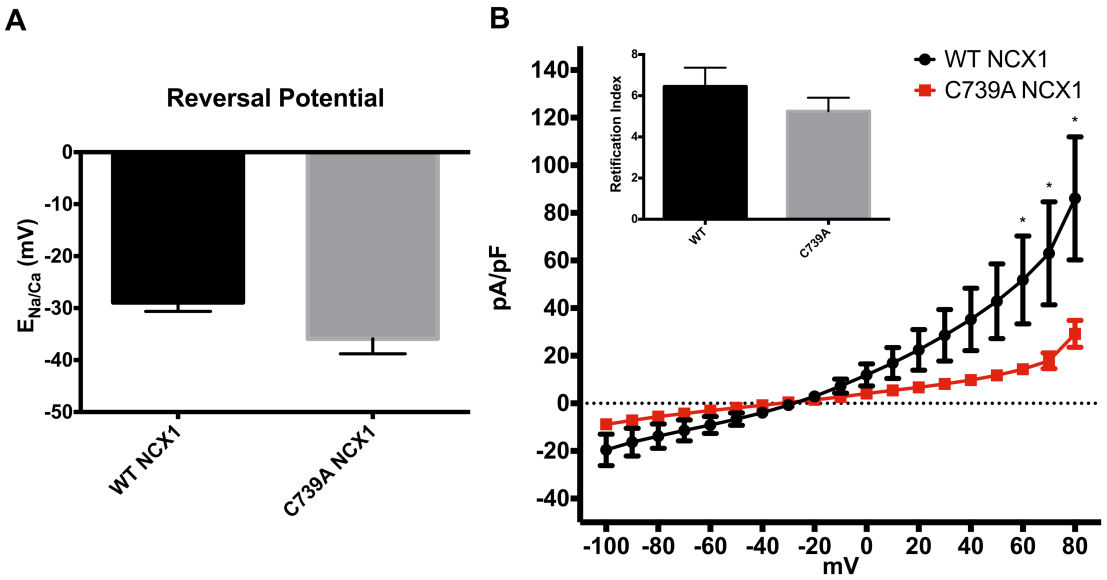


***Figure 6.5: C739A NCX1 Current Is Decreased Compared To WT NCX1 At Positive Voltages.*** ***A.*** *Reversal potential between WT NCX1 and C739A NCX1 was not statistically different.* ***B.*** *C739A NCX1 current at +80, +70 and +60 mV is significantly decreased compared to WT NCX1. Insert shows rectification index for WT and C739A NCX1 expressing cells at +80mV normalised to current obtained at -80mV. Statistical significance was calculated using the Holm-Sidak method with alpha 5%. WT NCX1 – n=6, C739A NCX1 n=5.*

## 6.5 Discussion

Palmitoylation has been reported to have a number of different roles in the regulation of ion transport (Shipston 2014). Palmitoylation has been described to regulate cell surface expression of ion transporters and channels. In addition, palmitoylation has been described to regulate activity of ion channels, namely predominantly through altered voltage sensitivity, such as Kv1.1 (Gubitosi-Klug et al. 2005), ENaC (Mueller et al. 2010) and α1BCa$^{2+}$ (Stephens et al. 2000). Therefore, elucidating the effect of palmitoylation on NCX1 will provide insight into how this post-translational modification modulates activity.

### Membrane Targeting Of NCX1 By Palmitoylation

As mentioned previously, palmitoylation regulates membrane targeting and cell surface localisation of a number of ion channels. Using FT293 cell lines stably expressing WT NCX1 or its non-palmitoylatable mutant, C739A, the cell surface localisation of NCX1 was investigated. Cell impermeable reagents were used to label the cell surface proteins with biotin, which was exploited to affinity purify cell surface proteins using streptavidin. The results revealed that inhibiting palmitoylation either pharmacologically or using mutagenesis had no effect on trafficking of NCX1 to the cell surface membrane. C739A NCX1, which is non-palmitoylated, is trafficked to the cell surface membrane. This is somewhat unsurprising as NCX1 has 10 transmembrane domains (Ren & Philipson 2013); therefore it is unlikely that a single lipid modification would alter trafficking to the membrane. Indeed, single lipid modifications have been described to promote transient membrane association (Shahinian & Silvius 1995; Salaun et al. 2010). Evidence regarding palmitoylation of the BK channel, which is a multi-pass transmembrane protein, suggests that palmitoylation of multiple residues can govern surface membrane localisation (Jeffries et al. 2010). The BK channel is palmitoylated on S0-S1 linker domain on 3 cysteine residues (Jeffries et al. 2010), which regulates its cell surface expression. Steady state cell surface expression levels were reduced by ~55% in non-palmitoylatable BK channels. It appears that in order to regulate cell membrane targeting of large multi-pass transmembrane proteins, multiple palmitoylated cysteine residues are required.

**Targeting Of NCX1 To Caveolae In Cardiac Muscle**

As palmitoylation does not appear to regulate cell surface expression of NCX1, influence on NCX1 targeting to lipid rafts was investigated. Few studies have determined whether NCX1 localises to caveolar domains and what the functional consequences of this localisation are. NCX1 was shown to associate with caveolin-3 in bovine cardiac sarcolemmal vesicles (Bossuyt et al. 2002). Additionally, evidence that annexin A5 interacts with NCX1 as part of a larger macromolecular complex, which includes caveolin-3 localised to caveolae in human ventricular myocytes (Camors et al. 2006). In contrast, co-immunoprecipitation failed to detect NCX1 and caveolin-3 interactions from rat ventricular myocardium or co-localisation using immunolabelled rat ventricular myocytes (Cavalli et al. 2007). The same study reported a large majority of NCX1 present in cardiac myocytes does not localise to caveolae (Cavalli et al. 2007). In order to determine whether NCX1 is found in caveolae within cardiac muscle, buoyant caveolin-enriched microdomains were prepared from isolated ARVM by floatation on a discontinuous sucrose gradient. NCX1 was found in caveolin containing fractions isolated from sucrose gradients. Moreover, palmitoylated NCX1 localised to caveolae in rat ventricular myocytes. Surprisingly, non-palmitoylated NCX1 was found in pooled fractions 4 and 5 fractions from sucrose gradients. These results suggest that palmitoylation is not required to target NCX1 to caveolae in cardiac muscle, as non-palmitoylated NCX1 is also present in buoyant caveolin-enriched fractions. NCX1 contains five possible caveolin-binding motifs (Bossuyt et al. 2002), therefore localisation to caveolae is most likely dependent on the interaction between NCX1 and caveolin-3 and not its palmitoylation.

Palmitoylation may not be involved in targeting to cell surface membranes in HEK293 cells or caveolae in cardiac myocytes, however it may serve as a signal to target NCX1 to t-tubules. Cardiac t-tubules are branched invaginations of cardiac myocyte sarcolemma (figure 6.7). T-tubules are highly involved in initiation of $Ca^{2+}$ transients and many of the proteins involved in $Ca^{2+}$ cycling appear to be concentrated at the t-tubule (Brette & Orchard 2003). Indeed, NCX1 has been described to localise to the sarcolemmal and t-tubular membrane within cardiac myocytes (Frank et al. 1992). Approximately 60% of NCX1 is localised to the t-tubular membrane (Despa et al. 2003), although other studies have reported higher levels (Z. Yang 2002). However, the mechanism by which proteins are targeted to t-tubules is unknown. L-type $Ca^{2+}$

channels are also targeted to t-tubules, which has in part been described as due to subunits which form the channel as well interaction with the scaffolding protein BIN1 (Shaw & Colecraft 2013). It is proposed that BIN1 may act as a membrane anchor to target L-type $Ca^{2+}$ channels to t-tubules. If a membrane anchor is required to target ion channels and transporters to t-tubules, palmitoylation may be involved. However, direct measurement of targeting of palmitoylation to specific microdomains within cells has not been achieved. If NCX1 exits the Golgi fully palmitoylated as previous data suggests, upon reaching the cell surface membrane, NCX1 may then be depalmitoylated that may lead to its lateral diffusion to other subdomains.

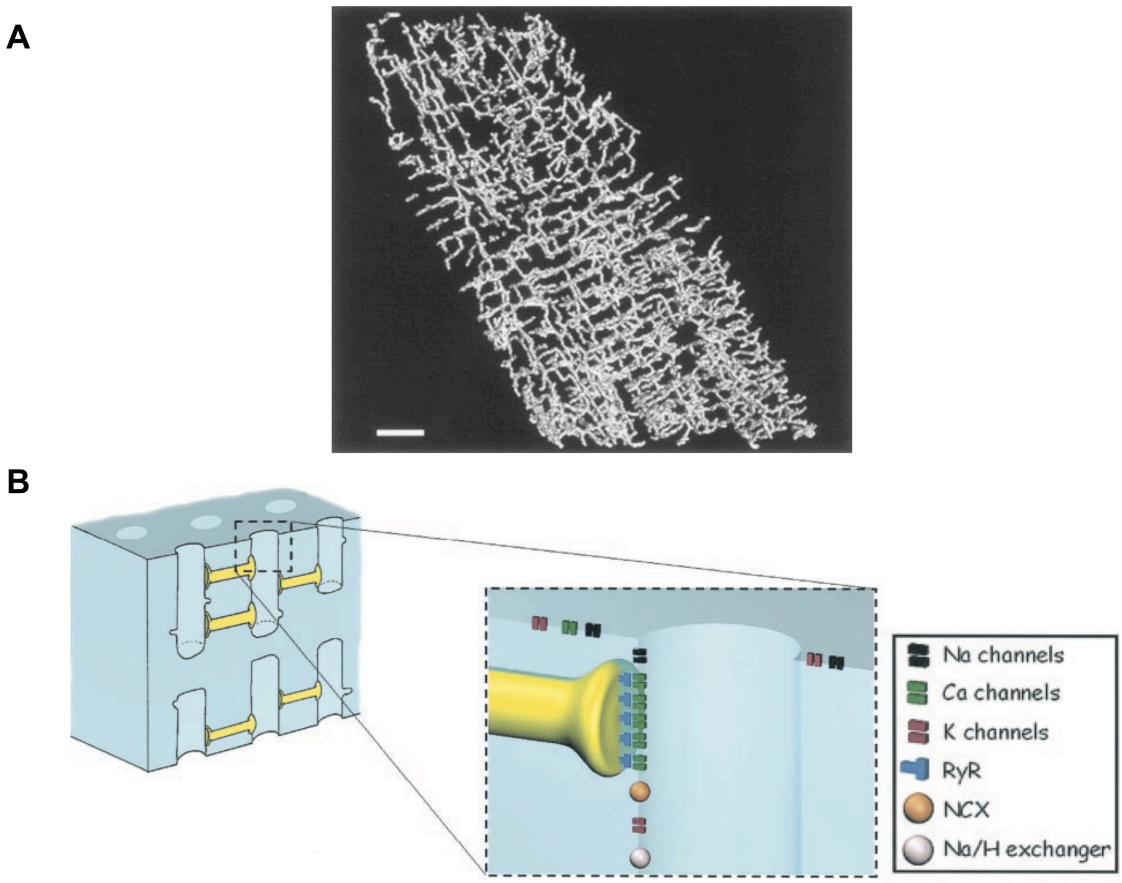


***Figure 6.6: T-Tubule Network And Protein Organisation. A.*** *3D structure of t-tubular system in rat ventricular myocyte, reconstructed from a stack of images of dextran-linked fluorescein fluorescence within t-tubules. Bar = 5µm.* ***B.*** *Schematic demonstrating protein distribution between t-tubules and sarcolemmal membrane based on immunohistological data. Both modified from (Brette & Orchard 2003).*

**NCX1 Exchange Current**

Inhibition of palmitoylation did not affect cell surface localisation of NCX1, nor was palmitoylation involved in targeting to caveolae. This suggests that palmitoylation may be involved in modulation of NCX1 activity. To address this, the current-voltage (I-V) relationship of WT NCX1 and its non-palmitoylated mutant C739A NCX1 was determined using whole cell electrophysiology. I-V relationships were determined using a voltage ramp protocol from +80mV to -100mV. NCX1 current measured from WT NCX1 and C739A NCX1 expressing cells showed sensitivity to $Li^+$ and $Mg^{2+}$, used to inhibit NCX1 current. In addition, a significant difference was observed in NCX1 current measured at positive potentials. NCX1 current was significantly decreased in C739A NCX1 expressing cells at +80mV, +70mV and +60mV compared to WT NCX1. NCX1 measured at positive potentials is indicative of outward exchange current. Additionally, lack of NCX1 palmitoylation has no effect on the reversal potential at the ion concentrations used. These results suggest that palmitoylation has a regulatory role in NCX1 current.

A potential reason for the decreased exchange current observed in C739A NCX1 expressing cells may be due to a change in $Ca^{2+}$ sensitivity. Experimental solutions were designed so NCX1 was not maximally $Ca^{2+}$ activated (free $Ca^{2+}$ = 2μM). $Ca^{2+}$ regulates NCX1 through binding to regulatory domains, CBD1 and CBD2 located within the intracellular loop domain. Recently, $Ca^{2+}$ regulation was described to feature a dual electrostatic switch mechanism (Hilge et al. 2009). $Ca^{2+}$-binding increases the electrostatic potential at the $Ca^{2+}$ binding sites and increases the attraction to negatively charged areas. As a result, $Ca^{2+}$ induced changes in electrostatic potential are regarded as switches that promote structural rearrangements (Shao et al. 1997). Following a rise in cytoplasmic $Ca^{2+}$, $Ca^{2+}$ ions bind to CBD1, increasing the electrostatic potential of CBD1. This results in CBD1 and CBD2 reorientation and thus a more compact conformation is adopted (figure 6.8, B). This initial activation step is termed $Ca^{2+}$-dependent activation and is the responsible for the initiation of $Na^+/Ca^{2+}$ exchange (Hilgemann, Collins & Matsuoka 1992b). In order to maintain activation and counteract $Na^+$-dependent inactivation, CBD2 must also bind $Ca^{2+}$ ions, thus inducing a change in electrostatic potential for CBD2 (figure 6.8, C). Following a decrease in cytoplasmic $Ca^{2+}$ below the CBD1 $Ca^{2+}$ affinity, this reverses the activation steps and NCX becomes inactive (figure 6.8, A). Based on the solutions used in these experiments, it may be the

second step (panel B) of $Ca^{2+}$-dependent activation that is modulated by palmitoylation. CBD2 is closer to the palmitoylation site, which may govern the influence of palmitoylation to regulate the conformation change in response to $Ca^{2+}$.

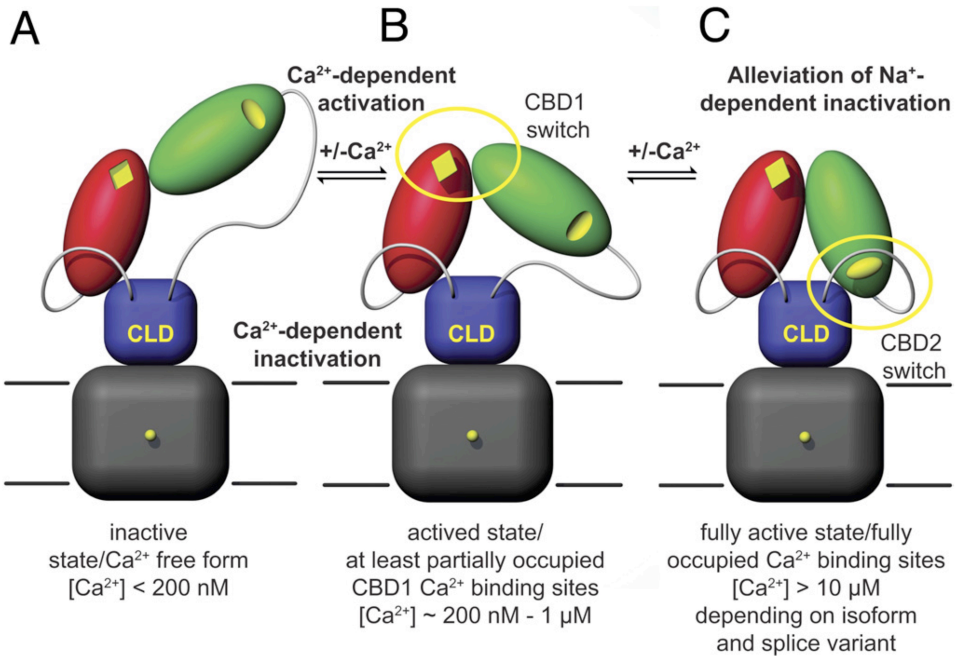


***Figure 6.7: Hypothetical Dual Electrostatic Switch Mechanism In NCX Regulation.*** ***A.*** *Inactive, $Ca^{2+}$-free NCX in an extended conformation.* ***B.*** *Submicromolar $Ca^{2+}$ concentrations induce conformation change in CBD1 via the electrostatic switch.* ***C.*** *Binding of $Ca^{2+}$ to CBD2 results in sustained $Na^{+}$-$Ca^{2+}$ exchange and removes $Na^{+}$-dependent inactivation. CBD1 is shown in red, CBD2 is shown in green. CLD - catenin-like domain. Modified from (Hilge et al. 2009).*

Palmitoylation of NCX1 may result in a change in the secondary structure. This could lead to a change in the $Ca^{2+}$ sensitivity required for activation, potentially an increase in the $Ca^{2+}$ affinity for CBD1 (Hilge et al. 2009). However, more likely is the ability of CBD2 to overcome $Na^{+}$-dependent inactivation. Introduction of a membrane anchor may promote the ability of $Ca^{2+}$ to bind to CBD2 and induce the second electrostatic switch that is required to overcome $Na^{+}$-dependent inactivation. To address whether it is $Ca^{2+}$ sensitivity that is adversely affected in the absence of palmitoylation, further electrophysiological experiments are required. Additionally, whether $Na^{+}$-dependent inactivation is more pronounced in C739A NCX1 required further investigation, which is beyond the scope of this thesis.

NCX1 has also been described to be regulated by $PIP_2$ (Hilgemann & Ball 1996; Yaradanakul et al. 2007; Shen et al. 2007). In excised patches, exogenous application of $PIP_2$ results in stimulation of NCX1 current, which inactivates upon removal of $Ca^{2+}$ or increasing cytoplasmic $Na^+$. This is modulated by direct interaction of $PIP_2$ and the XIP domain, located within the intracellular loop domain (Matsuoka et al. 1997), which is proposed to be at the N-terminal end of the intracellular loop. In addition to modulation by $PIP_2$, NCX1 was also demonstrated to be regulated by intracellular acyl CoAs (Riedel et al. 2006), as acyl CoA activated outward exchange current. These results suggest that anionic lipids regulate NCX1 exchange activity, predominantly the outward exchange current. However, the majority of these studies were performed in excised patches and applying exogenous $PIP_2$ or acyl CoAs. Further investigation will be required to determine whether $PIP_2$ or indeed acyl CoAs are capable of modulating exchange current in a physiological setting. It is possible that palmitoylation may influence the regulation by anionic lipids. The addition of a lipid anchor towards the C-terminal end of the intracellular loop may impact protein-protein interactions or interactions with mediators. Further work is required to determine whether C739A NCX1 would be regulated by $PIP_2$ in the absence of palmitoylation.

**Summary**

These results suggest that palmitoylation is not involved in membrane trafficking or indeed targeting to lipid rafts such as caveolae. Palmitoylation, does however, appear to regulate exchange activity of NCX1, predominantly the outward mode. The mechanism by which palmitoylation influences regulation by secondary messengers like $PIP_2$, if that indeed is the case, remains to be explored. The observed decrease in outward NCX1 current in the absence of palmitoylation may point to a change in regulation of the exchanger by $Ca^{2+}$ and $Na^+$. Further experiments are required to tease out the mechanism by which palmitoylation regulates NCX1 activity.

# Chapter 7: NCX1 Palmitoylation In Disease

## 7.1 NCX1 Palmitoylation In Left Ventricular Heart Failure

Contractile abnormalities during the development of left ventricular hypertrophy and heart failure are a result of an imbalance between SERCA2a and NCX1. This ultimately leads to more $Ca^{2+}$ removal from the cytosol (via overactive NCX1), resulting in decreased $Ca^{2+}$ being sequestered back into intracellular stores (via reduced SERCA2a activity) and ultimately leading to decreased contractility (Pogwizd et al. 1999; Hobai & O'Rourke 2000). The role of palmitoylation in cardiovascular disease has not been investigated. As NCX1 is often upregulated in heart failure, it was investigated whether NCX1 palmitoylation was changed in a model of heart failure. Heart failure was induced in adult rats via aortic banding, in which the ascending aorta was constricted with a titanium clip. Animals were allowed to recover and monitored by echocardiography. Once ejection fraction decreased to below 45%, animals were sacrificed and tissue collected. Prior to tissue collection, cardiac function measurements were recorded using Millar pressure-conductance catheters, which provide direct measurements of LV pressure-volume relationships and is the gold standard method for ejection fraction measurements. Compensated hypertrophy, evident at 16-20 weeks, progressed to heart failure by approximately 25 weeks. Heart tissue, which was normalised by assessing protein concentration, was used in acyl rac to determine palmitoylation of specific targets followed by SDS-PAGE gel electrophoresis and western blotting. Both sham operated and banded animals were investigated.

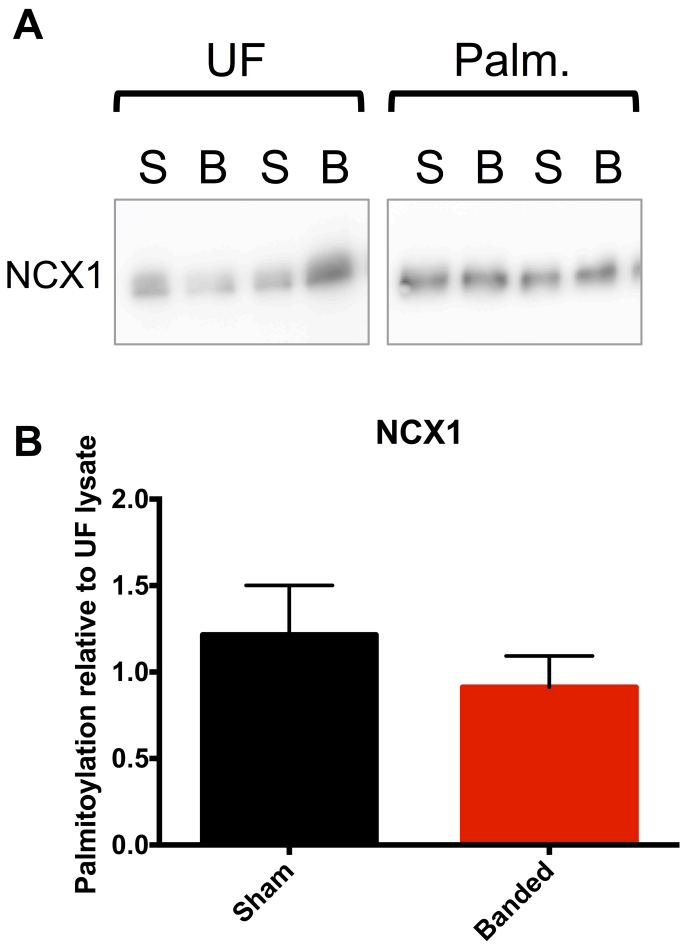


***Figure 7.1: NCX1 Expression and Palmitoylation Are Unchanged In A Rat Model Of Heart Failure. A.*** *NCX1 palmitoylation is not affected by heart failure.* ***B.*** *Statistical analysis revealed no significant difference between sham and banded animals. n=4-5, sham mean 1.215 ± 0.2864, banded mean 0.9123 ± 0.1810. UF – unfractionated, Palm. – palmitoylated, S – sham, B – banded.*

UF samples in figure 7.1 reveal that NCX1 expression is variable between banded hearts, sham 418545 ± 67340 A.U and banded 455282 ± 154744 A.U. Despite inconsistencies in NCX1 expression, palmitoylation of NCX1 is consistent between sham and banded hearts. Statistical analyses revealed that there is no significant difference between NCX1 palmitoylation in sham and banded hearts. These results suggest that NCX1 palmitoylation is unaffected by left ventricular heart failure in this model.

In addition to NCX1 upregulation, SERCA2a is downregulated in heart failure (O'Rourke et al. 1999; Hasenfuss & Schillinger 2004). To validate the heart failure

model used in this study, SERCA2a expression was determined. Shown in figure 7.2, banded hearts show decreased SERCA2a expression compared to sham hearts (panel A, figure 7.2). Statistical analysis revealed that the difference in SERCA2a expression observed on western blotting is not significant (panel B, figure 7.2). The results suggest that in this model of heart failure, SERCA2a expression does not change. However, post hoc power analysis revealed power to be 55.1%, suggesting that this study is underpowered to see an effect of banding on SERCA2a expression.

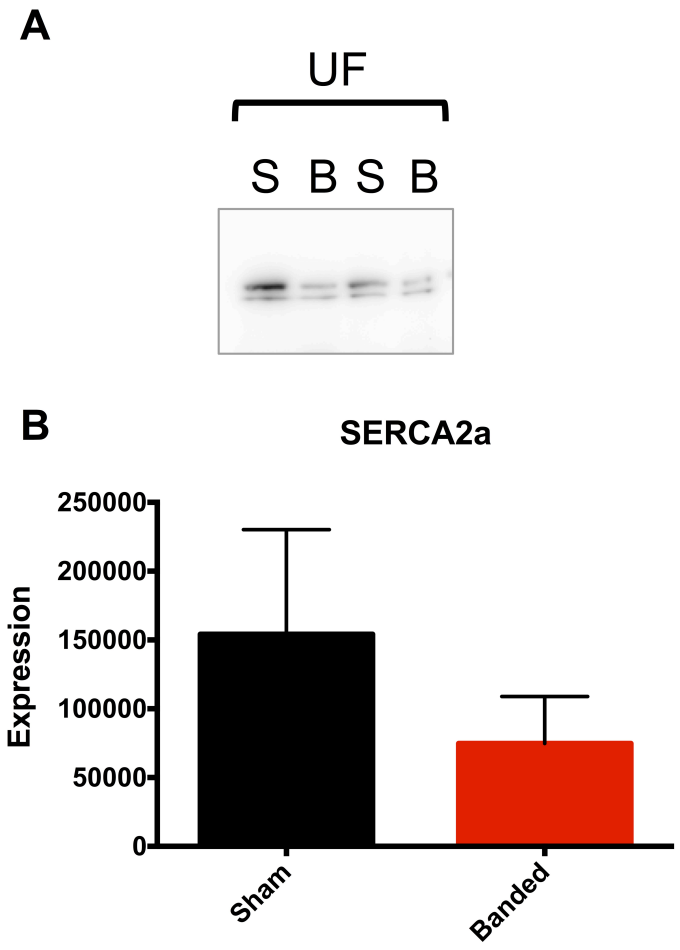


***Figure 7.2: SERCA2a Expression Is Unchanged In Heart Failure.*** ***A.*** *SERCA2a expression shows a decrease in banded samples on western blots.* ***B.*** *Statistical analysis revealed that differences observed on western blots are not significant between sham and banded hearts. n=4-5, sham mean 154186 ± 76009, banded mean 74763 ± 34138. UF – unfractionated, S – sham, B – banded, A.U – arbitrary units.*

An underlying cause of contractile abnormalities in cardiac disease is the balance of $Ca^{2+}$ removal from the cytosol by SERCA2a and NCX1. During development of heart

failure, there is a shift towards NCX1, as has been demonstrated by increased activity in models of heart failure (Hobai & O'Rourke 2000; Pogwizd et al. 1999). To determine whether the ratio between SERCA2a and NCX1 was favouring NCX1, the ratio of SERCA2a expression was calculated against NCX1 expression. Shown in figure 7.3, the SERCA2a:NCX1 ratio is unchanged in banded animals compared to sham operated animals. However, SERCA2a:NCX1 ratio is slightly decreased in banded animals compared to sham, suggesting that the ratio is shifting towards NCX1, despite no statistical significance.

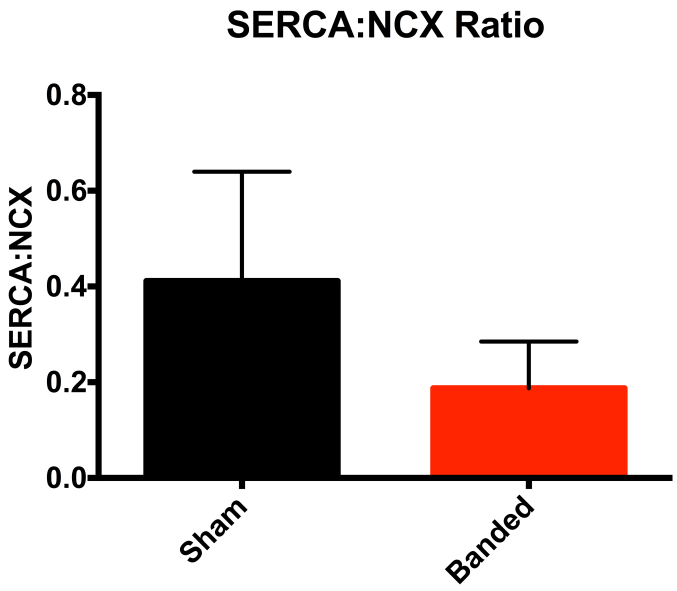


***Figure 7.3: SERCA2a:NCX1 Ratio In Heart Failure.*** *Ratio between SERCA2a and NCX1 expression in heart failure is unaffected by heart failure.*

Changes in caveolin-3 protein expression have been reported in models of heart failure (Woodman et al. 2002; Feiner et al. 2011; Ohsawa et al. 2003; Y. I. Lee et al. 2006). However, these reports are controversial. In a murine model of heart failure and in human failing heart, caveolin-3 was decreased (Feiner et al. 2011). In contrast, caveolin-3 knockout mice developed progressive cardiomyopathy (Woodman et al. 2002). In order to determine whether caveolin-3 expression and palmitoylation was affected in this rat model of heart failure, acyl rac samples from sham and banded hearts were investigated. In contrast to reports that find differences in caveolin-3 expression between failing and non-failing hearts, there was no difference between caveolin-3 expression between sham and banded hearts detected by western blotting (panel A, figure 7.4). Determining palmitoylation of caveolin-3 in sham and banded hearts

revealed no significant difference (panel B, figure 7.4). In this model of heart failure, caveolin-3 palmitoylation is unchanged.

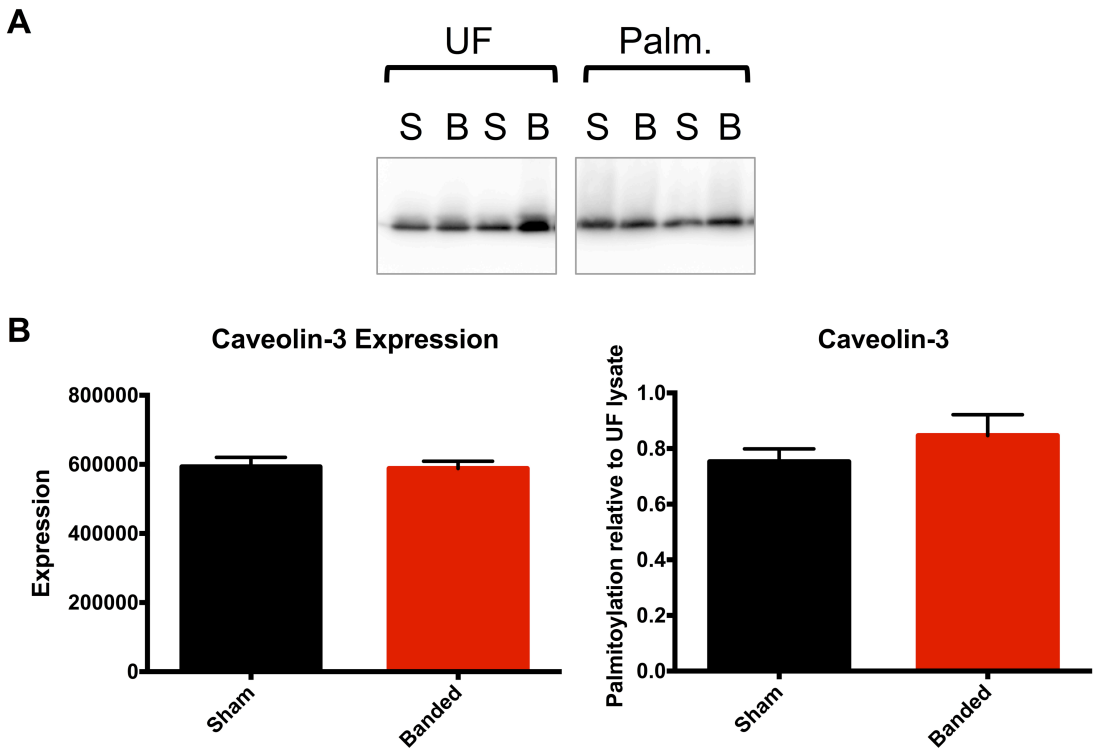


***Figure 7.4: Caveolin-3 Expression And Palmitoylation Is Unchanged In Heart Failure. A.*** *Caveolin-3 expression is not significantly affected by heart failure.* ***B.*** *Palmitoylation of caveolin-3 is comparable between sham and banded hearts. n=4-5, sham mean 0.7526 ± 0.04620, banded mean 0.8465 ± 0.07535. UF – unfractionated, Palm. – palmitoylated, S – sham, B – banded, Bds – beads.*

As caveolin-3 expression and palmitoylation is unchanged in this model, it was used to normalise the amount of NCX1 palmitoylation, to establish if NCX1 palmitoylation is altered in this model. Additionally, caveolin-3 palmitoylation serves as a control for acyl rac, as it is a constitutively palmitoylated protein and should be enriched during the assay. Shown in figure 7.5, NCX1 palmitoylation is unchanged following banding, compared to sham operated animals. This suggests that in this model, NCX1 palmitoylation is unchanged following induction of heart failure.

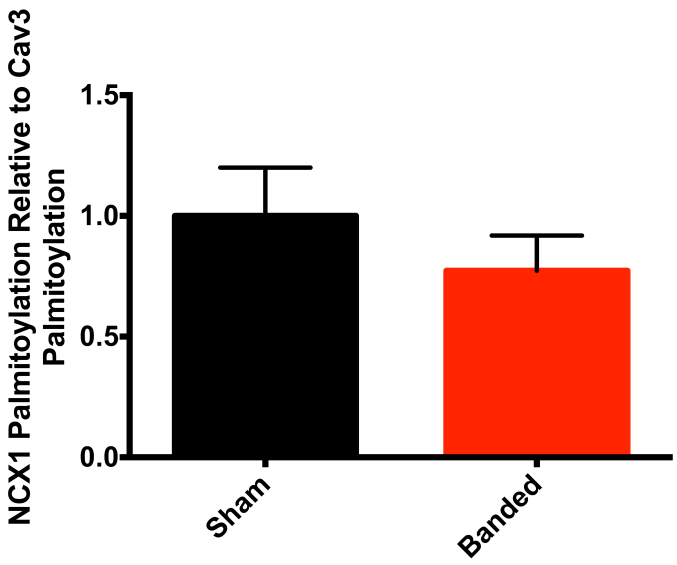


***Figure 7.5: NCX1 Palmitoylation Is Unchanged In Heart Failure When Normalised To Caveolin-3 Palmitoylation.*** *NCX1 palmitoylation is unchanged when expressed relative to caveolin-3 palmitoylation.*

## 7.2 NCX1 Palmitoylation During Development Of Left Ventricular Hypertrophy

NCX1 expression has been shown to increase during hypertrophy (Hobai & O'Rourke 2000; Pogwizd et al. 1999; Hasenfuss et al. 1994) but whether palmitoylation is affected has not been investigated. To determine the effect of hypertrophy on NCX1 palmitoylation, a rodent *in vivo* model of cardiac hypertrophy was used (Boguslavskyi et al. 2014). Myocardial hypertrophy was induced by pressure overload following suprarenal aortic constriction (banding) in 6-week old mice. Mice were sacrificed after 3 days, 2 weeks, 4 weeks and 8 weeks following surgery. Tissue was harvested and used in acyl rac to assess changes in protein palmitoylation.

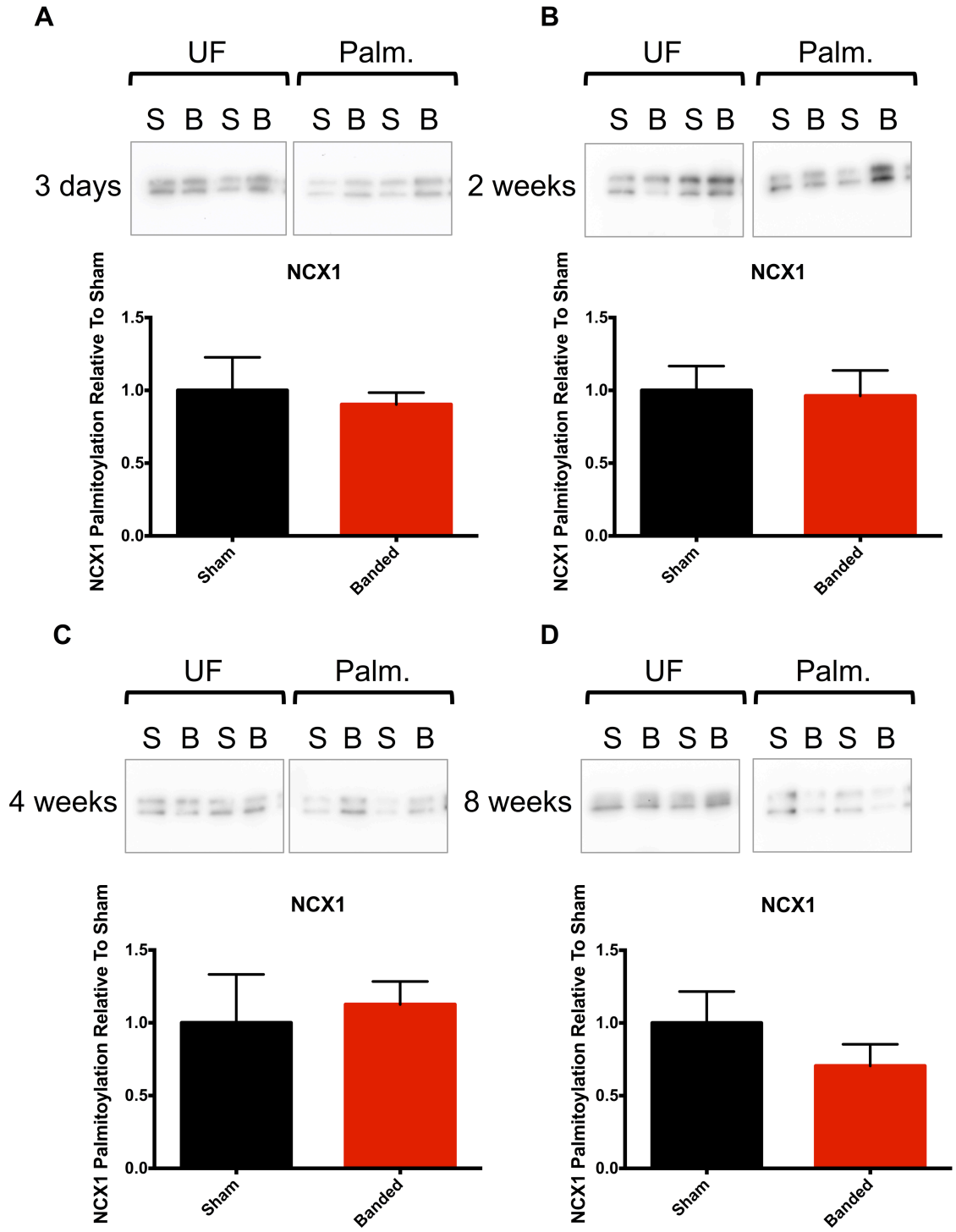


***Figure 7.6: NCX1 Palmitoylation Does Not Change During Development Of Left Ventricular Hypertrophy. A.*** *NCX1 palmitoylation is unchanged 3 days post banding, sham mean 1.00 ± 0.22 n=4, banded mean 0.90 ± 0.08 n=4.* ***B.*** *NCX1 palmitoylation does not change 2 weeks post banding, sham mean 1.00 ± 0.2 n=5, banded mean 0.96 ± 0.18 n=6.* ***C.*** *4 weeks of banding had no effect on NCX1 palmitoylation, sham mean 1.00 ± 0.33 n=3, banded mean 1.13 ± 0.16 n=6.* ***D.*** *8 weeks of banding had no effect on NCX1 palmitoylation, sham mean 1.00 ± 0.22 n=6, banded mean 0.70 ± 0.15 n=6. UF – unfractionated, Palm. – palmitoylated, S – sham, B – banded.*

Figure 7.6 shows a timecourse of NCX1 palmitoylation following banding in mice. NCX1 palmitoylation was unchanged at any of the timepoints investigated (figure 7.6). Statistical analysis revealed that there is no significant change in NCX1 palmitoylation between sham and banded animals at any timepoint. These results suggest that in the samples analysed, there is no significant change in NCX1 palmitoylation in this model of cardiac hypertrophy.

## 7.3 Changes In Caveolin-3 And SERCA2a During Development Of Left Ventricular Hypertrophy

As previously discussed, changes in caveolin-3 expression have been reported in various models of cardiovascular disease. In order to determine whether caveolin-3 palmitoylation was changed in hypertrophy, samples used in NCX1 palmitoylation analysis were used to assess changes in caveolin-3 palmitoylation between sham and banded animals. Additionally, caveolin-3 palmitoylation can determine how efficiently acyl rac captured palmitoylated proteins and can be used to normalise relative palmitoylation of other targets investigated.

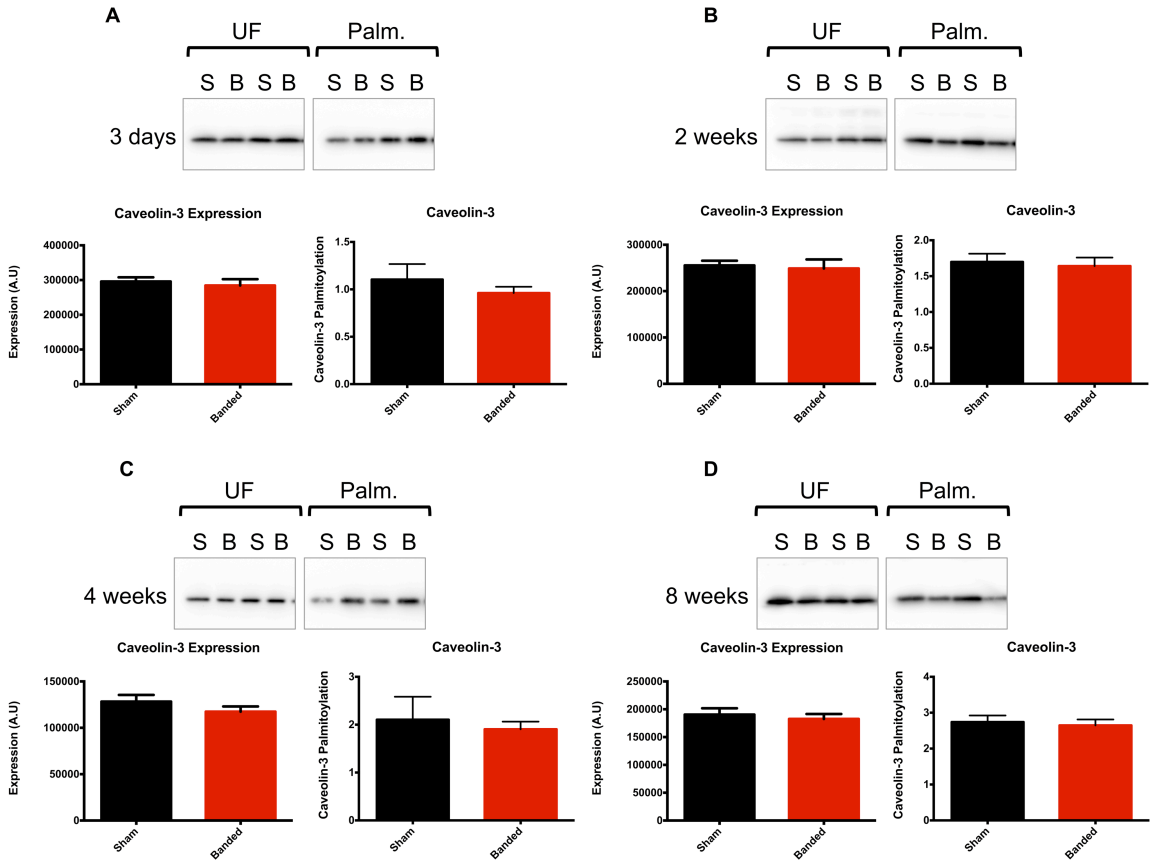


***Figure 7.7: Caveolin-3 Expression And Palmitoylation Does Not Change During Development Of Hypertrophy. A.*** *Caveolin-3 expression or palmitoylation does not change 3 days post banding.* ***B.*** *2 weeks post banding had no effect on caveolin-3 palmitoylation.* ***C.*** *4 weeks post banding had no effect on caveolin-3 palmitoylation.* ***D.*** *8 weeks post banding does not change caveolin-3 palmitoylation. UF – unfractionated, Palm. – palmitoylated, S – sham, B – banded. Graphs represent mean data ± sem.*

Shown in figure 7.7, caveolin-3 expression and palmitoylation following banding at 4 time points. At all timepoints investigated, caveolin-3 expression and palmitoylation is unchanged during left ventricular hypertrophy development. Statistical analysis of the mean data revealed that palmitoylation of caveolin-3 does not change between sham and banded samples. Based on these results, caveolin-3 palmitoylation does not significantly change in response to cardiac hypertrophy.

As described previously, normalising palmitoylation of targets to caveolin-3 can serve as an additional control to account for variability in acyl rac to capture palmitoylated proteins. Shown in figure 7.8 is mean NCX1 palmitoylation data expressed relative to palmitoylated caveolin-3. NCX1 palmitoylation is unchanged at 3 days; 2 weeks and 8 weeks post surgery. Surprisingly, expressing NCX1 palmitoylation relative to caveolin-

3 palmitoylation revealed a significant increase in NCX1 palmitoylation at 4 weeks. This indicates that the acyl rac was too variable at this time point to determine an effect of hypertrophy development on NCX1 palmitoylation. Normalising to caveolin-3 palmitoylation accounts for the variability and allows effects of hypertrophy development to be observed.

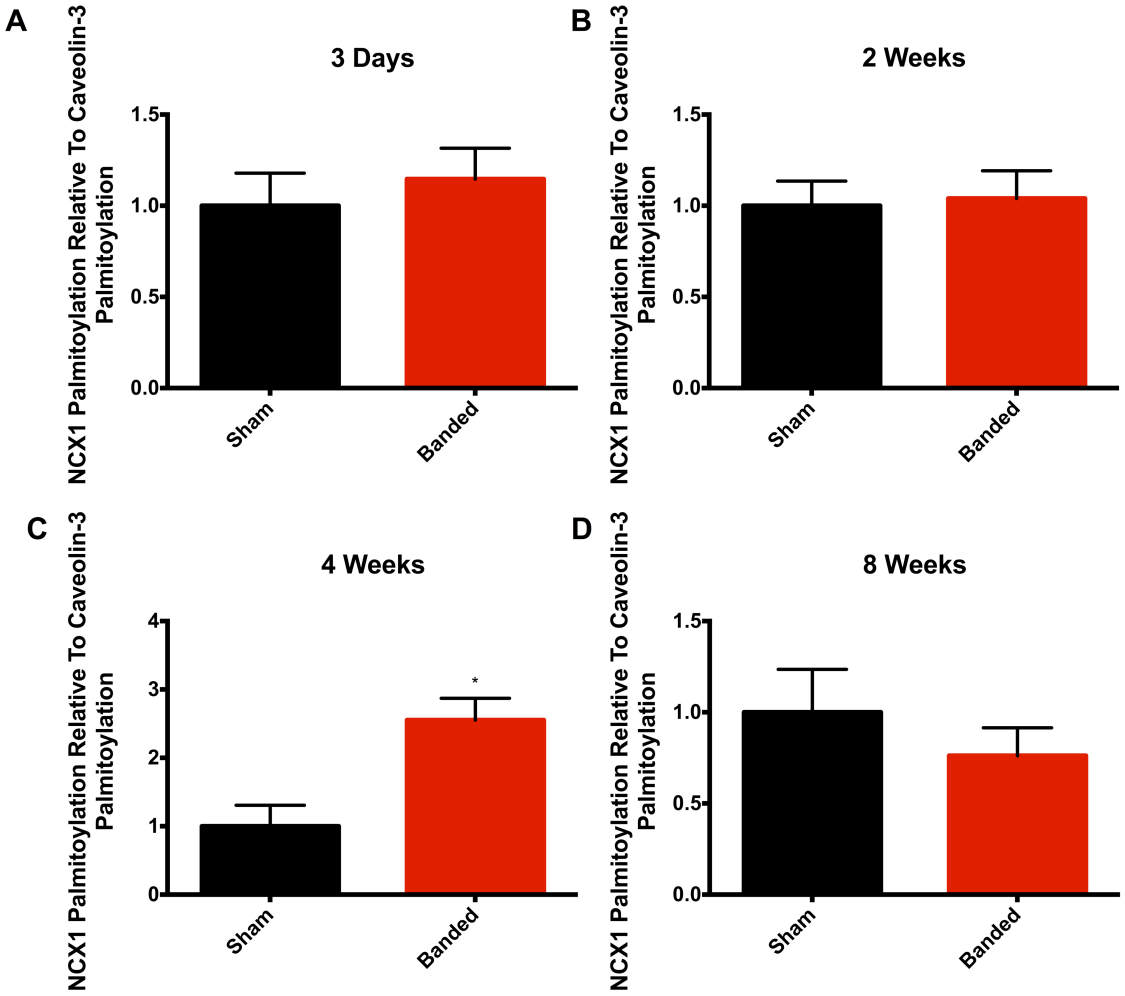


***Figure 7.8: NCX1 Palmitoylation Is Significantly Increased At 4 Weeks Post Banding Relative To Caveolin-3 Palmitoylation.*** ***A.*** *NCX1 palmitoylation is unchanged at 3 days post banding compared to sham operated animals when expressed relative to caveolin-3 palmitoylation.* ***B.*** *NCX1 palmitoylation is unchanged at 2 weeks post banding relative to caveolin-3 palmitoylation.* ***C.*** *NCX1 palmitoylation is significantly increased at 4 weeks post banding relative to caveolin-3 palmitoylation. Sham mean 1.00 ± 0.30, banded mean, 2.55 ± 0.32.* ***D.*** *NCX1 palmitoylation is unchanged at 8 weeks post banding relative to caveolin-3 palmitoylation.*

Downregulation of SERCA2a is associated with cardiac dysfunction (O'Rourke et al. 1999; Hasenfuss & Schillinger 2004). To determine whether SERCA2a expression was

downregulated in this model, heart samples from a timecourse of hypertrophy development were used to analyse expression. Shown in figure 7.9 is SERCA2a expression following banding for 3 days, 2 weeks, 4 weeks or 8 weeks. At 3 days following banding, SERCA2a expression is decreased slightly in banded heart, however this is not significantly different (panel A, figure 7.9). Following banding for 2 weeks, SERCA2a is significantly decreased in banded hearts compared to sham (panel B, figure 7.9). In some hearts examined, SERCA2a is virtually undetectable by western blotting. At 4 weeks post banding, the initial decrease in SERCA2a observed at 2 weeks is lost, with no significant difference in SERCA2a expression between sham and banded hearts (panel C, figure 7.9). By 8 weeks post banding, there is no significant difference in SERCA2a expression between sham and banded hearts, despite SERCA2a expression appearing decreased in some hearts analysed (panel D, figure 7.9). Taken together, these results suggest that SERCA2a is downregulated as early as 2 weeks following pressure overload. However this downregulation does not appear to be maintained during the development of left ventricular hypertrophy.

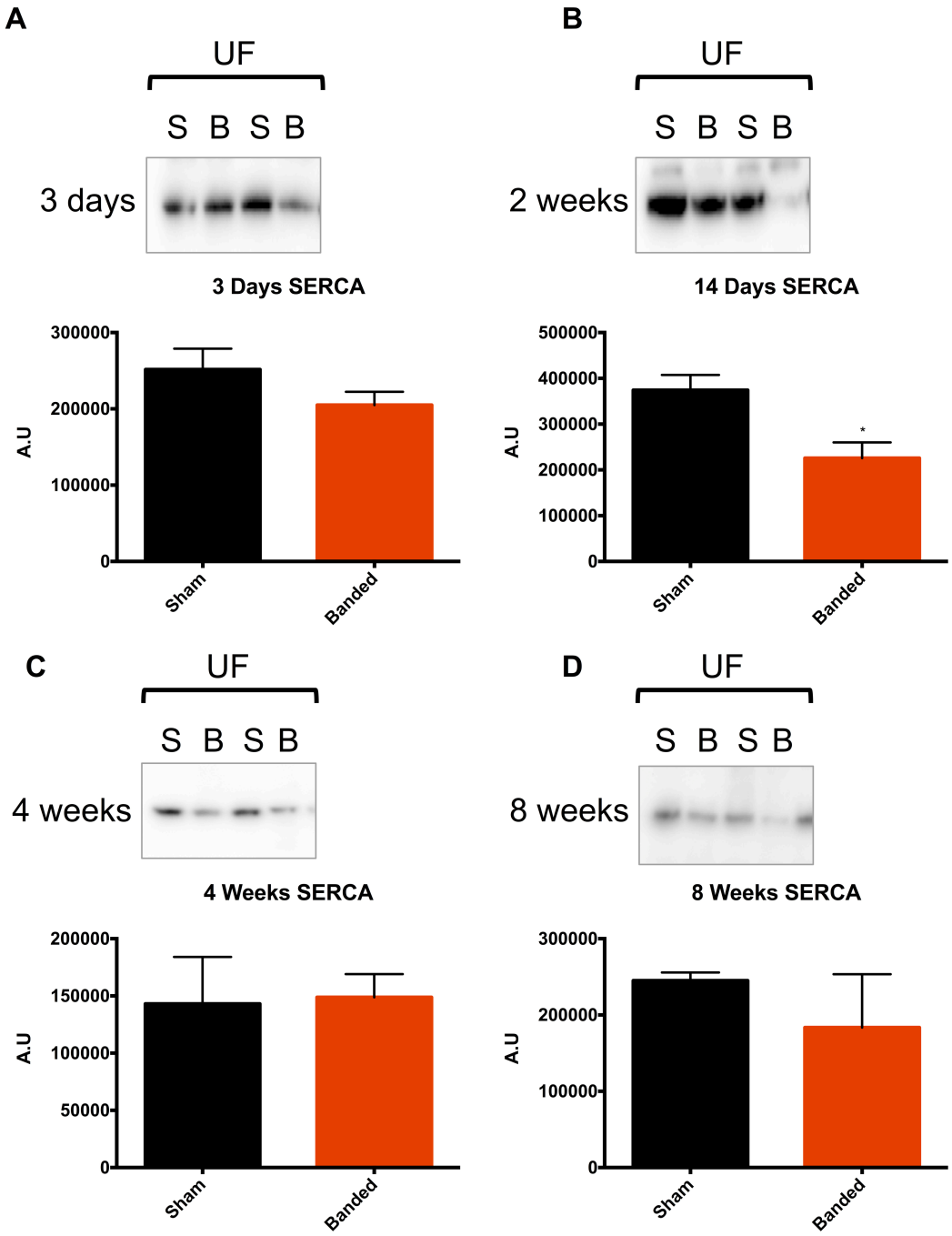


***Figure 7.9: SERCA2a Is Downregulated At 2 Weeks Post Banding In Hypertrophy.*** ***A.*** *SERCA2a is unchanged following 3 days post banding, sham mean 251561 ± 27348 n=4, banded mean 204871 ± 17447 n=4.* ***B.*** *By 2 weeks post banding, SERCA2a is significantly decreased, sham mean 374069 ± 33373 n=5, banded mean 225761 ± 34177 n=6, $p<0.05$.* ***C.*** *4 weeks post banding, SERCA2a expression is unchanged following banding, sham mean 143048 ± 41045 n=3, banded mean 148778 ± 20301 n=5.* ***D.*** *Following 8 weeks post banding, SERCA2a expression does not change, sham mean 245058 ± 10688 n=6, banded mean 183486 ± 69983 n=6.*

As discussed previously, the balance of $Ca^{2+}$ extrusion from the cytosol during diastole between SERCA2a and NCX1 is altered during cardiac hypertrophy (Boguslavskyi et al. 2014). The balance shifts towards NCX1, resulting in decreased $Ca^{2+}$ within the sarcoplasmic reticulum, leading to decreased contraction. Using the data presented previously, the ratio of SERCA2a to NCX1 was determined. Shown in panel A of figure 7.10, NCX1 expression gradually increased following banding. However this increase was not significant compared to sham operated animals. SERCA2a expression decreased significantly at 2 weeks in banded animals compared to sham operated animals (panel B, figure 7.10). In addition, the ratio of SERCA2a to NCX1 significantly decreased as early as 3 days compared to sham operated animals, and decreased further at 2 weeks (panel C, figure 7.10). This effect was then lost by 8 weeks. This suggests that in this model, the ratio of SERCA to NCX1 is shifting to favour $Ca^{2+}$ extrusion by NCX1.

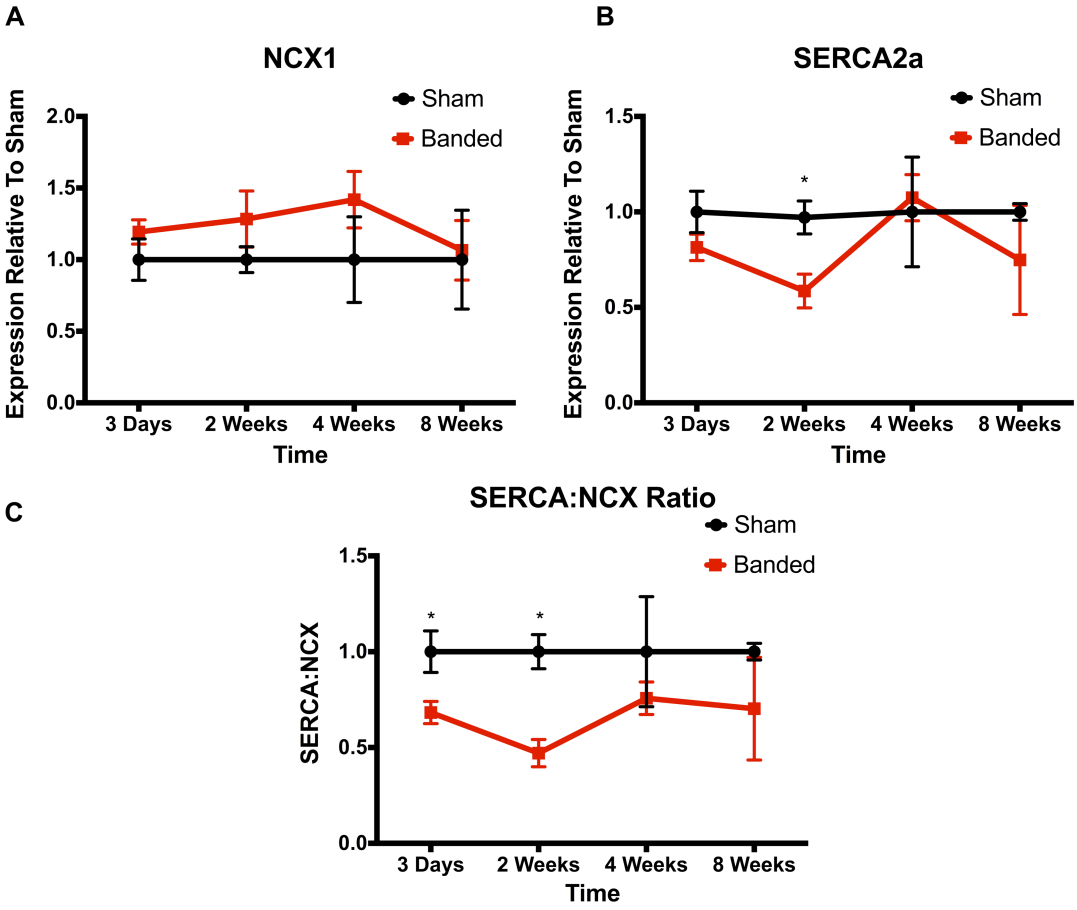


***Figure 7.10: SERCA:NCX1 Ratio Significantly Decreased By 3 Days During Development Of Left Ventricular Hypertrophy.*** ***A.*** *NCX1 expression is not significantly increased during development of left ventricular hypertrophy.* ***B.*** *SERCA2a expression is significantly decreased at 2 weeks following banding.* ***C.*** *SERCA:NCX ratio is significantly decreased by 3 days and continues to decline by 2 weeks. This effect is lost by 4 weeks.*

## 7.4 Discussion

NCX1 has a well-documented role in heart failure. NCX1 is upregulated at the mRNA and protein level in heart failure (Menick et al. 2007). Increase NCX1 activity is also associated with animal models of heart failure (Pogwizd et al. 1999; O'Rourke et al. 1999). Despite evidence for increased expression and activity, whether regulation of the exchanger is affected is relatively unexplored. One group has demonstrated an increase in NCX1 phosphorylation in failing hearts (Wei 2003), however whether NCX1 is directly phosphorylated is controversial. To date, there is no published data regarding NCX1 palmitoylation in models of heart failure. In order to determine NCX1 palmitoylation altered during cardiac dysfunction, a rat model of heart failure and a murine model of left ventricular hypertrophy were used.

### Left Ventricular Heart Failure

The first model was established in Dr Sarah Calaghan's group at University of Leeds. This is a rat model of left ventricular heart failure, induced by constricting the ascending aorta. Rats were monitored with echocardiography until ejection fraction dropped below 45%. Prior to tissue collection, LV-pressure volume relationships were measured using Millar pressure-conductance catheters. Despite echocardiography indicating that rats were in established heart failure, pressure-conductance catheters provide more sensitive measures of cardiac function. As a result, some rats that echocardiography had indicated were in heart failure, were not, and as such were excluded from analysis. This resulted in lower n numbers for comparison between groups. NCX1 palmitoylation was unchanged in this model. In addition, NCX1 expression is not upregulated as is described in many other models (Pogwizd et al. 1999; Hobai & O'Rourke 2000; Menick et al. 2007). This indicates that the model needs developed further to recapitulate all the parameters associated with heart failure. There may also be an issue with protein degradation following harvest, which would impact any results drawn from these samples. Therefore, NCX1 palmitoylation may be affected, however this experiment would need to be repeated following establishment of the model and with fresh tissue.

In addition to NCX1 palmitoylation, SERCA2a expression was examined. As previously discussed, decrease in SERCA2a expression is associated with heart failure (Hasenfuss et al. 1994; Hobai & O'Rourke 2001). SERCA2a expression was

investigated in UF lysates from acyl rac. Surprisingly, SERCA2a expression is not significantly different between sham and banded hearts. Mean data (panel B, figure 7.2) indicates a decrease in SERCA2a expression, as well as decreases in SERCA2a expression in banded samples detected by western blotting. In addition, the ratio of SERCA2a to NCX1 was unchanged in banded animals compared to sham operated, suggesting that in this model, there is not a shift to favour $Ca^{2+}$ extrusion via NCX1. The number of animals subjected to this procedure is small, with sham animals at n=4 and banded animals at n=5. To increase statistical power, increased sample number would be required. However, this is a labour-intensive and expensive experiment, with some rats taking over 25 weeks to progress to established heart failure following aortic banding.

Caveolin-3 is a scaffolding protein, integral to the formation of caveolae in cardiac myocytes. Mice lacking caveolin-3 develop progressive cardiomyopathy (Woodman et al. 2002). This phenotype is characterised by myocytes hypertrophy. Therefore, the authors argue that loss of caveolin-3 expression and cardiac myocyte caveolae is sufficient to induce activation of a hypertrophic program in cardiac myocytes (Woodman et al. 2002). In agreement with this, data from an overexpression model of caveolin-3 indicates that caveolin-3 overexpression confers protection from cardiac ischemia, similar to ischemic preconditioning (Tsutsumi et al. 2008). Using spontaneous hypertensive rat (SHR) model, Lee and colleagues demonstrated a decrease in caveolin-3 in non-exercised SHR compared to Wistar-Kyoto (WK) rats, which was increased upon exercising SHR (Y. I. Lee et al. 2006). These studies suggest that caveolin-3 is downregulated in heart disease, and when overexpressed, conveys protection against ischemic insults. In contrast, overexpression of a mutant caveolin-3 associated with autosomal dominant limb-girdle muscular dystrophy 1C (LGMD1C) results in hypertrophic cardiomyopathy and enhanced contractility (Ohsawa et al. 2003). This hypertrophic cardiomyopathy is associated with increased endothelial nitric oxide synthase activity. Feiner and colleagues show that left ventricular dysfunction in both murine models of heart failure and failing human heart is associated with a decrease in the expression of caveolin-3 (Feiner et al. 2011).

In contrast, dogs with pacing induced heart failure demonstrated increased levels of caveolin-3 (Hare et al. 2000). In agreement with these results, failing human heart obtained during placement of a left ventricular assist device showed increase caveolin-3

mRNA when compared to non-failing heart, however caveolin-3 mRNA levels increase further following left ventricular unloading (Uray et al. 2003). Although the role of caveolin-3 in heart failure is still under investigation, the role of post-translational modifications of caveolin-3 in heart failure is unexplored. Examining palmitoylation of caveolin-3 in a model of left ventricular heart failure revealed no significant difference in palmitoylation between sham operated and banded hearts. Caveolin-3 expression is consistent between sham and banded hearts in this model, resulting in comparable palmitoylation between each group. Therefore, in this model of heart failure, caveolin-3 is unchanged, which directly contrasts previous reports of increased and decreased expression. If caveolin-3 expression was increased, an increase in palmitoylation may be expected. However, the role of DHHCs in heart failure is unknown, and differential regulation of palmitoylation may determine degree of palmitoylation for different targets.

Taken together, these results suggest that this particular model needs to be further developed to establish basic changes in SERCA2a expression, which is consistent with heart failure. Increasing statistical power with more biological and technical replicates will also enable detection of changes in expression and palmitoylation of target proteins associated with heart failure.

**Cardiac Hypertrophy**

To further determine the role of palmitoylation in heart disease, palmitoylation was assessed in hearts from a mouse model of left ventricular hypertrophy. Hypertrophy was induced in these animals by pressure overload, achieved through suprarenal aortic constriction (banding) in wild-type C57BL/6J mice (Boguslavskyi et al. 2014). Reproducibility of aortic constriction was assessed post-mortem by measurement of residual luminal area (RLA) and constrictions outwith predefined limits were excluded (see supplementary material for (Boguslavskyi et al. 2014) for further explanation). Following surgery, mice were allowed to recover for 3 days, 2 weeks, 4 weeks and 8 weeks, after which heart tissue was collected, homogenised and snap frozen. Palmitoylation of NCX1 and Caveolin-3 was assessed at all time points. No significant differences in palmitoylation between sham and banded hearts were observed for either NCX1 or caveolin-3. Normalising NCX1 palmitoylation to caveolin-3 palmitoylation at 4 weeks results in a significant increase in NCX1 palmitoylation in banded animals

compared to sham operated animals. This suggests that palmitoylation may be an important post-translational modification in the regulation of NCX1 during development of hypertrophy. The increase in NCX1 palmitoylation at 4 weeks may also indicate a decrease in thioesterase activity. However, activity of thioesterase has not been measured from this model, nor the level of thioesterase present. Contrastingly, NCX1 palmitoylation does appear to be decreasing by 8 weeks, however this change was not statistically significant. Caveolin-3 palmitoylation is consistently unchanged at all time points investigated. In addition, a significant decrease in SERCA2a expression was observed at 2 weeks post-banding. However this effect was lost at 4 weeks. However, only 3 sham hearts were available for 4 week timepoint, which may explain the variability in SERCA2a expression observed. By 8 weeks, SERCA2a appears to be decreased, however this did not reach statistical significance. Significant decreases in SERCA2a expression was observed in this model previously (Boguslavskyi et al. 2014), which validates the model. The ratio of SERCA2a to NCX1 is significantly decreased in banded animals compared to sham operated animals at 3 days and 2 weeks post surgery. This suggests that changes in the balance between SERCA2a and NCX1 to remove $Ca^{2+}$ from the cytosol are altered as early as 3 days during development of hypertrophy. The samples used here have undergone freeze-thaw cycles, which may explain the lack of significant decreases in SERCA2a expression at other timepoints. The protein may have degraded through proteolysis. Therefore, to elucidate a role for palmitoylation in this model, acyl rac should be performed on freshly isolated tissue.

**Summary**

These results suggest that palmitoylation of NCX1 does not change in two clinically relevant models of chronic disease. A more in-depth study of NCX1 palmitoylation in heart disease is required. Perhaps measurement of NCX1 palmitoylation in failing human heart may give indication of the role of palmitoylation in heart failure. In agreement with data from left ventricular heart failure, caveolin-3 palmitoylation is unchanged in hypertrophy. This suggests that in these particular models, caveolin-3 palmitoylation does not contribute to cardiac remodelling. Quantitative proteomic analysis of palmitoylated proteins isolated from control and failing hearts could provide insight into whether palmitoylation does change. Given the role of palmitoylation in membrane targeting of proteins, changes in palmitoylation following cardiac remodelling may occur. However, as palmitoylation regulates protein function in a

variety of different ways depending on substrate, changes in palmitoylation may vary from target to target. This would make it difficult to make a blanket hypothesis that palmitoylation is beneficial or detrimental to heart failure progression.

# Chapter 8: Concluding Remarks And Future Work

# 8 Concluding Remarks

The aim of this work was to analyse the biochemical and functional effect of palmitoylation on the cardiac Na+/$Ca^{2+}$ exchanger (NCX1) using mass spectrometry, affinity chromatography, site-directed mutagenesis and whole cell electrophysiology.

## Key Findings

This work has identified that NCX1.1 is palmitoylated in cardiac muscle. In addition, the site of palmitoylation was identified and was shown to be within the large intracellular loop of NCX1. This domain has been documented to be involved in the regulation of NCX1 (Matsuoka & Hilgemann 1992; Hilgemann, Collins & Matsuoka 1992b; Hilgemann, Matsuoka, Nagel & Collins 1992d). Co-immunoprecipitation of the intracellular loop domain of NCX fused to YFP with DHHCs identified protein-protein interactions with DHHC5, DHHC9, DHHC12 and DHHC18. Overexpression of catalytically inactive DHHC5, DHHC9, DHHC12 and DHHC18 revealed that DHHC9 is the major protein acyl transferase that palmitoylates NCX1. DHHC9 is predominantly expressed in the Golgi apparatus (Ohno et al. 2006), suggesting that NCX1 palmitoylation occurs within the secretory pathway. Finally, genetic ablation of NCX1 palmitoylation results in decreased outward current, indicated by I-V relationship analysis using whole-cell electrophysiology.

## Palmitoylation Site Conservation In $Na^{+}$-$Ca^{2+}$ Family

NCX1 is a member of the $Ca^{2+}$-cation exchanger superfamily, characterised by presence of α-repeats in hydrophobic domains separated by a hydrophilic loop (Philipson & Nicoll 2000). The $Na^{+}$-$Ca^{2+}$ exchanger family shares a large amount of sequence homology (figure 8.1), particularly in the transmembrane domains. In addition to the $Na^{+}$-$Ca^{2+}$ exchanger family, another family also part of the superfamily is $Na^{+}$-$Ca^{2+}$-$K^{+}$ exchangers. These exchangers share homology within their transmembrane domains and also contain α-repeats (Philipson & Nicoll 2000), however there is little sequence similarity between NCX and NCKX exchanger families within their N-terminal and cytoplasmic loop domains. Alignment of NCX1, NCX2, NCX3 and NCKX1 reveals that the palmitoylation site is conserved in NCX family members (figure 8.1, red box), but not other $Ca^{2+}$-cation family members.

**A**

```
NKC1, human          [Na/Ca/K family] EEEEEEEEEKG-NEEP---------LSLDWPETRQK------------------------
CAX1, Arabadopsis    [H/Ca family]    YDDDVEQ-ETA-------------------------------------------------
NKC6, human          [CCX family]     PEILSDSEEDRVSSNTNSYDYGDEYRPLFFYQETTAQILVRALNPLDYMKWRRKSAYWK-
YrbG, E. coli        [YRBG family]    ------------------------------------------------------------
NCX1, human          [NCX family]     AGEDDDDDECGEEKLPSCFDYVMHFLTVFW------KVL---------FAFVPPTEYWNG
```

**B**

```
gi|6492237|gb|AAF14229.1|AF109178_1|magnesium/proton exchanger|AtMHX[Arabidopsis thaliana]LRIAKSFWHLLLAPWKLLFAFVPPCNIAHGWIAFICSLLFISGVAFVVTRFTDLISCVTG 398
gi|392900568|ref|NP_501984.2|Protein NCX-3 [Caenorhabditis elegans]                        ATVSDCILHALAFPWKFAFAFLPPPTIFYGYPCFVVALIGIGLVTAVVGDVASIFGCMVG 686
gi|115533320|ref|NP_001041182.1|Protein NCX-1,isoform a [Caenorhabditis elegans]          VTTMEKVMHYIALPWKLLFALIPPTDYFNGWLCFVVAIAMIGLLTAFIGDIAAAFGCTVG 736
gi|71983528|ref|NP_504414.4|Protein NCX-2,isoform a [Caenorhabditis elegans]              PGCMDYVMHVLTVPWKLTFATIPPTDYFGGWATFVVAIFMIGVLTAVVGDLASQFGCWVG 832
gi|2266953|gb|AAB63464.1|CALX [Drosophila melanogaster]                                   PSCFSYVSHFVCLFWKVLFAFVPPTDICGGYVTFVVSIFVIGVITAIIGDAASYFGCALN 807
gi|1947092|gb|AAB52920.1|Na/Ca exchanger [Doryteuthis opalescens]                         PSCMDYIMHFVCLFWKVLFAFVPPTDYWGGWACFTVSIILIGVLTAFIGDLATYFGCTIG 749
gi|57163987|ref|NP_055878.1|sodium/calcium exchanger 2 precursor [Homo sapiens]          PSCFDYVMHFLTVFWKVLFACVPPTEYCHGWACFGVSILVIGLLTALIGDLASHFGCTVG 778
gi|17530967|ref|NP_511174.1|sodium/calcium exchanger 2 precursor [Rattus norvegicus]     PSCFDYVMHFLTVFWKVLFACLPPTEYCHGWACFGVCILVIGLLTALIGDLASHFGCTVG 778
gi|530404521|ref|XP_005268074.1|sodium/calcium exchanger 3 isoform X1 [Homo sapiens]     PSCFDYVMHFLTVFWKVLFACVPPTEYCHGWACFAVSILIIGMLTAIIGDLASHFGCTIG 785
gi|30851385|gb|AAH52435.1|sodium/calcium exchanger 3 [Mus musculus]                       PSCFDYVMHFLTVFWKVLFACVPPTEYCHGWACFVVSILIIGMLTAIIGDLASHFGCTIG 778
gi|17530969|ref|NP_511175.1|sodium/calcium exchanger 3 [Rattus norvegicus]               PSCFDYVMHFLTVFWKVLFACVPPTEYCHGWACFVVSILIIGMLTAIIGDLASHFGCTIG 784
gi|6755564|ref|NP_035536.1|sodium/calcium exchanger, member1 [Mus musculus]              PSCFDYVMHFLTVFWKVLFAFVPPTEYWNGWACFIVSILMIGLLTAFIGDLASHFGCTIG 827
gi|1346652|sp|Q01728.3|Sodium/calcium exchanger 1 [Rattus norvegicus]                     PSCFDYVMHFLTVFWKVLFAFVPPTEYWNGWACFIVSILMIGLLTAFIGDLASHFGCTIG 828
gi|1346649|sp|P48766.1|Sodium/calcium exchanger 1 [Cavia porcellus]                       PSCFDYVMHFLTVFWKVLFAFVPPTEYWNGWACFIVSILMIGLLTAFIGDLASHFGCTIG 827
gi|28603740|ref|NP_788805.1|sodium / calcium exchanger 1 [Bos taurus]                    PSCFDYVMHFLTVFWKVLFAFVPPTEYWNGWACFIVSILMIGLLTAFIGDLASHFACTIA 827
gi|10863913|ref|NP_066920.1|sodium / calcium exchanger 1 [Homo sapiens]                  PSCFDYVMHFLTVFWKVLFAFVPPTEYWNGWACFIVSILMIGLLTAFIGDLASHFGCTIG 830
gi|127793|sp|P23685.1|Sodium/calcium exchanger 1 [Canis lupus familiaris]                PSCFDYVMHFLTVFWKVLFAFVPPTEYWNGWACFIVSILMIGILTAFIGDLASHFGCTIG 827
gi|1346650|sp|P48767.1|Sodium/calcium exchanger 1 [Felis catus]                          PSCFDYVMHFLTVFWKVLFAFVPPTEYWNGWACFIVSILMIGILTAFIGDLASHFGCTIG 827
gi|1279782|gb|AAA97928.1|Na/Ca exchanger [Oryctolagus cuniculus]                         PSCFDYVMHFLTVFWKVLFAFVPPTEYWNGWACFIVSILMIGLLTAFIGDLASHFGCTIG 798
gi|4140706|gb|AAD04173.1|sodium-calcium exchanger isoform NCX1.3 [Macaca mulatta]        PSCFDYVMHFLTVFWKVLFAFVPPTEYWNGWACFIVSILMIGLLTAFIGDLASHFGCTIG 791
gi|62637560|gb|AAP37041.2|sodium calcium exchanger [Oreochromis mossambicus]            PSCFDYVMHFLTIFWKLLFAFVPPTDYWNGWACFVVSITVIGMLTAVIGDLASHFGCTVG 814
gi|6273849|gb|AAF06363.1|cardiac sodium-calcium exchanger [Oncorhynchus mykiss]          PSCFDYVMHFLTVFWKLLFAFVPPTDYWNGWACFVVSISMIGLLTAFIGDLASHFGCTVG 825
```

***Figure 8.1: Clustal Alignment Of Exchanger Superfamily Members.*** ***A.*** *Clustal alignment of representative members of $Ca^{2+}$-cation superfamily. Only NCX1 family members have palmitoylation site.* ***B.*** *Clustal alignment of NCX family members. Only NCX in Drosophila melanogaster and above have palmitoylation site (highlighted by red box). Aligned using Clustal Omega.*

Additionally, an NCX1 orthologue from *Drosophila Melanogaster*, Calx was also aligned with NCX and NCKX family members. NCX proteins expressed in *Drosophila Melanogaster* and higher organisms show conservation of the palmitoylated cysteine residue (figure 8.1, red box), as *C.elegans* NCX1 and NCX2 isoforms and *Arabidopsis thaliana* do not have this cysteine residue. The conservation of the cysteine suggests that palmitoylation is an important post-translational modification in the regulation of NCX family members. Previous data presented in this thesis (Chapter 3 results) revealed that the palmitoylated cysteine is conserved within splice variants of NCX1, which are also palmitoylated. Functional analysis of NCX1, NCX2 and NCX3 did not reveal major differences (Linck et al. 1998). NCX1 is regulated by $Ca^{2+}$ (Hilgemann, Collins & Matsuoka 1992b), increases in intracellular $Ca^{2+}$ results in activation of NCX1. Calx shares 49% amino acid homology with NCX1. In addition, Calx show similar $Na^{+}$-dependent inactivation, current-voltage relationships and regulation by the peptide XIP (Hryshko et al. 1996) and like NCX1, Calx is regulated by $Ca^{2+}$. In contrast to NCX proteins, cytoplasmic $Ca^{2+}$ in the micromolar range inhibits Calx. Chimeric transfer of CBD1 from NCX1 to Calx results in $Ca^{2+}$ stimulation of Calx (Dyck et al. 1998). It is possible that the conserved palmitoylation site of NCX and Calx may play a role in $Ca^{2+}$ regulation as NCKX proteins do not possess this conserved palmitoylation residue (figure 8.1). Palmitoylation may influence the electrostatic mechanism that regulates $Ca^{2+}$ binding to CBDs within the intracellular loop domain as discussed previously. Whether palmitoylation influences $Ca^{2+}$ regulation of NCX1 remains to be determined experimentally.

**TMD Tilting Of NCX1**

The crystal structure of NCX_Mj, a prokaryotic NCX1 homolog, revealed that TMD6 is significantly longer than other TMDs within NCX1 (Liao et al. 2012). As a result, this TMD is modelled to be at a 45° angle to the membrane. TMD6 is proposed to move significantly during the conformation change from outward-facing to inward-face conformations (figure 8.2). In the outward-facing conformation, TMD6 is parallel to the rest of the molecule, allowing access to the ion binding sites. However in the inward-facing conformation, TMD6 moves to occlude the ion binding sites on the extracellular side (Liao et al. 2012). Movements of TMD6 is hinged at bends between TMD2A and 2B and TMD7A and TMD7B and may involve sliding across a central flat hydrophobic patch that is centred around conserved proline residues from the α-repeats (Liao et al.

2012). C739 is located upstream of TMD6, within the large intracellular loop. It is possible that the addition of palmitate at this position would serve as an additional membrane anchor, and influence titling of the transmembrane domain (Nyholm et al. 2007; Shipston 2014). Such an addition at this site would also confer conformational constraints on the protein. Indeed, this precise mechanism has been proposed to control ER exit of the regulatory β4 subunits of BK channels (Chen et al. 2013). Depalmitoylation of a cysteine residue located near TMD2 may result in hydrophobic mismatch at the ER, resulting in reduced ER exit and may also yield a conformation that is not favourable for interaction with BK channel α subunits and thus decreasing BK channel α subunits cell surface expression (Chen et al. 2013). It has been proposed that palmitoylation may result in structural rearrangement. Evidence from the BK channel also supports this hypothesis. The large C-terminal domain of the BK channel is cytosolic, which is palmitoylated (Tian et al. 2008). Palmitoylation of this domain results in association with the membrane, however in the absence of palmitoylation, this domain remains cytosolic. Palmitoylation in this region is thought to cause a structural rearrangement of the channel, impacting its activity. Upstream of the palmitoylated cysteine residues is a polybasic domain. Mutation of this domain results in inhibition of palmitoylation and a right-shift in channel half-maximal voltage for activation (Jeffries et al. 2012). PKA-dependent phosphorylation of a single serine residue within the polybasic region results in channel inhibition and reduced palmitoylation. This data suggests that the polybasic region in control palmitoylation of the cytosolic domain and that phosphorylation of this region acts as an electrostatic switch (Jeffries et al. 2012). Therefore it appears that palmitoylation can alter conformation of ion channels, thus resulting in regulation of their activity.

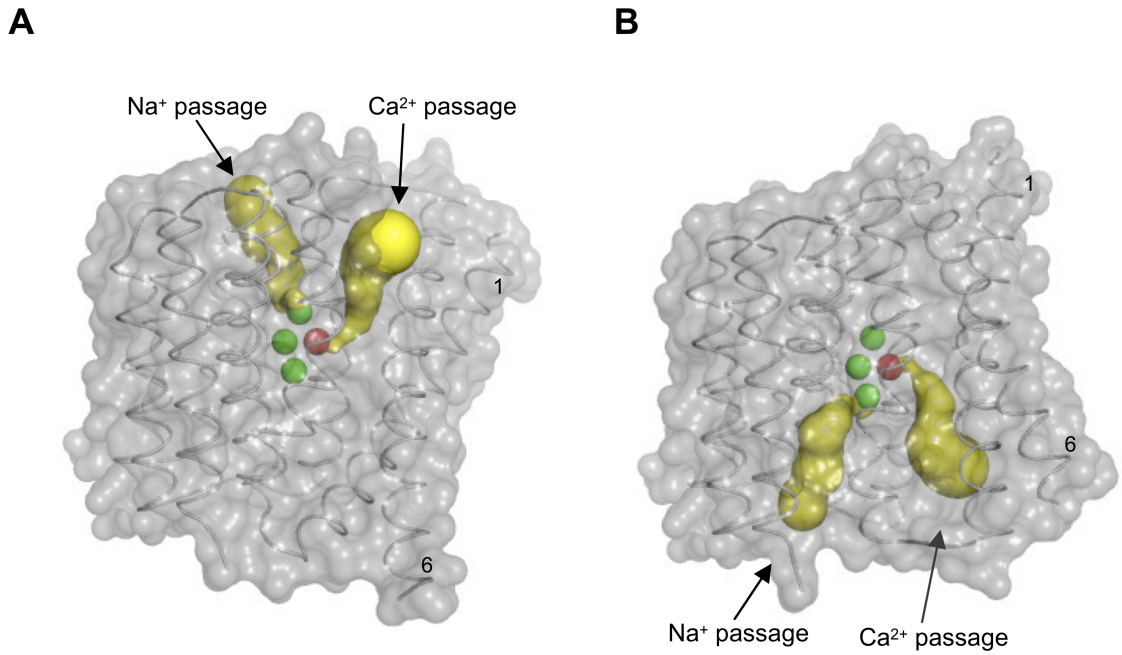


***Figure 8.2: TMD6 Moves Considerably During NCX1 Transport. A.*** *Surface rendered structure of NCX1 in the outward-facing conformation. TMD6 is parallel to the ion permeation pathway, whereas TMD1 is tilted at a 45° angle.* ***B.*** *Surface rendered structure of NCX1 in the inward-facing conformation. TMD6 is now at a 45° angle to the ion permeation pathway, occluding the outward-facing binding sites. Modified from (Liao et al. 2012).*

Although the recent crystal structure of NCX_Mj provides structural insight into TMDs of NCX, insight into the regulatory intracellular loop domain is lacking as NCX_Mj does not contain this domain. This suggests that NCX1 and NCX_Mj must be regulated through different mechanisms. Recently, evidence that NCX_Mj transports $Ca^{2+}$ slower than its mammalian counterpart was published (Almagor et al. 2014). The authors suggest that the large intracellular loop controls the intrinsic equilibrium and rates of bidirectional $Ca^{2+}$ in NCX proteins. NCX_Mj does not have a regulatory domain like the mammalian NCX proteins, meaning that 6 of the cysteine residues predicted to lie within this domain are not represented in this structural homolog. It may be that palmitoylation is involved in stabilising the outward-facing (extracellular) access, given that $Ca^{2+}$ movement from the cytosol to the extracellular side is faster than the opposite direction (Almagor et al. 2014) in NCX_Mj chimeras possessing the intracellular loop domain. During the exchange cycle, NCX1 undergoes significant conformation changes (Liao et al. 2012). TMD6 moves significantly during this cycle. Inhibition of

palmitoylation may result in this domain being less anchored and more flexible. This may result in less ordered movements of TMD6 during the exchange cycle, potentially impacting the efficiency of this cycle.

**Thioesterase Activity Mediating NCX1 Palmitoylation**

Overexpression of DHHCs results in decreased NCX1 palmitoylation. This suggests that in the presence of increased DHHC expression, depalmitoylation of NCX1 is increased. Protein depalmitoylation is predominantly mediated by acyl thioesterases, which belong to the serine hydrolase superfamily (Zeidman et al. 2009; Bachovchin et al. 2010). However the thioesterase responsible for the depalmitoylation of NCX1 has not been identified to date. The extent to which serine hydrolases exhibit thioesterase activity towards different ion channels and transporters is unknown (Shipston 2014). Control of depalmitoylation of proteins is largely affected by a family of cytosolic thioesterases, which includes APT1 (Yeh et al. 1999; Devedjiev et al. 2000) and APT2 (Tomatis et al. 2010). APT1 and APT2 do show selectivity for different palmitoylated peptides (Tomatis et al. 2010). The depalmitoylation of the S0-S1 loop of BK channels is mediated by APT1 but not APT2 (Tian et al. 2012). Depalmitoylation of BK channels results in Golgi retention, which may indicate that reversible palmitoylation provides a checkpoint to regulate exit from the Golgi, thus controlling cell surface expression (Tian et al. 2012). However, mechanisms that determine whether proteins are depalmitoylated remain to be determined. Regulation of thioesterases themselves by palmitoylation is important for their association with membranes (Kong et al. 2013; Vartak et al. 2014). Additionally, APTs have been described to regulate the spatial organisation of palmitoylated membrane proteins (Vartak et al. 2014). Depalmitoylated APTs were found to be soluble and depalmitoylated substrates on all membranes. Palmitoylated APTs localise to the Golgi, which serves as a homeostatic regulatory mechanism that ensures partitioning of APT substrates between the plasma membrane and the Golgi (Vartak et al. 2014). The depalmitoylating activity of APTs serves as a release factor for mislocalised palmitoylated proteins. It is possible that APTs regulate the spatial organisation of NCX1 within the cell surface membrane. Furthermore, lysosomal degradation of protein often results in their depalmitoylation mediated by PPT1 (Verkruyse & Hofmann 1996). In the absence of PPT1, total expression and surface membrane abundance of GluA4 AMPA receptor subunit was decreased, but no effect

was observed on GluA1 or GluA2 AMPA subunits or NMDA receptor subunits (Finn et al. 2011). For the majority of ion transporters and channels, the wherebouts depalmitoylation occurs within the cell and the time course of palmitoylation-depalmitoylation cycles is unknown (Shipston 2014). Whether depalmitoylation of NCX1 plays a role in the regulation of its activity or spatial organisation remains to be determined.

**Site-Recognition By DHHCs**

Overexpression of catalytically inactive DHHCs (Mitchell et al. 2006) revealed that DHHC9 is responsible for palmitoylation of NCX1 (Chapter 5 results). To date, no consensus sequence has been identified for palmitoylation (Salaun et al. 2010). Palmitoylation prediction algorithms are being constantly developed to aid in the identification of palmitoylation sites. Using PalmPred (Kumari et al. 2014), a recently developed palmitoylation prediction algorithm, palmitoylation sites of specific proteins can be identified. Indeed, PalmPred correctly identifies C739 as the NCX1 palmitoylation site. Examining other known DHHC9 substrates can generate insight into potential sequence features that may be involved in directing the DHHC to the appropriate site. As a result of clustal alignment, it was revealed that DHHC9 substrates have a proline residue at the -2 position relative to the target cysteine residue (Chapter 5, discussion). Performing *in silico* mutation of the proline residue results in loss of the palmitoylation predicition by PalmPred (Figure 8.3). Panel A of figure 8.3 shows WT human NCX1. The prediction algorithm correctly predicts Cys739 (note: analysis run without removal of signal peptide, so numbering is +35 to account for signal peptide) as palmitoylated. However, shown in panel B of figure 8.3, changing the proline at the – 2 position results in loss of the palmitoylation prediction of Cys739. This suggests that the sequence surrounding the target cysteine may be important for its palmitoylation. In addition, the proline residue at the -2 position is highly conserved among $Na^+$-$Ca^{2+}$ exchanger family members, even in NCKX1, which does not possess the palmitoylation site (figure 8.1). This suggests that this proline may not only be important for palmitoylation but for overall function of these proteins. DHHC9 substrates share a large amount of homology with NCX1 upstream of the palmitoylation site, suggesting that areas outwith this region may confer substrate specificity for DHHC9.

**A**

| Protein | Cys-Peptide | Cys-Position | Prediction |
|---|---|---|---|
| seq | NETGECTGSYY | 49 | Non-Palmitoyl |
| seq | TGSYYCKKGVI | 55 | Non-Palmitoyl |
| seq | SVIEVCGHNFT | 157 | Non-Palmitoyl |
| seq | IIIALCVYVVP | 186 | Non-Palmitoyl |
| seq | FFFPICVVFAW | 245 | Non-Palmitoyl |
| seq | QGTYQCLENCG | 418 | Non-Palmitoyl |
| seq | QCLENCGTVAL | 422 | Non-Palmitoyl |
| seq | VSTLACLGSPS | 520 | Non-Palmitoyl |
| seq | DFEDTCGELEF | 592 | Non-Palmitoyl |
| seq | DDDDECGEEKL | 765 | Non-Palmitoyl |
| seq | EKLPSCFDYVM | 773 | Palmitoyl |
| seq | WNGWACFIVSI | 803 | Non-Palmitoyl |
| seq | ASHFGCTIGLK | 827 | Non-Palmitoyl |
| seq | KLLTSCLFVLL | 949 | Non-Palmitoyl |
| seq | SLEAYCHIKGF | 968 | Non-Palmitoyl |

Any 'X' in Peptide is only to complete the window, it does not represent an amino acid residue

**B**

| Protein | Cys-Peptide | Cys-Position | Prediction |
|---|---|---|---|
| seq | NETGECTGSYY | 49 | Non-Palmitoyl |
| seq | TGSYYCKKGVI | 55 | Non-Palmitoyl |
| seq | SVIEVCGHNFT | 157 | Non-Palmitoyl |
| seq | IIIALCVYVVP | 186 | Non-Palmitoyl |
| seq | FFFPICVVFAW | 245 | Non-Palmitoyl |
| seq | QGTYQCLENCG | 418 | Non-Palmitoyl |
| seq | QCLENCGTVAL | 422 | Non-Palmitoyl |
| seq | VSTLACLGSPS | 520 | Non-Palmitoyl |
| seq | DFEDTCGELEF | 592 | Non-Palmitoyl |
| seq | DDDDECGEEKL | 765 | Non-Palmitoyl |
| seq | EKLASCFDYVM | 773 | Non-Palmitoyl |
| seq | WNGWACFIVSI | 803 | Non-Palmitoyl |
| seq | ASHFGCTIGLK | 827 | Non-Palmitoyl |
| seq | KLLTSCLFVLL | 949 | Non-Palmitoyl |
| seq | SLEAYCHIKGF | 968 | Non-Palmitoyl |

Any 'X' in Peptide is only to complete the window, it does not represent an amino acid residue

***Figure 8.3: In Silico Mutagenesis Of Proline At Position 737 (771) to Alanine Results In Loss Of Palmitoylation Prediction.*** ***A.*** *PalmPred predicts Cys739 is palmitoylated in WT NCX1.* ***B.*** *In silico mutagenesis reveals that proline at position 737 may be important for palmitoylation of NCX1, as palmitoylation prediction is lost when mutated to alanine.*

### NCX1 Palmitoylation And Cardiovascular Disease

As previously discussed, during development of cardiac dysfunction as a result of heart failure or cardiac hypertrophy, the balance of $Ca^{2+}$ extrusion from the cytosol during diastole shifts to favour extrusion by NCX1. This can also be accompanied by an increase in NCX1 expression. As NCX1 is electrogenic, increased outward mode

exchange during diastole can result in arrhythmogenic delayed afterdepolarisations (Voigt et al. 2012; Venetucci et al. 2007). In ischemia reperfusion, outward mode exchange is responsible for $Ca^{2+}$ overload and ultimately necrotic cell death (Ohtsuka et al. 2004). Shown in this thesis, outward mode of NCX1 is decreased in the absence of palmitoylation. As palmitoylation of NCX1 most likely occurs in the Golgi, changes within NCX1 palmitoylation would be expected to occur over a longer time scale, such as in the case of hypertrophic remodelling. However, as $Ca^{2+}$ overload is caused by NCX1 outward mode, targeting this mode of NCX1 could be a potential therapeutic target for ischemia reperfusion. Altering NCX1 exchange has been demonstrated previously to be associated with less ischemia damage (Sipido et al. 2002; Hobai et al. 2004). As outward mode appears to be enhanced by palmitoylation, selectively targeting NCX1 palmitoylation may serve as a potentially promising therapeutic target for ischemia reperfusion. NCX1 palmitoylation may increase during ischemia reperfusion, which may lead to a stabilisation of the outward mode, thus leading to greater $Ca^{2+}$ influx into the cell and perpetuating $Ca^{2+}$ overload and eventually cell death. However, further work is required to determine the role of NCX1 palmitoylation in ischemia reperfusion, and indeed cardiac dysfunction in general.

**Conclusions And Future Work**

The work presented in this thesis demonstrated that palmitoylation is important in the regulation of NCX1 activity. Although NCX1 shows a decrease in outward current of C739A NCX1 compared to WT NCX1, whether $Ca^{2+}$ sensitivity or $Na^{+}$-dependent inactivation is affected is unknown. Further electrophysiological studies are required to determine whether non-palmitoylatable NCX1 has altered $Ca^{2+}$ sensitivity. Using excised patch or pipette-perfusion techniques would allow for a throughout assessment of $Ca^{2+}$ sensitivity (Hilgemann, Collins & Matsuoka 1992b). Using this technique would also allow investigation of the effect of palmitoylation on $Na^{+}$-dependent inactivation modulation by cytoplasmic Ca2+. Furthermore, $PIP_2$ has previously been reported to regulate NCX1 activity (Hilgemann 2007). NCX1 has previously been described to be within close proximity of $PIP_2$ within the membrane (Ottolia et al. 2006). Palmitoylation may influence the interaction between $PIP_2$ or subcellular localisation of NCX1 relative to $PIP_2$.

Although palmitoylation did not control membrane localisation or caveolar localisation of NCX1, the mechanism targeting of proteins to t-tubular domains present within cardiac myocytes is unknown. Direct imaging of palmitoylated NCX1 would be required to determine whether this influences its localisation to t-tubular membranes. Furthermore, viral infection of cardiac myocytes with C739A NCX1 or a knock-in mouse possessing the same mutation may also provide insight into membrane targeting of NCX1. Generation of a cardiac specific NCX1 knockout resulted only a mild phenotype (Henderson et al. 2004). Mice show decreased contractility by 7.5 weeks of age. However no adaptation of the myocardium was detected. In addition, L-type $Ca^{2+}$ channel current is decreased by 50%, with the number of channels unchanged (Henderson et al. 2004). Cardiac-specific ablation of NCX1 confers protection against ischemia/reperfusion injury (Imahashi et al. 2005). Therefore, it appears that NCX1 contributes significantly to ischemic injury during reperfusion. Generation of a knock-in C739A NCX1 expressing mouse would provide insight into whether palmitoylation has an observable effect of NCX1 function within cardiac muscle or contributes to NCX-mediated pathologies in other tissues. NCX1 palmitoylation stoichiometry is higher in myocytes than in HEK293 cells (chapter 4). Reducing palmitoylation from 60% to 0% rather than 30% to 0% would likely result in a greater observable difference in NCX1 activity in the absence of palmitoylation compared to wild-type.

Finally, as discussed previously, regions outwith the target cysteine residues of substrates may be important for directing DHHCs. Extensive mutational analysis of regions within the intracellular loop region that are conserved between NCX1 and other known DHHC9 substrates would elucidate which regions are important for DHHC9:NCX1 interactions. Additionally, mutational analysis of DHHC9 could also provide insight into functional domains important for substrate interaction. Recently, a similar study was conducted for DHHC5 and its interaction with phospholemman (Howie et al. 2014). It is clear more work is required to build upon the results presented here on the regulation of NCX1 by palmitoylation.

# Chapter 9: References

## 9 References

Achour, L. et al., 2011. Using Quantitative BRET to Assess G Protein-Coupled Receptor Homo- and Heterodimerization. *Methods In Molecular Biology*, 756, pp.183–200.

Alexander, J.K. et al., 2009. Palmitoylation of Nicotinic Acetylcholine Receptors. *Journal of Molecular Neuroscience*, 40(1-2), pp.12–20.

Almagor, L. et al., 2014. Functional Asymmetry of Bidirectional Ca2+-Movements in an Archaeal Na+-Ca2+ Exchanger (NCX_Mj). *Cell Ca2+*, pp.1–24.

Ander, B. et al., 2007. Differential sensitivities of the NCX1.1 and NCX1.3 isoforms of the Na+–Ca2+ exchanger to α-linolenic acid. *Cardiovascular Research*, 73(2), pp.395–403.

Apolloni, A. et al., 2000. H-ras but Not K-ras Traffics to the Plasma Membrane through the Exocytic Pathway. *Molecular and Cellular Biology,* 20(7), pp.1–13.

Bachovchin, D.A. et al., 2010. Superfamily-wide portrait of serine hydrolase inhibition achieved by library-versus-library screening. *PNAS*, pp.20941–20946.

Baker, P.F. et al., 1969. The Influence Of Ca2+ On Na+ Efflux In Squid Axons. *Journal of Physiology*, 200, pp.431–458.

Baker, T.L. et al., 2003. Distinct Rates of Palmitate Turnover on Membrane-bound Cellular and Oncogenic H-Ras. *Journal of Biological Chemistry*, 278(21), pp.19292–19300.

Balijepalli, R.C. & Kamp, T.J., 2008. Caveolae, ion channels and cardiac arrhythmias. *Progress in Biophysics & Molecular Biology*, 98(2-3), pp.149–160.

Barr, F.A. et al., 1997. GRASP65, a Protein Involved in the Stacking of Golgi Cisternae. *Cell*, 91, pp.253–262.

Bartels, D.J. et al., 1999. Erf2, a novel gene product that affects the localization and palmitoylation of Ras2 in Saccharomyces cerevisiae. *Molecular and Cellular Biology*, 19(10), pp.6775–6787.

Bennion, B.J. & Daggett, V., 2003. The molecular basis for the chemical denaturation of proteins by urea. *PNAS*, 100(9), pp.5142–5147.

Bers, D.M., 2002. Cardiac excitation-contraction coupling. *Nature*, 415, pp.198–205.

Besserer, G.M. et al., 2007. The second Ca2+-binding domain of the Na+/Ca2+ exchanger is essential for regulation: crystal structures and mutational analysis. *PNAS*, 104(47), pp.18467–18472.

Bhuyan, A.K., 2010. On the mechanism of SDS-induced protein denaturation. *Biopolymers*, 93(2), pp.186–199.

Bijlmakers, M. & Marsh, M., 2003. The on–off story of protein palmitoylation. *Trends*

*in Cell Biology*, 13(1), pp.32–42.

Blaskovic, S. et al., 2014. Chemistry and Physics of Lipids. *Chemistry and Physics of Lipids*, 180, pp.44–52.

Blaskovic, S., Blanc, M. & van der Goot, F.G., 2013. What does S-palmitoylation do to membrane proteins? *FEBS Journal*, 280(12), pp.2766–2774.

Blaustein, M.P. & Christie Ector, A., 1976. Carrier-mediated Na+-dependent and Ca2+-dependent Ca2+ efflux from pinched-off presynaptic nerve terminals (synaptosomes) in vitro. *Biochimica et Biophysica Acta (BBA) - Biomembranes*, 419(2), pp.295–308.

Blaustein, M.P. & Lederer, W.J., 1999. Na+/Ca2+ Exchange: Its Physiological Implications. *Physiological Reviews*, 79(3), pp.763–854.

Blaustein, M.P. & Santiago, E.M., 1977. Effects of internal and external cations and of ATP on Na+-Ca2+ and Ca2+-Ca2+ exchange in squid axons. *Biophysical Journal*, 20(1), pp.79–111.

Boguslavskyi, A. et al., 2014. Cardiac hypertrophy in mice expressing unphosphorylatable phospholemman. *Cardiovascular Research*, 104(1), pp.72–82.

Bossuyt, J. et al., 2002. Evidence for cardiac Na+–Ca2+ exchanger association with caveolin-3. *FEBS Letters*, 511, pp.113–117.

Brette, F. & Orchard, C.H., 2003. T-Tubule Function in Mammalian Cardiac Myocytes. *Circulation Research*, 92(11), pp.1182–1192.

Brown, D.A., 2006. Lipid Rafts, Detergent-Resistant Membranes, and Raft Targeting Signals. *Physiology*, 21(6), pp.430–439.

Camors, E. et al., 2006. Association of annexin A5 with Na+/Ca2+ exchanger and caveolin-3 in non-failing and failing human heart. *Journal of Molecular and Cellular Cardiology*, 40(1), pp.47–55.

Camp, L.A. & Hofmann, S.L., 1993. Properties of a Palmitoyl-Protein Thioesterase That Cleaves Palmitate From H-Ras. *Journal of Biological Chemistry*, 268(30), pp.22566–22574.

Cavalli, A. et al., 2007. Localization of sarcolemmal proteins to lipid rafts in the myocardium. *Cell Ca2+*, 42(3), pp.313–322.

Chen, L. et al., 2013. Palmitoylation of the  4-subunit regulates surface expression of large conductance Ca2+-activated potassium channel splice variants. *Journal of Biological Chemistry*, 288(18), pp.13136–13144.

Cheng, G. et al., 2010. Basis for MAP4 Dephosphorylation-related Microtubule Network Densification in Pressure Overload Cardiac Hypertrophy. *Journal of Biological Chemistry*, 285(49), pp.38125–38140.

Chernysh, O., Condrescu, M. & Reeves, J.P., 2008. Na+-dependent inactivation of Na+/Ca2+ exchange in transfected Chinese hamster ovary cells. *AJP: Cell*

*Physiology*, 295(4), pp.C872–C882.

Cho, C. et al., 2003. Partial rescue of the Na+-Ca2+ exchanger (NCX1) knock-out mouse by transgenic expression of NCX1. *Experimental and Molecular Medicine*, 35(2), pp.125–135.

Cho, C. et al., 2001. The Na+-Ca2+ Exchanger Is Essential for Embryonic Heart Development in Mice. *Molecules and Cells*, 10(6), pp.712–722.

Choy, E. et al., 1999. Endomembrane Trafficking of Ras:The CAAX Motif Targets Proteins to the ER and Golgi. *Cell*, 98, pp.69–80.

Cole, C., Barber, J.D. & Barton, G.J., 2008. The Jpred 3 secondary structure prediction server. *Nucleic Acids Research*, 36(Web Server), pp.W197–W201.

Condrescu, M. et al., 1995. ATP-dependent Regulation of Na+-Ca2+ Exchange in Chinese Hamster Ovary Cells Transfected with the Bovine Cardiac Na+-Ca2+ Exchanger. *Journal of Biological Chemistry*, 270(16), pp.9137–9146.

Corrotte, M. et al., 2013. Caveolae internalization repairs wounded cells and muscle fibres. *eLife*, 2, pp.1–30.

Craven, S.E., El-Husseini, A. & Bredt, D.S., 1999. Synaptic Targeting of the Postsynaptic Density Protein PSD-95 Mediatedby Lipid and Protein Motifs. *Neuron*, 22, pp.497–509.

Davda, D. et al., 2013. Profiling Targets of the Irreversible Palmitoylation Inhibitor 2-Bromopalmitate. *ACS Chemical Biology*, 8(9), pp.1912–1917.

Dekker, F.J. et al., 2010. Small-molecule inhibition of APT1 affects Ras localization and signaling. *Nature Methods*, 6(6), pp.449–456.

Despa, S. et al., 2003. Na/Ca Exchange and Na/K-ATPase Function Are Equally Concentrated in Transverse Tubules of Rat Ventricular Myocytes. *Biophysical Journal*, 85, pp.3388–3396.

Deval, E. et al., 2000. Expression of the Na+/Ca2+ Exchanger in Mammalian Skeletal Muscle Cells in Primary Culture. *Experimental Cell Research*, 255(2), pp.291–302.

Devedjiev, Y. et al., 2000. Crystal Structure of the HumanAcyl Protein Thioesterase Ifrom a Single X-Ray Data Set to 1.5 A˚. *Structure*, 8, pp.1137–1146.

Dietzen, D.J., Hastings, W.R. & Lublin, D.M., 1995. Caveolin Is Palmitoylated on Multiple Cysteine Residues: Palmitoylation Is Not Necessary For Localization Of Caveolin To Caveolae. *Journal of Biological Chemistry*, 270(12), pp.6838–6842.

Dipolo, R. & Beaugé, L., 1990. Asymmetrical properties of the Na-Ca exchanger in voltage-clamped, internally dialyzed squid axons under symmetrical ionic conditions. *The Journal of General Physiology*, 95(5), pp.819–835.

Dipolo, R. & Beaugé, L., 2002. MgATP counteracts intracellular proton inhibition of the Na+-Ca2+ exchanger in dialysed squid axons. *Journal of Physiology*, 539(3), pp.791–803.

Dipolo, R. & Beaugé, L., 2006. Na+/Ca2+ Exchanger: Influence of Metabolic Regulation on Ion Carrier Interactions. *Physiological Reviews*, 86(1), pp.155–203.

Djurovic, S. et al., 2004. Comparison of Nonviral Transfectionand Adeno-Associated Viral Transduction on Cardiomyocytes. *Molecular Biotechnology*, 28, pp.21–31.

Doering, A.E. et al., 1998. Topology of a functionally important region of the cardiac Na+/Ca2+ exchanger. *The Journal of Biological Chemistry*, 273(2), pp.778–783.

Drisdel, R.C., Manzana, E. & Green, W.N., 2004. The Role of Palmitoylation in Functional Expression of Nicotinic  7 Receptors. *Journal of Neuroscience*, 24(46), pp.10502–10510.

Duncan, J.A., 2002. Characterization of Saccharomyces cerevisiae Acyl-protein Thioesterase 1, the Enzyme Responsible for G Protein alpha Subunit Deacylation in Vivo. *Journal of Biological Chemistry*, 277(35), pp.31740–31752.

Duncan, J.A. & Gilman, A.G., 1998. A Cytoplasmic Acyl-Protein Thioesterase That Removes Palmitate from G Protein alpha Subunits and p21RAS. *Journal of Biological Chemistry*, 273(25), pp.15830–15837.

Duncan, J.A. & Gilman, A.G., 1996. Autoacylation of G Protein α Subunits. *The Journal of Biological Chemistry*, 271(38), pp.23594–23600.

Dunn, J. et al., 2002. The Molecular Determinants of Ionic Regulatory Differences between Brain and Kidney Na+/Ca2+ Exchanger (NCX1) Isoforms. *The Journal of Biological Chemistry*, 277(37), pp.33957–33962.

Durkin, J.T. et al., 1991. Purification and amino-terminal sequence of the bovine cardiac Na+-Ca2+ exchanger: Evidence for the presence of a signal sequence. *Archives of Biochemistry and Biophysics*, 290(2), pp.369–375.

Dyck, C. et al., 1999. Ionic Regulatory Properties of Brain and Kidney Splice Variants of the NCX1 Na+-Ca2+ Exchanger. *Journal of General Physiology*, 114, pp.701–711.

Dyck, C. et al., 1998. Structure-Function Analysis of CALX1.1, a Na+-Ca2+ Exchanger from Drosophila: Mutagenesis Of Ionic Regulatory Sites. *Journal of Biological Chemistry*, 273(21), pp.12981–12987.

El-Husseini, A.E. et al., 2000. Dual Palmitoylation of PSD-95 Mediates Its Vesiculotubular Sorting, Postsynaptic Targeting, and Ion Channel Clustering. *The Journal of Cell Biology*, 148(1), pp.159–171.

Feiner, E.C. et al., 2011. Left Ventricular Dysfunction in Murine Models of Heart Failure and in Failing Human Heart is Associated With a Selective Decrease in the Expression of Caveolin-3. *Journal of Cardiac Failure*, 17(3), pp.253–263.

Finn, R., Kovács, A.D. & Pearce, D.A., 2011. Altered glutamate receptor function in the cerebellum of the Ppt1−/− mouse, a murine model of infantile neuronal ceroid lipofuscinosis. *Journal of Neuroscience Research*, 90(2), pp.367–375.

Fontana, G., Rogowski, R.S. & Blaustein, M.P., 1995. Kinetic properties of the Na+-

Ca2+ exchanger in rat brain synaptosomes. *Journal of Physiology*, 485(2), pp.349–364.

Forrester, M.T. et al., 2011. Site-Specific Analysis of Protein S-Acylation by Resin-Assisted Capture (Acyl-RAC). *Journal of Lipid Research*, 52(2), pp.393–398.

Frank, J.S. et al., 1992. Distribution of the Na-Ca exchange protein in mammalian cardiac myocytes: an immunofluorescence and immunocolloidal gold-labeling study. *The Journal of Cell Biology*, 117(2), pp.337–345.

Fraysse, B. et al., 2001. Expression of the Na+/Ca2+exchanger in skeletal muscle. *AJP: Cell Physiology*, 280, pp.C146–C154.

Fukata, M. et al., 2004. Identification of PSD-95 Palmitoylating Enzymes. *Neuron*, 44, pp.987–996.

Fukata, Y., Iwanaga, T. & Fukata, M., 2006. Systematic screening for palmitoyl transferase activity of the DHHC protein family in mammalian cells. *Methods*, 40(2), pp.177–182.

Fuller, W. et al., 2009. FXYD1 phosphorylation in vitro and in adult rat cardiac myocytes: threonine 69 is a novel substrate for protein kinase C. *AJP: Cell Physiology*, 296(6), pp.C1346–C1355.

Fuller, W. et al., 2004. Ischemia-induced phosphorylation of phospholemman directly activates rat cardiac Na/K ATPase. *The FASEB Journal*, 18(1), pp.197–199.

Fuller, W. et al., 2012. Regulation of the cardiac Na+ pump. *Cellular and Molecular Life Sciences*.

Gadsby, D.C. et al., 1991. Influence of External Monovalent Cations on Na-Ca Exchange Current-Voltage Relationships in Cardiac Myocytes. *Annals of the New York Academy of Sciences*, 639, pp.140–146.

Gao, X. et al., 2011. Membrane targeting of palmitoylated Wnt and Hedgehog revealed by chemical probes. *FEBS Letters*, 585(15), pp.2501–2506.

Gauthier-Kemper, A. et al., 2014. Interplay between phosphorylation and palmitoylation mediates plasma membrane targeting and sorting of GAP43. *Molecular Biology of the Cell*, 25(21), pp.3284–3299.

Ghosh, A.K. et al., 2008. CGI-58, the Causative Gene for Chanarin-Dorfman Syndrome, Mediates Acylation of Lysophosphatidic Acid. *The Journal of Biological Chemistry*, 283(36), pp.24525–24533.

Gonnord, P. et al., 2009. Palmitoylation of the P2X7 receptor, an ATP-gated channel, controls its expression and association with lipid rafts. *The FASEB Journal*, 23(3), pp.795–805.

Goodwin, J.S. et al., 2005. Depalmitoylated Ras traffics to and from the Golgi complex via a nonvesicular pathway. *The Journal of Cell Biology*, 170(2), pp.261–272.

Greaves, J. & Chamberlain, L.H., 2007. Palmitoylation-dependent protein sorting. *The*

*Journal of Cell Biology*, 176(3), pp.249–254.

Greaves, J. & Chamberlain, L.H., 2010. S-acylation by the DHHC protein family. *Biochemical Society Transactions*, 38(2), p.522.

Greaves, J. et al., 2008. Palmitoylation and Membrane Interactions of the Neuroprotective Chaperone Cysteine-string Protein. *Journal of Biological Chemistry*, 283(36), pp.25014–25026.

Greaves, J. et al., 2009. The Hydrophobic Cysteine-rich Domain of SNAP25 Couples with Downstream Residues to Mediate Membrane Interactions and Recognition by DHHC Palmitoyl Transferases. *Molecular Biology of the Cell*, 20, pp.1845–1854.

Greaves, J., Carmichael, J.A. & Chamberlain, L.H., 2011. The palmitoyl transferase DHHC2 targets a dynamic membrane cycling pathway: regulation by a C-terminal domain. *Molecular Biology of the Cell*, 22(11), pp.1887–1895.

Gubitosi-Klug, R.A., Mancuso, D.J. & Gross, R.W., 2005. The human Kv1.1 channel is palmitoylated,modulating voltage sensing: Identificationof a palmitoylation consensus sequence. *PNAS*, 102(17), pp.5964–5968.

Hancock, J.F., Paterson, H. & Marshall, C.J., 1990. A Polybasic Domain or Palmitoylation Is Required in Addition to the CAAX Motif to Localize ~21"s to the Plasma Membrane. *Cell*, 63(1), pp.133–139.

Hare, J.M. et al., 2000. Contribution of Caveolin Protein Abundance to Augmented Nitric Oxide Signaling in Conscious Dogs With Pacing-Induced Heart Failure. *Circulation Research*, 86(10), pp.1085–1092.

Hasenfuss, G. & Schillinger, W., 2004. Is Modulation of Na+-Ca2+ Exchange a Therapeutic Option in Heart Failure? *Circulation Research*, 95(3), pp.225–227.

Hasenfuss, G. et al., 1994. Relation between myocardial function and expression of sarcoplasmic reticulum Ca(2+)-ATPase in failing and nonfailing human myocardium. *Circulation Research*, 75(3), pp.434–442.

Hayashi, T., Rumbaugh, G. & Huganir, R.L., 2005. Differential Regulation of AMPA Receptor Subunit Trafficking by Palmitoylation of Two Distinct Sites. *Neuron*, 47(5), pp.709–723.

Hayashi, T., Thomas, G.M. & Huganir, R.L., 2009. Dual Palmitoylation of NR2 Subunits Regulates NMDA Receptor Trafficking. *Neuron*, 64(2), pp.213–226.

He, L.P. et al., 2003. Molecular determinants of cAMP-mediated regulation of the Na+-Ca2+ exchanger expressed in human cell lines. *The Journal of Physiology*, 548(3), pp.677–689.

He, S. et al., 1998. Isoform-Specific Regulation of the Na+/Ca2+ Exchanger in Rat Astrocytes and Neurons by PKA. *The Journal of Neuroscience*, 18(13), pp.4833–4841.

He, Z. et al., 2000. Interaction of PIP2 with the XIP region of the cardiac Na/Ca exchanger. *American Journal of Physiology: Cell Physiology*, 278(4), pp.C661–

C666.

Hellsten, E. et al., 1996. Human palmitoyl protein thioesterase: evidence for lysosomal targeting of the enzyme and disturbed cellular routing in infantile neuronal ceroid lipofuscinosis. *The EMBO Journal*, 15(19), pp.5240–5245.

Henderson, S.A. et al., 2004. Functional Adult Myocardium in the Absence of Na+-Ca2+ Exchange: Cardiac-Specific Knockout of NCX1. *Circulation Research*, 95(6), pp.604–611.

Hilge, M. et al., 2009. Ca2+ regulation in the Na+/Ca2+ exchanger features a dual electrostatic switch mechanism. *PNAS*, pp.1–6.

Hilge, M., Aelen, J. & Vuister, G.W., 2006. Ca2+ Regulation in the Na+/Ca2+ Exchanger Involves Two Markedly Different Ca2+ Sensors. *Molecular Cell*, 22(1), pp.15–25.

Hilgemann, D.W., 2007. On the physiological roles of PIP2 at cardiac Na+ Ca2+ exchangers and KATP channels: a long journey from membrane biophysics into cell biology. *The Journal of Physiology*, 582(3), pp.903–909.

Hilgemann, D.W., 1990. Regulation and deregulation of cardiac Na+–Ca2+ exchange in giant excised sarcolemmal membrane patches. *Nature*, 344(6263), pp.242–245.

Hilgemann, D.W. & Ball, R., 1996. Regulation of Cardiac Na+,Ca2+ Exchange and KATP Potassium Channels by PIP2. *Science*, 273, pp.956–959.

Hilgemann, D.W. et al., 2013. Massive endocytosis triggered by surface membrane palmitoylation under mitochondrial control in BHK fibroblasts. *eLife*, 2(0), pp.e01293–e01293.

Hilgemann, D.W., Collins, A. & Matsuoka, S., 1992a. Steady-State and Dynamic Properties of Cardiac Na+-Ca2+ Exchange. Secondary Modulation by Cytoplasmic Ca2+ and ATP. *Journal of General Physiology*, 100, pp.933–961.

Hilgemann, D.W., Matsuoka, S., Nagel, G.A. & Collins, A., 1992b. Steady-State and Dynamic Properties of Cardiac Na+-Ca2+ Exchange. Na+-Dependent Inactivation. *The Journal of General Physiology*, 100(6), pp.905–932.

Hobai, I.A. & O'Rourke, B., 2001. Decreased Sarcoplasmic Reticulum Ca2+ Content Is Responsible for Defective Excitation-Contraction Coupling in Canine Heart Failure. *Circulation*, 103(11), pp.1577–1584.

Hobai, I.A. & O'Rourke, B., 2000. Enhanced Ca2+-Activated Na+-Ca2+ Exchange Activity in Canine Pacing-Induced Heart Failure. *Circulation Research*, 87, pp.690–698.

Hobai, I.A., Maack, C. & O'Rourke, B., 2004. Partial Inhibition of Na+/Ca2+ Exchange Restores Cellular Ca2+ Handling in Canine Heart Failure. *Circulation Research*, 95(3), pp.292–299.

Hornemann, T., 2014. Palmitoylation and depalmitoylation defects. *Journal of Inherited Metabolic Disease*.

Hou, H. et al., 2009. Analysis of DHHC Acyltransferases Implies Overlapping Substrate Specificity and a Two-Step Reaction Mechanism. *Traffic*, 10(8), pp.1061–1073.

Howie, J. et al., 2013. Regulation of the cardiac Na +pump by palmitoylation of its catalytic and regulatory subunits. *Biochemical Society Transactions*, 41(1), pp.95–100.

Howie, J. et al., 2014. Substrate recognition by the cell surface palmitoyl transferase DHHC5. *PNAS*, p.201413627.

Hryshko, L., 2008. What regulates Na+/Ca2+ exchange? Focus on "Na+-dependent inactivation of Na+/Ca2+ exchange in transfected Chinese hamster ovary cells." *AJP: Cell Physiology*, 295(4), pp.C869–C871.

Hryshko, L.V. et al., 1996. Anomalous regulation of the Drosophila Na+ –Ca2+ exchanger by Ca2. *Journal of General Physiology*, 108, pp.67–74.

Hryshko, L.V. et al., 1993. Biosynthesis and initial processing of the cardiac sarcolemmal Na+-Ca2+ exchanger. *Biochimica et Biophysica Acta (BBA) - Biomembranes*, 1151(1), pp.35–42.

Huang, D.W., Sherman, B.T. & Lempicki, R.A., 2008. Systematic and integrative analysis of large gene lists using DAVID bioinformatics resources. *Nature Protocols*, 4(1), pp.44–57.

Huang, K. et al., 2009. Neuronal palmitoyl acyl transferases exhibit distinct substrate specificity. *FASEB Journal*, 23(8), pp.2605–2615.

Hurtado, C. et al., 2006. Cells expressing unique Na+/Ca2+ exchange (NCX1) splice variants exhibit different susceptibilities to Ca2+ overload. *AJP: Heart and Circulatory Physiology*, 290(5), pp.H2155–H2162.

Imahashi, K. et al., 2005. Cardiac-Specific Ablation of the Na+-Ca2+ Exchanger Confers Protection Against Ischemia/Reperfusion Injury. *Circulation Research*, 97(9), pp.916–921.

Iwamoto, T., 2000. The Na+/Ca2+ Exchanger NCX1 Has Oppositely Oriented Reentrant Loop Domains That Contain Conserved Aspartic Acids Whose Mutation Alters Its Apparent Ca2+ Affinity. *Journal of Biological Chemistry*, 275(49), pp.38571–38580.

Iwamoto, T. et al., 1996. Phosphorylation-dependent Regulation of Cardiac Na+/Ca2+ Exchanger via Protein Kinase C. *Journal of Biological Chemistry*, 271(23), pp.13609–13615.

Iwamoto, T. et al., 2000. The Na+/Ca2+ Exchanger NCX1 Has Oppositely Oriented Reentrant Loop Domains That Contain Conserved Aspartic Acids Whose Mutation Alters Its Apparent Ca2+ Affinity. *Journal of Biological Chemistry*, 275(49), pp.38571–38580.

Iwamoto, T. et al., 1999. Unique topology of the internal repeats in the cardiac Na/Ca

exchanger. *FEBS Letters*, 446, pp.264–268.

Jeffries, O. et al., 2012. An Electrostatic Switch Controls Palmitoylation of the Large Conductance Voltage- and Ca2+-activated Potassium (BK) Channel. *Journal of Biological Chemistry*, 287(2), pp.1468–1477.

Jeffries, O. et al., 2010. Palmitoylation of the S0-S1 Linker Regulates Cell Surface Expression of Voltage- and Ca2+-activated Potassium (BK) Channels. *Journal of Biological Chemistry*, 285(43), pp.33307–33314.

Jennings, B.C. & Linder, M.E., 2012. DHHC protein S-acyltransferases use a similar ping-pong kinetic mechanism but display different acyl-CoA specificities. *The Journal of Biological Chemistry*, 287(10), pp.7236–7245.

Jennings, B.C. et al., 2008. 2-Bromopalmitate and 2-(2-hydroxy-5-nitro-benzylidene)-benzo[b]thiophen-3-one inhibit DHHC-mediated palmitoylation in vitro. *The Journal of Lipid Research*, 50(2), pp.233–242.

Jennings, R.B., 2013. Historical Perspective on the Pathology of Myocardial Ischemia/Reperfusion Injury. *Circulation Research*, 113, pp.428–438.

John, S.A. et al., 2011. Ca2+-dependent structural rearrangements within Na+–Ca2+ exchanger dimers. *PNAS*, 108(4), pp.1699–1704.

Keller, C.A. et al., 2004. The γ2 subunit of GABAA receptors is a substrate for palmitoylation by GODZ. *Journal of Neuroscience*, 24(26), pp.5881–5891.

Kinlough, C.L. et al., 2006. Recycling of MUC1 Is Dependent on Its Palmitoylation. *Journal of Biological Chemistry*, 281(17), pp.12112–12122.

Kofuji, P., Lederer, W.J. & Schulze, D.H., 1994. Mutually exclusive and cassette exons underlie alternatively spliced isoforms of the Na/Ca exchanger. *The Journal of Biological Chemistry*, 269(7), pp.5145–5149.

Komuro, II et al., 1992. Molecular cloning and characterization of the human cardiac Na+/Ca2+ exchanger cDNA. *PNAS*, 89(10), pp.4769–4773.

Kong, E. et al., 2013. Dynamic Palmitoylation Links Cytosol-Membrane Shuttling of Acyl-protein Thioesterase-1 and Acyl-protein Thioesterase-2 with That of Proto-oncogene H-Ras Product and Growth-associated Protein-43. *Journal of Biological Chemistry*, 288(13), pp.9112–9125.

Korycka, J. et al., 2012. Human DHHC proteins: A spotlight on the hidden player of palmitoylation. *European Journal of Cell Biology*, pp.107–117.

Koushik, S.V. et al., 2001. Targeted inactivation of the Na+-Ca2+ exchanger (Ncx1) results in the lack of a heartbeat and abnormal myofibrillar organization. *The FASEB Journal*, 15, pp.1209–1211.

Kumari, B., Kumar, R. & Kumar, M., 2014. PalmPred: An SVM Based Palmitoylation Prediction Method Using Sequence Profile Information G. P. S. Raghava, ed. *PloS one*, 9(2), p.e89246.

Lai, J. & Linder, M.E., 2013. Oligomerization of DHHC Protein S-Acyltransferases. *Journal of Biological Chemistry*, 288(31), pp.22862–22870.

Lariccia, V. et al., 2011. Massive Ca2+–activated endocytosis without involvement of classical endocytic proteins. *Journal of General Physiology*, 137(1), pp.111–132.

Lee, C. & Hryshko, L.V., 2004. SEA0400: A Novel Na+-Ca2+ Exchange Inhibitor with Cardioprotective Properties. *Cardiovascular Drug Reviews*, 22(4), pp.334–347.

Lee, C. et al., 2004. Inhibitory Profile of SEA0400 [2-[4-[(2,5-Difluorophenyl)methoxy]phenoxy]-5-ethoxyaniline] Assessed on the Cardiac Na+-Ca2+ Exchanger, NCX1.1. *Journal of Pharmacology and Experimental Therapeutics*, 311(2), pp.748–757.

Lee, S.L., Yu, A.S. & Lytton, J., 1994. Tissue-specific expression of Na(+)-Ca2+ exchanger isoforms. *Journal of Biological Chemistry*, 269(21), pp.14849–14852.

Lee, Y.I. et al., 2006. Effects of exercise training on pathological cardiac hypertrophy related gene expression and apoptosis. *European Journal of Applied Physiology*, 97(2), pp.216–224.

Lemonidis, K. et al., 2014. The Golgi S-acylation machinery is comprised of zDHHC enzymes with major differences in substrate affinity and S-acylation activity. *Mol Biol Cell*, pp.1–28.

Levitsky, D.O., Nicoll, D.A. & Philipson, K.D., 1994. Identification of the high affinity Ca(2+)-binding domain of the cardiac Na(+)-Ca2+ exchanger. *Journal of Biological Chemistry*, 269(36), pp.22847–22852.

Léoty, C., 1984. Na+ withdrawal contractures in Rat Slow Twitch Skeletal Muscle. *General Physiology and Biophysics*, 3(5), pp.413–429.

Li, Z. et al., 1991. Identification of a peptide inhibitor of the cardiac sarcolemmal Na(+)-Ca2+ exchanger. *Journal of Biological Chemistry*, 266(2), pp.1014–1020.

Liao, J. et al., 2012. Structural Insight into the Ion-Exchange Mechanism of the Na+/Ca2+ Exchanger. *Science*, 335(6069), pp.686–690.

Liebler, D.C. & Ham, A.L., 2009. Spin filter–based sample preparation for shotgun proteomics. *Nature Methods*, 6(11), pp.785–785.

Lin, D.-T. et al., 2009. Regulation of AMPA receptor extrasynaptic insertion by 4.1N, phosphorylation and palmitoylation. *Nature Publishing Group*, 12(7), pp.879–887.

Lin, M.J. et al., 2013. Massive palmitoylation-dependent endocytosis during reoxygenation of anoxic cardiac muscle. *eLife*, 2(0), pp.e01295–e01295.

Linck, B. et al., 1998. Functional comparison of the three isoforms of the $Na^+/Ca^{2+}$ exchanger (NCX1, NCX2, NCX3). *American Journal of Physiology: Cell Physiology*, 274(2), pp.C415–C423.

Linder, M.E., 2001. Reversible modification of proteins with thioester-linked fatty acids F. Tamanoi & D. S. Sigman, eds. *The Enzymes: Protein Lipidation*, 21, pp.215–

240.

Linder, M.E. & Deschenes, R.J., 2003. New Insights into the Mechanisms of Protein Palmitoylation †. *Biochemistry*, 42(15), pp.4311–4320.

Linder, M.E. & Deschenes, R.J., 2007. Palmitoylation: policing protein stability and traffic. *Nature Reviews Molecular Cell Biology*, 8(1), pp.74–84.

Linder, M.E. et al., 1993. Lipid modifications of G proteins: subunits are palmitoylated. *PNAS*, 90, pp.3675–3679.

Lobo, S. et al., 2002. Identification of a Ras Palmitoyltransferase in Saccharomyces cerevisiae. *The Journal of Biological Chemistry*, 277(43), pp.41268–41273.

Lord, C.C., Thomas, G. & Brown, J.M., 2013. Biochimica et Biophysica Acta. *BBA - Molecular and Cell Biology of Lipids*, 1831(4), pp.792–802.

Low, W., Kasir, J. & Rahamimoff, H., 1993. Cloning of the rat heart Na+-Ca2+ exchanger* and its functional expression in HeLa cells. *FEBS Letters*, 316(1), pp.63–67.

Lu, J.Y. & Hofmann, S.L., 1995. Depalmitoylation of CAAX motif proteins. Protein structural determinants of palmitate turnover rate. *The Journal of Biological Chemistry*, 270(13), pp.7251–7256.

Lu, J.Y., Verkruyse, L.A. & Hofmann, S.L., 1996. Lipid thioesters derived from acylated proteins accumulate in infantile neuronal ceroid lipofuscinosis: correction of the defect in lymphoblasts by recombinant palmitoyl-protein thioesterase. *PNAS*, 93, pp.10046–10050.

Lyly, A. et al., 2008. Deficiency of the INCL protein Ppt1 results in changes in ectopic F1-ATP synthase and altered cholesterol metabolism. *Human Molecular Genetics*, 17(10), pp.1406–1417.

Lynch, S.J. et al., 2014. The Differential Palmitoylation States of N-Ras and H-Ras Determine Their Distinct Golgi Sub-compartment Localizations. *Journal of Cellular Physiology*, pp.n/a–n/a.

Maack, C. et al., 2005. Cardiac Na+-Ca2+ Exchanger Is Regulated by Allosteric Ca2+ and Exchanger Inhibitory Peptide at Distinct Sites. *Circulation Research*, 96(1), pp.91–99.

Magee, A.I. et al., 1987. Dynamic fatty acylation of p21N-ras. *EMBO*, 6(11), pp.3353–3357.

Martin, B.R. & Cravatt, B.F., 2009. Large-scale profiling of protein palmitoylation in mammalian cells. *Nature Methods*, 6(2), pp.135–138.

Martin, B.R. et al., 2011. Global profiling of dynamic protein palmitoylation. *Nature Methods*.

Matsuoka, S. & Hilgemann, D.W., 1994. Inactivation of outward Na+-Ca2+ exchange current in guinea-pig ventricular myocytes. *Journal of Physiology*, 476(3), pp.443–

458.

Matsuoka, S. & Hilgemann, D.W., 1992. Steady-State and Dynamic Properties of Cardiac Na+-Ca2+ Exchange: Ion and Voltage Dependencies of the Transport Cycle. *Journal of General Physiology*, 100, pp.963–1001.

Matsuoka, S. et al., 1997. Regulation of cardiac Na+-Ca2+ exchanger by the endogenous XIP region. *Journal of General Physiology*, 109(2), pp.273–286.

Matsuoka, S. et al., 1995. Regulation of the cardiac Na(+)-Ca2+ exchanger by Ca2+. Mutational analysis of the Ca(2+)-binding domain. *The Journal of General Physiology*, 105(3), pp.403–420.

Melkonian, K.A. et al., 1999. Role of Lipid Modifications in Targeting Proteins to Detergent-resistant Membrane Rafts: Many Raft Proteins Are Acylated, While Few Are Prenylated. *Journal of Biological Chemistry*, 274(6), pp.3910–3917.

Menick, D.R. et al., 2007. Regulation of Ncx1 Gene Expression in the Normal and Hypertrophic Heart. *Annals of the New York Academy of Sciences*, 1099(1), pp.195–203.

Mi, H. et al., 2013. Large-scale gene function analysis with the PANTHER classification system. *Nature Protocols*, 8(8), pp.1551–1566.

Mitchell, D.A., 2006. Protein palmitoylation by a family of DHHC protein S-acyltransferases. *Journal of Lipid Research*, 47(6), pp.1118–1127.

Mitchell, D.A. et al., 1994. A polybasic domain allows nonprenylated Ras proteins to function in Saccharomyces cerevisiae. *Journal of Biological Chemistry*, 269(34), pp.21540–21546.

Mitchell, D.A. et al., 2006. Protein palmitoylation by a family of DHHC protein S-acyltransferases. *Journal of Lipid Research*, 47(6), pp.1118–1127.

Mollner, S. et al., 1998. Nonenzymatic palmitoylation at Cys 3 causes extra-activation of the B-subunit of the stimulatory GTP-binding protein Gs. *European Journal of Biochemistry*, 257, pp.236–241.

Montero-Moran, G. et al., 2010. CGI-58/ABHD5 is a coenzyme A-dependent lysophosphatidic acid acyltransferase. *Journal of Lipid Research*, 51(4), pp.709–719.

Morad, M., Cleemann, L. & Menick, D.R., 2011. NCX1 phosphorylation dilemma: a little closer to resolution. Focus on “Full-length cardiac Na+/Ca2+ exchanger 1 protein is not phosphorylated by protein kinase A.” *AJP: Cell Physiology*, 300(5), pp.C970–C973.

Morrow, I.C. et al., 2002. Flotillin-1/Reggie-2 Traffics to Surface Raft Domains via a Novel Golgi-independent Pathway: Identification Of A Novel Membrane Targeting Domain And A Role For Palmitoylation. *Journal of Biological Chemistry*, 277(50), pp.48834–48841.

Mueller, G.M. et al., 2010. Cys Palmitoylation of the  Subunit Modulates Gating of the

Epithelial Na+ Channel. *Journal of Biological Chemistry*, 285(40), pp.30453–30462.

Nadolski, M.J. & Linder, M.E., 2009. Molecular Recognition of the Palmitoylation Substrate Vac8 by Its Palmitoyltransferase Pfa3. *Journal of Biological Chemistry*, 284(26), pp.17720–17730.

Nardini, M. & Dijkstra, B.W., 1999. α/β Hydrolase fold enzymes: the family keeps growing. *Current Opinion in Structural Biology*, 9, pp.732–737.

Nicoll, D.A. et al., 1999. A new topological model of the cardiac sarcolemmal Na+-Ca2+ exchanger. *Journal of Biological Chemistry*, 274(2), pp.910–917.

Nicoll, D.A. et al., 2006. The Crystal Structure of the Primary Ca2+ Sensor of the Na+/Ca2+ Exchanger Reveals a Novel Ca2+ Binding Motif. *The Journal of Biological Chemistry*, 281(31), pp.21577–21581.

Nicoll, D.A., Hryshko, L.V., et al., 1996a. Mutation of Amino Acid Residues in the Putative Transmembrane Segments of the Cardiac Sarcolemmal Na+-Ca2+ Exchanger. *Journal of Biological Chemistry*, 271(23), pp.13385–13391.

Nicoll, D.A., Longoni, S. & Philipson, K.D., 1990. Molecular cloning and functional expression of the cardiac sarcolemmal Na(+)-Ca2+ exchanger. *Science*, pp.562–565.

Nicoll, D.A., Quednau, B.D., et al., 1996b. Cloning of a third mammalian Na+-Ca2+ exchanger, NCX3. *The Journal of Biological Chemistry*, 271(40), pp.24914–24921.

Noritake, J. et al., 2009. Mobile DHHC palmitoylating enzyme mediates activity-sensitive synaptic targeting of PSD-95. *Journal of Cell Biology*, 186(1), pp.147–160.

Nyholm, T.K.M., Özdirekcan, S. & Killian, J.A., 2007. How Protein Transmembrane Segments Sense the Lipid Environment. *Biochemistry*, 46(6), pp.1457–1465.

O'Brien, P.J. et al., 1987. Acylation of Disc Membrane Rhodopsin May Be Nonenzymatic. *Journal of Biological Chemistry*, 262(11), pp.5210–5215.

O'Rourke, B. et al., 1999. Mechanisms of Altered Excitation-Contraction Coupling in Canine Tachycardia-Induced Heart Failure, I: Experimental Studies. *Circulation Research*, 84, pp.562–570.

Ohno, Y. et al., 2006. Intracellular localization and tissue-specific distribution of human and yeast DHHC cysteine-rich domain-containing proteins. *Biochimica et Biophysica Acta (BBA) - Molecular and Cell Biology of Lipids*, 1761(4), pp.474–483.

Ohsawa, Y. et al., 2003. Overexpression of P104L mutant caveolin-3 in mice develops hypertrophic cardiomyopathy with enhanced contractility in association with increased endothelial nitric oxide synthase activity. *Human Molecular Genetics*, 13(2), pp.151–157.

Ohtsuka, M. et al., 2004. Role of Na+–Ca2+ exchanger in myocardial

ischemia/reperfusion injury: evaluation using a heterozygous Na+–Ca2+ exchanger knockout mouse model. *Biochemical and Biophysical Research Communications*, 314(3), pp.849–853.

Ollis, D.L. et al., 1992. The a/|3 hydrolase fold. *Protein Engineering*, 5(3), pp.197–211.

Ottolia, M. et al., 2006. Fluorescent Na+-Ca+ Exchangers: Electrophysiological And Optical Characterization. *Journal of Biological Chemistry*, 282(6), pp.3695–3701.

Ottolia, M. et al., 2010. Interactions between Ca2+ binding domains of the Na+-Ca2+ exchanger and secondary regulation. *Channels*, 4(3), pp.159–162.

Ottolia, M. et al., 2007. Shedding Light on the Na+/Ca2+ Exchanger. *Annals of the New York Academy of Sciences*, 1099(1), pp.78–85.

Ottolia, M. et al., 2001. Split Na+-Ca2+ Exchangers. Implications for Function and Expression. *Journal of Biological Chemistry*, 276(22), pp.19603–19609.

Ottolia, M., Nicoll, D.A. & Philipson, K.D., 2005. Mutational Analysis of the α-1 Repeat of the Cardiac Na+-Ca2+ Exchanger. *Journal of Biological Chemistry*, 280(2), pp.1061–1069.

Ottolia, M., Nicoll, D.A. & Philipson, K.D., 2009. Roles of Two Ca2+-binding Domains in Regulation of the Cardiac Na+-Ca2+ Exchanger. *Journal of Biological Chemistry*, 284(47), pp.32735–32741.

Ozdemir, S. et al., 2008. Pharmacological Inhibition of Na/Ca Exchange Results in Increased Cellular Ca2+ Load Attributable to the Predominance of Forward Mode Block. *Circulation Research*, 102(11), pp.1398–1405.

Parenti, M. et al., 1993. A novel N-terminal motif for palmitoylation of G-protein a subunits. *Biochemical Journal*, 291, pp.349–353.

Pavlovic, D., McLatchie, L.M. & Shattock, M.J., 2010. The rate of loss of T-tubules in cultured adult ventricular myocytes is species dependent. *Experimental Physiology*, 95(4), pp.518–527.

Pepinsky, R.B. et al., 1998. Identification of a Palmitic Acid-modified Form of Human Sonic hedgehog. *Journal of Biological Chemistry*, 273(22), pp.14037–14045.

Petaja-Repo, U.E. et al., 2006. Distinct Subcellular Localization for Constitutive and Agonist-modulated Palmitoylation of the Human Opioid Receptor. *Journal of Biological Chemistry*, 281(23), pp.15780–15789.

Philipson, K.D. & Nicoll, D.A., 2000. Na+-Ca2+ Exchange: A Molecular Perspective. *Annual Review of Physiology*, (62), pp.111–133.

Philipson, K.D., Longoni, S. & Ward, R., 1988. Purification of the cardiac Na+-Ca2+ exchange protein. *Biochimica et Biophysica Acta (BBA) - Biomembranes*, 945(2), pp.298–306.

Philipson, K.D., Quednau, B.D. & Nicoll, D.A., 2004. The Na+/Ca2+ exchanger family-SLC8. *Pflugers Archive European Journal of Physiology*, 447(5), pp.543–

548.

Pickering, D.S. et al., 2005. Palmitoylation of the GluR6 kainate receptor. *PNAS*, 92, pp.12090–12094.

Pieske, B. et al., 1999. Ca2+ Handling and Sarcoplasmic Reticulum Ca2+ Content in Isolated Failing and Nonfailing Human Myocardium. *Circulation Research*, 85, pp.38–46.

Pogwizd, S.M. et al., 1999. Upregulation of Na+/Ca2+ Exchanger Expression and Function in an Arrhythmogenic Rabbit Model of Heart Failure. *Circulation Research*, 85(11), pp.1009–1019.

Politis, E.G., Roth, A.F. & Davis, N.G., 2005. Transmembrane Topology of the Protein Palmitoyl Transferase Akr1. *Journal of Biological Chemistry*, 280(11), pp.10156–10163.

Ponimaskin, E. & Schmidt, M.F.G., 1998. Domain-structure of cytoplasmic border region is main determinant for palmitoylation of influenza virus hemagglutinin (H7). *Virology*, 249, pp.325–335.

Porzig, H. et al., 1993. Mapping of the cardiac Na+-Ca2+ exchanger with monoclonal antibodies. *American Journal of Physiology: Cell Physiology*, 265, pp.C748–C756.

Qiu, Z., Nicoll, D.A. & Philipson, K.D., 2001. Helix Packing of Functionally Important Regions of the Cardiac Na+-Ca2+ Exchanger. *Journal of Biological Chemistry*, 276(1), pp.194–199.

Quednau, B.D., Nicoll, D.A. & Philipson, K.D., 1997a. Tissue specificity and alternative splicing of the Na+/Ca2+ exchanger isoforms NCX1, NCX2, and NCX3 in rat. *AJP: Cell Physiology*, 272(4), pp.C1250–C1261.

Quednau, B.D., Nicoll, D.A. & Philipson, K.D., 1997b. Tissue specificity and alternative splicing of the Na+/Ca2+ exchanger isoforms NCXl, NCX2, and NCX3 in rat. *AJP: Cell Physiology*, 272, pp.C1250–C1261.

Quesnel, S. & Silvius, J.R., 1994. Cysteine-Containing Peptide Sequences Exhibit Facile Uncatalyzed Transacylation and Acyl-CoA-dependent Acylation at the Lipid Bilayer Interface. *Biochemistry*, 33, pp.13340–13348.

Rathenberg, J., Kittler, J.T. & Moss, S.J., 2004. Palmitoylation regulates the clustering and cell surface stability of GABAA receptors. *Molecular and Cellular Neuroscience*, 26(2), pp.251–257.

Reeves, J.P. & Condrescu, M., 2008. Ionic regulation of the cardiac Na+-Ca2+ exchanger. *Channels*, 2(5), pp.322–328.

Ren, J. et al., 2008a. CSS-Palm 2.0: an updated software for palmitoylation sites prediction. *Protein Engineering Design and Selection*, 21(11), pp.639–644.

Ren, X. & Philipson, K.D., 2013. The topology of the cardiac Na+/Ca2+ exchanger, NCX1. *Journal of Molecular and Cellular Cardiology*, 57, pp.68–71.

Ren, X. et al., 2008b. Intermolecular Cross-Linking of Na +−Ca 2+Exchanger Proteins: Evidence for Dimer Formation. *Biochemistry*, 47(22), pp.6081–6087.

Ren, X. et al., 2010. Transmembrane Segment Packing of the Na +/Ca 2+Exchanger Investigated with Chemical Cross-Linkers. *Biochemistry*, 49(39), pp.8585–8591.

Ren, X., Nicoll, D.A. & Philipson, K.D., 2006. Helix packing of the cardiac Na+-Ca2+ exchanger: proximity of transmembrane segments 1, 2, and 6. *Journal of Biological Chemistry*, 281(32), pp.22808–22814.

Resh, M.D., 2006. Palmitoylation of Ligands, Receptors, and Intracellular Signaling Molecules. *Science's STKE*, 2006(359), pp.re14–re14.

Riedel, M.J. et al., 2006. Metabolic regulation of Na+–Ca2+ exchange by intracellular acyl CoAs. *The EMBO Journal*, 25, pp.4605–4614.

Rocks, O. et al., 2005. An acylation cycle regulates localization and activity of palmitoylated Ras isoforms. *Science*, 307(5716), pp.1741–1746.

Rocks, O. et al., 2010. The Palmitoylation Machinery Is a Spatially Organizing System for Peripheral Membrane Proteins. *Cell*, 141(3), pp.458–471.

Roth, A.F. et al., 2006. Global Analysis of Protein Palmitoylation in Yeast. *Cell*, 125(5), pp.1003–1013.

Roth, A.F. et al., 2002. The yeast DHHC cysteine-rich domain protein Akr1p is a palmitoyl transferase. *Journal of Cell Biology*, 159(1), pp.23–28.

Roy, S. et al., 2005. Individual Palmitoyl Residues Serve Distinct Roles in H-Ras Trafficking, Microlocalization, and Signaling. *Molecular and Cellular Biology*, 25(15), pp.6722–6733.

Ruknudin, A. et al., 2000. Functional differences between cardiac and renal isoforms of the rat Na+—Ca2+ exchanger NCX1 expressed in Xenopus oocytes. *Journal of Physiology*, 529(3), pp.599–610.

Ruknudin, A.M. et al., 2007. Phosphorylation and Other Conundrums of Na/Ca Exchanger, NCX1. *Annals of the New York Academy of Sciences*, 1099(1), pp.103–118.

Rusch, M. et al., 2011. Identification of Acyl Protein Thioesterases 1 and 2 as the Cellular Targets of the Ras-Signaling Modulators Palmostatin B and M. *Angewandte Chemie International Edition*, 50(42), pp.9838–9842.

Salaun, C., Greaves, J. & Chamberlain, L.H., 2010. The intracellular dynamic of protein palmitoylation. *The Journal of Cell Biology*, 191(7), pp.1229–1238.

Santacruz-Toloza, L. et al., 2000. Functional Analysis of a Disulfide Bond in the Cardiac Na+-Ca2+ Exchanger. *Journal of Biological Chemistry*, 275(1), pp.182–188.

Schillinger, W. et al., 2000. Impaired contractile performance of cultured rabbit ventricular myocytes after adenoviral gene transfer of Na/Ca exchanger.

*Circulation Research*, 87, pp.581–587.

Schillinger, W. et al., 2003. Relevance of Na+–Ca2+ exchange in heart failure. *Cardiovascular Research*, 57(4), pp.921–933.

Schmidt, J.W. & Catterall, W.A., 1987. Palmitylation, Sulfation, and Glycosylation of the a Subunit of the Na+ Channel. *Journal of Biological Chemistry*, 262(28), pp.13713–13723.

Schulze, D.H. et al., 1996. Alternative Splicing of the Na+-Ca2+ Exchanger Gene, NCX1. *Annals of New York Academy of Sciences*, 779, pp.46–57.

Schulze, D.H. et al., 2003. Na+/Ca2+ Exchanger (NCX1) Macromolecular Complex. *Journal of Biological Chemistry*, 278(31), pp.28849–28855.

Schwarz, E.M. & Benzer, S., 1997. Calx, a Na-Ca exchanger gene of Drosophila melanogaster. *PNAS*, 94(19), pp.10249–10254.

Shahinian, S. & Silvius, J.R., 1995. Doubly-Lipid-Modified Protein Sequence Motifs Exhibit Long-Lived Anchorage to Lipid Bilayer Membranes. *Biochemistry*, 34, pp.3813–3822.

Shao, X. et al., 1997. Synaptotagmin-syntaxin interaction: The C2 domain as a Ca2□-dependent electrostatic switch. *Neuron*, 18, pp.133–142.

Shaw, R.M. & Colecraft, H.M., 2013. L-type Ca2+ channel targeting and local signalling in cardiac myocytes. *Cardiovascular Research*, 98(2), pp.177–186.

Shen, C. et al., 2007. Dual control of cardiac Na+ Ca2+ exchange by PIP2: analysis of the surface membrane fraction by extracellular cysteine PEGylation. *Journal of Physiology*, 582(3), pp.1011–1026.

Shigekawa, M. & Iwamoto, T., 2001. Cardiac Na+-Ca2+ Exchange : Molecular and Pharmacological Aspects. *Circulation Research*, 88(9), pp.864–876.

Shipston, M.J., 2011. Ion Channel Regulation by Protein Palmitoylation. *Journal of Biological Chemistry*, 286(11), pp.8709–8716.

Shipston, M.J., 2014. Ion channel regulation by protein S-acylation. *Journal of General Physiology*, 143(6), pp.659–678.

Sim, D.S., Dilks, J.R. & Flaumenhaft, R., 2007. Platelets Possess and Require an Active Protein Palmitoylation Pathway for Agonist-Mediated Activation and In Vivo Thrombus Formation. *Arteriosclerosis, Thrombosis, and Vascular Biology*, 27(6), pp.1478–1485.

Singaraja, R.R. et al., 2002. HIP14, a novel ankyrin domain-containing protein, links huntingtin to intracellular trafficking and endocytosis. *Human Molecular Genetics*, 11(23), pp.2815–2828.

Sipido, K.R. et al., 2002. Altered Na/Ca exchange activity in cardiac hypertrophy and heart failure: a new target for therapy?. *Cardiovascular Research*, 53, pp.782–805.

Smotrys, J.E. & Linder, M.E., 2004. Palmitoylation Of Intracellular Signaling Proteins: Regulation and Function. *Annual Review of Biochemistry*, 73(1), pp.559–587.

Smotrys, J.E. et al., 2005. The vacuolar DHHC-CRD protein Pfa3p is a protein acyltransferase for Vac8p. *The Journal of Cell Biology*, 170(7), pp.1091–1099.

Soyombo, A.A. & Hofmann, S.L., 1997. Molecular Cloning and Expression of Palmitoyl-protein Thioesterase 2 (PPT2), a Homolog of Lysosomal Palmitoyl-protein Thioesterase with a Distinct Substrate Specificity. *Journal of Biological Chemistry*, 272(43), pp.27456–27463.

Stan, R.V., 2005. Structure of caveolae. *Biochimica et Biophysica Acta (BBA) - Molecular Cell Research*, 1746(3), pp.334–348.

Stephens, G.J. et al., 2000. The α1B Ca2+ channel amino terminus contributes determinants for β subunit-mediated voltage-dependent inactivation properties. *Journal of Physiology*, 525(2), pp.377–390.

Sugimoto, H., Hayashi, H. & Yamashita, S., 1996. Purification, cDNA Cloning, and Regulation of Lysophospholipase from Rat Liver. *Journal of Biological Chemistry*, 271(13), pp.7705–7711.

Suzuki, H. et al., 2008. Formation of aquaporin-4 arrays is inhibited by palmitoylation of N-terminal cysteine residues. *Biochimica et Biophysica Acta (BBA) - Biomembranes*, 1778(4), pp.1181–1189.

Swarthout, J.T. et al., 2005. DHHC9 and GCP16 Constitute a Human Protein Fatty Acyltransferase with Specificity for H- and N-Ras. *Journal of Biological Chemistry*, 280(35), pp.31141–31148.

Thurneysen, T. et al., 2002. Na+/Ca2+ exchanger subtypes NCX1, NCX2 and NCX3 show cell-specific expression in rat hippocampus cultures. *Molecular Brain Research*, 107, pp.145–156.

Tian, L. et al., 2012. Distinct Acyl Protein Transferases and Thioesterases Control Surface Expression of Ca2+-activated Potassium Channels. *Journal of Biological Chemistry*, 287(18), pp.14718–14725.

Tian, L. et al., 2010. Multiple Palmitoyltransferases Are Required for Palmitoylation-dependent Regulation of Large Conductance Ca2+- and Voltage-activated Potassium Channels. *Journal of Biological Chemistry*, 285(31), pp.23954–23962.

Tian, L. et al., 2008. Palmitoylation gates phosphorylation-dependent regulation of BK potassium channels. *PNAS*, 105(52), pp.21006–21011.

Tomatis, V.M. et al., 2010. Acyl-Protein Thioesterase 2 Catalizes the Deacylation of Peripheral Membrane-Associated GAP-43 V. N. Uversky, ed. *PloS one*, 5(11), p.e15045.

Toyoda, T., Sugimoto, H. & Yamashita, S., 1999. Sequence, expression in Escherichia coli, and characterization of lysophospholipase II. *Biochimica et Biophysica Acta*, 1437, pp.182–193.

Tsutsumi, Y.M. et al., 2008. Cardiac-Specific Overexpression of Caveolin-3 Induces Endogenous Cardiac Protection by Mimicking Ischemic Preconditioning. *Circulation*, 118(19), pp.1979–1988.

Tulloch, L.B. et al., 2011. The Inhibitory Effect of Phospholemman on the Na+ Pump Requires Its Palmitoylation. *Journal of Biological Chemistry*, 286(41), pp.36020–36031.

Uray, I.P. et al., 2003. Mechanical unloading increases caveolin expression in the failing human heart. *Cardiovascular Research*, 59, pp.57–66.

Vartak, N. et al., 2014. The Autodepalmitoylating Activity of APT Maintains the SpatialOrganization of Palmitoylated Membrane Proteins. *Biophysical Journal*, 106(1), pp.93–105.

Veit, M. & Schmidt, M.F.G., 2001. Enzymatic Depalmitoylation of Viral Glycoproteins with Acyl-Protein Thioesterase 1 in Vitro. *Virology*, 288(1), pp.89–95.

Veit, M., Reverey, H. & Schmidt, M.F.G., 1996. Cytoplasmic tail length influences fatty acid selection for acylation of viral glycoproteins. *Journal of Biological Chemistry*, 318, pp.163–172.

Venetucci, L.A. et al., 2007. Na/Ca Exchange: Regulator of Intracellular Ca2+ and Source of Arrhythmias in the Heart. *Annals of the New York Academy of Sciences*, 1099(1), pp.315–325.

Verkruyse, L.A. & Hofmann, S.L., 1996. Lysosomal Targeting of Palmitoyl-protein Thioesterase. *Journal of Biological Chemistry*, 271(26), pp.15831–15836.

Vesa, J. et al., 1995. Mutations in the palmitoyl protein thioesterase gene causing infantile neuronal ceroid lipofuscinosis. *Nature*, 376, pp.584–587.

Voigt, N. et al., 2012. Enhanced Sarcoplasmic Reticulum Ca2+ Leak and Increased Na+-Ca2+ Exchanger Function Underlie Delayed Afterdepolarizations in Patients With Chronic Atrial Fibrillation. *Circulation*, 125, pp.2059–2070.

Wakimoto, K. et al., 2000. Targeted Disruption of Na+/Ca2+ Exchanger Gene Leads to Cardiomyocyte Apoptosis and Defects in Heartbeat. *Journal of Biological Chemistry*, 275(47), pp.36991–36998.

Wang, J. et al., 2007. SEA0400, a Novel Na+/Ca2+ Exchanger Inhibitor, Reduces Ca2+ Overload Induced by Ischemia and Reperfusion in Mouse Ventricular Myocytes. *Physiological Research*, 56, pp.17–23.

Wanichawan, P. et al., 2011. Full-length cardiac Na+/Ca2+ exchanger 1 protein is not phosphorylated by protein kinase A. *AJP: Cell Physiology*, 300(5), pp.C989–C997.

Wansleeben, C. et al., 2010. A novel mutant allele of Ncx1: a single amino acid substitution leads to cardiac dysfunction. *International Journal of Developmental Biology*, 54(10), pp.1465–1470.

Webb, Y., Hermida-Matsumoto, L. & Resh, M.D., 2000. Inhibition of Protein Palmitoylation, Raft Localization, and T Cell Signaling by 2-Bromopalmitate and

Polyunsaturated Fatty Acids. *Journal of Biological Chemistry*, 275(1), pp.261–270.

Wei, S.K., 2003. Protein Kinase A Hyperphosphorylation Increases Basal Current but Decreases beta-Adrenergic Responsiveness of the Sarcolemmal Na+-Ca2+ Exchanger in Failing Pig Myocytes. *Circulation Research*, 92(8), pp.897–903.

Woodman, S.E. et al., 2002. Caveolin-3 Knock-out Mice Develop a Progressive Cardiomyopathy and Show Hyperactivation of the p42/44 MAPK Cascade. *Journal of Biological Chemistry*, 277(41), pp.38988–38997.

Wright, L.P. & Philips, M.R., 2006. Thematic review series: Lipid Posttranslational Modifications. CAAX modification and membrane targeting of Ras. *Journal of Lipid Research*, 47(5), pp.883–891.

Wypijewski, K.J. et al., 2013. A separate pool of cardiac phospholemman that does not regulate or associate with the Na+ pump: multimers of phospholemman in ventricular muscle. *Journal of Biological Chemistry*, 288(19), pp.13808–13820.

Yang, G. et al., 2009. Subunit-selective palmitoylation regulates the intracellular trafficking of AMPA receptor. *European Journal of Neuroscience*, 30(1), pp.35–46.

Yang, J. et al., 2005. Submicromolar Concentrations of Palmitoyl-CoA Specifically Thioesterify Cysteine 244 in Glyceraldehyde-3-phosphate Dehydrogenase Inhibiting Enzyme Activity: A Novel Mechanism Potentially Underlying Fatty Acid Induced Insulin Resistance. *Biochemistry*, 44(35), pp.11903–11912.

Yang, W. et al., 2010. Proteome Scale Characterization of Human S-Acylated Proteins in Lipid Raft-enriched and Non-raft Membranes. *Molecular and Cellular Proteomics*, 9, pp.54–70.

Yang, Z., 2002. Na+-Ca2+ Exchange Activity Is Localized in the T-Tubules of Rat Ventricular Myocytes. *Circulation Research*, 91(4), pp.315–322.

Yaradanakul, A. et al., 2007. Dual control of cardiac Na+ Ca2+ exchange by PIP2: electrophysiological analysis of direct and indirect mechanisms. *The Journal of Physiology*, 582(3), pp.991–1010.

Yeh, D.C. et al., 1999. Depalmitoylation of Endothelial Nitric-oxide Synthase by Acyl-protein Thioesterase 1 Is Potentiated by Ca2+-Calmodulin. *Journal of Biological Chemistry*, 274(46), pp.33148–33154.

Zaika, O. et al., 2006. Angiotensin II regulates neuronal excitability via phosphatidylinositol 4,5-bisphosphate-dependent modulation of Kv7 (M-type) K+ channels. *The Journal of Physiology*, 575(1), pp.49–67.

Zeidman, R., Jackson, C.S. & Magee, A.I., 2009. *Protein acyl thioesterases*, Mol Membr Biol.

Zhang, L. et al., 2007. S-acylation regulates Kv1.5 channel surface expression. *AJP: Cell Physiology*, 293(1), pp.C152–C161.

# Chapter 10: Appendix

| Annotation Cluster 1 | Enrichment Score: 23.051356777242898 | | | | |
|---|---|---|---|---|---|
| Category | Term | Count | % | PValue | Genes |
| GOTERM_CC_FAT | GO:0030017~sarcomere | 29 | 10.24734982 | 2.02E-24 | Q01082, P10916, P50461, Q8WZ42, P06733, P04075, Q9NPC6, P02585, P13533, P35222, P35609, P19429, Q14896, Q14192, P02511, P17661, P29992, P08590, Q13936, P14923, Q92736, Q13813, P52179, Q14315, P09493, O75112, P56539, P11532, P45379 |
| Annotation Cluster 2 | Enrichment Score: 17.42753562708084 | | | | |
| Category | Term | Count | % | PValue | Genes |
| GOTERM_CC_FAT | GO:0031966~mitochondrial membrane | 47 | 16.60777385 | 8.97E-22 | P27105, O75431, O15239, Q86Y39, O96000, P45880, Q99714, P03905, O95674, O00483, P33121, O43678, Q96IX5, O96008, Q9UDW1, P21796, P05141, P17302, O75746, Q9Y512, Q02978, Q9Y6M9, P00403, O95167, O43920, Q9UJS0, Q16891, Q9NVH1, P03886, P14854, Q9P0J0, P51970, Q92523, P03915, P19367, P12235, Q9NZJ7, Q9UI09, O43169, Q9Y5U8, P21397, Q9NZ45, P03891, P53701, O43772, Q9Y277, Q9Y3D6 |
| Annotation Cluster 3 | Enrichment Score: 12.735748834017336 | | | | |
| Category | Term | Count | % | PValue | Genes |
| GOTERM_CC_FAT | GO:0005626~insoluble fraction | 55 | 19.43462898 | 9.71E-14 | Q07065, P51636, Q6PIU2, Q03135, Q9Y512, O60716, P17661, P05023, P29992, O00161, O75955, P05556, Q92523, P11717, Q9Y4J8, Q9BTU6, O75323, Q92736, Q13813, P48751, P56539, Q9UIQ6, Q9Y277, P27105, Q15836, Q9UP95, P33121, P35222, P16615, P04899, O96008, P48509, P02511, P13929, P07947, P55072, Q14118, Q6NZI2, Q5JWF2, Q14254, Q13936, P14923, O43306, P28907, O14880, P20338, P09471, P32418, O43169, P53985, P16671, P11532, P01111, Q14108, P01112 |
| Annotation Cluster 4 | Enrichment Score: 11.136199819293045 | | | | |

| Category | Term | Count | % | PValue | Genes |
|---|---|---|---|---|---|
| SP_PIR_KEYWORDS | respiratory chain | 18 | 6.360424028 | 2.01E-16 | P03886, O15239, P14854, O96000, Q86Y39, Q9P0J0, P51970, P03915, P03905, O00483, O43678, Q9UDW1, Q9UI09, Q9Y6M9, P00403, P03891, O95167, O43920 |
| Annotation Cluster 5 | Enrichment Score: 10.132955758953933 | | | | |
| Category | Term | Count | % | PValue | Genes |
| GOTERM_BP_FAT | GO:0006096~glycolysis | 14 | 4.946996466 | 7.85E-13 | P04406, P40925, P60174, P18669, P04075, P06733, P00338, P06744, P07195, P19367, P08237, P13929, P00558, P14618 |
| Annotation Cluster 6 | Enrichment Score: 9.047451586071642 | | | | |
| Category | Term | Count | % | PValue | Genes |
| GOTERM_BP_FAT | GO:0044275~cellular carbohydrate catabolic process | 16 | 5.653710247 | 1.55E-11 | P04406, P40925, P60174, P18669, P04075, P06733, P00338, P06744, P07195, P19367, P00558, P08237, P11217, P13929, P11216, P14618 |
| Annotation Cluster 7 | Enrichment Score: 9.013716248903663 | | | | |
| Category | Term | Count | % | PValue | Genes |
| SP_PIR_KEYWORDS | mitochondrion outer membrane | 13 | 4.593639576 | 3.90E-10 | O75431, P45880, Q92523, P33121, P19367, O96008, P21796, Q9Y512, O43169, P21397, Q9NZ45, Q9Y3D6, Q9Y277 |
| Annotation Cluster 8 | Enrichment Score: 6.435714036308812 | | | | |
| Category | Term | Count | % | PValue | Genes |
| GOTERM_MF_FAT | GO:0003924~GTPase activity | 19 | 6.713780919 | 1.31E-08 | Q5JWF2, Q05639, P62070, Q9NP72, P08134, P68371, P04899, P11233, Q14344, P20338, P13639, P10114, P68366, P09471, Q9BQE3, P10301, P01111, P01112, P29992 |
| Annotation Cluster 9 | Enrichment Score: 5.770799716264166 | | | | |
| Category | Term | Count | % | PValue | Genes |

| | | | | | |
|---|---|---|---|---|---|
| GOTERM_CC_FAT | GO:0031982~vesicle | 37 | 13.07420495 | 2.21E-07 | P27105, P21926, P00441, P51636, P04075, P35609, Q03135, P08133, P11142, P17302, P50995, Q6ZMU5, Q00610, A1A4Y4, P05023, O15126, O75955, Q5JWF2, O00161, P02787, Q07075, P27824, Q9H3Z4, P05556, P02768, P02786, P26678, P11717, Q9BTU6, Q14714, Q14344, P20338, P08238, Q86Y82, P16671, O75923 |
| Annotation Cluster 10 | Enrichment Score: 5.078913313496356 | | | | |
| Category | Term | Count | % | PValue | Genes |
| SP_PIR_KEYWORDS | transmembrane | 120 | 42.40282686 | 1.37E-09 | Q07065, Q9H0X4, P19022, Q86Y39, Q14524, Q9HCP6, P51636, Q9H7Z7, Q6PIU2, P13591, Q96IX5, O14786, Q5T3F8, O95870, Q02978, O15126, Q07075, P05556, Q96S97, P43121, Q00765, Q92523, Q14714, Q92736, Q9NZJ7, P20645, Q14126, Q9NZ45, P56539, O43772, Q8IWA5, Q9UP95, P45880, P33121, Q14165, P16615, Q5RI15, P17302, Q9P2B2, O14828, Q01628, P00403, O00168, Q6NTF9, Q9UJS0, P27824, P03886, P26678, P12235, O43306, Q9HBU9, O75110, P32418, P53985, Q9HCJ1, P03891, P19075, O75915, Q96FX8, P21926, Q92629, Q03135, P21796, P49961, Q9Y512, Q9H1E5, O15260, P05023, O15173, O95167, P02786, Q9P0J0, P11717, Q16585, Q16586, P48751, Q96ER9, Q86Y82, O75923, Q9Y277, Q9UIQ6, P27105, A5D6W6, O15239, Q13061, P29972, Q15836, P03905, O95674, Q96A26, O96008, P48509, P50895, P05141, Q9H0R3, Q9NRY6, O75746, Q14118, Q16891, O95183, Q9BUM1, Q6NXT6, P60033, Q9BX67, Q13936, P03915, Q9Y320, P56557, P28907, O14880, P28906, Q9BQJ4, O43169, Q687X5, Q9NRZ7, P21397, P16671, Q14108, Q9Y3D6 |
| Annotation Cluster 11 | Enrichment Score: 5.015294037106725 | | | | |
| Category | Term | Count | % | PValue | Genes |
| GOTERM_BP_FAT | GO:0060415~muscle tissue morphogenesis | 8 | 2.826855124 | 2.88E-07 | P19429, Q14896, P09493, P10916, Q8WZ42, P08590, P13533, P45379 |
| Annotation Cluster 12 | Enrichment Score: 4.710148595890581 | | | | |

| Category | Term | Count | % | PValue | Genes |
|---|---|---|---|---|---|
| GOTERM_BP_FAT | GO:0006461~protein complex assembly | 26 | 9.187279152 | 2.43E-06 | P27105, P19022, Q8WZ42, Q15836, P51636, Q99714, P04040, P35222, Q03135, P35609, P68371, P02511, P17302, P68366, Q9Y512, Q6ZMU5, Q9BQE3, P11047, Q14118, P55072, O43920, Q6NZI2, P14923, P08237, P01112 |
| Annotation Cluster 13 | Enrichment Score: 4.359567959489039 | | | | |
| Category | Term | Count | % | PValue | Genes |
| SP_PIR_KEYWORDS | nucleotide binding | 10 | 3.533568905 | 2.82E-05 | Q5JWF2, P20338, P13639, Q14204, P09471, P62070, P13533, P10301, P04899, P29992 |
| Annotation Cluster 14 | Enrichment Score: 4.325018055765178 | | | | |
| Category | Term | Count | % | PValue | Genes |
| GOTERM_BP_FAT | GO:0055066~di-, tri-valent inorganic cation homeostasis | 17 | 6.007067138 | 4.32E-06 | P02787, P50461, P02786, P26678, P00441, Q13936, P16615, Q03135, Q92736, P19429, P28907, Q14344, P11217, P32418, P56539, O00168, P23327 |
| Annotation Cluster 15 | Enrichment Score: 4.225164227979266 | | | | |
| Category | Term | Count | % | PValue | Genes |
| GOTERM_BP_FAT | GO:0030239~myofibril assembly | 6 | 2.120141343 | 2.46E-05 | P09493, P10916, P05556, Q8WZ42, P13533, P45379 |
| Annotation Cluster 16 | Enrichment Score: 4.065557745933812 | | | | |
| Category | Term | Count | % | PValue | Genes |
| GOTERM_BP_FAT | GO:0051924~regulation of calcium ion transport | 9 | 3.180212014 | 2.47E-05 | P17302, P26678, P29474, P09471, P32418, P56539, Q03135, Q92736, P04899 |
| Annotation Cluster 17 | Enrichment Score: 4.016801704461444 | | | | |
| Category | Term | Count | % | PValue | Genes |
| SMART | SM00173:RAS | 6 | 2.120141343 | 3.27E-06 | P11233, P10114, P62070, P10301, P01111, P01112 |

| Annotation Cluster 18 | Enrichment Score: 3.6917964715241163 | | | | |
|---|---|---|---|---|---|
| Category | Term | Count | % | PValue | Genes |
| SP_PIR_KEYWORDS | nucleotide-binding | 50 | 17.66784452 | 2.71E-06 | P62070, P06732, P08134, P68371, P11233, P11142, P10114, P49961, P68366, Q9BQE3, A1A4Y4, P05023, P29992, Q05639, P22314, Q9BTU6, Q92523, Q9H0U4, Q562R1, Q15772, Q14344, P08238, P00558, P08237, Q9Y277, P27105, Q8WZ42, P45880, P13533, P33121, P16615, P78527, P04899, P11217, P07947, P55072, Q5JWF2, P12277, Q9NP72, P19367, O43306, O75110, P20338, P13639, Q14204, P09471, P10301, P14618, P01111, P01112 |

| Annotation Cluster 19 | Enrichment Score: 3.5974830105810063 | | | | |
|---|---|---|---|---|---|
| Category | Term | Count | % | PValue | Genes |
| INTERPRO | IPR002113:Adenine nucleotide translocator 1 | 6 | 2.120141343 | 4.65E-05 | P05141, O75746, Q02978, O43772, P12235, Q9UJS0 |

| Annotation Cluster 20 | Enrichment Score: 3.5269674848426185 | | | | |
|---|---|---|---|---|---|
| Category | Term | Count | % | PValue | Genes |
| UP_SEQ_FEATURE | short sequence motif:Effector region | 10 | 3.533568905 | 1.13E-05 | P11233, P20338, P10114, P62070, Q9NP72, P10301, P08134, Q9H0U4, P01111, P01112 |

| Annotation Cluster 21 | Enrichment Score: 3.3796936264499227 | | | | |
|---|---|---|---|---|---|
| Category | Term | Count | % | PValue | Genes |
| GOTERM_CC_FAT | GO:0030055~cell-substrate junction | 11 | 3.886925795 | 1.28E-04 | Q14192, P18206, Q9Y490, P05556, Q9BX66, P51636, P13533, Q9Y4G6, P11532, Q03135, P35609 |

| Annotation Cluster 22 | Enrichment Score: 2.8854690297928114 | | | | |
|---|---|---|---|---|---|
| Category | Term | Count | % | PValue | Genes |
| SMART | SM00150:SPEC | 5 | 1.766784452 | 2.85E-04 | Q01082, P15924, P11532, P35609, Q13813 |

| Annotation Cluster 23 | Enrichment Score: 2.8033219552585225 | | | | |
|---|---|---|---|---|---|
| Category | Term | Count | % | PValue | Genes |
| UP_SEQ_FEATURE | repeat:ARM 8 | 5 | 1.766784452 | 2.75E-04 | O60716, P14923, O00192, Q99959, P35222 |

| Annotation Cluster 24 | Enrichment Score: 2.64540413703062 | | | | |
|---|---|---|---|---|---|
| Category | Term | Count | % | PValue | Genes |
| GOTERM_BP_FAT | GO:0009991~response to extracellular stimulus | 12 | 4.240282686 | 0.00161 5773 | P28907, O95870, P02768, P02786, P00441, P32418, P00338, O14828, P33121, Q03135, Q92736, P04899 |

| Annotation Cluster 25 | Enrichment Score: 2.5292499542067652 | | | | |
|---|---|---|---|---|---|
| Category | Term | Count | % | PValue | Genes |
| INTERPRO | IPR001925:Porin, eukaryotic type | 4 | 1.413427562 | 3.76E-05 | P45880, O96008, Q9Y277, P21796 |

| Annotation Cluster 26 | Enrichment Score: 2.5174462249316454 | | | | |
|---|---|---|---|---|---|
| Category | Term | Count | % | PValue | Genes |
| GOTERM_BP_FAT | GO:0015813~L-glutamate transport | 4 | 1.413427562 | 0.00163 5057 | O75915, O75746, P12235, Q9UJS0 |

| Annotation Cluster 27 | Enrichment Score: 2.487455069941237 | | | | |
|---|---|---|---|---|---|
| Category | Term | Count | % | PValue | Genes |
| UP_SEQ_FEATURE | domain:Laminin EGF-like 11 | 4 | 1.413427562 | 2.50E-04 | P07942, P11047, P55268, P24043 |

| Annotation Cluster 28 | Enrichment Score: 2.486694269091723 | | | | |
|---|---|---|---|---|---|
| Category | Term | Count | % | PValue | Genes |

| | | | | | |
|---|---|---|---|---|---|
| GOTERM_CC_FAT | GO:0005856~cytoskeleton | 56 | 19.78798587 | 2.34E-06 | Q01082, P04259, P54296, P02585, P35221, Q92629, P68371, P19429, Q14896, Q14192, P13645, P68366, P13647, Q9BQE3, P17661, P04264, Q99959, P29992, O75955, P15924, Q9Y490, Q16585, Q16586, Q562R1, Q13813, P09493, P45379, P27105, P10916, P18206, P50461, Q8WZ42, P04075, Q9NPC6, P13533, Q9Y4G6, P35222, P35609, P02511, P50995, P29474, Q14118, P22735, Q5JR59, Q9BX66, P08590, Q13936, P14923, Q9UN36, P52179, Q14315, O75112, Q14204, Q96AQ6, P11532 |
| Annotation Cluster 29 | Enrichment Score: 2.325439089301545 | | | | |
| Category | Term | Count | % | PValue | Genes |
| INTERPRO | IPR001019:Guanine nucleotide binding protein (G-protein), alpha subunit | 5 | 1.766784452 | 9.38E-05 | Q5JWF2, Q14344, P09471, P04899, P29992 |
| Annotation Cluster 30 | Enrichment Score: 2.0995507470640953 | | | | |
| Category | Term | Count | % | PValue | Genes |
| GOTERM_BP_FAT | GO:0048514~blood vessel morphogenesis | 11 | 3.886925795 | 0.00381 3792 | P19429, Q14344, Q07075, P50461, P29474, P19022, P06744, P07203, P35222, Q03135, O14786 |
| Annotation Cluster 31 | Enrichment Score: 2.086805963024401 | | | | |
| Category | Term | Count | % | PValue | Genes |
| INTERPRO | IPR001236:Lactate/malate dehydrogenase | 3 | 1.060070671 | 0.00648 1231 | P40925, P00338, P07195 |
| Annotation Cluster 32 | Enrichment Score: 2.044406220772395 | | | | |
| Category | Term | Count | % | PValue | Genes |
| GOTERM_BP_FAT | GO:0015909~long-chain fatty acid transport | 4 | 1.413427562 | 0.00546 2335 | P05413, Q92523, P16671, O43772 |
| Annotation Cluster 34 | Enrichment Score: 1.9601723462890719 | | | | |

| Category | Term | Count | % | PValue | Genes |
|---|---|---|---|---|---|
| UP_SEQ_FEATURE | repeat:Spectrin 4 | 4 | 1.413427562 | 0.00347 1338 | Q01082, P11532, P35609, Q13813 |
| Annotation Cluster 35 | Enrichment Score: 1.920799414903643 | | | | |
| Category | Term | Count | % | PValue | Genes |
| UP_SEQ_FEATURE | domain:Actin-binding | 4 | 1.413427562 | 0.00300 7971 | Q14315, Q01082, P11532, P35609 |
| Annotation Cluster 36 | Enrichment Score: 1.8430723495869428 | | | | |
| Category | Term | Count | % | PValue | Genes |
| PIR_SUPERFAMILY | PIRSF002419:CD9 antigen | 4 | 1.413427562 | 0.00718 9404 | P48509, P21926, P60033, P19075 |
| Annotation Cluster 37 | Enrichment Score: 1.8421619201373625 | | | | |
| Category | Term | Count | % | PValue | Genes |
| SMART | SM00054:EFh | 7 | 2.473498233 | 0.00378 7788 | P10916, O75746, P02585, Q92736, P35609, Q13813, Q9UJS0 |
| Annotation Cluster 38 | Enrichment Score: 1.829929023516856 | | | | |
| Category | Term | Count | % | PValue | Genes |
| GOTERM_BP_FAT | GO:0035150~regulation of tube size | 5 | 1.766784452 | 0.01336 7903 | P29474, P00441, P51636, P07203, Q03135 |
| Annotation Cluster 39 | Enrichment Score: 1.7304914666163667 | | | | |
| Category | Term | Count | % | PValue | Genes |
| INTERPRO | IPR018361:Caveolin, conserved site | 3 | 1.060070671 | 7.32E-04 | P51636, P56539, Q03135 |
| Annotation Cluster 40 | Enrichment Score: 1.6986812207587907 | | | | |

| Category | Term | Count | % | PValue | Genes |
|---|---|---|---|---|---|
| GOTERM_BP_FAT | GO:0007016~cytoskeletal anchoring at plasma membrane | 3 | 1.060070671 | 0.00785 2625 | Q9Y490, Q9Y4G6, P11532 |
| Annotation Cluster 41 | Enrichment Score: 1.6841650910788286 | | | | |
| Category | Term | Count | % | PValue | Genes |
| GOTERM_BP_FAT | GO:0010941~regulation of cell death | 24 | 8.480565371 | 0.01484 0197 | Q05639, Q96FX8, Q9H3Z4, P02768, P00441, Q9P0J0, P11717, Q04760, P04040, P07203, P78527, Q92736, P35609, P68371, P12235, P28907, Q9NZJ7, P02511, P29474, O95817, O75190, P55072, P01111, P01112 |
| Annotation Cluster 42 | Enrichment Score: 1.6382937034247793 | | | | |
| Category | Term | Count | % | PValue | Genes |
| GOTERM_BP_FAT | GO:0016310~phosphorylation | 24 | 8.480565371 | 0.01212 3408 | Q01082, P03886, O15239, P60033, Q8WZ42, P00441, O96000, P51636, P51970, P03915, P03905, O00483, O43678, P78527, P04899, Q15772, Q9UDW1, P00558, Q9Y6M9, P00403, P07947, P03891, O95167, O43920 |
| Annotation Cluster 43 | Enrichment Score: 1.6302161192897762 | | | | |
| Category | Term | Count | % | PValue | Genes |
| GOTERM_BP_FAT | GO:0046034~ATP metabolic process | 7 | 2.473498233 | 0.00995 4635 | O75110, P49961, P04075, P13533, P05023, P16615, Q9UJS0 |
| Annotation Cluster 44 | Enrichment Score: 1.5733513478938062 | | | | |
| Category | Term | Count | % | PValue | Genes |
| GOTERM_BP_FAT | GO:0030049~muscle filament sliding | 3 | 1.060070671 | 0.00998 1264 | P09493, P13533, P45379 |
| Annotation Cluster 45 | Enrichment Score: 1.5606627238158934 | | | | |
| Category | Term | Count | % | PValue | Genes |

| | | | | | |
|---|---|---|---|---|---|
| UP_SEQ_FEATURE | domain:Ig-like C2-type 3 | 7 | 2.473498233 | 0.00951 4356 | P50895, Q14896, Q9P2B2, P43121, P54296, P13591, P52179 |
| Annotation Cluster 46 | Enrichment Score: 1.5519088496657536 | | | | |
| Category | Term | Count | % | PValue | Genes |
| GOTERM_BP_FAT | GO:0051969~regulation of transmission of nerve impulse | 8 | 2.826855124 | 0.01430 4099 | P28907, P27105, P02787, P19022, P01111, P04899, P01112, P24043 |
| Annotation Cluster 47 | Enrichment Score: 1.4673440252853462 | | | | |
| Category | Term | Count | % | PValue | Genes |
| GOTERM_BP_FAT | GO:0034614~cellular response to reactive oxygen species | 4 | 1.413427562 | 0.01487 2429 | P09493, P00441, P04040, P07203 |
| Annotation Cluster 48 | Enrichment Score: 1.4282433313788871 | | | | |
| Category | Term | Count | % | PValue | Genes |
| GOTERM_CC_FAT | GO:0005764~lysosome | 10 | 3.533568905 | 0.03531 0376 | P20645, O00161, Q13510, P17302, P17174, P11717, P04040, P19075, P53634, Q14108 |
| Annotation Cluster 49 | Enrichment Score: 1.4277380351743758 | | | | |
| Category | Term | Count | % | PValue | Genes |
| GOTERM_BP_FAT | GO:0008645~hexose transport | 4 | 1.413427562 | 0.01487 2429 | P20645, Q9BX66, P07947, Q9BUM1 |
| Annotation Cluster 50 | Enrichment Score: 1.4255748657361815 | | | | |
| Category | Term | Count | % | PValue | Genes |
| GOTERM_BP_FAT | GO:0060548~negative regulation of cell death | 13 | 4.593639576 | 0.02389 1439 | Q05639, Q9H3Z4, P02768, P00441, Q04760, P04040, P07203, P12235, P02511, O95817, P29474, P01111, P01112 |
| Annotation Cluster 51 | Enrichment Score: | | | | |

| | 1.398772488459015 | | | | |
|---|---|---|---|---|---|
| Category | Term | Count | % | PValue | Genes |
| SMART | SM00060:FN3 | 7 | 2.473498233 | 0.01449 3044 | Q14896, Q8WZ42, P54296, P13591, P23327, Q15772, P52179 |

| Annotation Cluster 52 | Enrichment Score: 1.3476048173029478 | | | | |
|---|---|---|---|---|---|
| Category | Term | Count | % | PValue | Genes |
| SMART | SM00408:IGc2 | 9 | 3.180212014 | 0.00133 2961 | P50895, Q14896, Q8WZ42, P43121, Q9BX67, P54296, P13591, Q15772, P52179 |

| Annotation Cluster 53 | Enrichment Score: 1.2742839901779295 | | | | |
|---|---|---|---|---|---|
| Category | Term | Count | % | PValue | Genes |
| GOTERM_BP_FAT | GO:0034637~cellular carbohydrate biosynthetic process | 5 | 1.766784452 | 0.03189 4495 | P60174, P35573, P17174, P06744, Q9BUM1 |

| Annotation Cluster 54 | Enrichment Score: 1.2732587699024487 | | | | |
|---|---|---|---|---|---|
| Category | Term | Count | % | PValue | Genes |
| GOTERM_BP_FAT | GO:0006641~triglyceride metabolic process | 4 | 1.413427562 | 0.03838 6276 | P04040, P56539, P07203, Q03135 |

| Annotation Cluster 55 | Enrichment Score: 1.2548976646909955 | | | | |
|---|---|---|---|---|---|
| Category | Term | Count | % | PValue | Genes |
| UP_SEQ_FEATURE | domain:LIM zinc-binding 1 | 4 | 1.413427562 | 0.03745 2901 | Q14192, O75112, P50461, P52943 |

| Annotation Cluster 56 | Enrichment Score: 1.1920038723923674 | | | | |
|---|---|---|---|---|---|
| Category | Term | Count | % | PValue | Genes |
| GOTERM_BP_FAT | GO:0030193~regulation of blood coagulation | 4 | 1.413427562 | 0.02424 7336 | P29474, P04264, P19075, Q03135 |

| Annotation Cluster 57 | Enrichment Score: 1.1909064142830377 | | | | |
|---|---|---|---|---|---|
| Category | Term | Count | % | PValue | Genes |
| UP_SEQ_FEATURE | region of interest:Linker 12 | 5 | 1.766784452 | 0.01475 0471 | P13645, P04259, P13647, P17661, P04264 |

| Annotation Cluster 58 | Enrichment Score: 1.1544792210133155 | | | | |
|---|---|---|---|---|---|
| Category | Term | Count | % | PValue | Genes |
| GOTERM_BP_FAT | GO:0019217~regulation of fatty acid metabolic process | 4 | 1.413427562 | 0.05317 6559 | Q92523, P33121, Q03135, O43772 |

| Annotation Cluster 59 | Enrichment Score: 1.1334905153643626 | | | | |
|---|---|---|---|---|---|
| Category | Term | Count | % | PValue | Genes |
| GOTERM_BP_FAT | GO:0016477~cell migration | 10 | 3.533568905 | 0.05143 9762 | Q07075, P28906, P05556, P29474, P19022, P51636, P11047, P07203, O14786, P78527 |

| Annotation Cluster 60 | Enrichment Score: 1.1215871245727838 | | | | |
|---|---|---|---|---|---|
| Category | Term | Count | % | PValue | Genes |
| INTERPRO | IPR018316:Tubulin/FtsZ, 2-layer sandwich domain | 3 | 1.060070671 | 0.04629 5601 | P68366, Q9BQE3, P68371 |

| Annotation Cluster 61 | Enrichment Score: 1.1184660740837764 | | | | |
|---|---|---|---|---|---|
| Category | Term | Count | % | PValue | Genes |
| GOTERM_BP_FAT | GO:0051270~regulation of cell motion | 8 | 2.826855124 | 0.05111 371 | Q14344, P09493, P18206, P62070, P07942, P10301, O14786, P24043 |

| Annotation Cluster 62 | Enrichment Score: 1.1040884993077194 | | | | |
|---|---|---|---|---|---|
| Category | Term | Count | % | PValue | Genes |
| GOTERM_BP_FAT | GO:0046165~alcohol biosynthetic process | 4 | 1.413427562 | 0.04068 3363 | P60174, P17174, P06744, Q9BUM1 |

| Annotation Cluster 63 | Enrichment Score: 1.0419362041165432 | | | | |
|---|---|---|---|---|---|
| Category | Term | Count | % | PValue | Genes |
| GOTERM_BP_FAT | GO:0045792~negative regulation of cell size | 6 | 2.120141343 | 0.02905585 | P10916, P02511, Q9P0J0, P06733, P56539, O14786 |

| Annotation Cluster 64 | Enrichment Score: 1.0409730386702971 | | | | |
|---|---|---|---|---|---|
| Category | Term | Count | % | PValue | Genes |
| GOTERM_BP_FAT | GO:0043623~cellular protein complex assembly | 8 | 2.826855124 | 0.023079014 | P68366, Q9Y512, Q8WZ42, P51636, Q9BQE3, P68371, Q03135, O43920 |

| Annotation Cluster 65 | Enrichment Score: 1.0209343727996028 | | | | |
|---|---|---|---|---|---|
| Category | Term | Count | % | PValue | Genes |
| GOTERM_MF_FAT | GO:0030170~pyridoxal phosphate binding | 4 | 1.413427562 | 0.060016997 | P11217, P02768, P17174, P11216 |

| Annotation Cluster 66 | Enrichment Score: 1.0094481171891598 | | | | |
|---|---|---|---|---|---|
| Category | Term | Count | % | PValue | Genes |
| GOTERM_CC_FAT | GO:0005604~basement membrane | 7 | 2.473498233 | 0.006060758 | P02787, P49961, P07942, P11047, P55268, Q14118, P24043 |

| Annotation Cluster 67 | Enrichment Score: 0.9930304360167743 | | | | |
|---|---|---|---|---|---|
| Category | Term | Count | % | PValue | Genes |
| SP_PIR_KEYWORDS | myosin | 4 | 1.413427562 | 0.038754525 | P10916, P08590, P13533, P29992 |

| Annotation Cluster 68 | Enrichment Score: 0.9780987597335998 | | | | |
|---|---|---|---|---|---|
| Category | Term | Count | % | PValue | Genes |
| GOTERM_BP_FAT | GO:0055088~lipid homeostasis | 4 | 1.413427562 | 0.058631858 | Q9NRY6, P17174, P56539, Q03135 |

| Annotation Cluster 69 | Enrichment Score: 0.9239814046579772 | | | | |
|---|---|---|---|---|---|
| Category | Term | Count | % | PValue | Genes |
| GOTERM_BP_FAT | GO:0052547~regulation of peptidase activity | 5 | 1.766784452 | 0.06263 4488 | Q9NZJ7, O75190, P07203, P55072, Q03135 |

| Annotation Cluster 70 | Enrichment Score: 0.868933636011586 | | | | |
|---|---|---|---|---|---|
| Category | Term | Count | % | PValue | Genes |
| GOTERM_BP_FAT | GO:0008654~phospholipid biosynthetic process | 6 | 2.120141343 | 0.03247 3319 | P05413, P60033, Q9NRZ7, Q92523, Q9BTU6, O95674 |

| Annotation Cluster 71 | Enrichment Score: 0.8520610552914979 | | | | |
|---|---|---|---|---|---|
| Category | Term | Count | % | PValue | Genes |
| SMART | SM00271:DnaJ | 3 | 1.060070671 | 0.08967 6374 | Q9H3Z4, Q9NVH1, O75190 |

| Annotation Cluster 72 | Enrichment Score: 0.8468738490550688 | | | | |
|---|---|---|---|---|---|
| Category | Term | Count | % | PValue | Genes |
| INTERPRO | IPR003962:Fibronectin, type III subdomain | 3 | 1.060070671 | 0.09958 6357 | Q8WZ42, P54296, P52179 |

| Annotation Cluster 73 | Enrichment Score: 0.8466618194852193 | | | | |
|---|---|---|---|---|---|
| Category | Term | Count | % | PValue | Genes |
| GOTERM_BP_FAT | GO:0006754~ATP biosynthetic process | 5 | 1.766784452 | 0.06924 6346 | O75110, P04075, P05023, P16615, Q9UJS0 |

| Annotation Cluster 74 | Enrichment Score: 0.8294579560034017 | | | | |
|---|---|---|---|---|---|
| Category | Term | Count | % | PValue | Genes |
| GOTERM_BP_FAT | GO:0006518~peptide metabolic process | 4 | 1.413427562 | 0.06433 99 | P00441, Q04760, P07203, P11532 |

| Annotation Cluster 75 | Enrichment Score: 0.7692636409271687 | | | | |
|---|---|---|---|---|---|
| Category | Term | Count | % | PValue | Genes |
| GOTERM_BP_FAT | GO:0008542~visual learning | 3 | 1.060070671 | 0.07941 5283 | Q13936, P01111, P01112 |

| Annotation Cluster 76 | Enrichment Score: 0.7435437622251508 | | | | |
|---|---|---|---|---|---|
| Category | Term | Count | % | PValue | Genes |
| GOTERM_BP_FAT | GO:0032526~response to retinoic acid | 3 | 1.060070671 | 0.11177 2583 | P28907, P02786, O14828 |

| Annotation Cluster 77 | Enrichment Score: 0.7407998149339332 | | | | |
|---|---|---|---|---|---|
| Category | Term | Count | % | PValue | Genes |
| GOTERM_BP_FAT | GO:0030168~platelet activation | 3 | 1.060070671 | 0.10616 4702 | Q14344, P21926, P49961 |

| Annotation Cluster 78 | Enrichment Score: 0.7344959472105513 | | | | |
|---|---|---|---|---|---|
| Category | Term | Count | % | PValue | Genes |
| GOTERM_BP_FAT | GO:0046474~glycerophospholipid biosynthetic process | 4 | 1.413427562 | 0.11447 2387 | P05413, P60033, Q92523, Q9BTU6 |

| Annotation Cluster 79 | Enrichment Score: 0.7324304138556709 | | | | |
|---|---|---|---|---|---|
| Category | Term | Count | % | PValue | Genes |
| GOTERM_BP_FAT | GO:0043409~negative regulation of MAPKKK cascade | 3 | 1.060070671 | 0.03442 6366 | P27105, P56539, Q03135 |

| Annotation Cluster 80 | Enrichment Score: 0.7222184190298224 | | | | |
|---|---|---|---|---|---|
| Category | Term | Count | % | PValue | Genes |
| GOTERM_BP_FAT | GO:0006112~energy reserve metabolic process | 4 | 1.413427562 | 0.03838 6276 | Q5JWF2, P11217, P35573, P11216 |

| Annotation Cluster 81 | Enrichment Score: 0.7086494798288502 | | | | |
|---|---|---|---|---|---|
| Category | Term | Count | % | PValue | Genes |
| UP_SEQ_FEATURE | calcium-binding region:3 | 3 | 1.060070671 | 0.09855 0641 | O75746, P02585, Q9UJS0 |

| Annotation Cluster 82 | Enrichment Score: 0.6923067400003688 | | | | |
|---|---|---|---|---|---|
| Category | Term | Count | % | PValue | Genes |
| GOTERM_BP_FAT | GO:0046496~nicotinamide nucleotide metabolic process | 3 | 1.060070671 | 0.15290 7601 | P60174, P40925, P07195 |

| Annotation Cluster 83 | Enrichment Score: 0.6696447008566017 | | | | |
|---|---|---|---|---|---|
| Category | Term | Count | % | PValue | Genes |
| GOTERM_CC_FAT | GO:0005778~peroxisomal membrane | 3 | 1.060070671 | 0.13883 2466 | P04040, P33121, Q9Y3D6 |

| Annotation Cluster 84 | Enrichment Score: 0.6271102170185054 | | | | |
|---|---|---|---|---|---|
| Category | Term | Count | % | PValue | Genes |
| SP_PIR_KEYWORDS | atp-binding | 26 | 9.187279152 | 0.11722 1624 | P27105, Q8WZ42, P06732, P13533, P33121, P16615, P78527, P11142, P49961, P05023, P07947, P55072, P12277, P22314, Q9BTU6, Q92523, P19367, Q562R1, Q15772, O43306, O75110, P08238, P08237, Q14204, P00558, P14618 |

| Annotation Cluster 85 | Enrichment Score: 0.604333426583047 | | | | |
|---|---|---|---|---|---|
| Category | Term | Count | % | PValue | Genes |
| GOTERM_CC_FAT | GO:0032592~integral to mitochondrial membrane | 3 | 1.060070671 | 0.02551 7121 | O96008, Q16891, Q9Y3D6 |

| Annotation Cluster 86 | Enrichment Score: 0.5896982059689104 |
|---|---|

| Category | Term | Count | % | PValue | Genes |
|---|---|---|---|---|---|
| INTERPRO | IPR001757:ATPase, P-type, K/Mg/Cd/Cu/Zn/Na/Ca/Na/H-transporter | 3 | 1.060070671 | 0.10961 8011 | O75110, P05023, P16615 |
| Annotation Cluster 87 | Enrichment Score: 0.5821501573820184 | | | | |
| Category | Term | Count | % | PValue | Genes |
| GOTERM_BP_FAT | GO:0012501~programmed cell death | 15 | 5.300353357 | 0.17753 1953 | Q96FX8, Q9P0J0, P00441, P07203, P35222, P78527, P21796, Q9NZJ7, P17302, O95817, P14618, P55072, P01111, P01112, Q9Y3D6 |
| Annotation Cluster 88 | Enrichment Score: 0.576333996601938 | | | | |
| Category | Term | Count | % | PValue | Genes |
| GOTERM_BP_FAT | GO:0030324~lung development | 4 | 1.413427562 | 0.24704 9068 | Q13510, P29474, P51636, P35222 |
| Annotation Cluster 89 | Enrichment Score: 0.5602320779674103 | | | | |
| Category | Term | Count | % | PValue | Genes |
| GOTERM_BP_FAT | GO:0032956~regulation of actin cytoskeleton organization | 4 | 1.413427562 | 0.20137 3366 | P09493, Q01082, P56539, Q13813 |
| Annotation Cluster 90 | Enrichment Score: 0.5503500604223177 | | | | |
| Category | Term | Count | % | PValue | Genes |
| GOTERM_BP_FAT | GO:0030336~negative regulation of cell migration | 3 | 1.060070671 | 0.26056 1178 | P09493, P18206, P10301 |
| Annotation Cluster 91 | Enrichment Score: 0.5014275044450058 | | | | |
| Category | Term | Count | % | PValue | Genes |
| INTERPRO | IPR016044:Filament | 3 | 1.060070671 | 0.31327 | P13645, P13647, P17661 |

| Annotation Cluster 92 | Enrichment Score: 0.49826816150114267 | | | | |
|---|---|---|---|---|---|
| Category | Term | Count | % | PValue | Genes |
| GOTERM_BP_FAT | GO:0001569~patterning of blood vessels | 3 | 1.060070671 | 0.05081 3705 | Q14344, P35222, O14786 |

| Annotation Cluster 93 | Enrichment Score: 0.47994006094606917 | | | | |
|---|---|---|---|---|---|
| Category | Term | Count | % | PValue | Genes |
| GOTERM_MF_FAT | GO:0022832~voltage-gated channel activity | 6 | 2.120141343 | 0.22208 9066 | Q14524, P45880, Q13936, O96008, Q9Y277, P21796 |

| Annotation Cluster 94 | Enrichment Score: 0.45926530381818986 | | | | |
|---|---|---|---|---|---|
| Category | Term | Count | % | PValue | Genes |
| GOTERM_BP_FAT | GO:0006140~regulation of nucleotide metabolic process | 5 | 1.766784452 | 0.14323 9958 | Q5JWF2, O43306, P18669, P29474, P04899 |

| Annotation Cluster 95 | Enrichment Score: 0.3427264285259352 | | | | |
|---|---|---|---|---|---|
| Category | Term | Count | % | PValue | Genes |
| GOTERM_BP_FAT | GO:0031099~regeneration | 3 | 1.060070671 | 0.33766 8473 | P13929, P07203, P55268 |

| Annotation Cluster 96 | Enrichment Score: 0.33496021422415956 | | | | |
|---|---|---|---|---|---|
| Category | Term | Count | % | PValue | Genes |
| UP_SEQ_FEATURE | repeat:3 | 5 | 1.766784452 | 0.38648 1376 | P18206, Q96Q06, P11717, Q92736, P52179 |

| Annotation Cluster 97 | Enrichment Score: 0.33358374731217727 | | | | |
|---|---|---|---|---|---|
| Category | Term | Count | % | PValue | Genes |

| | | | | | |
|---|---|---|---|---|---|
| GOTERM_CC_FAT | GO:0033017~sarcoplasmic reticulum membrane | 3 | 1.060070671 | 0.04907 9377 | P16615, Q92736, P23327 |
| Annotation Cluster 98 | Enrichment Score: 0.31900827388492436 | | | | |
| Category | Term | Count | % | PValue | Genes |
| GOTERM_BP_FAT | GO:0043065~positive regulation of apoptosis | 9 | 3.180212014 | 0.47298 4557 | P28907, Q9NZJ7, Q96FX8, Q9P0J0, P00441, P07203, P68371, P78527, Q92736 |
| Annotation Cluster 99 | Enrichment Score: 0.3172831208392465 | | | | |
| Category | Term | Count | % | PValue | Genes |
| GOTERM_BP_FAT | GO:0048666~neuron development | 8 | 2.826855124 | 0.37788 7892 | Q9NZJ7, P17302, P00441, P09471, P07942, P55268, P11532, O14786 |
| Annotation Cluster 100 | Enrichment Score: 0.2898211938145993 | | | | |
| Category | Term | Count | % | PValue | Genes |
| GOTERM_BP_FAT | GO:0017038~protein import | 4 | 1.413427562 | 0.39846 9552 | O75431, Q01082, Q9P0J0, O96008 |
| Annotation Cluster 101 | Enrichment Score: 0.280113012730508 | | | | |
| Category | Term | Count | % | PValue | Genes |
| GOTERM_BP_FAT | GO:0048534~hemopoietic or lymphoid organ development | 6 | 2.120141343 | 0.47450 274 | P05556, P00441, P52943, P35222, P78527, P02144 |
| Annotation Cluster 102 | Enrichment Score: 0.2575710663722945 | | | | |
| Category | Term | Count | % | PValue | Genes |
| GOTERM_BP_FAT | GO:0006814~sodium ion transport | 4 | 1.413427562 | 0.39378 0041 | P32418, Q14524, Q9UP95, P05023 |
| Annotation Cluster 103 | Enrichment Score: 0.23827443003867488 | | | | |

| Category | Term | Count | % | PValue | Genes |
|---|---|---|---|---|---|
| SMART | SM00326:SH3 | 4 | 1.413427562 | 0.38600 0134 | Q9UKS6, Q9BX66, P07947, Q13813 |
| Annotation Cluster 104 | Enrichment Score: 0.22402483871252088 | | | | |
| Category | Term | Count | % | PValue | Genes |
| UP_SEQ_FEATURE | repeat:4 | 4 | 1.413427562 | 0.50245 4739 | Q96Q06, P11717, Q92736, P52179 |
| Annotation Cluster 105 | Enrichment Score: 0.22397594725518516 | | | | |
| Category | Term | Count | % | PValue | Genes |
| GOTERM_BP_FAT | GO:0034613~cellular protein localization | 8 | 2.826855124 | 0.57489 244 | O75431, Q01082, Q9P0J0, Q86Y82, Q00610, P35222, P55072, O96008 |
| Annotation Cluster 106 | Enrichment Score: 0.18902203968766013 | | | | |
| Category | Term | Count | % | PValue | Genes |
| GOTERM_BP_FAT | GO:0007605~sensory perception of sound | 3 | 1.060070671 | 0.50472 2793 | P00441, Q9Y6M9, P07203 |
| Annotation Cluster 107 | Enrichment Score: 0.18512967652967594 | | | | |
| Category | Term | Count | % | PValue | Genes |
| GOTERM_BP_FAT | GO:0008406~gonad development | 3 | 1.060070671 | 0.58245 4108 | P29474, P00441, Q99714 |
| Annotation Cluster 108 | Enrichment Score: 0.18233551157375058 | | | | |
| Category | Term | Count | % | PValue | Genes |
| GOTERM_BP_FAT | GO:0045859~regulation of protein kinase activity | 7 | 2.473498233 | 0.55666 3831 | O43306, P60033, Q8WZ42, P00441, P56539, Q03135, P04899 |
| Annotation Cluster 109 | Enrichment Score: 0.1528303342855841 | | | | |

| Category | Term | Count | % | PValue | Genes |
|---|---|---|---|---|---|
| GOTERM_BP_FAT | GO:0030098~lymphocyte differentiation | 3 | 1.060070671 | 0.536915637 | P05556, P35222, P78527 |
| Annotation Cluster 110 | Enrichment Score: 0.1412266740922575 | | | | |
| Category | Term | Count | % | PValue | Genes |
| GOTERM_BP_FAT | GO:0032990~cell part morphogenesis | 5 | 1.766784452 | 0.653237191 | P17302, P55268, P11532, O14786, Q9Y3D6 |
| Annotation Cluster 111 | Enrichment Score: 0.13903899904263536 | | | | |
| Category | Term | Count | % | PValue | Genes |
| GOTERM_BP_FAT | GO:0006302~double-strand break repair | 3 | 1.060070671 | 0.292840357 | P00441, P55072, P78527 |
| Annotation Cluster 112 | Enrichment Score: 0.11690792395668144 | | | | |
| Category | Term | Count | % | PValue | Genes |
| INTERPRO | IPR005821:Ion transport | 3 | 1.060070671 | 0.518519158 | Q14524, Q13936, Q92736 |
| Annotation Cluster 113 | Enrichment Score: 0.11410860838284909 | | | | |
| Category | Term | Count | % | PValue | Genes |
| GOTERM_BP_FAT | GO:0045860~positive regulation of protein kinase activity | 4 | 1.413427562 | 0.747790571 | O43306, P60033, P00441, P04899 |
| Annotation Cluster 114 | Enrichment Score: 0.07552626558706478 | | | | |
| Category | Term | Count | % | PValue | Genes |
| GOTERM_BP_FAT | GO:0043193~positive regulation of gene-specific transcription | 3 | 1.060070671 | 0.447982242 | P35222, P78527, Q96BS2 |

| Annotation Cluster 115 | Enrichment Score: 0.06979581613734355 | | | | |
|---|---|---|---|---|---|
| Category | Term | Count | % | PValue | Genes |
| KEGG_PATHWAY | hsa03010:Ribosome | 3 | 1.060070671 | 0.74663 9189 | P36578, Q92901, Q07020 |

| Annotation Cluster 116 | Enrichment Score: 0.04121532942215029 | | | | |
|---|---|---|---|---|---|
| Category | Term | Count | % | PValue | Genes |
| GOTERM_MF_FAT | GO:0043167~ion binding | 64 | 22.61484099 | 0.87209 3775 | P19022, Q14524, P06733, Q6PIU2, P02585, P08133, Q14192, P49961, Q6ZMU5, P35573, P05023, O15173, P02787, Q07075, Q9BTU6, Q9Y4J8, Q16586, Q92736, Q13813, P08237, Q14126, Q86TD4, Q9NZ45, P53634, Q96BS2, Q9UIQ6, P10916, P50461, Q8WZ42, P00441, Q9UP95, Q8N490, P04040, P33121, P16615, P35609, Q9NRY6, P13929, P50995, O75746, P29474, P00403, Q14118, O00168, P02144, Q9UJS0, P22735, P27824, Q68D91, P02768, P08590, Q13936, Q04760, O43306, O75110, O75112, O43169, P32418, Q687X5, P52943, P14618, P11532, P53701, P23327 |

| Annotation Cluster 117 | Enrichment Score: 0.016846629137158713 | | | | |
|---|---|---|---|---|---|
| Category | Term | Count | % | PValue | Genes |
| GOTERM_BP_FAT | GO:0045892~negative regulation of transcription, DNA-dependent | 4 | 1.413427562 | 0.94933 2805 | Q9P0J0, P06733, O75190, P35222 |

| Annotation Cluster 118 | Enrichment Score: 0.008193428462753395 | | | | |
|---|---|---|---|---|---|
| Category | Term | Count | % | PValue | Genes |
| GOTERM_BP_FAT | GO:0051173~positive regulation of nitrogen compound metabolic process | 7 | 2.473498233 | 0.97044 7253 | P27105, Q14192, P08238, P35222, P78527, P01112, Q96BS2 |

| Annotation Cluster | Enrichment Score: |
|---|---|

| 119 | 0.0020758457613709773 | | | | |
|---|---|---|---|---|---|
| Category | Term | Count | % | PValue | Genes |
| SP_PIR_KEYWORDS | Protease | 3 | 1.060070671 | 0.993983857 | Q07075, P53634, Q9UIQ6 |

| Annotation Cluster 120 | Enrichment Score: 0.002062957657555977 | | | | |
|---|---|---|---|---|---|
| Category | Term | Count | % | PValue | Genes |
| GOTERM_BP_FAT | GO:0000278~mitotic cell cycle | 3 | 1.060070671 | 0.989218791 | P05556, Q14204, Q8WZ42 |

| Annotation Cluster 121 | Enrichment Score: 1.6602543354317433E-5 | | | | |
|---|---|---|---|---|---|
| Category | Term | Count | % | PValue | Genes |
| GOTERM_CC_FAT | GO:0031974~membrane-enclosed lumen | 21 | 7.4204947 | 0.999902874 | Q6NZI2, Q01082, P14854, P02768, Q9P0J0, P00441, P45880, P13533, P11717, P04040, P35222, P78527, P35609, P21796, P05141, P38117, P29474, P50995, Q86TD4, P55072, P23327 |

| Annotation Cluster 122 | Enrichment Score: 2.775459811399698E-11 | | | | |
|---|---|---|---|---|---|
| Category | Term | Count | % | PValue | Genes |
| SP_PIR_KEYWORDS | transcription regulation | 5 | 1.766784452 | 1 | Q6NZI2, Q14192, O60716, P06733, P35222 |